Oxidation of Alkanes, Alkenes and Alcohols Catalyzed by Transition Metal Complexes

Thèse présentée à la Faculté des Sciences
Institut de Chimie
Université de Neuchâtel

Pour l'obtention du grade de Docteur ès Sciences

Par

Vladimir B. Romakh

Chimiste diplômé de l'Université d'Etat de Moscou
(Russie)

Acceptée sur proposition du jury :
Prof. Dr. Georg Süss-Fink, directeur de thèse
Prof. Dr. Titus Jenny, rapporteur
Prof. Dr. Georgiy B. Shul'pin, rapporteur
Prof. Dr. Thomas Ward, rapporteur

Soutenue le 19 septembre 2006

Université de Neuchâtel
2006

Université de Neuchâtel

IMPRIMATUR POUR LA THESE

Oxidation of Alkanes, Alkenes and Alcohols Catalyzed by Transition Metal Complexes

Vladimir Bogdanovich ROMAKH

UNIVERSITE DE NEUCHATEL

FACULTE DES SCIENCES

La Faculté des sciences de l'Université de Neuchâtel,
sur le rapport des membres du jury

MM.G. Süss-Fink (directeur de thèse),
T. Ward, T. Jenny (Fribourg)
et G.B. Shul'pin (Moscou)

autorise l'impression de la présente thèse.

Neuchâtel, le 30 octobre 2006

UNIVERSITE DE NEUCHATEL
FACULTE DES SCIENCES
Secrétariat-décanat de la faculté
Rue Emile-Argand 11 - CP 158
CH-2009 Neuchâtel

Le doyen :

J.-P. Derendinger

■ **Faculté des Sciences**
■ Rue Emile-Argand 11 ■ CP 158 ■ CH-2009 Neuchâtel
■ Téléphone : +41 32 718 21 00 ■ Fax : +41 32 718 21 03 ■ E-mail : secretariat.sciences@unine.ch ■ www.unine.ch

Remerciements

Les travaux reportés dans la présente thèse ont été effectués au sein du Laboratoire de Chimie des Organométalliques et de Catalyse Moléculaire de l'Université de Neuchâtel, sous la direction du Professeur Georg Süss-Fink.

En premier lieu, j'adresse mes remerciements les plus sincères au Professeur Georg Süss-Fink. Je le remercie de m'avoir accueilli dans son équipe de recherche et de m'avoir fait totalement confiance durant ces quatre années. Je le remercie également pour sa disponibilité, son soutien, ses conseils et ses grandes qualités humaines. Je remercie très sincèrement le Professeur Georgiy Borisovich Shul'pin d'avoir accepté de lire ce manuscrit avec attention et de m'avoir fait part de sa chimie fascinante. Je le remercie également pour sa disponibilité, son soutien et ses conseils scientifiques avisés.

Je tiens à remercier les Professeurs Thomas Ward et Titus Jenny d'avoir accepté de prendre connaissance de mon travail de thèse et d'y avoir porté un jugement. Je les remercie également de m'avoir fait part de leurs remarques pertinentes concernant ce manuscrit.

Je remercie toutes les personnes qui ont participé de près comme de loin à la réalisation de ce travail de thèse et qui m'ont permis d'avancer plus rapidement: Prof. Helen Stoeckli-Evans, Prof. Tawan Sooknoi, Dr. Yuriy Kozlov, Dr. Alex Kitaygorodskiy, Dr. Péter Buglyó, les étudiant(e)s Cyril Kopp, Inga Zaitseva, Inès Hafner et Youri Sauser. Je remercie tous les membres du laboratoire et de l'institut qui ont su faire régner une ambiance conviviale et sincère durant ces quatre années. Un clin d'oeil tout particulier à Dr. Frédéric Chérioux, Dr. Sylvain Burger, Dr. Ludovic Vieille-Petit, Dr. Mathieu Tschan, Anca Pordea, Ludovic Chahen, Jérôme Canivet, Mathieu Auzias, Michael Gras. Je remercie particulièrement le Docteur Bruno Therrien pour son aide très précieuse durant la rédaction des publications et pour sa disponibilité, notamment pour les mesures radiocristallographiques.

Je remercie l'Université de Neuchâtel et le Fonds National Suisse de la Recherche Scientifique qui ont soutenu financièrement ce projet. Enfin, un GRAND MERCI à mes amis proches qui m'ont toujours soutenu et encouragé dans mes démarches, depuis mes premiers jours sur les bancs de la fac. Une pensée toute particulière à Olya Sereda et Julieta Gradinaru, ainsi qu'à Seva, Inga, Andrij, Magi, Denis, Anton et François.

Abstract

The robust nature of alkanes is one of the major challenges for chemists from both a fundamental and a practical point of view. The present work deals in particular with the catalytic activation and selective functionalization of carbon-hydrogen bonds in alkanes including methane. The catalytic systems studied and developed in this thesis have been used for the oxidation of alkanes, alkenes and alcohols.

In a first approach, a detailed spectroscopic and kinetic study of the known catalytic system vanadate/pyrazine-2-carboxylic acid has been carried out. It revealed that this binary system catalyzes the oxidation of alkanes and alcohols with hydrogen peroxide via different routes. The mechanistic scheme proposed according to these findings gives a satisfactory interpretation of the experimental data.

In a second approach, based on biomimetic considerations, six new 1,4,7-triazacyclononane-derived ligands as well as thirteen new transition metal complexes thereof have been synthesized and characterized. Three novel types of dinuclear Mn(III)-Mn(IV) and Co(III)-Co(III) as well of tetranuclear Fe(III)-Fe(III)-Fe(III)-Fe(III) complexes have been structurally characterized. The catalytic activities and selectivities of manganese, iron, cobalt and ruthenium catalysts containing 1,4,7-triazacyclononane-derived ligands as well as those of *in situ* prepared systems have been studied for oxidation reactions. Activity and selectivity can be tuned by: a) using a co-catalyst that acts as a ligand or/and as reducing agent, b) introducing a functionality (carboxylato or hydroxo pendant arm) or/and chirality in the 1,4,7-triazacyclononane macrocycle. The oxidation of alcohols, alkenes and even alkanes such as methane has been studied in acetonitrile as well as in water as solvent. In some cases enantio- and stereoselectivity has been observed. The tetranuclear iron(III) complex containing four 1,4,7-triazacyclononane-derived ligands with a pendant carboxylato arm can be considered as a structural and functional model for methane monooxygenase.

In a third approach, a solid titanosilicalite catalyst with nanopores (TS-1) has been studied for the oxidative functionalization of alkanes. It turned out that the regioselectivity in the case of higher *n*-alkanes, controlled by the nanopores, can be improved by introducing certain alcohols into the reaction mixture.

In conclusion, this work describes improved known as well as new selective catalytic systems for oxidation reactions using the environmentally friendly oxidant H_2O_2. The biomimetic approach combined with detailed mechanistic investigations provides new insights into oxidation reactions of alcohols, alkenes and alkanes.

Keywords

Oxidation, Selectivity, Iron, Manganese, Ruthenium, Cobalt, Vanadium Complexes, Enantioselective Catalysis, Hydrogen Peroxide, Methane, Carbon-Hydrogen Bonds, Activation.

Mots Clés

Oxydation, Sélectivité, Fer, Manganèse, Ruthénium, Cobalt, Vanadium Complexes, Catalyse Enantiosélective, Peroxyde d’Hydrogène, Méthane, Liaisons Carbone-Hydrogène, Activation.

Table of Contents

1 Oxidative Functionalization of Hydrocarbons: A Challenge for the Chemical Community

The functionalization of hydrocarbons, the main natural oil and gas constituents, has been identified as a key research strategy for the development of economical and sustainable global carbon management [1, 2]. Undoubtedly one of the most important functionalizations is selective oxidation; in particular the selective aerobic oxidation of methane to methanol would be of great industrial interest [3, 4].

Unlike other types of catalytic processes, the oxidation of organic material is usually strongly exothermic. However, the more negative the free reaction enthalpy ΔH^o is, the smaller are the activation energy separations for the desired product formation versus the formation of other products. Usually, the activation energy, E_a, for the formation of a desired hydrocarbon oxidation product is higher than that for the subsequent products. Thus, the selective oxidation of hydrocarbons to valuable oxygenates represents a significant challenge, since initial oxidation products are susceptible to complete combustion to give CO_2.

The transformation of hydrocarbons into simple oxygenated organic compounds such as alcohols, aldehydes, ketones, carboxylic acids and peroxides has been extensively studied over the last decades, because such products are important intermediates of the industrial production [1, 5]. Given the chemical inertness of alkanes, it is difficult to activate these substrates under mild conditions, necessary for selective oxidation.

1.1 Activation of Aliphatic C−H Bonds

The functionalization of alkanes, including methane, is in principle known for a long time. These reactions involve the formation of radicals and the interaction with molecular oxygen from air (burning). Hence, industrial transformations of alkanes occur at elevated temperatures (higher than 300^{o}C) and are usually characterized by a lack of selectivity.

Over the past decades, the rapid development of metal-complex catalysis allowed the beginning of an essentially new chemistry of saturated hydrocarbons [6]. Indeed, reactions

with metal complexes occur at relatively low temperatures and can be selective. “Activation” of a certain molecule by a metal complex, although a rather vague concept, usually means that the molecule or part of it becomes a ligand in the coordination sphere of the complex and then undergoes a subsequent chemical transformation. Generally, “activation” of a molecule means that the reactivity of this molecule increases due to some action.

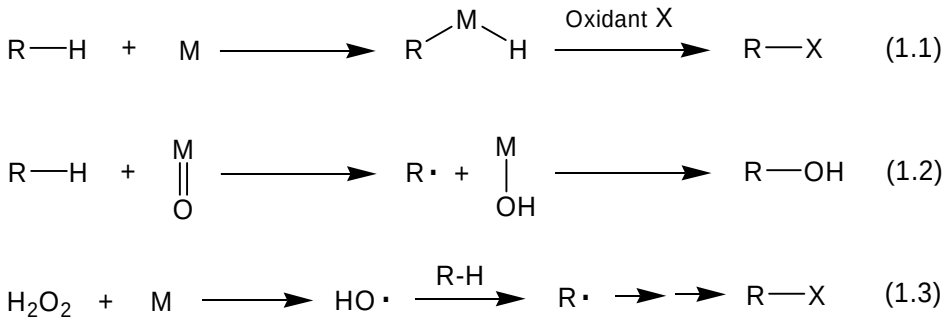

Scheme 1. Three types of oxidative activation of C−H bonds [1]

From the mechanistic point of view, C−H activation processes can be divided into three types [7]. The first group includes reactions where organometallic derivatives (*i.e.*, compounds containing a metal-carbon σ-bond) are formed as an intermediate or as the final product (Scheme 1, eq. 1.1). The second group involves reactions in which the contact between the complex and the C−H bond is achieved via a ligand, leading to C−H bond cleavage, a σ-C−M bond not being generated at any stage (eq. 1.2). In these reactions, the function of the metal complex usually consists in abstracting an electron or a hydrogen atom from the hydrocarbon. Finally, in the processes that belong to the third type, a complex activates initially not the hydrocarbon but another reactant (*e.g.* hydrogen peroxide (eq. 1.3) or molecular oxygen). The reactive species formed (*e.g.* hydroxyl radical) then attacks the hydrocarbon molecule without any participation of the metal complex in the latter process. The metal catalyst does not take part in the direct “activation” of the C−H bond by the radical.

1.2 Transition-Metal Catalyzed Oxidation of C−H Bonds

Although alkanes are generally unreactive toward soluble transition-metal complexes, chemists have identified several classes of compounds that react readily with the C−H bonds of hydrocarbons, including alkanes, under mild conditions (first type of activation). Five general mechanisms have been proposed (Scheme 2) [8]: (1) oxidative addition of the C−H bond to a low-valent, electron-rich transition-metal center, yielding an alkyl hydride product (eq. 1.4); (2) σ-bond metathesis of the C−H bond with highvalent electrophilic metal hydrides or hydrocarbyls to exchange the alkyl fragments between metal and hydrogen (eq. 1.5: R, R' = H, alkyl, alkenyl, alkynyl); (3) 1,2-addition of the C−H bond across the metal-element double bond for metal imido or oxo complexes, yielding the corresponding metal amido (hydroxo) alkyl product (eq. 1.6: X = NR, O) [9, 10]; (4) homolytic cleavage of the C−H bond (especially for methane) by two metal-centered radicals to afford a metal alkyl and a metal hydride product (eq. 1.7) [11]; (5) electrophilic activation (eq. 1.8: X = halide, hydroxide, *etc*.).

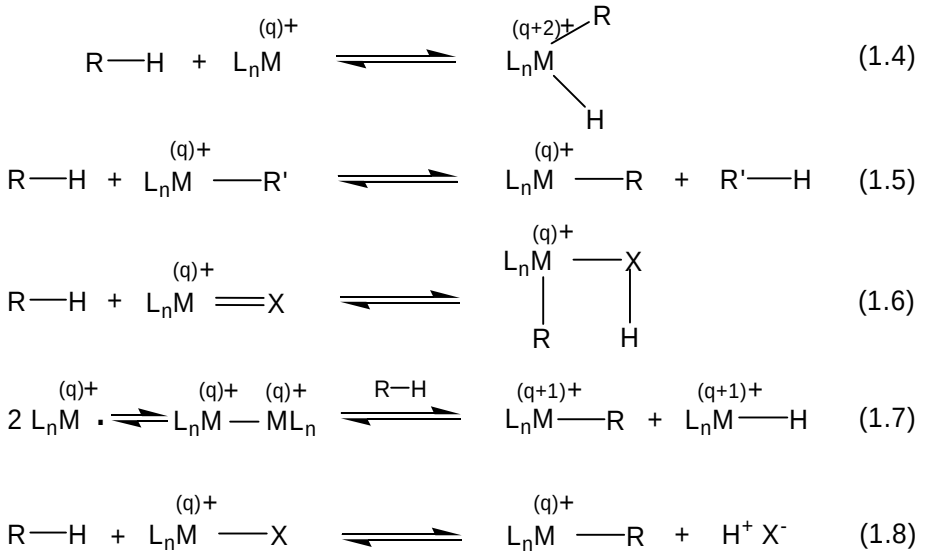

Scheme 2. Five mechanisms for homogeneous C−H bond activation with organometallic compounds (q = oxidation state of the metal center)

Although the first four processes represent highly significant developments in contemporary chemistry, the applications of these reaction types for the catalytic oxidative functionalization of hydrocarbons are still rare [8, 12].

Electrophilic activation, according to eq. 1.8, by late transition-metal ions such as Pt(II) [6, 13], Pd(II) [14, 15], Rh [16], Au(I)/Au(III) [17, 18] and Hg(II)[19] stands in marked contrast to the first four processes. Indeed, frontier orbital considerations indicate, that "soft" electophiles with low lying, polarizable LUMOs* of σ-symmetry would be effective for this mode of C−H bond activation [20]. Starting from the early work of Snyder and Grosse in 1950 [21], employing an $HgSO_4$ catalyst for methane oxidation with fuming sulphuric acid at 263°C, it was found that the reaction is mediated by the Hg(II)/Hg(I) redox couple [19]. In the 1970s, Shilov discovered that Pt(II)/Pt(IV) is capable of oxidizing alkanes to alcohols in water [22]; recently with Pt(II) chelated by a bipyrimidine ligand and SO_3 as the oxidant, methane was oxidized to a 72% yield of methanol and its esters [13]. In 2004 Periana and co-workers reported that the combination of gold as a catalyst and H_2SeO_4 as the oxidant results in a 94% selectivity for CH_3OSO_3H at 28% CH_4 conversion [17]. The step towards gold then seems straightforward, since Au(I) is isoelectronic with Hg(II), and Au(III) shares its electronic configuration with Pt(II).

Such electrophilic systems have been shown to effect both stoichiometric and catalytic oxidations of alkanes, including methane. The most attractive feature of these systems is their selectivity: the reactivity of the methyl group is substantially greater than that of a functionalized methylene or methylidene group (by as much as 100 times). Most of these systems operate in a strong acidic media at elevated temperatures (> 180 °C), but none of them is practical, since none display acceptable rates or uses air as the oxidant.

An important aspect of the Pd- [23, 24] and Rh-based [16] systems is their ability to simultaneously activate dioxygen and alkane. Both operate in protic media at moderate temperatures (70−100 °C), but require a co-reductant (carbon monoxide or dihydrogen) [25].

Although the mechanisms of the reaction with C−H bonds are in many cases unknown, processes of oxygen atom insertion rarely begin from the formation of the σ-metal-carbon bond [7] (first type of activation, Scheme 1). From the mechanistic point of view, all hydrocarbon oxidations occurring in living organisms are of the second and third type (Scheme 1) [26, 27], the metal center activating the C−H bond via a ligand or another reactant.

* Low unoccupied molecular orbital(s)

Transition metal ions are often used in catalytic low-temperature hydrocarbon oxidations with air. Catalytic systems consisting of cobalt or manganese acetate and sodium bromide efficiently catalyzes the oxidation of methylarenes to corresponding arenecarboxylic acids in acetic acid solution [28]. The catalytic oxidation of cyclohexane in the presence of manganese or cobalt naphthenate to give a mixture of cyclohexanone and cyclohexanol is an important industrial process [29]. Ishii and co-workers described the oxidation of hydrocarbons by molecular oxygen catalyzed by *N*-hydroxyphthalimide (NHPI) combined with manganese acetylacetonate (Scheme 3) or transition metal (mainly cobalt) salts [30]. Although air is the cheapest source of oxygen, it provides the lowest selectivity in many reactions [31]. Over the past decades, new catalysts have been developed for the use of oxidants called “oxygen atom donors”, such as hydrogen peroxide, alkylhydroperoxides, peracids, hypochlorite, iodosobenzene, nitrous oxide.

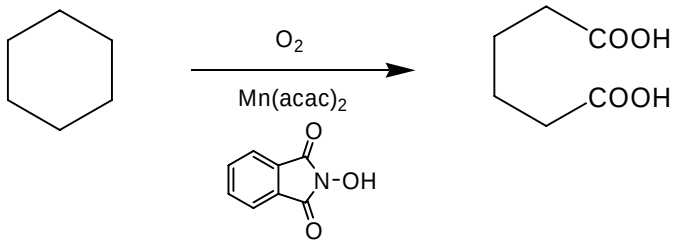

Scheme 3. Oxidation of cyclohexane to adipic acid catalyzed by *N*-hydroxyphthalimide (NHPI)

The oxidation of hydrocarbons with oxygen donors is an important field of research, since some industrial processes are based on these reactions [32], e.g. textile and paper bleaching [33]. In many cases the key step includes the interaction of an oxygen atom donor, such as hydrogen peroxide, with a low-valent form of the metal affording free oxygen centered radicals [31, 34] or/and high-valent metal-oxo species [35]. The classical Fenton system, a stoichiometric mixture of Fe(II) with H_2O_2, is transformed gradually into the catalytic Fe(III)-Fe(II)-H_2O_2 system in the course of the hydrogen peroxide decomposition, generating hydroxyl radicals. Other catalytic systems for the selective oxyfunctionalization of hydrocarbons with oxygen atom donors have been described by D. H. R. Barton (Gif systems, i.e. iron complexes in pyridine/acetic acid) [36], L. Que, Jr. [37], G. J. P. Britovsek [38] (non-heme transition metal catalysts containing polydentate nitrogen ligands), D. Mansuy [39] (manganese and iron porphyrinates with imidazole), E. N. Jacobsen [40, 41] (manganese Schiff-base complexes, Scheme 4) and W. Herrmann [42, 43] (methyltrioxorhenium/H_2O_2, Scheme 5).

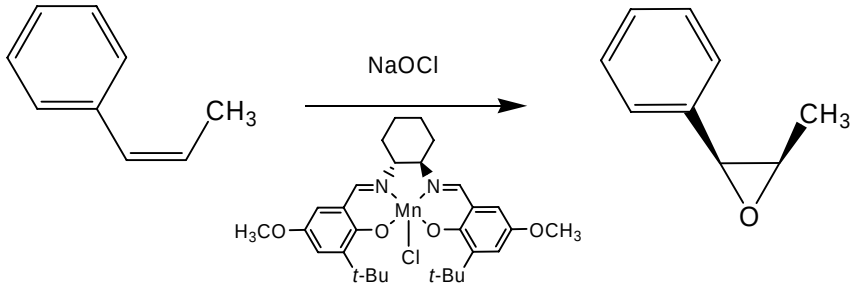

Scheme 4. Enantioselective epoxidation of cis-β-methylstyrene catalyzed by Jacobsen's catalyst

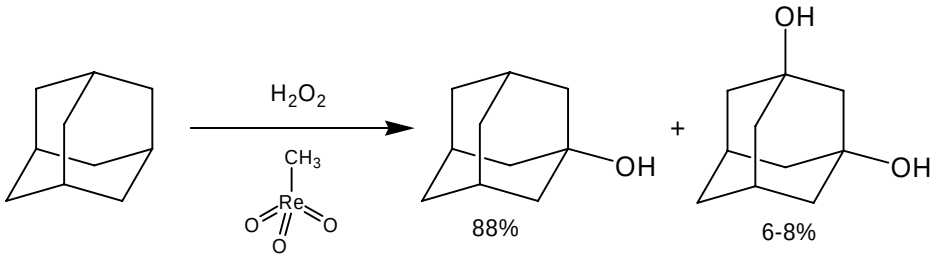

Scheme 5. Oxidation of adamantane catalyzed by methyltrioxorhenium (MTO)

Finally, we can conclude that the dioxygenase route (insertion of both oxygen atoms from the O_2 molecule) can be successfully used for the oxidation of compounds with C−H and C−C bonds activated by neighbouring oxo or hydroxyl groups. The radical-chain oxidation of saturated hydrocarbons under mild conditions is possible only in the case of compounds containing relatively weak C−H bonds. Usually this process is non-selective. The monooxygenase route (insertion of only one oxygen atom from the O_2 molecule, while the second oxygen atom is reduced to water by a reductant) is much more selective: the hydroxylation of alkanes can be carried out at room temperature like biological oxidations. Such oxidations normally require certain additives as co-catalyst [44]. These additives, which often are potential ligands, have been found during biomimetic studies or by chance. Aminoacids or heterocyclic amines can mimic the protein environment around the enzyme reaction center [45, 46]. It is very interesting that in many cases only particular molecules can play the role of efficient co-catalysts and even very similar compounds turn out to be inefficient in catalysis.

1.3 Biological Systems in Oxidation Catalysis

Enzymes are the most efficient oxidation catalysts found in nature, and examples are cytochrome P450 [47], the antitumor drug bleomycin (BLM) and methane monooxygenase (MMO). The general oxygenation mechanism includes the reduction of the metal center (mainly iron or copper) of such an enzyme by a biological reductant AH_2 prior to activation of molecular oxygen for the interaction with the hydrocarbon.

$$R{-}H + O_2 + AH_2 \xrightarrow{\text{monooxygenase}} R{-}OH + H_2O + A$$

The cytochrome P450s (CYP450s) are a large family of heme-type enzymes responsible for the metabolism of toxic hydrocarbons. CYP450s catalyze aromatic and aliphatic hydroxylations, epoxidations, or sulfoxides formation using NADPH (nicotinamide adenine dinucleotide phosphate, reduced form) as a reducing agent and O_2 as a substrate. Molecular oxygen coordinates to the reduced Fe(II) form of the CYP450, which contains a negatively charged sulphur atom of a conserved proximal cysteine as the axial ligand to the heme iron (Scheme 6). To form a peroxide state, the second electron is introduced via a flavin-containing electron-transport chain. Starting then from a (porphyrin)Fe(III)-O-OH intermediate, it has been believed [47] that a radical is formed at the porphyrin ring in the O-O splitting reaction step, but several researchers have suggested the formation of a sulfur radical in thiolate-heme proteins [48] producing an active Fe(IV)-O species.

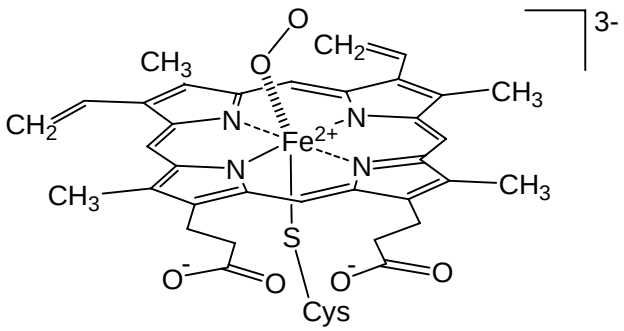

Scheme 6. Oxy ferrous species observed for the CYP450 during molecular oxygen activation

Bleomycin (BLM), a histidine-containing glycopeptide antibiotic produced by strains of *Streptomyces verticillus*, is a clinically useful antitumor agent (Blenoxane) that catalyzes oxidative DNA cleavage [49]. This oxidation is both O_2- and Fe(II)-dependent. BLM

coordinates Fe(II) to form a square pyramidal environment with the iron center being ligated to five nitrogens (Scheme 7). The sixth coordination site can be occupied by O_2, and a subsequent one-electron reduction forms activated bleomycin (ABLM), the last detectable species in its mechanism of action. This species can also be generated with Fe(III)-BLM and H_2O_2. ABLM has been characterized by different methods to be a low-spin Fe(III)-OOH species [50].

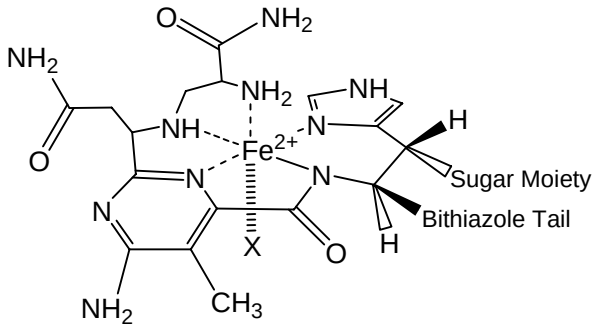

Scheme 7. Proposed structure for Fe(II)-bleomycin [50]

Methanemonooxygenases (MMOs) are a group of enzymes from methanotrophic bacteria capable of directly converting methane to methanol using NADH (nicotinamide adenine dinucleotide, reduced form) as a reducing agent and molecular oxygen as oxidant. Two varieties of MMO have been discovered: The first is copper-containing, membrane bound particulate MMO (pMMO) [51]; the second one, a soluble iron-containing MMO (sMMO) has been characterized more thoroughly [52].

The pMMO structure reveals an unexpected arrangement of three subunits named A, B, C. Two of the three metal cites, present as mononuclear and dinuclear copper units, are located within the soluble regions of the B subunit [53] (Scheme 8). The third metal-containing center, occupied by zinc, lies within the membrane with ligands derived from both C and A subunits. Direct electron transfer between metal centers may be possible. Neither the site of methane oxidation nor the pathway(s) of substrate entry and product release have been identified so far.

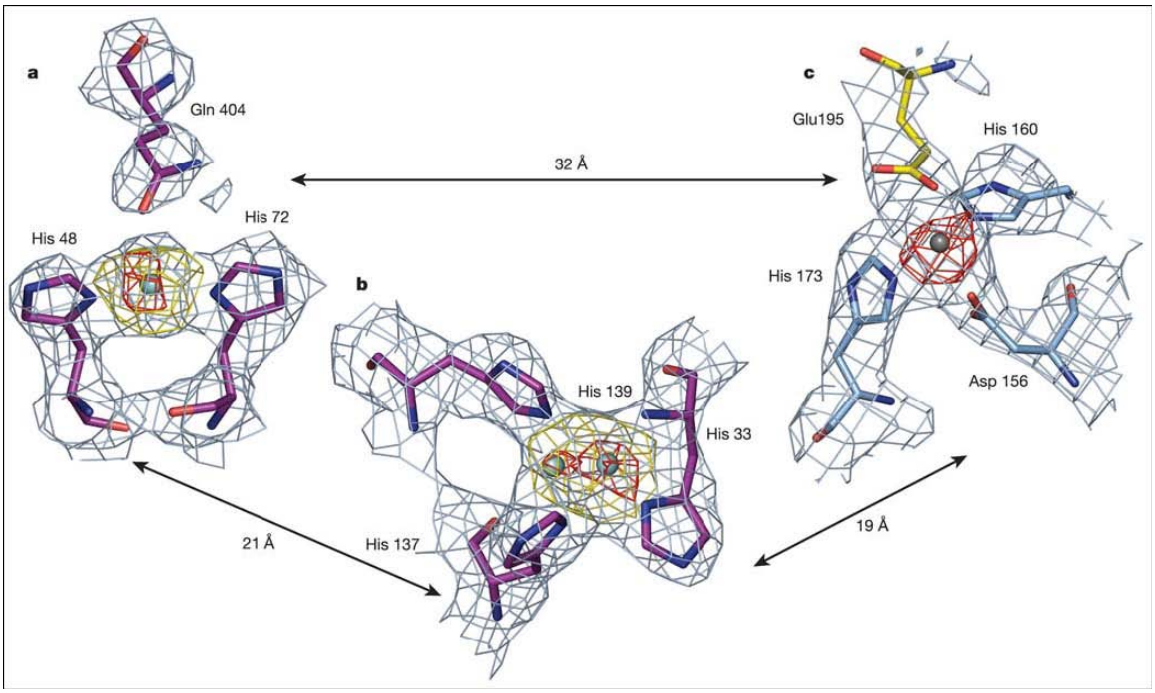

Scheme 8. The pMMO metal centers: (**a**) the mononuclear copper site, (**b**) the dinuclear copper site, (**c**) the zinc site. The distances are measured between metal ions.

By contrast, sMMO contains a dinuclear iron unit in the active site [54], Scheme 9. Its ability to hydroxylate unactivated hydrocarbon substrates is ascribed to a high-valent Fe(IV)-O intermediate [55]. Theoretical (DFT) studies on methane-to-methanol oxidation by sMMO [56, 57] and P450 [47] confirm the consensus oxygen-rebound mechanism for both systems, supported by the high measured and calculated kinetic isotope effects [58]. The rate-limiting step is the methane H-abstraction, via a linear Fe−O--H--C complex, forming a $\cdot CH_3$ radical, which can rearrange to form the alcohol in the rebound step [59].

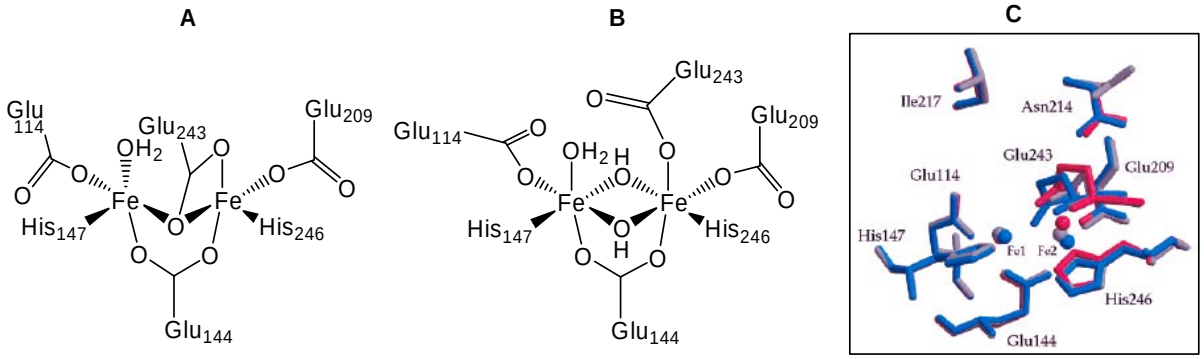

Scheme 9. Dinuclear iron active sites in *M. capsulatus* (Bath) sMMO, (A) – reduced form, (B) – oxidized form, (C) - superposition of the oxidized (gray), mixed-valent (red), and reduced (blue) diiron sites demonstrating the range of observed motions. Fe1 maintains the same position in all structures, while Fe2 moves significantly.

Nature's catalysts can oxygenate methane in aqueous solution at moderate temperatures and pressures, but require the use of sacrificial reducing agents for oxygen activation and are non-suitable for bulk production. Therefore, there is significant interest in non-biological systems for selective activation of saturated C−H bonds. In this context, controlled aerobic oxidation of methane in water is a key research objective [60]. Nowadays methanol is commercially produced in a two-step process via synthesis gas, which is thermodynamically less efficient. To improve industrially applied catalysts, study of these enzymes can be very helpful.

1.4 Methane Functionalization in Water: Dream or Reality?

The conversion of methane to methanol appears to be a straightforward exothermic reaction [61, 62]. Nevertheless, in practice it is very difficult to prevent the reaction from proceeding even explosively to afford carbon dioxide and water.

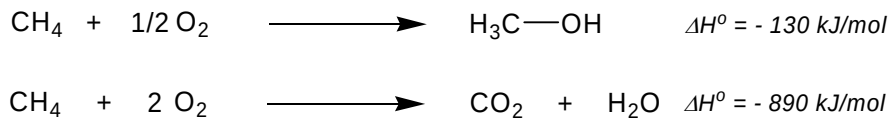

The value of the C−H dissociation energy for methane (104 kcal mol^{-1}) is comparable to the one in the dihydrogen molecule. In contrast to ethylene, acetylene and benzene, compounds with stronger C−H bonds (106, 120 and 109 kcal mol^{-1}), methane contains neither π- nor n-electrons. Both the abundance of methane and its extremely low reactivity have attracted chemists active in fundamental as well as in applied research.

Of particular interest in this context is the electrophilic methane activation and oxidation in aqueous solution by Pt(II)/Pt(IV) complexes, originally reported by Shilov [6]. A key feature of the "Shilov system" is that the first step involves electrophilic attack by Pt(II) at the methane C−H bond, generating a methyl-platinum(II) species with a polarized $Pt^{\delta+}-C^{\delta-}$ bond, followed by the oxidation by $[PtCl_6]^{2-}$ to give a platinum (IV) species with the bond polarity being reversed to $Pt^{\delta-}-C^{\delta+}$, which allows a nucleophilic attack at the carbon atom in the third step. A complication with the original "Shilov chemistry" involving only water and chloride ligands for platinum arises from the fact that the Pt(IV)/Pt(II) couple and the Pt(II)/Pt(0) couple have virtually the same redox potentials. Hence, Pt(II) may compete with Pt(IV) in the oxidation step and Pt(0) deposits from solution.

In 1998, it was found that a combination of sodium vanadate with pyrazine-2-carboxylic acid can be effectively used for methane oxidation in water, employing hydrogen peroxide as a promoter [63]. At low temperatures (20−70 °C) methyl hydroperoxide was identified as a main oxidation product, whereas at high temperatures (90−120 °C) the reaction yields predominantly formic acid.

Recently, a new system for selective oxidation of methane in water with hydrogen peroxide has been reported by G. B. Shul'pin *et al*., using the dinuclear manganese(IV) tri-μ-oxo complex containing 1,4,7-trimethyl-1,4,7-triazacyclononane ligands with oxalic acid as a co-catalyst [64].

Another recent discovery in this field, reported in 2004 by R. Neumann *et al*., can be considered as a breakthrough: The authors succeeded in oxidising methane to give methanol by air in aqueous solution under mild conditions, using a bipyrimidinylplatinum–polyoxometalate hybrid complex supported on silica as the catalyst [65].

Although a series of reagents have been identified and developed for selective oxidation of methane to methanol, most catalysts that activate methane still suffer from low yields (10−33 TONs[*]) and are not stable under reaction conditions. Low molecular weight alkanes, particularly methane, however, are readily available and are less expensive than olefins and aromatics. As a consequence, one can envision the replacement of highly endothermic processes needed to generate unsaturated precursors with exothermic, single-step alkane-oxidation processes that, if properly operated, would generate energy as well as chemical products. If catalysts could be developed that can do this selectively, a green chemical process technology with enormous economic benefits would result.

1.5 Project of this Work

The general goal of this work is to develop new oxidation catalysts that are selective (chemo-, regio- and stereoselective) for many substrates, with high conversion, stable, inexpensive and environmentally friendly. In the best cases, these catalysts should also work for oxidative functionalization of methane, if possible, in aqueous solution.

[*] Catalyst turnover number, mol products per mol of catalyst

In particular, it was the aim of the present work: (1) to get new mechanistic insights into the oxidation of alkanes and alcohols with the known vanadium(V)-based catalytic system; (2) to synthesize new transition metal complexes mimicking monooxygenase enzymes, and (3) to use redox-active molecular sieves as oxidation catalysts. Without any doubt the catalytic methane conversion is one of the most challenging topics of the present research project, methane being one of the most inert chemicals.

2 Vanadium-Based Systems

Vanadium is an important element in biology, inorganic chemistry and organic syntheses [66], vanadium compounds can heterogeneously or homogenously catalyze selective oxidation reactions of alkanes, alkenes, aromatics, alcohols, halides [1, 67, 68]. The development of new oxidation catalysts based on vanadium(V) is one of the most important fields in modern chemical research [69].

2.1 The Binary System Vanadate and Pyrazine-2-Carboxylic Acid: State of the Art

In 1983 H. Mimoun and co-workers demonstrated that vanadate peroxo complexes containing picolinic (Scheme 10, **A**) or pyrazine-2-carboxylic acid (pcaH, **B**) are versatile reagents for the stoichiometric oxygenation of hydrocarbons, including alkanes [70]. Ever since 1993, a binary catalytic system based on vanadate and pyrazine-2-carboxylic acid has found much interest for the efficient oxidation of organic compounds [71, 72], based on the pioneering work of G. Shul'pin *et al*. [73]. In our group it has been demonstrated that even the most inert substrates – ethane and methane – can be oxygenized by this system using hydrogen peroxide as a promoter and atmospheric oxygen as oxidant in acetonitrile [74, 75] as well as in aqueous solution [63, 76]. The anionic complexes *cis*-$[V(O)(OO)(pca)_2]^-$ (Scheme 15, page 27, **V1**) and *trans*-$[V(O)(OO)(pca)_2]^-$ (**V2**) have been isolated from the catalytic mixture and structurally characterized in our group [77].

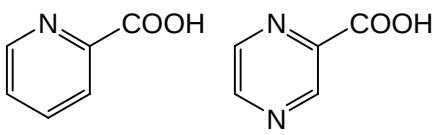

(**A**) (**B**)

Scheme 10. Picolinic (**A**) and pyrazine-2-carboxylic (**B**) acids

Alkanes are oxidized under mild conditions (20−70°C) to give predominantly the corresponding alkyl hydroperoxides, which are partially decomposed in the course of the reaction into more stable ketones and alcohols (Scheme 11).

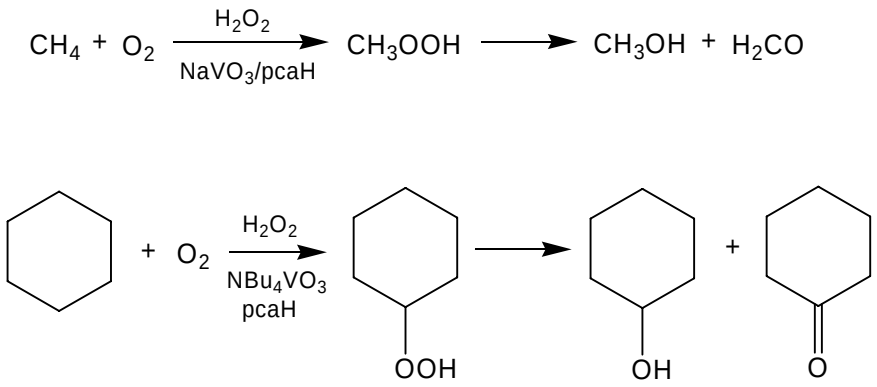

Scheme 11. Oxygenation of methane and cyclohexane catalyzed by the binary system vanadate/pcaH under mild conditions (20−70 °C)

The mechanistic aspects of the oxidation catalyzed by the system "vanadate – pcaH - H_2O_2" system in acetonitrile have been thoroughly investigated [78]. The rate-limiting step of the catalytic reaction is ascribed to the monomolecular decomposition of the complex containing one coordinated pca ligand (Scheme 12):

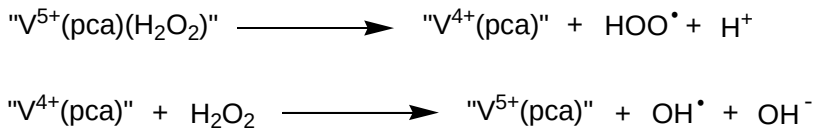

Scheme 12. Formation of hydroperoxyl and hydroxyl radicals from H_2O_2 induced by the vanadate−pcaH system

The vanadium(IV) species thus formed react further with the second H_2O_2 molecule to generate the hydroxyl radical, which is capable to abstract a hydrogen atom from the alkane molecule. Alkyl radicals, R· then rapidly combine with molecular oxygen to give alkylperoxyl radicals, ROO·, resulting finally in the formation of alkyl hydroperoxides. Thus, it can be concluded that the oxidative potential of this system is due to the hydroxyl radical formation in the hydrogen peroxide decomposition.

The co-catalyst pcaH is assumed to accelerate the proton transfer from a hydrogen peroxide molecule to oxo or hydroxy ligands in the coordination sphere of vanadium complex ("robot's arm mechanism", Scheme 13) [78].

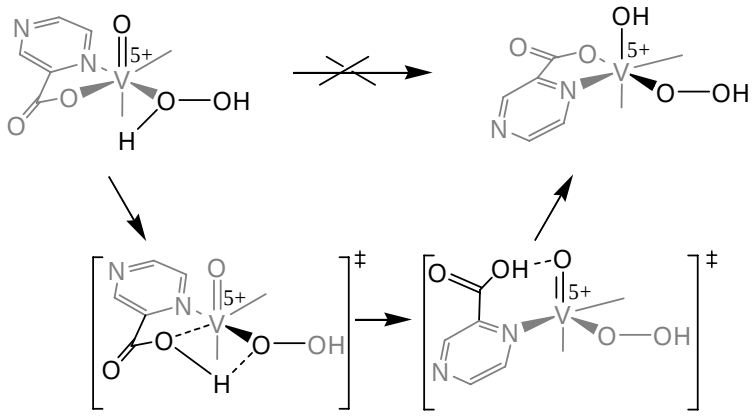

Scheme 13. The «robot's arm mechanism« for the proton transfer in the vanadate/pcaH system

Recently A. Bell and co-workers published the density functional theory (DFT) calculation results concerning the hydroxylation mechanism of the vanadate/pcaH system [79]. Indeed, the pca-ligand-assisted transfer of hydrogen atom was found to be more thermodynamically favoured than the direct proton transfer to the vanadium-oxo group (steps I, III in Scheme 14) and occurs via migration of hydrogen atom from coordinated H_2O_2 molecule to the oxygen of a pca ligand connected to the vanadium center (Scheme 13).

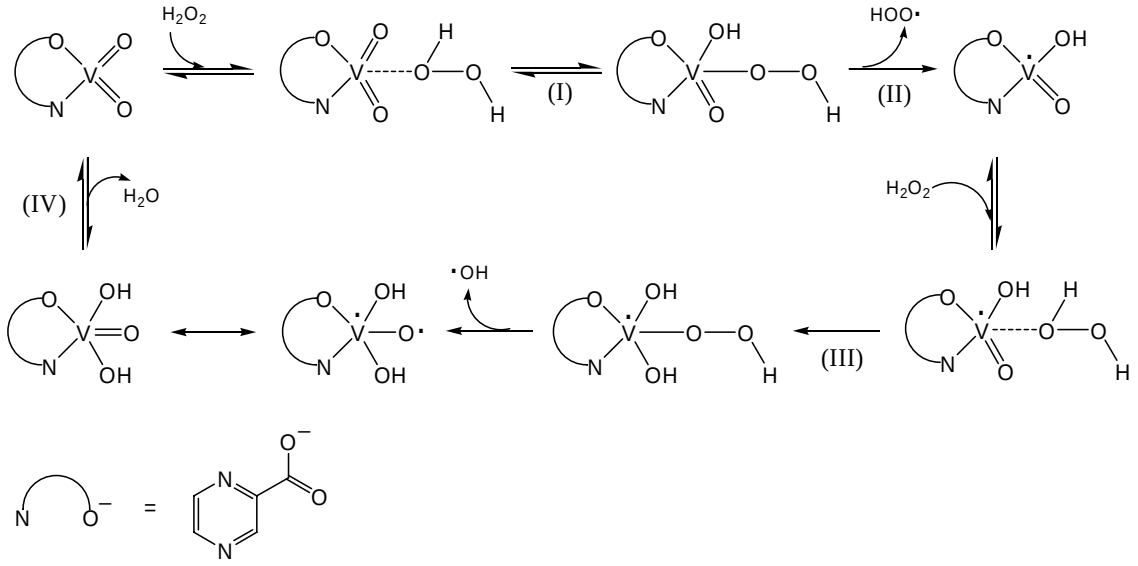

Scheme 14. Proposed catalytic cycle for hydroperoxyl and hydroxyl radicals generation [79] catalyzed by the vanadate/pcaH system

Furthermore, the activation energy of HOO· radical generation (rate-determining step II, Scheme 14) is substantially decreased, if a sequence of additional steps *via* diperoxo complexes is involved. Otherwise, the activation barrier for the V−OOH bond cleavage would be too high. Finally, it was demonstrated, that the solvent coordination to vanadium complexes can play a significant role in this system.

In the present chapter we report new results concerning the crucial role of vanadium diperoxo complexes as well as the solvent effect in alkane and alcohol oxidation catalyzed by the binary vanadate/pcaH system in acetonitrile, 2-propanol and aqueous solution.

2.2 New Insights into the Vanadium-Catalyzed C−H Oxidation

The oxidation of alkanes and alcohols catalyzed by the vanadate/pcaH system has been well studied in acetonitrile solution [73−75, 80], which is not the case as far as the oxidation in aqueous solution is concerned. On the other hand, water would be an ideal solvent for methane oxidation, since it cannot be oxidized and it is cheap and environmentally friendly.

2.2.1 Oxidation of Methane in Water

Although the oxidation of methane with air and hydrogen peroxide using the KVO_3/pcaH system (1:4) in water has been reported [63, 76], it was not possible to reproduce these results under the conditions reported. We therefore decided to study this reaction again, in order to find out the reason for reproducibility problems.

$$CH_4 + O_2 \xrightarrow[KVO_3/pcaH]{H_2O_2} CH_3OOH + CH_3OH + H_2CO + HCOOH$$

All reactions were carried out in a stainless-steel autoclave. After a subsequent cooling two aliquots of the reaction mixture were analyzed by UV-Vis spectroscopy to determine the H_2O_2 consumption (at 230 nm, $\varepsilon = 81\ M^{-1}\ cm^{-1}$) as well as by NMR spectroscopy to detect the oxygenation products formation (using CD_3CN or D_2O as solvents and CH_3NO_2 or CH_3CN as internal standards). In all cases the GC analysis of the liquid phase as well as the gaseous phase were performed. No CO or CO_2 formation was observed under these conditions.

Table 1. Methane oxygenation in acetonitrile and water using the vanadate/pcaH catalytic system; conditions: 10 bars of air, 75 bars of methane; TON* − catalyst turnover number, mol of products per mol catalyst

Solvent	$[NBu_4VO_3]$ (mM)	[pcaH] (mM)	Temp. (°C)	Time (h)	$[H_2O_2]_o$ (mM)	$[H_2O_2]_{final}$ (mM)	TON* (analysis)
CH_3CN (0.7M H_2O)	0.1	0.4	23	16	200	150	180 (GC)
CH_3CN (1.6M H_2O)	0.1	0.4	23	24	200	200	< 1 (NMR/GC)

Solvent	$[KVO_3]$ (mM)	[pcaH] (mM)	Temp. (°C)	Time (h)	$[H_2O_2]_o$ (mM)	$[H_2O_2]_{final}$ (mM)	TON* (analysis)
D_2O/H_2O	0.1	0.1−0.4	50	4−24	200	190−200	< 1 (NMR/GC)
D_2O/H_2O (pH 2.0−9.0)	0.1-1.0	0.4−4.0	50	4−24	200	50−200	< 1 (NMR)
D_2O	1.0	4.0	80	4	200	170	4 (NMR)
D_2O	0.1	10	80	4	200	170	45 (NMR)

The data of Table 1 show that, in acetonitrile solution, the increase of the water content from 0.7 M (1.3 vol%) to 1.6 M (2.8 vol%) dramatically suppresses the oxidation reaction at 23 °C. In D_2O solution, methane oxygenation products are not observed even at 50 °C and at different pH values (at pH 8.0−9.0 a significant non-productive decomposition of H_2O_2 is observed). Only at 80 °C the oxidation of methane takes place producing mainly formic acid, it increases substantially, if the KVO_3/pcaH ratio is increased to 1:100 (last line of Table 1).

In addition to the analysis of the product distribution, NMR spectroscopy also allows to see the characteristic signals of the co-catalyst pcaH after the catalytic reaction. It turned out that, unlike in acetonitrile, where it is stable, in aqueous solution pcaH decomposes under the catalytic conditions with H_2O_2, evidenced by the disappearance of the ^1H NMR signals of pcaH. This can explain why the oxidation of methane with H_2O_2/O_2 catalyzed by the vanadate/pcaH system in water [63] is not reproducible, if a KVO_3/pcaH of 1:4 is used. However, with a KVO_3/pcaH ratio of 1:100, the reported catalytic activity [63] for methane oxidation in water can be reproduced.

Table 2. Temperature effect on the product accumulation and the co-catalyst (pcaH) degradation in the methane oxidation in water catalyzed by the vanadate/pcaH system; conditions: 10^{-4} M KVO_3, 10^{-2} M pcaH (100 eqv. to vanadate), 0.20 M H_2O_2, 10 bars of air, 75 bars of methane, (*) − no H_2O_2 added

Temp.	Time	TON
50	4	< 1
60	4	< 1
70	4	10
80	4	45
90	4	69
90	8	79
90*	4	0

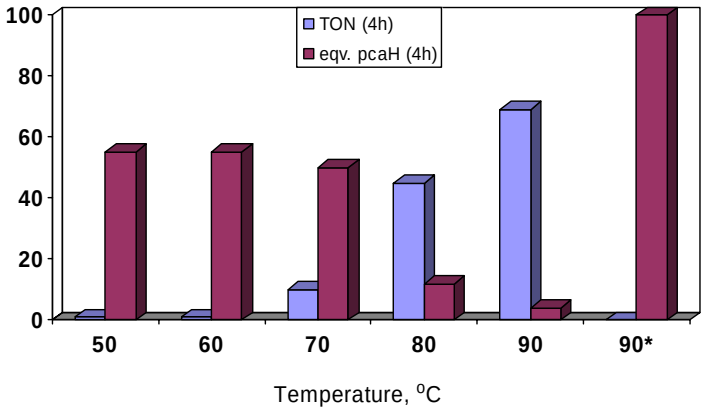

In the absence of hydrogen peroxide (Table 2), pcaH is stable under reaction conditions even at 90 °C, whereas upon addition of H_2O_2 the pcaH concentration is diminished to half (after 4 hours, 50−70 °C); while at 80–90 °C less then 12% of the initial quantity of pcaH can be detected after 4 hours of the reaction.

It is noteworthy to mention the effect of strong inorganic acids, added to the reaction mixture in a 0.10 M concentration (Table 3). Despite of the increased conversion (formic acid being the major product), this effect can be attributed to the instability of H_2O_2 itself under such drastic conditions (90 °C, pH = 1), especially in the case of perchloric acid (blank tests).

Although we found the working conditions for the methane oxygenation in water, it is evident, that in aqueous solution the oxidation mechanism is different from those in acetonitrile.

Table 3. Product distribution upon addition of 0.10 M strong acid in the methane oxidation in water catalyzed by the vanadate/pcaH system; conditions: 90 °C, 4 hours of the reaction, 10^{-4} M KVO_3, 10^{-2} M pcaH, 0.20 M H_2O_2, 10 bars of air, 75 bars of methane

Acid	TON
---	69
H_2SO_4	88
CF_3COOH	102
$HClO_4$	182

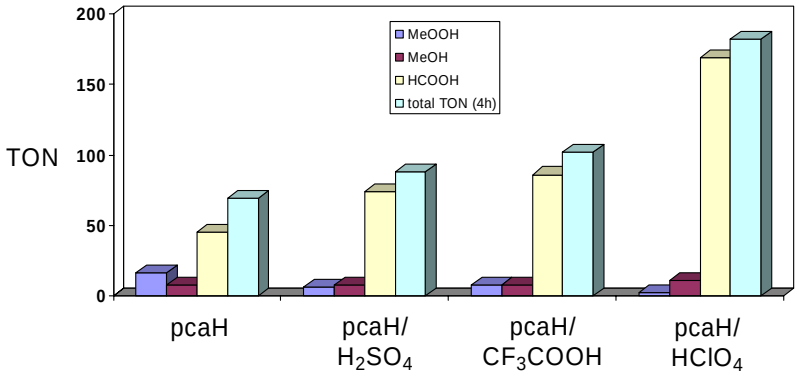

In order to get further insights in the oxidation mechanism of the vanadate/pcaH system, we performed a detailed spectroscopic and kinetic study of oxygenation of 2-propanol as a model substrate in aqueous solution.

2.2.2 Main Features of the Oxidation of 2-Propanol in Water

Isopropanol is easily oxidized to give acetone by hydrogen peroxide in air using vanadate/pcaH catalytic system in water (Figure 1, 2). In these water/2-propanol mixtures, tetrabutylammonium vanadate was used for solubility reasons.

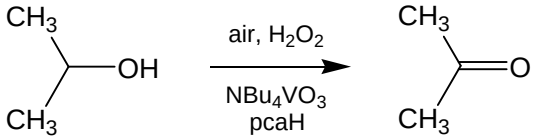

However, the dependence of the initial reaction rate of acetone accumulation W_0 at various concentrations of water shows that water added to the reaction solution at high concentration (> 10 M) sufficiently retards the oxidation of isopropanol (Figure 1).

The yield of acetone is significantly lower, if the reaction is carried out in an argon atmosphere (Figure 3). This testifies that atmospheric oxygen takes part in the oxidation.

However, the initial rates of the reaction in argon and in air are the same. Thus, in all further kinetic experiments only initial rates of the oxidation can be used.

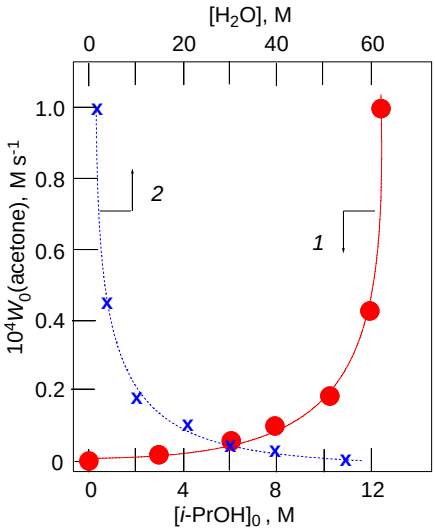

Figure 1. Isopropanol oxidation in water, catalyzed by the vanadate/pcaH system: dependences of the initial rate of acetone accumulation (*Wo*) on initial isopropanol concentration (curve *1*) and water concentration (curve *2*). Conditions: [*n*-Bu_4NVO_3] = 1 mM, [pcaH] = 4 mM, $[H_2O_2]_0$ = 0.50 M, 50 °C

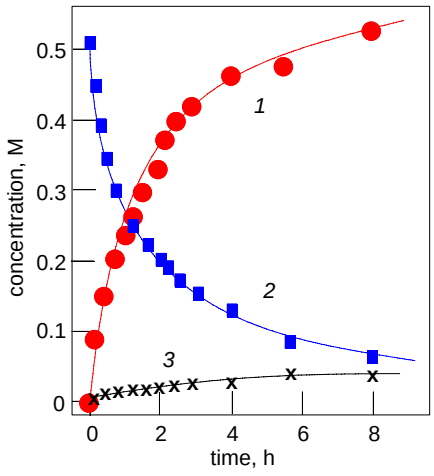

Figure 2. Oxidation of isopropanol (12.4 M) with H_2O_2 ($[H_2O_2]_0$ = 0.51 M) in the presence of water (2.2 M) catalyzed by *n*-Bu_4NVO_3 (1 mM) and pcaH (4 mM) at 50 °C in air. Accumulation of acetone (curve *1*), consumption of hydrogen peroxide (curve *2*) and consumption of O_2 from air (curve *3*) with time are shown

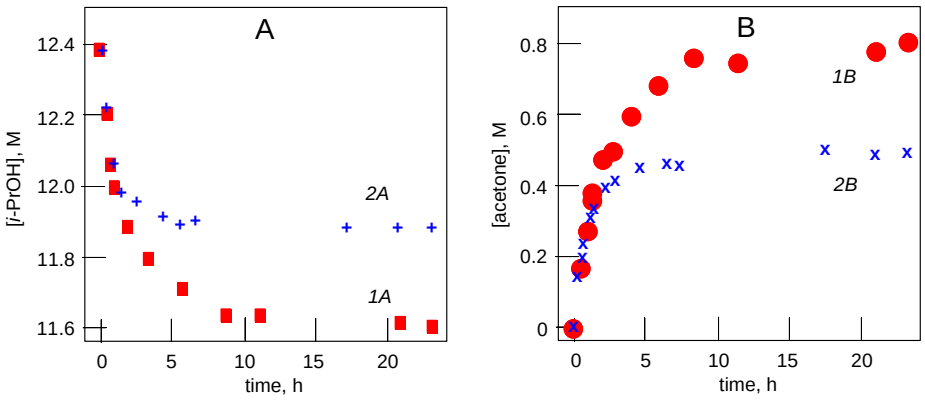

Figure 3. Consumption of isopropanol (***A***) and accumulation of acetone (***B***) in the oxidation of isopropanol (12.4 M) with H_2O_2 (0.5 M) in the presence of water (2.2 M) catalyzed by *n*-Bu_4NVO_3 (1 mM) and pcaH (4 mM) at 50 °C in air (points *1A*, *1B*) and in an argon atmosphere (points *2A*, *2B*)

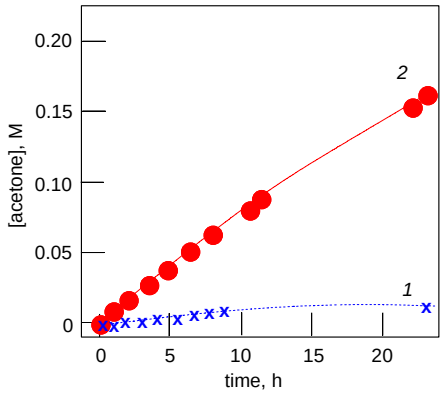

Figure 4. Accumulation of acetone in oxidation of isopropanol (12.4 M) with air in the presence of low concentration of H_2O_2 (0.01 M) and water (2.2 M) catalyzed by *n*-Bu_4NVO_3 (1 mM) in the absence (curve *1*) and in the presence of pcaH (4 mM; curve *2*) at 50 °C

Using vanadate as a catalyst, isopropanol can be slowly oxidized with atmospheric oxygen, if only a small quantity of hydrogen peroxide is added to the solution [81]. In the presence of pcaH a significant acceleration of the reaction is observed (Figure 4).

2.2.3 Distribution of Species in the Vanadate/Pyrazine-2-Carboxylic Acid System in Water

The pH-potentiometric titration combined with spectroscopic techniques is a useful tool for vanadium distribution studies [82]. The analogous method is applied for the vanadate/pcaH system speciation in aqueous solution, the pH-range 2−8 being monitored at the fixed ionic strength at 25.0 °C (Figure 5).

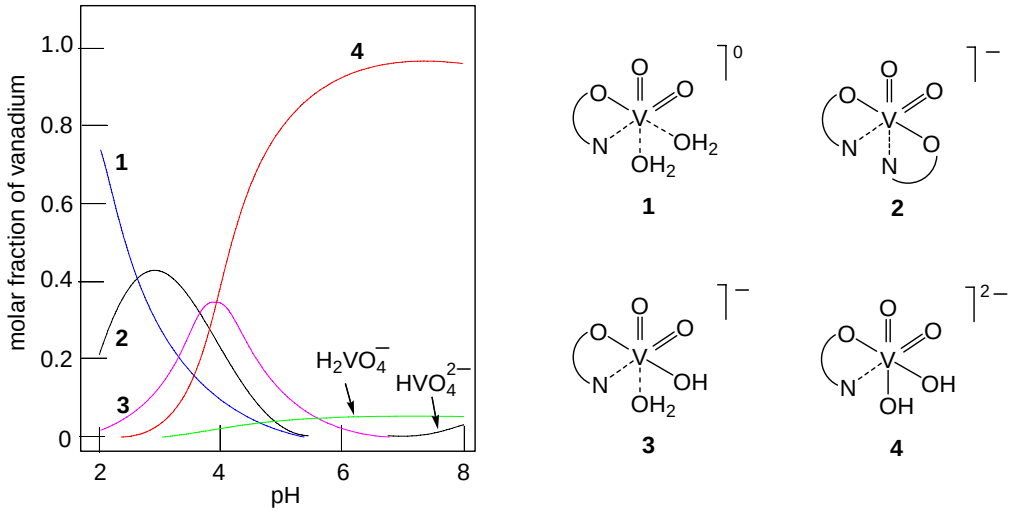

Figure 5. Distribution curves for the vanadate/pcaH system in water; conditions: $[KVO_3]_o$ = 1.0 mM, $[pcaH]_o$ = 4 mM, ionic strength (KCl) 0.200 M, 25 °C

Under catalytic conditions (pH 2.0−4.0) in aqueous solution at least 60% of vanadium(V) species contain only one pca ligand in the coordination sphere (Figure 5, complexes **1**, **3**, **4**), providing the possibility to form peroxo- and diperoxo complexes upon addition of an excess of H_2O_2. The diperoxo vanadium complexes formation is facilitated at low pH values (pH < 2), where two neutral solvent molecules should be displaced, especially at low water concentration. Thus, the improved catalytic results upon addition of a strong acid or/and decreasing a water content can be rationalized in terms of a predominant formation of diperoxo vanadium complexes containing one pca ligand, but additional spectroscopic (NMR, UV-vis) evidences should be provided.

2.2.4 NMR Spectra

For the starting point of the NMR study an isopropanol solution with the fixed water concentration (2.2 M) is chosen, where the vanadate/pcaH catalytic system exhibits a high

oxidation activity (see Figure 2). The ^{51}V NMR spectrum of a 1 mM Bu_4NVO_3 solution in this isopropanol/water mixture is shown in Figure 6a. The spectrum consists of a major peak at −570 ppm (with the line width $W_{1/2}$ 80 Hz) (A) and two minor peaks at −563 ppm ($W_{1/2}$ 80 Hz) (B) and −631 ppm ($W_{1/2}$ 26 Hz) (C). Two signals in the low field are located in a region typical for vanadate alkyl esters in isopropanol, while peak C is considerably shifted upfield from that region. Analysis of the literature data shows that the compound $VO(O-i\text{-}Pr)_3$ give rise to a very sharp vanadium signal around −630 ppm [83, 84]. Therefore, on the basis of the chemical shift and the linewidth, resonance C can be ascribed to $VO(O-i\text{-}Pr)_3$, which is formed from Bu_4NVO_3 in *i*-PrOH at minor quantities (3% of overall vanadium concentration). Addition of excess of strong trifluoroacetic acid to this solution leads to complete conversion of all other species into $VO(O-i\text{-}Pr)_3$ and the ^{51}V NMR spectrum consists of a single signal at −631 ppm.

In the presence of 4-fold excess of pcaH, the spectrum of Bu_4NVO_3 in isopropanol/water consists of two signals (Figure 6b). The high field signal is the same as resonance C in the first spectrum and belongs to $VO(O-i\text{-}Pr)_3$. The relative intensity of this signal significantly increases in the presence of pcaH (from 3% to 28% of overall vanadium concentration). Clearly, pcaH also facilitates the formation of $VO(O-i\text{-}Pr)_3$ from Bu_4NVO_3 in *i*-PrOH (while treating the spectra 6a and 6b with the same line broadening, the linewidths of signal C in these spectra become identical). The second signal observed at −546 ppm (D) is very broad ($W_{1/2}$ 2500 Hz), and it originates from a vanadium complex with pcaH. In acetonitrile-d_3, the analogous vanadium chemical shift −532 ppm (−538 ppm in the presence of 2.2 M H_2O) was observed for the $[VO_2(pca)_2]^-$ complex [78]. Thus, the chemical shift of D is reasonably attributed to $[VO_2(pca)_2]^-$ (in aqueous solution the concentration of D can be estimated from Figure 5).

The proton NMR spectrum of 1 mM *n*-Bu_4NVO_3 + 4 mM pcaH in isopropanol/water shows three signals from free pcaH (9.25, 8.81 and 8.77 ppm) in the aromatic region as well as three signals of equal intensity from vanadium-pcaH complex (9.30, 8.96 and 8.65 ppm) with chemical shifts relatively close to those observed in CD_3CN (9.22, 8.77, and 8.45 ppm) (Figure 7a). On the basis of close NMR chemical shifts, we assume that the structure of this species is similar in both solvents. Slightly different chemical shifts of the pca signal may be due to different composition of the solvation shell in these two solvents. In mixed acetonitrile-

isopropanol solvents of different composition the vanadium spectra contain no new, previously undetected resonances.

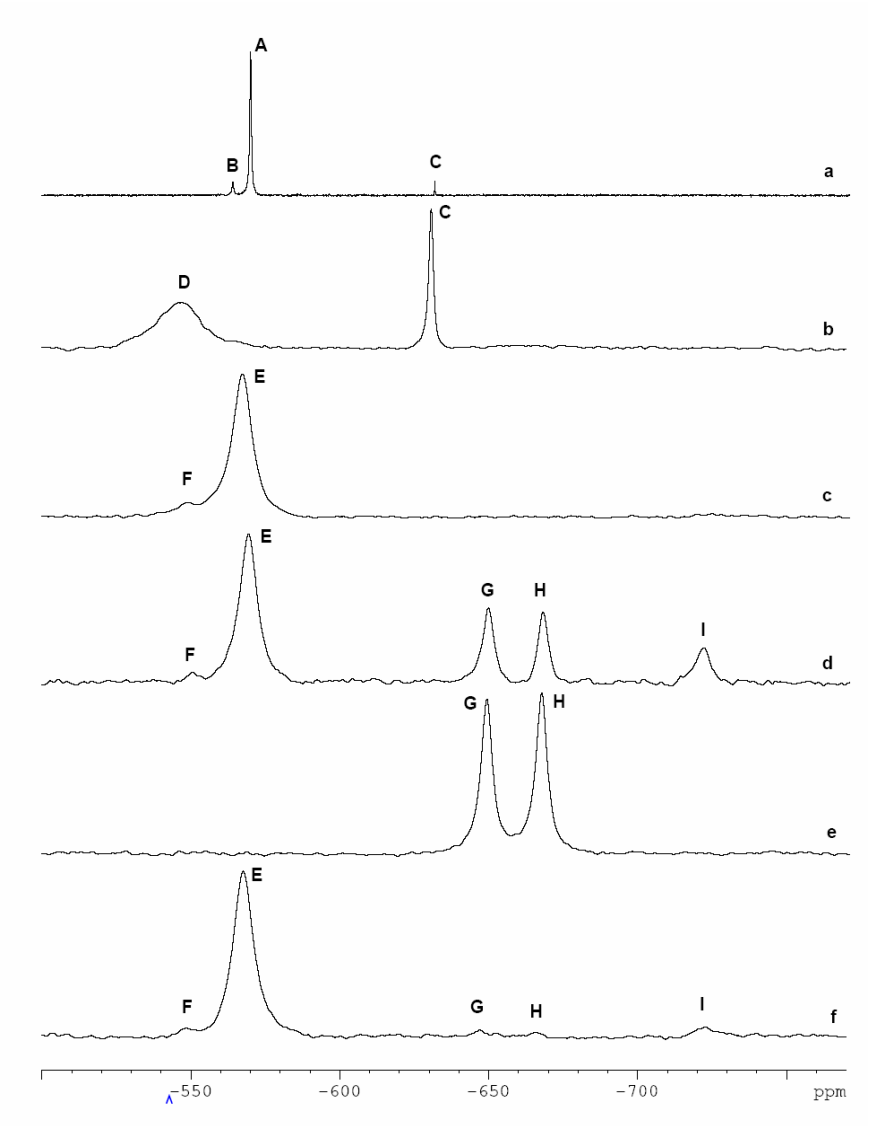

Figure 6. ^{51}V NMR spectra of (a) *n*-Bu_4NVO_3 (1 mM); (b) *n*-Bu_4NVO_3 (1 mM) + pcaH (4 mM); (c) *n*-Bu_4NVO_3 (1 mM) + pcaH (4 mM) + H_2O_2 (1 mM); (d) *n*-Bu_4NVO_3 (1 mM) + pcaH (4 mM) + H_2O_2 (0.5 M); (e) *n*-Bu_4NVO_3 (1 mM) + H_2O_2 (0.5 M); (f) *n*-Bu_4NVO_3 (1 mM) + pcaH (12 mM) + H_2O_2 (0.5 M). All spectra were recorded in isopropanol containing 2.2 M H_2O.

Addition of one equivalent of H_2O_2 (with respect to vanadium, 1 mM) to the isopropanol/water solution results in dramatic transformations experienced by the vanadate species. Both signals C and D vanish, while a new major resonance E appears (δ −568 ppm, $W_{1/2}$ 760 Hz) (Figure 6c). While peak E is considerably sharper than signal D, it is still much broader that the major resonance in similar mixtures in acetonitrile (760 *vs*. 135 Hz). Once

again, the chemical shifts are rather close, which is suggestive of similar structures for the peroxo species formed in these two solvents.

Even stronger evidence for the structural similarity of the species in both solvents comes from the ^{1}H NMR data. The proton spectrum of the vanadate/pcaH/H_2O_2 mixture in the aromatic region shows six resonances in addition to the three signals of free pcaH. Two of these resonances overlap giving a signal of double intensity [δ 9.92 (1 H), 9.46 (1 H), 9.40 (2 H), 9.38 (1 H) and 9.21 (1 H)] (Figure 7b). A similar pattern was observed in acetonitrile-d_3, and it was explained by the formation of the oxo-peroxo complex $[VO(OO)(pca)_2]^-$ [78]. This species has a pentagonal bipyramidal structure with two nonequivalent pca ligands (see Scheme 15) [77]. All six aromatic protons in this complex are non-equivalent, which should result in six different proton signals in the aromatic region. Thus, it is reasonable to assume an oxo- peroxo-vanadate complex to be responsible for resonance E.

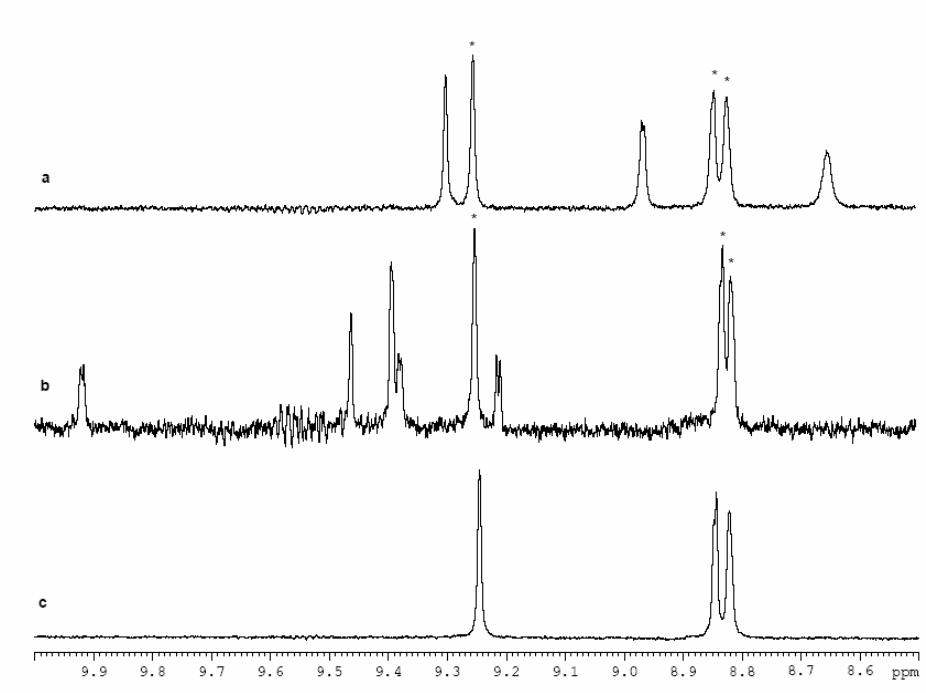

Figure 7. ^{1}H NMR spectra of (a) *n*-Bu_4NVO_3 (4 mM) + pcaH (16 mM); (b) *n*-Bu_4NVO_3 (1 mM) + pcaH (4 mM) + H_2O_2 (1 mM); (c) pcaH (16 mM). Peaks indicated by asterisks are due to free pcaH. All spectra were recorded in isopropanol containing 2.2 M H_2O.

The NMR data show that the oxo-peroxo complex $[VO(OO)(pca)_2]^-$ **(V1)** is not the active catalytic species: it is stable and can even be isolated and characterized [77]. The difference in chemical shifts of the pca ligands of this complex in acetonitrile and in isopropanol suggests solvent molecules to be involved in the outer sphere of the vanadium

complex. However, these changes are too subtle to consider them as strong evidence for isopropanol entering the first coordination sphere of vanadium for these oxo-peroxo complexes.

The spectrum in Figure 6c contains also a minor component F at −547 ppm, which is at about the same position as resonance D (in spectrum Figure 6b). However, these resonances belong to different species: the resonance D is considerably broader than F and the resonance F appears with approximately the same intensity even at higher peroxide concentrations (Figure 6d). In acetonitrile two vanadium signals observed in the presence of peroxide were tentatively assigned to different isomers of monoperoxo anions *trans*-$[V(O)(OO)(pca)_2]^-$ (**V1**) and *cis*-$[V(O)(OO)(pca)_2]^-$ (**V2**) (Scheme 15) [78]. Possibly, the peak F also belongs to a minor isomer of this complex.

Further addition of H_2O_2 produces three new vanadium resonances of comparable intensities in the high field region: δ −649 ($W_{1/2}$ 400 Hz) (G), −667 ($W_{1/2}$ 390 Hz) (H), and −721 ($W_{1/2}$ 700 Hz) (I) (Figure 6d). At 0.5 M H_2O_2, about 40−45% of all vanadium have been transformed into these new species. Interestingly, increasing peroxide concentration in acetonitrile-d_3 does not generate any new species [78] and this fact may explain the very different properties of these two solvents, when we deal with the reactivity of the vanadate/pcaH system.

To identify these new complexes, we recorded the spectrum obtained under the same conditions as in Figure 6d but with one exception – no pcaH was added. It turned out that the two low field signals (G and H) are formed also in the absence of pcaH, they are the only signals observed in such mixtures (Figure 6e). Conte and co-workers [85, 86] attributed the upfield component to an aqua-diperoxovanadium species, while the downfield resonance – to diperoxo species containing isopropanol molecule under comparable conditions. Thus, the same complexes can be responsible for signals H **(**$[VO(OO)_2(H_2O)]^-$) and G ($[VO(OO)_2(i\text{-}PrOH)]^-$) in the ^{51}V NMR spectra. At the water concentration we used (2.2 M), the intensities of signals G and H are similar, whereas at higher water concentrations the relative intensity H (corresponding to the aqua-diperoxo species) grows and exceeds the intensity of G.

The ^{51}V NMR signal I is located in the range typical for diperoxo vanadate complexes [87], therefore it can be assumed that the corresponding vanadium complex also contains two peroxo ligands. The exact composition of other ligands present in the vanadium coordination

sphere of this complex is still unknown. Whereas no diperoxo species were observed in acetonitrile under similar conditions [78], and species corresponding to I is not formed in the absence of pcaH, we assume that the coordination sphere of this complex can include both pcaH and *i*-PrOH ligands.

Thus, under the catalytic conditions, five vanadium-containing species are detectable (Figure 6c, d, f): two isomers of the monoperoxo vanadium complex $[VO(OO)(pca)_2]^-$ (**V1**, **V2**) [77], as well as diperoxo species with a tentative description $[VO(OO)(OOH)(pca)]^-$ (**V3**, this work) $[VO(OO)_2(i\text{-PrOH})]^-$ (**V4**) and $[VO(OO)_2(H_2O)]^-$ (**V5**) [85, 86].

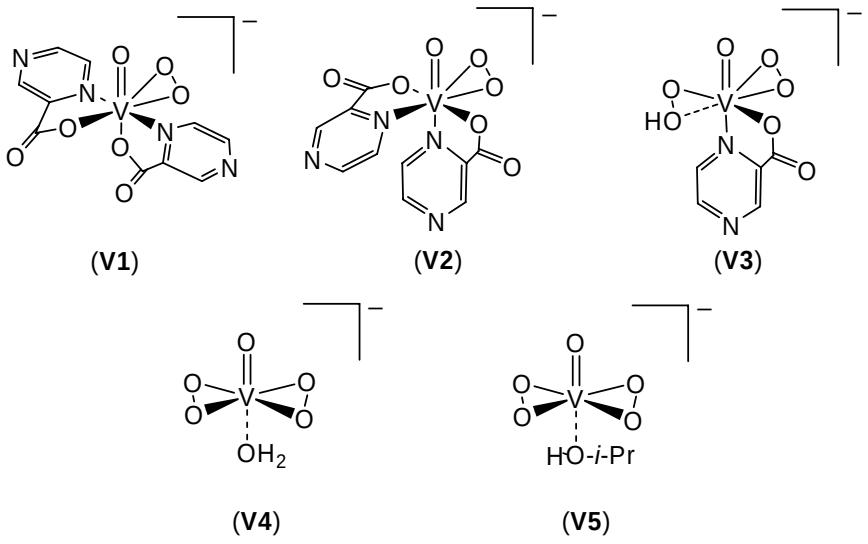

Scheme 15. Vanadium containing species detected by ^{51}V NMR in the oxidation of isopropanol with H_2O_2, catalyzed by the vanadate/pcaH system

The monoperoxo-diperoxo conversion is less efficient at higher pcaH concentrations (Figure 6f). It is reasonable to assume that pcaH competes with H_2O_2 for coordination sites and, at high concentrations, stabilizes monoperoxo complexes $[VO(OO)(pca)_2]^-$, whereas the formation of the diperoxo species, being the plausible catalytically active form according to DFT calculations [79], is suppressed. Obviously, there should be an "optimal" pcaH concentration, at which the degree of such monoperoxo–diperoxo conversion reaches the maximum.

2.2.5 Electronic Spectra

The data obtained by the NMR-spectroscopy indicate the formation of catalytically active peroxovanadium complexes containing pca ligands. The UV-Vis investigations provide additional evidences for this hypothesis.

Thus, the addition of pcaH to the vanadate (10^{-3} M) and H_2O_2 (0.5 M) solution in isopropanol containing water (2.2 M) leads to the appearance of a new absorption band in the visible region with maximum at 457 nm (Figure 8A). As this absorption does not exist in the absence of either H_2O_2 or pcaH, it can be attributed to the formation of the peroxovanadium complexes containing pcaH molecule in the coordination sphere (**V1, V2 or V3**). The intensity of absorption at 457 nm increases with subsequent addition of pcaH and attains maximum value at [pcaH] > 6 mM, depending upon the initial H_2O_2 concentration (Figure 8B). The maximal value D_{457} is not dependent on H_2O_2 concentration (in the range 0.004−0.5 M) as well as on pcaH concentration (in the range 0.01−0.024 M), but is directly proportional to the concentration of vanadate at constant concentrations of all other components (Figure 9).

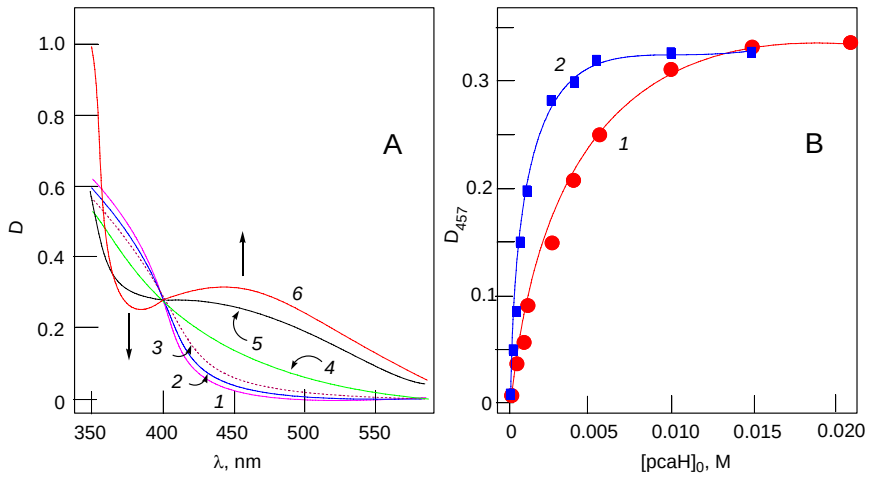

Figure 8. (**A**) - electronic spectra of the solution of *n*-Bu_4NVO_3 (1 mM) and H_2O_2 (0.5 M) in isopropanol/ water (2.2 M) at various concentrations of added pcaH: 0.0 (**1**), 0.001 (**2**), 0.0015 (**3**), 0.003 (**4**), 0.006 (**5**), 0.015 M (**6**); the components were mixed at 50 °C 2 min before the spectra were recorded; (**B**) - dependence of the D_{457} value on concentration of pcaH added to the solution of *n*-Bu_4NVO_3 (1 mM) at two different concentrations H_2O_2 (0.5 M: curve *1* and 0.004 M: curve *2*) in 2-propanol/ water (2.2 M) at 50 °C

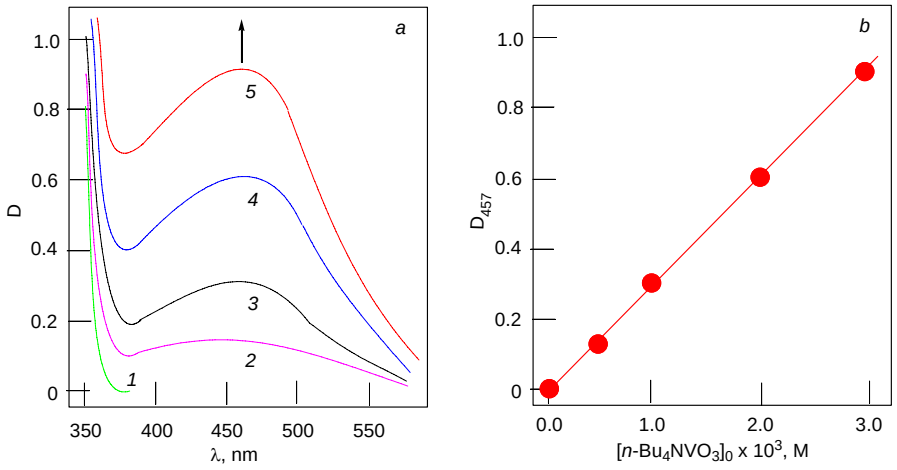

Figure 9. (**a**) - electronic spectra of the pcaH (0.015 M) and H_2O_2 (0.50 M) in isopropanol/ water (2.2 M) solution at various concentrations of *n*-Bu_4NVO_3: 0.0 (*1*), 0.0005 (*2*), 0.0010 (*3*), 0.0020 (*4*), 0.0030 (*5*) M; the components were mixed at 50 °C 2 min before the spectra were recorded; (*b*) - dependence of D_{457} on concentration of *n*-Bu_4NVO_3 derived form graph *a*

Figure 10 demonstrates changes in absorption spectra of the vanadate/pcaH (1:10 ratio) solution upon addition of various amounts of hydrogen peroxide, the water concentration being constant (2.2 M). At low H_2O_2 concentrations (≤ 0.004 M) the optical density at 457 nm increases, corresponding to the growth of a peroxovanadium complexes concentration containing pcaH in the coordination sphere (Figure 10a).

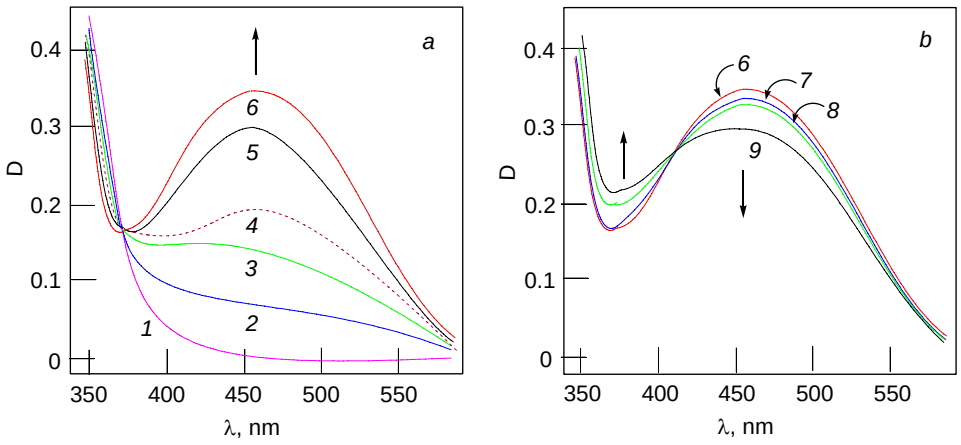

Figure 10. Electronic spectra of *n*-Bu_4NVO_3 (1 mM) and pcaH (10 mM) in isopropanol/ water (2.2 M) solution at various concentrations of H_2O_2: 0.0 (1), 0.0002 (2), 0.0004 (3), 0.0006 (4), 0.001 (5), 0.004 (6), 0.024 (7), 0.025 (8), 0.50 M (9); the components were mixed at 50 °C 2 min before the spectra were recorded

With a 4-fold excess of H_2O_2 over the vanadate concentration, almost complete transformation of a vanadate-pca complex into its peroxo derivative is observed (Figure 10a). The linear dependence of D_{457} absorption on concentration of hydrogen peroxide ($[H_2O_2]_0$ =

0−0.001 M) as well as NMR spectroscopy data (Figure 6f) show that absorption at D_{457} is predominantly due to the $[VO(OO)(pca)_2]^-$ complex formation and its molar extinction coefficient equals to ε_{457} = 350±10 M^{-1} cm^{-1} (it is almost the only vanadium species in solution, Figure 8A curve *6*, Figure 6f). Clearly, pcaH, H_2O_2 as well as the complexes **4** and **5** have no absorption in this region (Figure 8A curve *1*, Figure 6e).

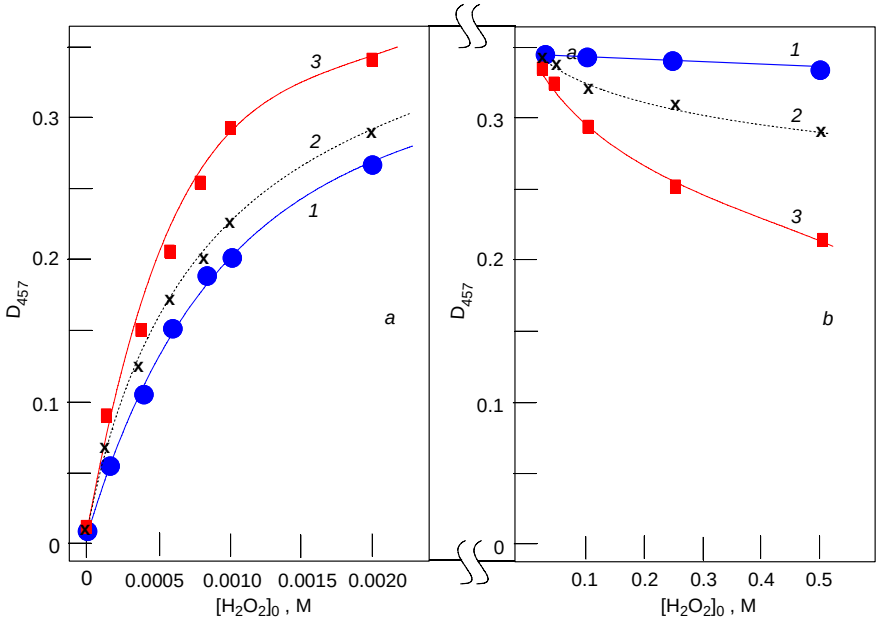

Figure 11. Dependence of D_{457} on concentration of hydrogen peroxide in electronic spectra of the *n*-Bu_4NVO_3 (1 mM) solution in isopropanol/water (2.2 M) at three different concentrations of pcaH: 0.024 (curves *1*), 0.010 (*2*), 0.004 M (*3*); the components were mixed at 50 °C 2 min before the spectra were recorded

At high concentrations of hydrogen peroxide (0.02−0.5 M, Figure 11b, curve *3*) the concentration of **V2** decreases, giving rise to **V3**, **V4** and **V5** complexes formation. At 0.5 M H_2O_2 the equilibrium distribution of these complexes can be calculated from ^{51}V NMR spectrum in Figure 6d. Thus, $[\mathbf{V1} + \mathbf{V2}]_{6d}$ = 0.58 mM and the corresponding D_{457} gives a value 0.203±0.006. The experimental value D_{457} is 0.211 and corresponds to $[\mathbf{V3}]_{6d}$ = 0.118 mM. Apparently, $\varepsilon_{457}(\mathbf{V1} + \mathbf{V2})$ is substantially bigger than those of the complex **V3** which have an absorption maximum in a short-wave region of the spectrum (see Figure 12).

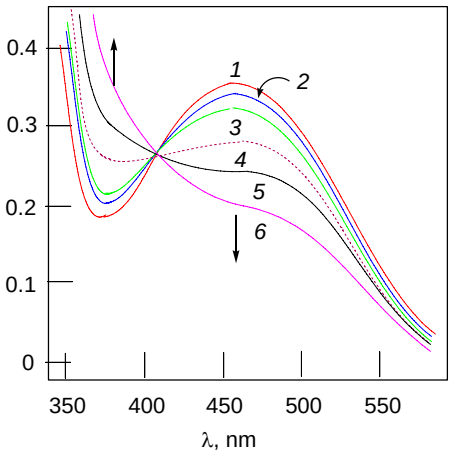

Figure 12. Electronic spectra of the *n*-Bu_4NVO_3 (1 mM) and pcaH (0.004 M) solution in isopropanol/ water (2.2 M) at various concentrations of added H_2O_2: 0.002 (*1*), 0.004 (*2*), 0.024 (*3*), 0.10 (*4*), 0.25 (*5*), 0.50 (*6*) M; the components were mixed at 50 °C 2 min before the spectra were recorded

The transformation of monoperoxo to diperoxo derivatives (Figure 11b) occurs to high extent, if the concentration of pcaH is low, and even if hydrogen peroxide is added. These results testify that pcaH and H_2O_2 compete for a site in the coordination sphere of vanadium.

2.2.6 Kinetics of the Oxidation of 2-Propanol to Acetone

A kinetic study was performed in aqueous as well as in moist 2-propanol solutions, using hydrogen peroxide as a promoter. The oxidation products were analyzed by GC using acetonitrile as internal standard. The dependences of initial rate W_0 of acetone accumulation on initial concentration of vanadate, pcaH and hydrogen peroxide are given in Figure 13 and Figure 14.

The kinetic data (Figure 13) demonstrate that the rate of 2-propanol oxidation is directly proportional to the vanadate concentration, which is in line with the monovanadate species being involved in the oxidation reaction. In the absence of pcaH the initial rate *Wo* is low, therefore, the catalytic activity of the vanadium complexes **V4** and **V5**, which do not contain a pca ligand in the coordination sphere, is low.

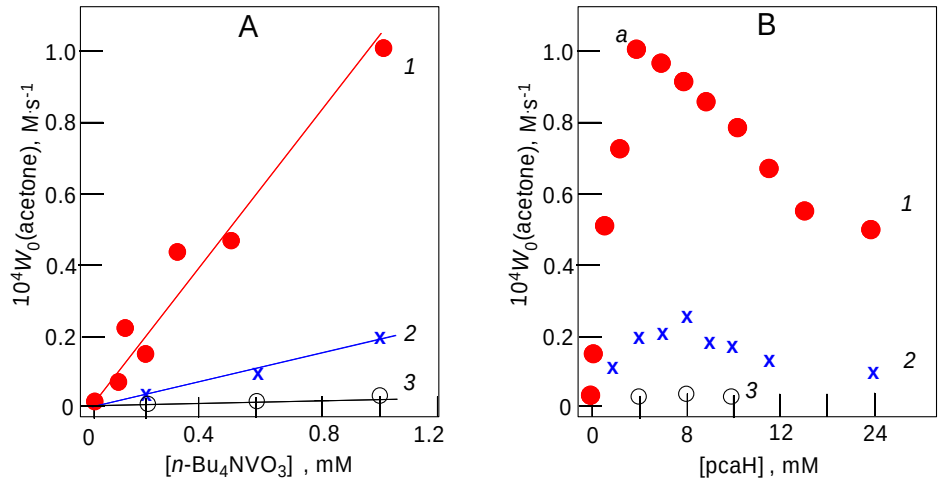

Figure 13. Dependences of the initial rate of acetone accumulation on initial concentration of *n*-Bu_4NVO_3 (**A**, $[pcaH]_0$ = 4 mM) and pcaH (**B**, $[n\text{-}Bu_4NVO_3]_0$ = 1 mM) in isopropanol oxidation at various isopropanol/water ratios; (**1**): [*i*-PrOH]/[H_2O] = 12.4 M / 2.2 M; (**2**): 10.4 M / 10.5 M; (**3**): 3.0 M / 42.1 M. Conditions: $[H_2O_2]_0$ = 0.50 M, 50 °C.

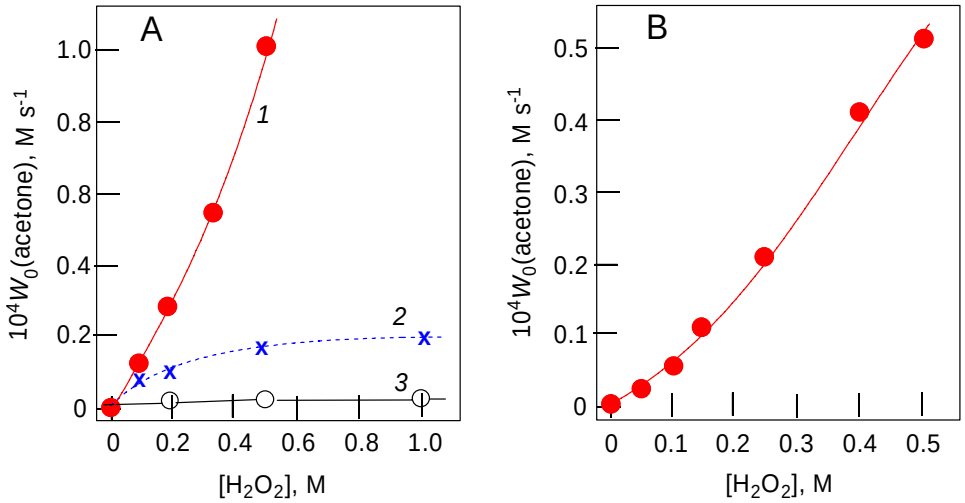

Figure 14. Dependences of the initial rate of acetone accumulation on initial concentration of H_2O_2 in isopropanol oxidation (**A**): $[n\text{-}Bu_4NVO_3]_0$ = 1 mM, $[pcaH]_0$ = 4 mM, (**1**): [*i*-PrOH]/[H_2O] = 12.4 M / 2.2 M; (**2**): 10.4 M / 10.5 M; (**3**): 3.0 M / 42.1 M; (**B**), $[n\text{-}Bu_4NVO_3]_0$ = 1 mM, $[pcaH]_0$ = 24 mM, [*i*-PrOH]/[H_2O] = 12.4 M / 2.2 M; 50 °C.

In the presence of pcaH the concentrations of the monoperoxo vanadium species and the corresponding absorption at 457 nm attain maximum values (Figure 10a, 11a) at low H_2O_2 concentrations (0–0.01 M), but the reaction rate is still low (Figure 14). An increase in the reaction rate upon further addition of H_2O_2 is accompanied by the transformation of the monoperoxo vanadium complex $[VO(OO)(pca)_2]^-$ (**V1**, **V2**), being the predominant vanadium species under the catalytic conditions, into the diperoxo vanadium complexes (Figure 10b, 12). However, ^{51}V NMR results testify that the major product of this transformation – the

diperoxo vanadium complex $[VO(OO)(OOH)(pcaH)]^-$ (**V3**) − does not participate in the rate-determining step of the oxidation reaction (Figure 6d, 6f and 13B): the corresponding resonance I has almost disappeared upon addition of a 10-fold excess of pcaH, whereas the oxidation rate is decreased only by 20%. Therefore, the rate-determining step can be ascribed to a monomolecular transformation of another low-abundant diperoxo vanadium derivative (**X**) containing one pca ligand, which is formed from complex **V1** and/or **V2** upon addition of H_2O_2. Tentatively, we assume **X** to be a complex $[V(O)(OO)(H_2O_2)(pca)]$.

$$[V(O)(OO)(pca)_2]^- (\mathbf{V2}) + H^+ + H_2O_2 \rightleftharpoons [V(O)(OO)(H_2O_2)(pca)] (\mathbf{X}) + pcaH \qquad K_X \qquad (2.3)$$

Thus, an increase of the isopropanol oxidation rate at $[pcaH]_0$ = 0–0.004 M (see Figure 13B) is in line with the increase of the **V2** concentration, whereas at high initial pcaH concentrations (0.006–0.024 M) the reaction rate is decreased due to the equilibrium 2.3, the concentration of **X** being diminished. This hypothesis is supported by DFT calculations [79], as well as by the fact that vanadium diperoxo complexes are usually more reactive in comparison with analogous monoperoxo derivatives [88, 89].

2.2.7 Mechanistic Description of the Vanadate/pcaH System Transformation

Taking into account the considerations mentioned above and using the experimental NMR and UV-Vis spectroscopic data, a kinetic scheme of the isopropanol oxidation can be proposed, based on the observed species. The description of equilibrium transformations in the vanadate–H_2O_2–pcaH system in moist 2-propanol when $[H_2O_2]_o >> [pcaH]_o > [VO_3^-]_o$ (the product formation is low) includes the following set of equations (2.3–2.9).

$$[V(O)(OO)_2(H_2O)]^- (\mathbf{V4}) + i\text{-PrOH} \rightleftharpoons [V(O)(OO)_2(i\text{-PrOH})]^- (\mathbf{V5}) + H_2O \qquad K_1 \qquad (2.4)$$

$$[V(O)(OO)_2(H_2O)]^- (\mathbf{V4}) + pcaH \rightleftharpoons [V(O)(OO)_2(pcaH)]^- (\mathbf{V3}) + H_2O \qquad K_2 \qquad (2.5)$$

$$[V(O)(OO)_2(i\text{-PrOH})]^- (\mathbf{V5}) + pcaH \rightleftharpoons [V(O)(OO)(OOH)(pca)]^- (\mathbf{V3}) + i\text{-PrOH} \qquad K_3 \qquad (2.6)$$

$$[V(O)(OO)(OOH)(pca)]^- (\mathbf{V3}) + pcaH \rightleftharpoons [V(O)(OO)(pca)_2]^- (\mathbf{V2}) + H_2O_2 \qquad K_4 \qquad (2.7)$$

$$[V(O)(OO)(pca)_2]^- (\mathbf{V2}) + H^+ + H_2O_2 \rightleftharpoons [V(O)(OO)(H_2O_2)(pca)] (\mathbf{X}) + pcaH \qquad K_X \qquad (2.3)$$

$$[V(O)(OO)(H_2O_2)(pca)] (\mathbf{X}) + H_2O \rightleftharpoons [V(O)(OO)(H_2O)(pca)] (\mathbf{Y}) + H_2O_2 \qquad K_Y \qquad (2.8)$$

$$pcaH \rightleftharpoons pca^- + H^+ \qquad K_a \quad (2.9)$$

$$[V(O)(OO)(H_2O_2)(pca)]\ (\mathbf{X}) \longrightarrow (\mathbf{X'}) \longrightarrow \cdot OOH \qquad k_{obs}$$

The equation 2.4 was described earlier [85, 86] and represents a solvent molecule exchange between two corresponding vanadium diperoxocomplexes **V4** and **V5**. The K_1 value can be estimated from Figure 6e and equals to 0.16. The next two equations (2.5 and 2.6) reflect the affinity of added pcaH to the vanadium diperoxocomplexes with the subsequent formation of $[V(O)(OO)_2(pcaH)]^-$ (**V3**). K_2 and K_3 values can be calculated using the integration of the NMR signals from Figure 6d and give 700 and 3130, respectively. Thus, the isopropanol ligand is 4.5 times more easely replaced by pcaH from the vanadium coordination sphere than the aqua ligand. Alternatively, K_2 can be determined by using the assosiation constant of **V4** and pcaH in water [86], considering the experimentally determined pH of the solution (4.68), in this case K_2 is found to be 810.

Equations 2.7 and 2.3 describe a competitive process between pcaH and H_2O_2 in the vanadium coordination sphere. In **V2** the two pca ligands are not equivalent, which results in the formation of two different substitution products upon addition of hydrogen peroxide. The equilibrium constant K_4 associated with the major substitution product (**V3**) can be estimated from Figure 6d using equation 2.10 as being equal to 883, the concentrations of catalytically active complexes containing one pca ligand being negligeble.

$$[pcaH] = [pcaH]o - 2\,[\mathbf{V1}] - 2\,[\mathbf{V2}] - [\mathbf{V3}] \qquad (2.10)$$

The active vanadium diperoxo species **X** is the minor substitution product. Its formation requires one of the two pca ligands in **V2** to be protonated prior to substitution by a H_2O_2 molecule. In **X**, the oxo and hydrogen peroxide ligands should be in trans configuration with respect to each other (Scheme 16, step I). In this configuration the pca ligand can transfer a proton from the H_2O_2 ligand to the vanadium oxo/hydroxo moiety with the lower activation barrier ("robot's arm mechanism"), according to the DFT calculations [79] (Scheme 16, steps II, IV).

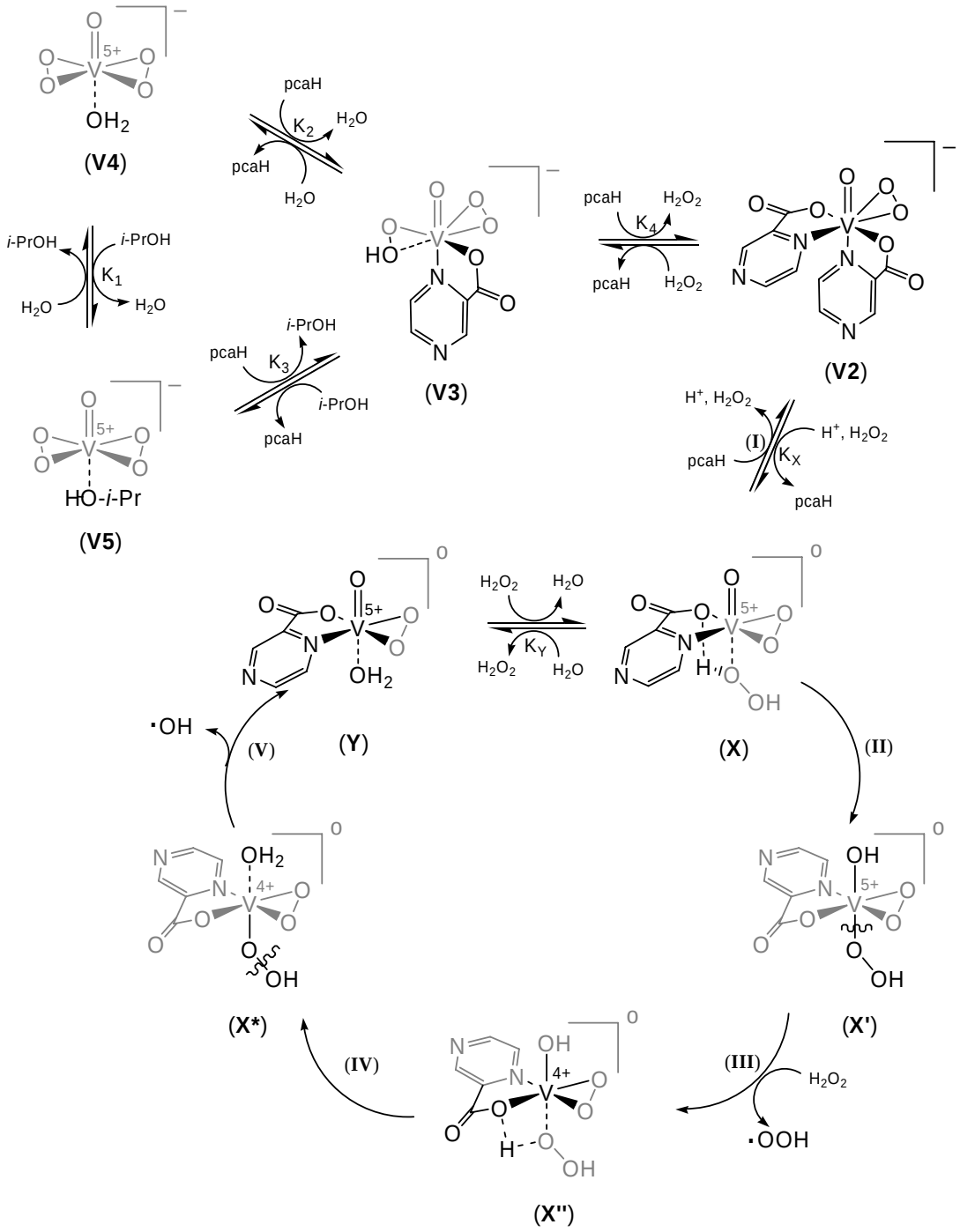

Scheme 16. Proposed mechanistic scheme for the vanadium/pcaH catalytic system in moist 2-propanol

However, the activation energy of the pca-assisted proton transfer (Scheme 16, step II) in the complex **X** is comparable to those of step III (the hydroperoxo radical release from **X'**). Therefore, both steps could determine the overall oxidation rate and we can assume:

$[V(O)(OO)(H_2O_2)(pca)]$ (**X**) ⟶ ·OOH $\qquad Wo = k_{obs}$ [**X**]

In addition, water can compete with H_2O_2 for the place in the vanadium coordination sphere of the complex **X** (eq. 2.8). The aqua-complex **Y** has been characterized [90] and terminates the proposed catalytic cycle (Scheme 16).

Given that for the initial reaction rates, we can assume $[H_2O_2] \approx [H_2O_2]_o >> [pcaH]_o$ and $[VO_3^-]_o$, only two mass balance equations on pcaH (eq. 2.10) and vanadate (eq. 2.11) can be used, which is reorganized into equations 2.12 and 2.13.

$$[VO_3^-]_o = [\mathbf{V1}] + [\mathbf{V2}] + [\mathbf{V3}] + [\mathbf{V4}] + [\mathbf{V5}] + [\mathbf{X}] + [\mathbf{X'}] + [\mathbf{X^*}] + [\mathbf{Y}] \approx [\mathbf{V1} + \mathbf{V2}] + [\mathbf{V3}] + [\mathbf{V4}] + [\mathbf{V5}] \quad (2.11)$$

$$[\mathbf{V1} + \mathbf{V2}] = \frac{[VO_3^-]_o}{(1 + [H_2O_2]_o/(K_4[pcaH]) + [H_2O_2]_o([H_2O]_o/K_2 + [i\text{-}PrOH]_o/K_3)/(K_4[pcaH]^2)} \quad (2.12)$$

$$[pcaH] = \frac{1}{2}([pcaH]_o - 2[\mathbf{V1} + \mathbf{V2}] + (4[\mathbf{V1} + \mathbf{V2}]^2 - 4[pcaH]_o[\mathbf{V1} + \mathbf{V2}] + [pcaH]_o^2 - 4[\mathbf{V1} + \mathbf{V2}][H_2O_2]_o/K_4)^{1/2}) \quad (2.13)$$

The initial oxidation rate is described by equation 2.14, where [**V1** + **V2**] can be calculated from the system of eq. 2.12–2.13 or determined from the corresponding UV-Vis spectra (Figure 8 and Figure 12, ε_{457}(**V1** + **V2**) = 350 M^{-1} cm^{-1}).

$$Wo = k_{obs}[\mathbf{X}] = k_{obs} \frac{K_x[\mathbf{V1} + \mathbf{V2}][H_2O_2]_o K_a^{1/2}}{[pcaH]^{1/2}(1 + K_Y[H_2O]/[H_2O_2]_o)} \quad (2.14)$$

The dissociation constant K_a was obtained using the experimentally determined pH values under reaction conditions and for isopropanol/water 12.4/2.2 M ratio gives 1.6×10^{-7} M. K_Y was estimated from Figure 1 fit as 0.4, and using the literature data [86] $K_Y K_X$ = 1/0.8 M = 1.25 M, K_X = 3.13 M^{-1}. The last parameter k_{obs} was determined from Figure 13 and Figure 14 fit and gives 40 ± 5 s^{-1}.

The proposed kinetic scheme of isopropanol oxidation satisfactorily describes the experimentally dependencies observed (Figure 15). The calculated vanadium complexes distribution in moist isopropanol shows that the total concentration of the catalytically active species does not exceed 0.3% of the total vanadium content (Figure 16). The equillibrium constant parameters are summarized in Table 4.

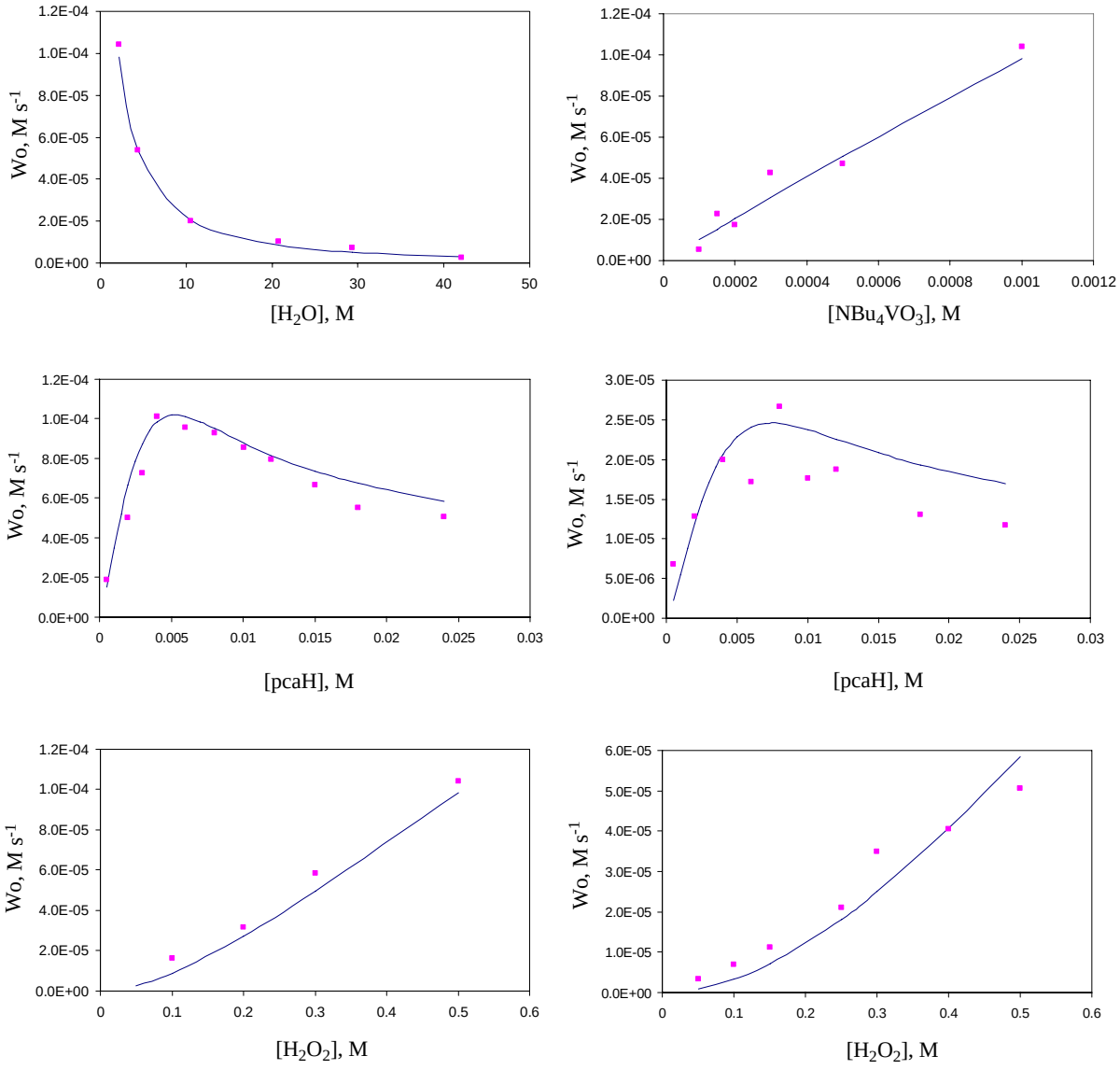

Figure 15. Experimental values (■) and predicted dependencies (–), calculated on the basis of the proposed mechanism of 2-propanol oxidation by the vanadate/pcaH catalytic system; for the reaction conditions see the corresponding figures

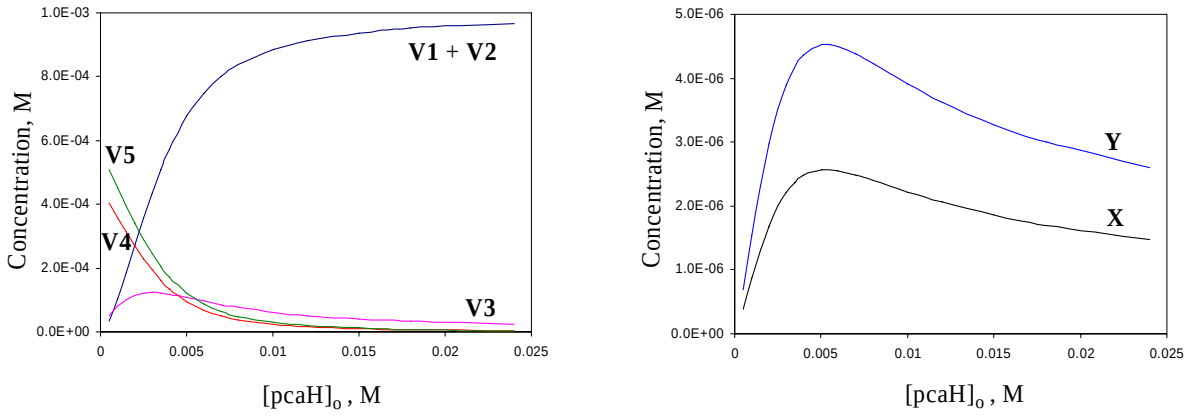

Figure 16. Distribution of the vanadium complexes according to the proposed oxidation mechanism by vanadate/pcaH catalytic system; conditions: $[n\text{-}Bu_4NVO_3]_0$ = 1 mM, $[H_2O_2]_0$ = 0.50 M, [*i*-PrOH] = 12.4 M, $[H_2O]$ = 2.2 M

Table 4. Parameters calculated from experimental data for the vanadium/pcaH catalytic system in isopropanol oxidation with H_2O_2

	Value
K_1	0.16
K_2	700
K_3	3130
K_4	883
K_X	3.13 M^{-1}
K_Y	0.4
k_{obs}	40 s^{-1}

It is interesting to compare the oxidation mechanisms of the binary vanadate/pcaH catalytic system in water, in isopropanol and in acetonitrile solution.

2.2.8 A Comparison of the Oxidation of Alkanes in Acetonitrile and 2-Propanol

A kinetic study was performed in moist 2-propanol and acetonitrile solutions using hydrogen peroxide as a promoter and 2-propanol and cyclohexane as substrates. The oxidation products were analyzed by GC using acetonitrile or nitromethane as internal standards (cyclohexylhydroperoxide is not stable under the analysis conditions and is reduced with triphenylphosphine, PPh_3, prior to injection).

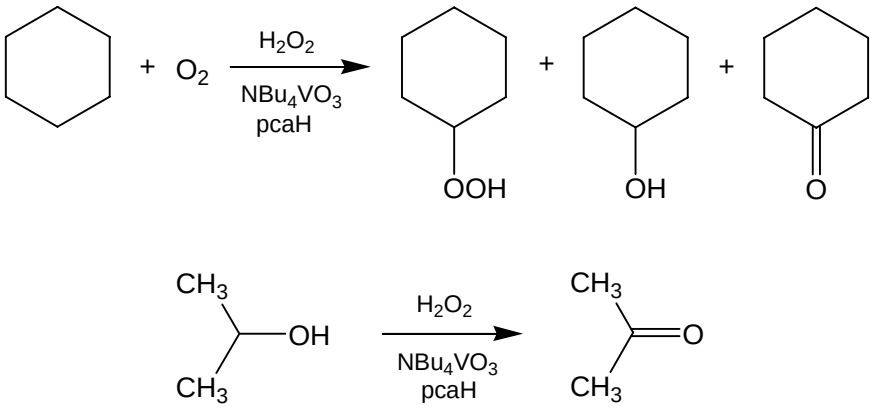

Scheme 17. Oxidation of cyclohexane and 2-propanol catalyzed by vanadate/pcaH system

The initial rate (W_o) dependences for the oxygenate formation in the simultaneous competitive oxidation of 2-propanol and cyclohexane in 2-propanol solution are shown in Figure 17. These results testify of a competitive behavior between 2-propanol and cyclohexane toward an active transient species (**X''**).

$$i\text{-PrOH} + \mathbf{X''} \longrightarrow (CH_3)_2CO \qquad k_1 \qquad (2.15)$$

$$C_6H_{12} + \mathbf{X''} \longrightarrow C_6H_{11}OOH \qquad k_2 \qquad (2.16)$$

The total oxidation rate W_i can be represented by eq. 2.17, and as follows from Figure 17, the sum of the rates of acetone and cyclohexyl hydroperoxide formation remains constant at various cyclohexane concentrations.

$$W_i = \{k_1[i\text{-PrOH}] + k_2[C_6H_{12}]\}[\mathbf{X''}] = 10^{-4}\ \mathrm{M\ s^{-1}} \qquad (2.17)$$

As the cyclohexane oxidation rate is much lower than the isopropanol oxidation rate under the conditions studied, therefore:

$$\frac{d[C_6H_{11}OOH]}{dt} = k_2[C_6H_{12}][\mathbf{X''}] = \frac{W_i}{1 + \dfrac{k_1[i\text{-PrOH}]}{k_2[C_6H_{12}]}} \simeq \frac{k_2[C_6H_{12}]\ W_i}{k_1[i\text{-PrOH}]} \qquad (2.18)$$

The tangent of the straight line slope in the dependence of $d[C_6H_{11}OOH]/dt$ on $[C_6H_{12}]_o$ (Figure 17) is equal to 5×10^{-6} s^{-1}. Thus, from eq. 2.18, $k_2/k_1 = 0.6$ ($[i\text{-PrOH}]_0 = 12$ M), so that the reactivities of cyclohexane and isopropanol toward species **X''** are close.

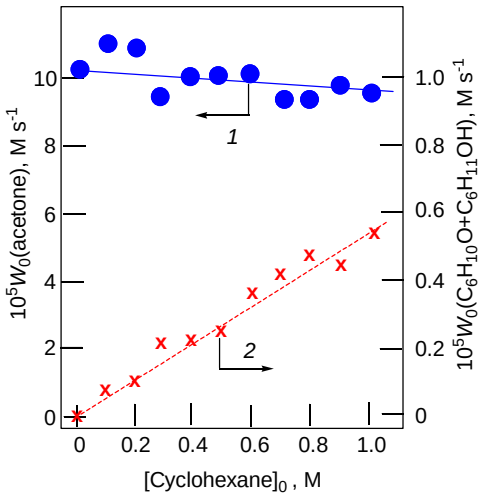

Figure 17. Dependence of the initial rate of oxygenates accumulation in the competitive 2-propanol/cyclohexane oxidation in moist 2-propanol. Conditions: $[n\text{-}Bu_4NVO_3]_0$ = 1 mM, $[pcaH]_0$ = 4 mM, $[H_2O_2]_0$ = 0.50 M, $[H_2O]$ = 2.2 M, $[i\text{-PrOH}]$ = 12 M, 50 °C

In acetonitrile solution, such a competition for a transient oxidizing species exists between cyclohexane and acetonitrile [78, 80] and is observed for 2-propanol and acetonitrile (Figure 18A). Low values of selectivity parameters in the alkane oxidation suggest that the hydroxyl radical is the oxidizing species, which operates in the vanadate/pcaH catalytic system in acetonitrile.

Analysis of the data presented in Figure 18A shows the ratio of the rate constants for the hydroxyl radical interactions with acetonitrile and isopropanol to be 0.012. The calculated dependence of the acetone accumulation rate on the initial concentration of isopropanol, using this constant ratio (Figure 18A, a dotted curve), gives a good agreement between experimental and calculated data.

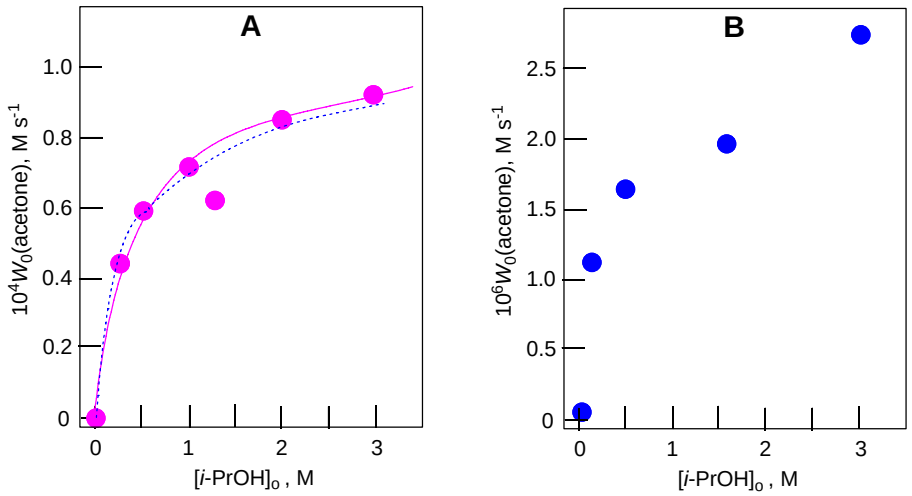

Figure 18. Dependence of the initial rate of acetone accumulation in isopropanol oxidation in acetonitrile solution (**A**) - catalyzed by the vanadate/pcaH system: [*n*-Bu_4NVO_3]$_0$ = 1 mM, [pcaH]$_0$ = 4 mM, 50 °C; (**B**) - under UV ($\lambda \geq 253$ nm) irradiation at 20 °C. Conditions: [H_2O_2]$_0$ = 0.50 M, [H_2O] = 2.2 M

Figure 18B presents the results of photochemical experiments, where the rate of acetone formation in acetonitrile has been measured at various concentrations of isopropanol. This dependence also corresponds to the competition between acetonitrile and isopropanol for hydroxyl radicals. The estimated ratio of the rate constants for these two substrates gives the following value: $k(HO^{\cdot} + CH_3CN)/k(HO^{\cdot} + i\text{-PrOH}) = 0.008$, which is comparable to those obtained for the vanadate/pcaH catalytic system. Given that the reactivities of cyclohexane and isopropanol toward the oxidizing species are close, we can assume that hydroxyl radicals are the oxidizing species both in acetonitrile and in isopropanol solution. Taking into account that $k(HO^{\cdot} + i\text{-PrOH}) = 1.9 \times 10^9$ $M^{-1}s^{-1}$ [91], we can calculate the following constants: $k(HO^{\cdot} + CH_3CN) = 1.5 \times 10^7$ $M^{-1}s^{-1}$ and $k(HO^{\cdot} + \text{cyclohexane}) = 1.1 \times 10^9$ $M^{-1}s^{-1}$.

In acetonitrile as well as in isopropanol solution, the absorption maximum at 457 nm can be observed due to the formation of the monoperoxo vanadium complexes containing two pca ligands (**V1** + **V2**). The modes of D_{457} value decrease upon further addition of H_2O_2 in these solutions are the same (Figure 19 and Figure 12), which is in line with the comparable acetone accumulation rates in both solvents (Figure 17, Figure 18A) and correlates with the similar modes of W_0 dependences on the initial H_2O_2 concentration (Figure 14 and Figure 20). Thus, the mechanisms of the generation of the oxidizing species in both solvents are similar and can include the monomolecular transformation of the vanadium diperoxo complex in the rate limiting step to produce hydroperoxyl and hydroxyl radicals.

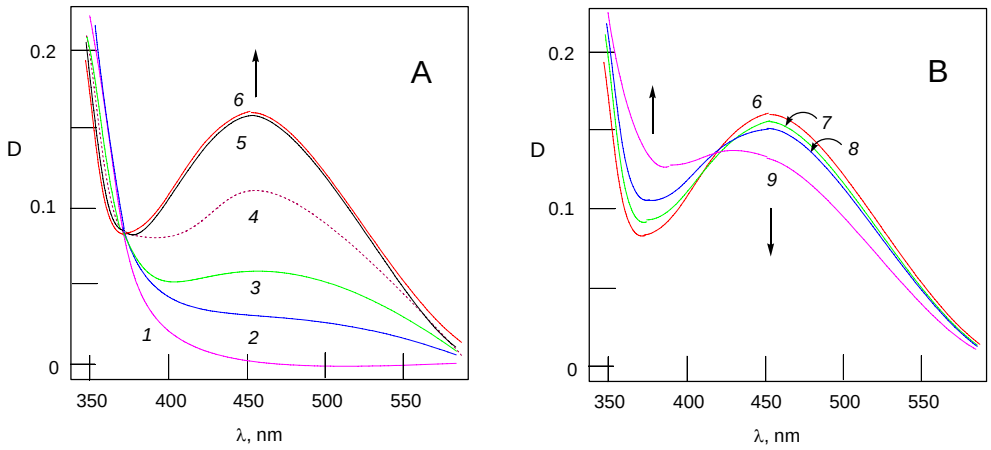

Figure 19. Electronic spectra of the acetonitrile solution containing *n*-Bu_4NVO_3 (0.5 mM), pcaH (2 mM), and water (2.2 M) at various concentrations of added H_2O_2: 0.0 (1), 0.0002 (2), 0.0004 (3), 0.0010 (4), 0.0020 (5), 0.0040 (6), 0.024 (7), 0.25 (8), 0.50 (9) M; the components were mixed at 40 °C 2 min before the spectra were recorded

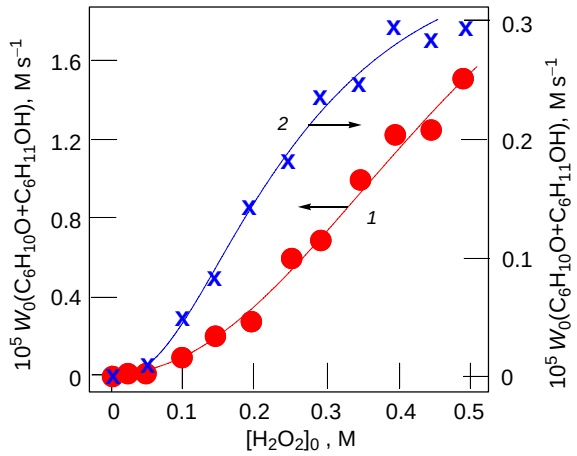

Figure 20. Dependences of the initial rate of cyclohexane oxidation in CH_3CN on initial concentration of H_2O_2; conditions: $[H_2O]$ = 2.2 M, 40 °C; curve 1: $[n\text{-}Bu_4NVO_3]_0$ = 0.5 mM, $[pcaH]_0$ = 2 mM, $[CH_3CN]$ = 17.2 M, $[Cyclohexane]_0$ = 0.46 M; curve 2: $[n\text{-}Bu_4NVO_3]_0$ = 0.1 mM, $[pcaH]_0$ = 0.4 mM, $[CH_3CN]$ = 17.7 M, $[Cyclohexane]_0$ = 0.20 M

In the alkane oxygenation, the hydroxyl radical abstracts the hydrogen atom from the cyclohexane molecule (eq. 2.19) and the cyclohexyl radical thus formed reacts rapidly with an oxygen molecule (eq. 2.20).

$$C_6H_{12} + \cdot OH \longrightarrow \cdot C_6H_{11} + H_2O \qquad (2.19)$$

$$\cdot C_6H_{11} + O_2 \longrightarrow C_6H_{11}OO\cdot \qquad (2.20)$$

$$C_6H_{11}OO\cdot + \cdot OOH \longrightarrow C_6H_{11}OOH + O_2 \qquad (2.21)$$

$$\text{Sum: } C_6H_{12} + \cdot OH + \cdot OOH \longrightarrow C_6H_{11}OOH + H_2O$$

In order to close the cycle we can introduce reaction (2.21), which affords cyclohexyl hydroperoxide as a product. Therefore, in the alkane oxidation two hydrogen peroxide molecules are sacrificially used by the vanadate/pcaH system for one hydrocarbon molecule.

The 2-propanol oxygenation in air can proceed with the regeneration of H_2O_2 used for the formation of the oxidizing species.

$$(CH_3)_2CHOH + \cdot OH \longrightarrow (CH_3)_2C\cdot(OH) + H_2O \qquad (2.22)$$

$$(CH_3)_2CHOH + \cdot OOH \longrightarrow (CH_3)_2C\cdot(OH) + HOOH \qquad (2.23)$$

$$(CH_3)_2C\cdot(OH) \rightleftharpoons (CH_3)_2CHO\cdot \qquad (2.24)$$

$$(CH_3)_2CHO\cdot + O_2 \longrightarrow (CH_3)_2CO + \cdot OOH \qquad (2.25)$$

$$(CH_3)_2C\cdot(OH) + \cdot OOH \longrightarrow (CH_3)_2CO + HOOH \qquad (2.26)$$

$$\text{Sum: } 2\,(CH_3)_2CHOH + \cdot OH + \cdot OOH + O_2 \longrightarrow 2\,(CH_3)_2CO + 2\,HOOH + H_2O$$

In this scheme hydroxyl and hydroperoxyl radicals, formed in the catalytic cycle, can both abstract a hydrogen atom from the activated secondary C–H bond of two isopropanol molecules (eq. 2.22−2.23). The hydroxyalkyl radicals thus formed can rearrange (eq. 2.24) or/and react with molecular oxygen to give one acetone molecule (eq. 2.25). The hydroperoxyl radical is regenerated affording the second acetone and hydrogen peroxide molecules in the last step (2.26). This reactivity scheme can explain the experimental data (Figure 4), when the isopropanol oxidation proceeds, formally, without H_2O_2 consummation. However, in the absence of atmospheric oxygen, the system requires one hydrogen peroxide molecule to produce one acetone molecule.

2.3 Conclusion

In this chapter we provide new insights into the hydroxylation of alkanes and alcohols catalyzed by the binary vanadate/pyrazine-2-carboxylic acid (pcaH) system with hydrogen peroxide. The detailed spectroscopic and kinetic studies revealed that in isopropanol and in acetonitrile solution the catalytic oxidation reaction proceeds via the similar routes. The rate limiting step is ascribed to the monomolecular decomposition of the diperoxo vanadium complex containing one pca ligand with the tentative description [V(O)(OO)(H_2O_2)(pca)] (**X**).

This species is formed from the known $[V(O)(OO)(pca)_2]^-$ (**V2**) complex containing two inequivalent pca ligands by attack of the H_2O_2 molecule on the protonated pca ligand in trans-coordination with respect to the vanadium-oxo moiety. The mechanistic scheme proposed satisfactorily describes the experimental data.

Although, the kinetic analysis indicates the decomposition of complex **X** to be the rate-determining step of the catalytic reaction, it can be composed of several steps. Thus, the intramolecular pca-assisted migration of a proton from the coordinated hydrogen peroxide molecule in complex **X** ("robot's arm mechanism") as well as the subsequent hydroperoxyl radical release from complex **X'** possess the comparable activation energy values, according to DFT calculations [79] and can determine the overall rate of the process. Hydroperoxyl and hydroxyl radicals, being released in the catalytic cycle, attack the substrates with activated C−H bonds (isopropanol), whereas in the alkane oxidation only hydroxyl radicals are the oxidizing species.

Water substentially decreases the catalytic activity of the vanadate/pcaH system. However, in aqueous solution even methane can be oxygenated using an excess of pcaH (100 eqv. with respect to vanadate) at the elevated temperatures (70–90 °C), unfortunately, the co-catalyst (pcaH) being not stable under these reaction conditions.

3 Manganese-Based Systems

Manganese complexes containing macrocyclic ligands with three nitrogen-donor atoms have found much interest as model complexes for biologically active systems [92]. In particular, the coordination chemistry of 1,4,7-triazacyclononane and its derivatives has been pioneered by K. Wieghardt in the 1980s.

3.1 Wieghardt's Complexes: A Breakthrough in Oxidation Catalysis

1,4,7-Triazacyclononane (L) and 1,4,7-trimethyl-1,4,7-triazacyclononane (L-Me_3) were found to react with manganese(III) acetate to give the dinuclear manganese(III) complexes $[L_2Mn_2(O)(OOCMe)_2]^{2+}$ and $[(L\text{-}Me_3)_2Mn_2(O)(OOCMe)_2]^{2+}$ [93], the latter one reacts in basic media under aerobic conditions to give the manganese(IV) tri-μ-oxo complex $[(L\text{-}Me_3)_2Mn_2(O)_3]^{2+}$ [94], while the analogous reaction of the first one leads to the tetranuclear manganese(IV) complex $[L_4Mn_4O_6]^{4+}$ [94, 95]. A full series of dinuclear Mn(II)-Mn(II), Mn(III)-Mn(III) and Mn(III)-Mn(IV) di-μ-acetato complexes, containing 1,4,7-trimethyl-1,4,7-triazacyclononane $[(L\text{-}Me_3)_2Mn_2(OH)(OOCMe)_2]^{+}$, $[(L\text{-}Me_3)_2Mn_2(O)(OOCMe)_2]^{2+}$ and $[(L\text{-}Me_3)_2Mn_2(O)(OOCMe)_2]^{3+}$ have been described by Wieghardt as model complexes for the active centre of photosystem II [96]. Dinuclear Mn(II)-Mn(III) bis-acetato complexes with 1,4,7-triazacyclononane derived ligand have been reported by Hendrickson and co-workers [97].

After the discovery of the catalytic activity of these and other Mn(III) and Mn(IV) complexes containing 1,4,7-triazacyclononane derived ligands for low-temperature bleaching [98], the catalytic oxidation potential of this type of complexes has been demonstrated for the oxidation of phenols [99, 100] and sulfides [101], as well as for the cis-hydroxylation [102] and for the epoxidation [103, 104] of olefins with hydrogen peroxide. The results of the asymmetric epoxidation catalysis using enantiomerically pure analogues of 1,4,7-triazacyclononane have been recently reviewed [105].

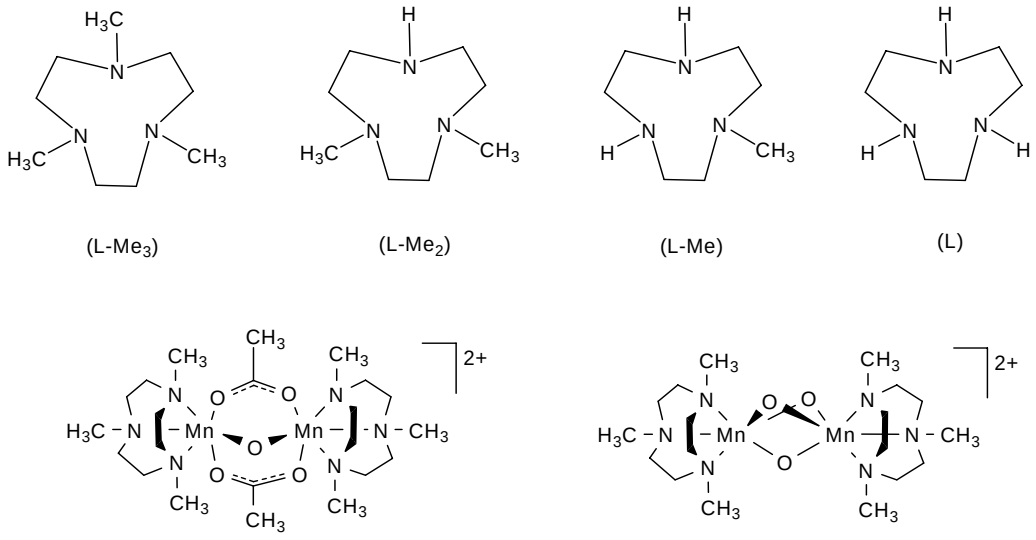

Scheme 18. Triazacyclononane ligands and dinuclear manganese complexes containing the trimethyl derivative

In 1998 G. B. Shul'pin discovered that the presence of acetic or other carboxylic acids strongly increases the catalytic oxidation potential of the dinuclear manganese(IV) complex $[(L\text{-}Me_3)_2Mn_2(O)_3]^{2+}$ (Wieghardt's complex) [106, 107], so that even alkanes, including ethane and methane could be oxidized with hydrogen peroxide in acetonitrile [108, 109] or water [64]. The importance of a carboxylate buffer for this catalyst was also demonstrated a few years later for the oxidation of benzylic groups [110]. The role of the carboxylic acid seems to consist in converting $[(L\text{-}Me_3)_2Mn_2(O)_3]^{2+}$ into $[(L\text{-}Me_3)_2Mn_2(O)_2(OH)]^{+}$, which than reacts with H_2O_2 to form highly active dinuclear Mn(III)-Mn(IV) and even Mn(IV)-Mn(V) species [111, 112].

Whereas the methyl substituents in L-Me_3 can be replaced by other alkyl groups without much change in the coordination chemistry [113], replacing only one of the three methyl groups for hydrogen inhibits the formation of the $Mn_2(O)_3$ core [114]. Thus, with the ligand 1,4-dimethyl-1,4,7-triazacyclononane (L-Me_2) only the Mn(III)-Mn(III) complex $[(L\text{-}Me_2)_2Mn_2(O)(OOCMe)_2]^{2+}$ is known [114], the mixed-valence Mn(III)-Mn(IV) complex $[(L\text{-}Me_2)_2Mn_2(O)_2(OOCMe)]^{2+}$ has been postulated without being isolated and characterized [114].

The basic cyclization procedures for the 1,4,7-triazacyclononane ring synthesis were reported by Richman and Atkins [115], however, in the particular cases [116, 117] the yields are low and additional improvement should be applied to the general synthetic route [118].

The general strategy of the 1,4,7-triazacyclononane ring synthesis includes the cyclization procedure of the disodium salt of fully tosylated triamine (L_N, Scheme 19) with the ditosyl derivative of 1,2-ethanediol (L_O), readily obtained according to the published methods [119, 120], giving the 1,4,7-triazacyclononane tritosylate derivative (L-Ts_3).

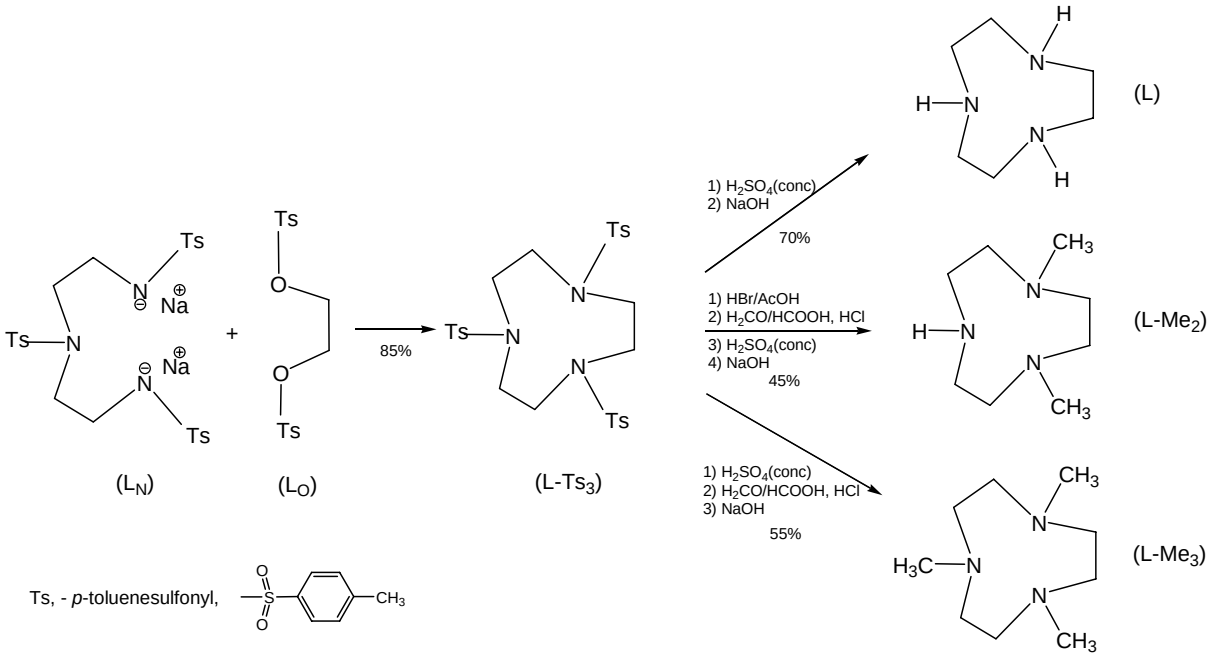

Scheme 19. General procedure for the 1,4,7-triazacyclononanes synthesis, including Eschweiler-Clarke methylation

Given that Wieghardt's type catalysts are much more active in the catalytic oxidation reactions in the presence of carboxylic acids [108, 121], it is interesting to introduce the carboxylate function into the 1,4,7-triazacyclononane ring. The mono- (L-Ac, Scheme 20) [122, 123] and triacetato-substituted (L-Ac_3) macrocycles [124] as well as two mononuclear Mn(II) $[(L\text{-}Ac_3)Mn]^-$ and Mn(III) $[(L\text{-}Ac_3)Mn]$ complexes [124] are known, however, their catalytic potential has not been exploited.

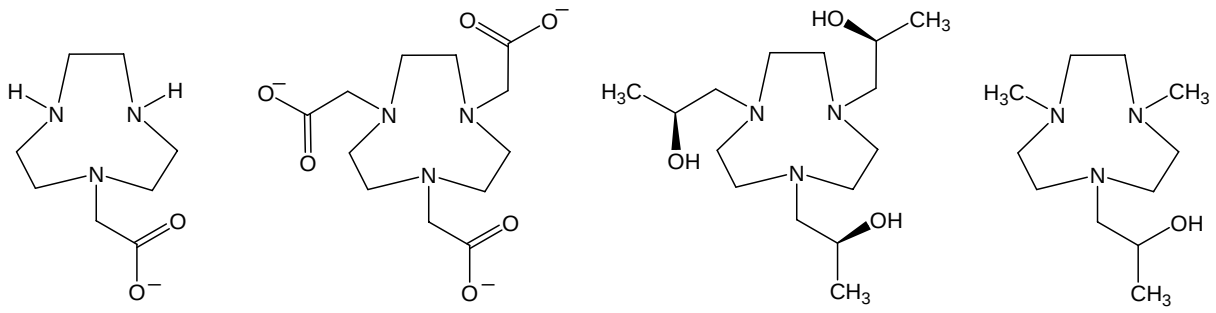

Scheme 20. Known 1,4,7-triazacyclononanes containing carboxylato- and hydroxo-pendant arms

Since $[(L\text{-}Me_3)_2Mn_2(O)_3]^{2+}$ catalyses the hydroxylation of hydrocarbons with a high degree of regio- and stereoselectivity [64, 125], it is interesting to introduce an alkyl or alkyl-functionalized substituent bearing a stereogenic center into L and apply the corresponding manganese complex in the asymmetric epoxidation catalysis. The syntheses of the racemic mono- ($R^1L\text{-}Me_2$, Scheme 20) [126] and the tri-(*S*)-2-hydroxypropyl substituted ($L\text{-}(R^{1S})_3$) [127] macrocycles have been reported, the latter one combined *in situ* with manganese (II) acetate catalyze enantioselective olefin epoxidation with the enantiomeric excess (*ee*) up to 55% [128].

Since three 1,4,7-triazacyclononane ligands (L, $L\text{-}Me_2$ and $L\text{-}Me_3$) were already known [118, 129], we decided to use L and $L\text{-}Me_2$ for the preparation of new macrocyclic ligands. Whereas bulky N-alkyl substituents (ethyl, *i*-propyl, *etc.*) provide low yields in the complexation with manganese salts, the oxidation potential of the corresponding manganese complexes is decreased [113, 114].

Thus, 1,4-dimethyl-1,4,7-triazacyclononane ($L\text{-}Me_2$) has been chosen as a starting material to introduce a functionality into the 1,4,7-triazacyclononane ring. Indeed, replacing only one of the three methyl groups in $L\text{-}Me_3$ (the most active catalyst precursor) could provide new insights into the oxidation mechanism as well as the possibility to tune the electronic and steric properties of the corresponding manganese complexes.

3.2 New Triazacyclononane Ligands

3.2.1 Selective Introduction of Alkyl Groups into a Triazacyclononane Skeleton

The selective alkylation procedure based on the L-Ts_3 is well studied [130]. However, the subsequent coupling of L-Me_2 with alkyl halogenides gives only low yields [114, 131].

For the selective incorporation of one chiral substituent into the 1,4,7-triazacyclononane ring another strategy can be applied (Scheme 21). The methine-bridged triamine L-CH (1,4,7-triazatricyclo[5.2.1.$0^{4,10}$]decane) can give the only product of the nucleophilic substitution [R^{2S}L-CH][I] ((*S*)-1-(2-methylbutyl)-4,7-diaza-1-azoniatricyclo[5.2.1.$0^{4,10}$]decane iodide) converted further to a newly prepared Wieghardt-type ligand R^{2S}L-Me_2.

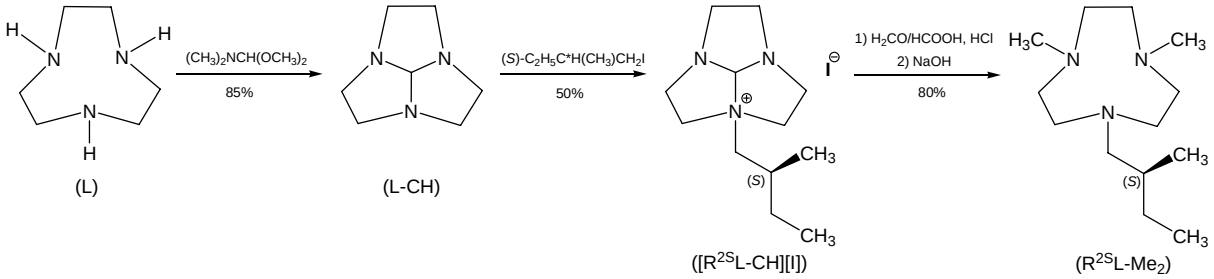

Scheme 21. Synthesis of the (*S*)-1-(2-methylbutyl)-4,7-dimethyl-1,4,7-triazacyclononane (R^{2S}L-Me_2)

The ESI mass spectrum of [R^{2S}L-CH][I] consists of a major peak at *m/z* 210.2 (60%, $[R^{2S}L\text{-}CH]^+$) and minor peaks at 200.4 (24%, $[R^{2S}L + H]^+$), 228 (8%, $[R^{2S}L\text{-}COH + H]^+$, the methine-bridge opening), 340.3 (6%, $[R^{2S}L\text{-}CH + I + 3H]^{3+}$) in the positive mode. The MS/MS experiment on the *m/z* 210.2 fragment reveals the loss of a *m/z* 70.1 fragment (the 2-methylbutyl substituent). The ^{1}H NMR spectrum of the CD_3OD solution shows the non-equivalence of the two (CH_3-*CH_2*-C*H) methylene protons, caused by the chiral carbon center, with δ 1.41(m) and 1.61(m) ppm. The ^{1}H resonances at δ 5.65(s) and ^{13}C δ 129.4 are characteristic of the methine-bridged triamine. The circular dichroism (CD) spectrum is bisignate and related to the strong UV absorbance in the 200−270 nm region (Figure 21). The difference in the molar extinction coefficients is maximal at λ ($\Delta\varepsilon$, M^{-1} cm^{-1}) 243 (+ 2.34) and 239.5 (– 5.1) nm.

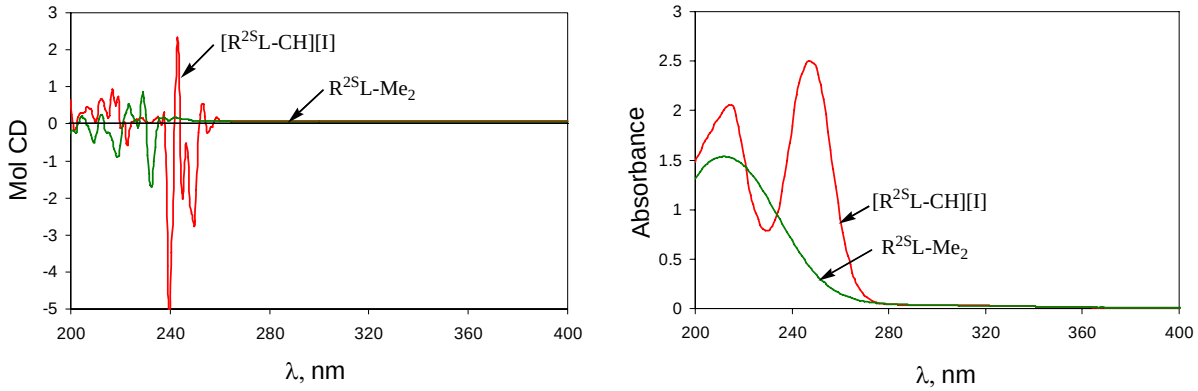

Figure 21. Molar circular dichroism (CD) and UV spectra of [R^{2S}L-CH][I] precursor and R^{2S}L-Me_2 ligand in acetonitrile ([(R^{2S}L-CH)$^+$]=[R^{2S}L-Me_2]= 0.20 mM)

R^{2S}L-Me_2 has been isolated in the form of the free base (colorless oil) using fractional distillation under reduced pressure and is applied for *in situ* catalytic experiments (Chapter 3.3.2). The ESI-MS spectrum presents one peak at *m/z* 228.2 ([R^{2S}L-Me_2 + H]$^+$) in the positive mode. The ^{1}H NMR spectrum of the CD_3OD solution reflects the non-equivalence of the two (CH_3-*CH_2*-C*H) methylene protons, caused by the chiral carbon center, with δ 1.12(m) and 1.49(m) ppm. The CD spectrum is bisignate and related to the strong UV absorbance with a maximum centered around 212 nm. For the R^{2S}L-Me_2 ligand the difference in the molar extinction coefficients is maximal at λ (Δε, M^{-1} cm^{-1}) 232.5 (– 1.7) and 229 (+ 0.87) nm.

3.2.2 Functionalization of 1,4-Dimethyl-1,4,7-Triazacyclononane

Four new 1,4,7-triazacyclononane derivatives have been synthesized (Scheme 22). Two chiral ligands R^{1S}L-Me_2 and R^{1R}L-Me_2 are obtained using the ring-opening of the corresponding enantiomerically pure epoxides. The nucleophylic attack was shown to be 100% regiospecific and proceeds at the less hindered carbon atom of the epoxide, so the absolute configuration at the neighbouring carbon center is conserved [127].

The ESI-MS spectra of both R^{1S}L-Me_2 and R^{1R}L-Me_2 contain one peak at *m/z* 216 ([R^1L-Me_2 + H]$^+$) in the positive mode. In C_6D_6, the ^{1}H and ^{13}C NMR spectra of R^{1S}L-Me_2 are the same as those for the racemic R^1L-Me_2 [126]. The ^{1}H NMR (400 MHz) spectrum of R^{1R}L-Me_2 in $CDCl_3$ gives δ 3.76 (m, 1H, $NCH_2CH(OH)CH_3$), 2.70–2.60 (m, 12H,

NC*H*$_2$C*H*$_2$N), 2.60–2.37 (m, 2H, NC*H*$_2$CH(OH)CH$_3$), 2.20 (s, 6H, NC*H*$_3$) and 1.03 (d, 3H, NCH$_2$CH(OH)C*H*$_3$, ^3J = 6.3 Hz), while the ^{13}C NMR (100 MHz) spectrum shows seven resonances with δ 66.1 (NC*H*$_2$CH(OH)CH$_3$), 65.9 (NCH$_2$*C*H(OH)CH$_3$), 58.7, 58.1, 57.0 (3 × NC*H*$_2$C*H*$_2$N), 46.3 (N*C*H$_3$) and 19.6 (NCH$_2$CH(OH)*C*H$_3$) ppm. The CD spectra of the R^{1S}L-Me$_2$ and R^{1R}L-Me$_2$ solutions in hexane indicate the enantiomeric relationship between these two molecules and result in the mirror images of each other (Figure 22). The CD curves are bisignate and related to the strong UV absorbance in the 220−260 nm region. For the R^{1R}L-Me$_2$ enantiomer, the molar CD spectrum shows four maxima centered around λ (Δε, M^{-1} cm^{-1}) 249 (– 0.15), 238 (+ 0.38), 233 (– 0.62) and 228 (+ 0.78) nm; for the R^{1S}L-Me$_2$ enantiomer: λ (Δε, M^{-1} cm^{-1}) 246 (+ 0.15), 238 (– 0.24), 234 (+ 0.65) and 229 (– 0.73) nm.

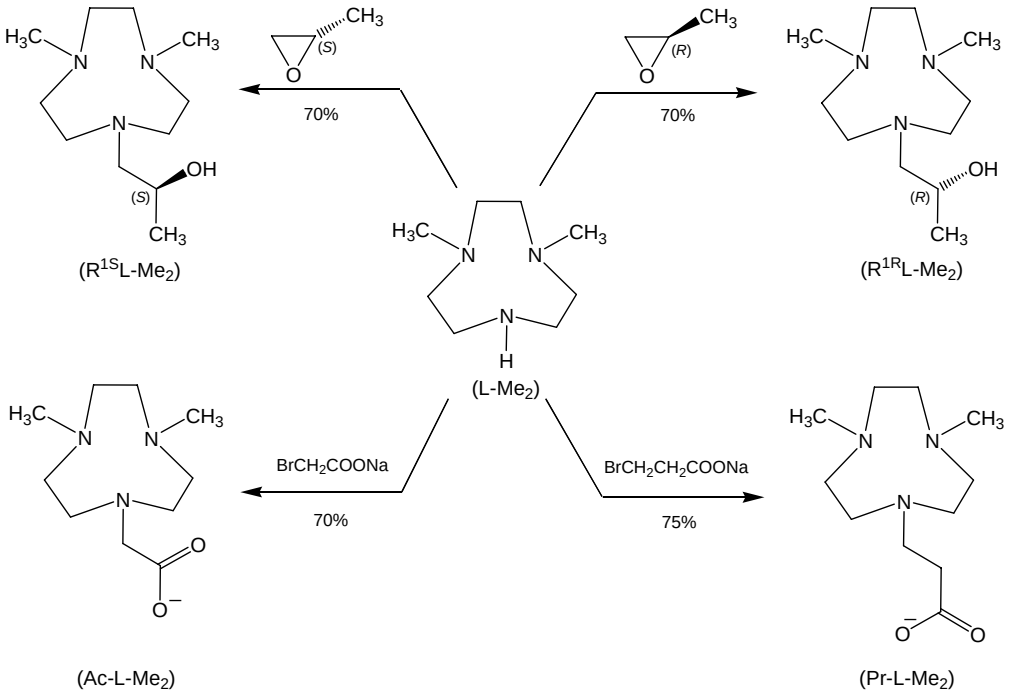

Scheme 22. Syntheses of new 1,4-dimethyl-1,4,7-triazacyclononane (L-Me$_2$) derived ligands

The ligands Ac-L-Me$_2$ and Pr-L-Me$_2$ containing pendant carboxylato arm are readily obtained by reaction of the 1,4-dimethyl-1,4,7-triazacyclononane (L-Me$_2$) with sodium bromoacetate or 3-bromopropionate, by modification of previously described procedure for L-Ac$_3$ [103, 124]. In contrast to L-Ac$_3$, both Ac-L-Me$_2$ and Pr-L-Me$_2$ can be successfully isolated from the alkaline aqueous solution (by extraction with dichloromethane) in the form of the corresponding sodium salts.

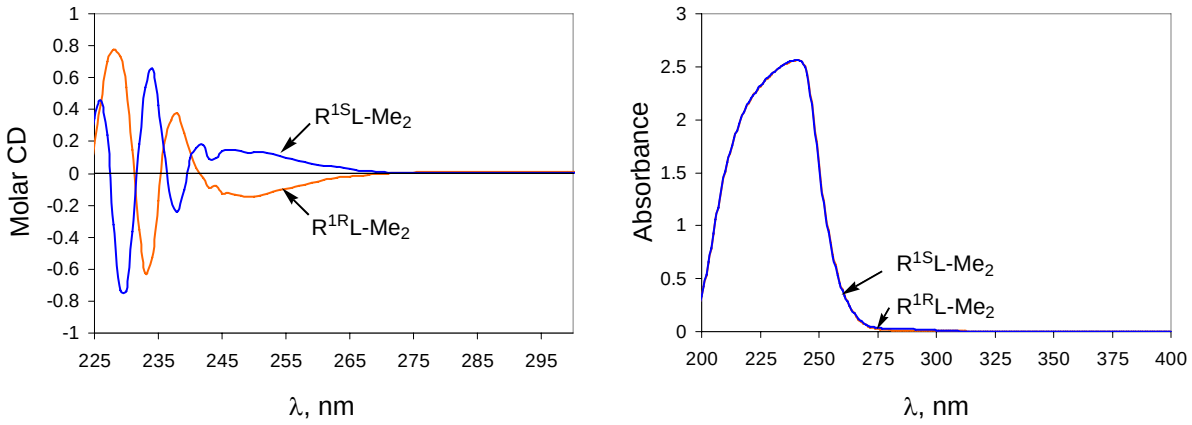

Figure 22. Molar circular dichroism (CD) and UV spectra of (*R*) and (*S*) isomers of 1-(2-hydroxypropyl)-4,7-dimethyl-1,4,7-triazacyclononane in hexane ([R^{1R}L-Me_2]=[R^{1S}L-Me_2]= 1.45 mM)

The ESI-MS spectrum of Ac-L-Me_2 contains one peak at *m/z* 215 ([Ac-L-Me_2]$^-$) in the negative mode. The ^{1}H NMR (400 MHz, $CDCl_3$) spectrum shows resonances: δ 3.10 (s, 2H, NCH_2COONa), 2.55−2.48 (m, 12H, NCH_2CH_2N) and 2.33 (s, 6H, NCH_3); the ^{13}C NMR (100 MHz, $CDCl_3$) spectrum reveals six resonances at δ 177.2 (NCH$_2$*C*OONa), 63.7 (N*C*H$_2$COONa), 55.0, 54.8, 53.2 (3 × N*C*H$_2$*C*H$_2$N) and 45.9 (N*C*H$_3$).

The ESI-MS spectrum of Pr-L-Me_2 contains one peak at *m/z* 228.3 ([Pr-L-Me_2]$^-$) in the negative and two peaks at *m/z* 230.3 ([Pr-L-Me_2 + 2H]$^+$) and 252.1 ([Pr-L-Me_2 + H + Na]$^+$) in the positive mode. The ^{1}H NMR (400 MHz, CD_3OD) spectrum shows resonances at δ 2.80 (t, 2H, NCH_2CH$_2$COONa, ^3J = 7.0 Hz), 2.65−2.63 (m, 12H, NCH_2CH_2N), 2.38 (s, 6H, NCH_3) and 2.36 (t, 2H, NCH$_2$CH_2COONa, ^3J = 9.9 Hz); the ^{13}C NMR (100 MHz, CD_3OD) spectrum gives seven resonances at δ 181.1 (NCH$_2$CH$_2$*C*OONa), 56.5, 56.1, 55.5 (3 × N*C*H$_2$*C*H$_2$N), 53.7 (N*C*H$_2$CH$_2$COONa), 46.1 (N*C*H$_3$) and 36.6 (NCH$_2$*C*H$_2$COONa). The ν_{as}(C−O) stretching frequencies for Pr-L-Me_2 (1581 cm^{-1}) and for Ac-L-Me_2 (1594 cm^{-1}) are close; ν_s(C−O) frequency for Pr-L-Me_2 (1420 cm^{-1}) are comparable to those in Ac-L-Me_2 (1405 cm^{-1}).

3.2.3 Preparation of the C_2-Symmetric *SS-trans*-2,5,8-Trimethyl-2,5,8-Triazabicyclo[7.4.0^{1,9}] Tridecane

Given that the C_2-element of symmetry plays an important role in epoxidation catalysis [132], we introduced this element also in the asymmetric analogue of 1,4,7-

triazacyclononane. Thus, we synthesized *SS-trans*-2,5,8-trimethyl-2,5,8-triazabicyclo[7.4.0^{1,9}] tridecane (L^{SS}-Me_3, Scheme 23), however, as in the case of its known *RR*-enantiomer [116, 133], the yields are quite low.

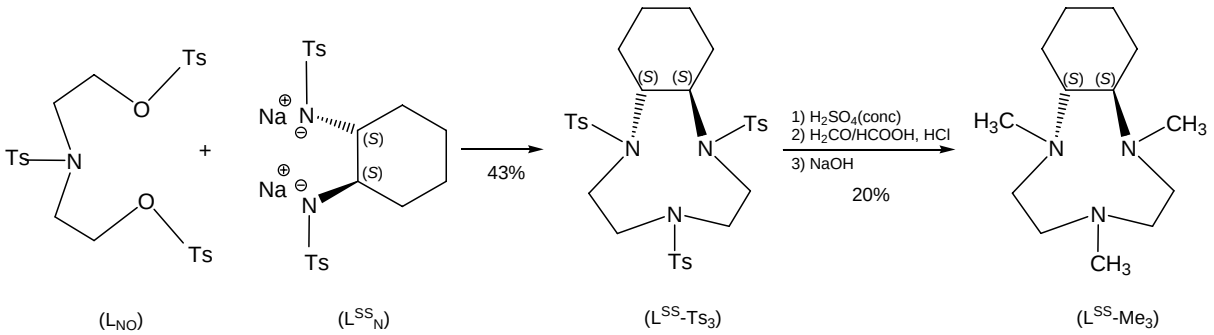

(L_{NO}) ($L^{SS}{}_N$) (L^{SS}-Ts_3) (L^{SS}-Me_3)

Scheme 23. Synthesis of the C_2-symmetric enantimerically pure L^{SS}-Me_3 (*SS-trans*-2,5,8-trimethyl-2,5,8-triazabicyclo[7.4.0^{1,9}]tridecane

The ESI-MS spectrum of L^{SS}-Me_3 contains one peak at *m/z* 226.2 ($[L^{SS}\text{-}Me_3 + H]^+$ in the positive mode. ^{1}H NMR (400 MHz, $CDCl_3$) spectrum of L^{SS}-Me_3 shows δ 2.7–2.4 (m, 8H, NCH_2CH_2N), 2.35 (br, 2H, NC*HC*HN), 2.26 (s, 3H, NCH_3), 2.22 (s, 6H, NCH_3), 1.80 (br, 2H), 1.71 (br, 2H) and 1.13 (br, 4H, cyclohexyl ring) ppm. The chiroptical properties of the L^{SS}-Me_3 solution in hexane result in the CD spectrum shown in Figure 23. The CD curve is bisignate and related to the strong UV absorbance in the 200−300 nm region. For the L^{SS}-Me_3 molar CD spectrum gives five maxima centered around λ (Δε, M^{-1} cm^{-1}) 263 (+ 0.49), 245 (– 0.33), 230 (+ 0.57), 222 (– 1.41) and 210 (+ 0.45) nm.

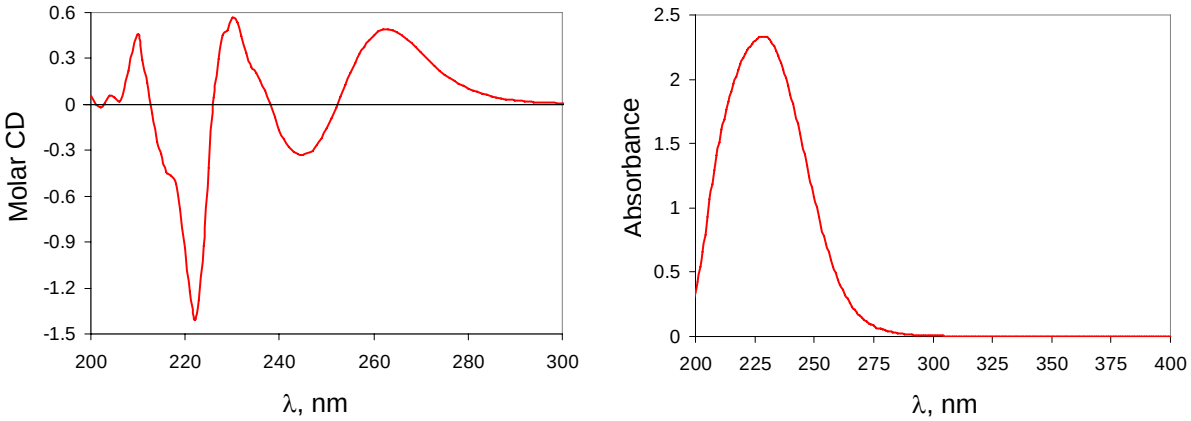

Figure 23. Molar circular dichroism (CD) and UV spectra of *SS-trans*-2,5,8-trimethyl-2,5,8-triazabicyclo[7.4.0^{1,9}] tridecane in hexane ($[L^{SS}\text{-}Me_3]$ = 1.06 mM)

The catalytic oxidation potential of manganese complexes containing such a 2,5,8-triazabicyclo[7.4.0^{1,9}]tridecane motive has not been reported. Thus, we decided to combine the L^{SS}-Me$_3$ ligand with a manganese salt in hydroxylation and asymmetric epoxidation studies.

3.3 New Results with Dinuclear Manganese Complexes Containing Triazacyclononane-Derived Ligands

While the system containing 1,4,7-triazacyclononane (L) added to the manganese(II) sulphate aqueous solution turns out to be inactive in the alcohol oxidation with hydrogen peroxide, we found that upon addition of L-Me$_3$ the catalytic oxidation reaction results in the corresponding aldehydes/carboxylic acid or ketone formation, see Table 5.

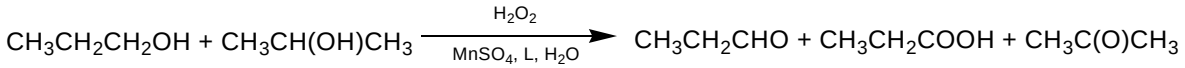

Table 5. Oxalic acid effect in the oxidation of 1:1 isomeric propanols mixture in aqueous solution catalyzed by the *in situ* prepared combinations containing 1,4,7-triazacyclononane (L) and 1,4,7-trimethyl-1,4,7-triazacyclononane (L-Me$_3$) ligands; conditions: 22 °C, 1 hour, 0.34 mM $MnSO_4$, 0.52 mM ligand, 0.50 H_2O_2, 0.46 M sum of alcohols; oxa - oxalate

Ligand	pH	Promoter, mM	Yield, % (product)	TON
L	6.0	---	0	0
L	3.7	0.5 oxaH_2, 0.5 oxaNa_2	0	0
L-Me$_3$	6.0	---	0.3 (CH_3CH_2CHO), 1.1 ($CH_3C(O)CH_3$)	19
L-Me$_3$	3.7	0.5 oxaH_2, 0.5 oxaNa_2	7 (CH_3CH_2CHO), 5 (CH_3CH_2COOH), 31 ($CH_3C(O)CH_3$)	580

The accelerating effect of oxalates added in 3:1 ratio relative manganese catalyst containing L-Me$_3$ was originally reported by De Vos [134]. Since 1997 the carboxylates effect on the catalytic activity of the dinuclear Mn(IV)-Mn(IV) complex $[(L\text{-}Me_3)_2Mn_2(O)_3]^{2+}$ has been intensively studied [64, 112, 135].

3.3.1 Dinuclear Manganese Complexes Containing 1,4-Dimethyl-1,4,7-Triazacyclononane Ligands as well as Carboxylato and Oxo Bridges

1,4-Dimethyl-1,4,7-triazacyclononane (L-Me_2) appears to be a convenient material to launch the systematic tuning of the electronic and steric properties around the manganese center. The classical synthesis of the manganese(III)-manganese(III) complexes $[L_2Mn_2(O)(OOCMe)_2]^{2+}$ and $[(L\text{-}Me_3)_2Mn_2(O)(OOCMe)_2]^{2+}$ from manganese(III) acetate and L or L-Me_3 in moist ethanol, reported by K. Wieghardt *et al*. [93], fails in the case of L-Me_2; the analogous complex $[(L\text{-}Me_2)_2Mn_2(O)(OOCMe)_2]^{2+}$ was synthesised by J. Koek *et al*. by adding one equivalent of a strong acid to the acetonitrile solution of the triazamacrocycle prior to coordination [114]. Presumably the monoprotonation of L-Me_2 preorganizes the conformation of the macrocycle suitable for complexation.

We extended this idea to the synthesis of $(L\text{-}Me_2)_2Mn_2$ complexes containing various carboxylato bridges in the presence of *p*-$CH_3C_6H_4SO_3H$ as strong acid and hydrogen peroxide as oxidant, see Scheme 24. We found that the nature of the dinuclear complexes formed depends on the nature of the carboxylate used: with formate, the Mn(III)-Mn(IV) complex $[(L\text{-}Me_2)_2Mn_2(O)_2(OOCH)]^{2+}$ (**Mn1**) is obtained, while benzoate gives the Mn(III)-Mn(III) complex $[(L\text{-}Me_2)_2Mn_2(O)(OOCPh)_2]^{2+}$ (**Mn2**). With acetate, both cations the green Mn(III)-Mn(IV) complex $[(L\text{-}Me_2)_2Mn_2(O)_2(OOCMe)]^{2+}$ (**Mn3**) and the violet-brown [114] Mn(III)-Mn(III) complex $[(L\text{-}Me_2)_2Mn_2(O)(OOCMe)_2]^{2+}$ (**Mn4**) are accessible, depending on the molar ratio of sodium acetate to manganese(II) chloride tetrahydrate.

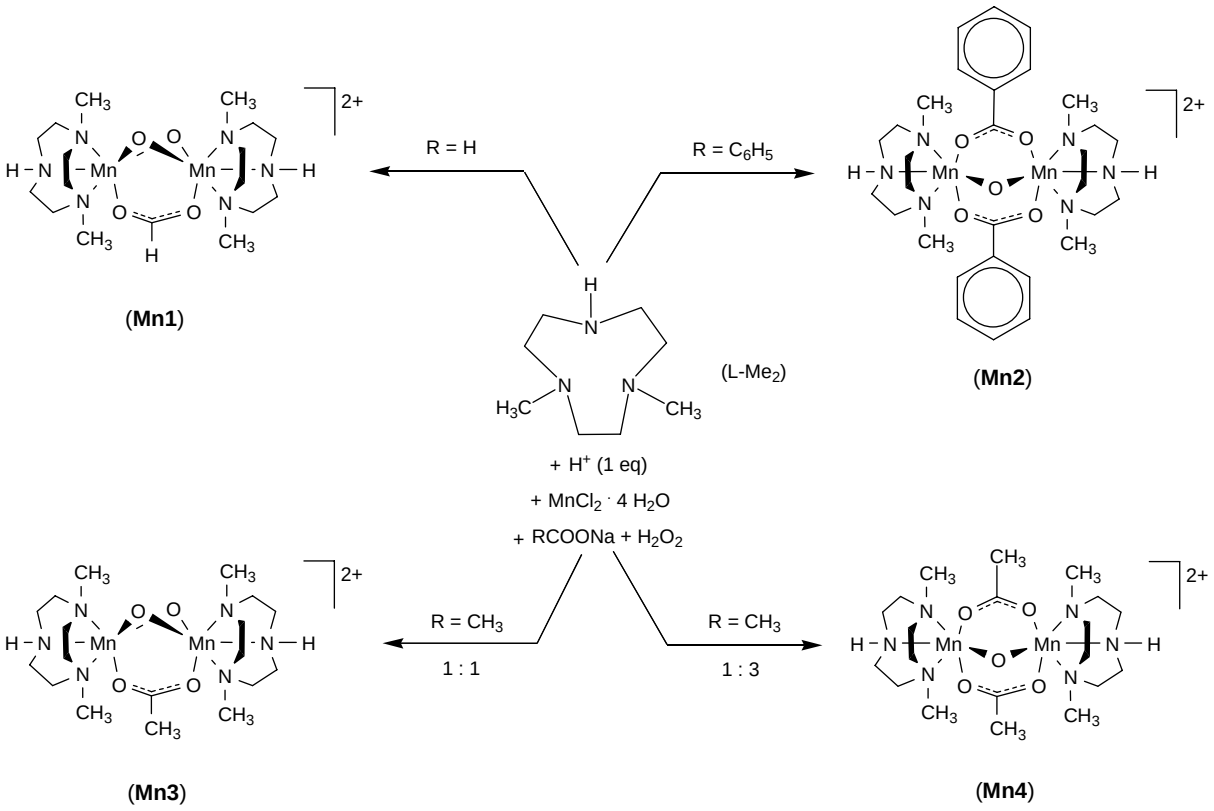

Scheme 24. Reaction of 1,4-dimethyl-1,4,7-triazacyclononane (L-Me_2) with manganese(II) chloride tetrahydrate in the presence of hydrogen peroxide and the corresponding sodium carboxylate

All complexes **Mn1** – **Mn4** are paramagnetic and could be isolated as the hexafluorophosphate salts, which are well soluble in acetone and acetonitrile, but sparingly soluble in ethanol, isopropanol and water.

Green X-ray quality crystals of [**Mn1**][PF_6]$_{1.5}$[Cl]$_{0.5}$ · 1.5 H_2O and [**Mn3**][PF_6]$_2$ · $(CH_3)_2CO$ were obtained by slow diffusion of ether into an acetone solution containing **Mn1** and **Mn3** respectively. In [**Mn3**][PF_6]$_2$ · $(CH_3)_2CO$, there are two crystallographically independent Mn(III)-Mn(IV) cations of **Mn3** per unit cell. The molecular structure of **Mn1** and **Mn3** are shown in Figure 24 and Figure 25 respectively. Similarly, red-violet crystals of [**Mn4**][PF_6]$_2$ are obtained by slow diffusion of ether into an acetone solution containing **Mn4**. The molecular structure of **Mn4** is presented in Figure 26.

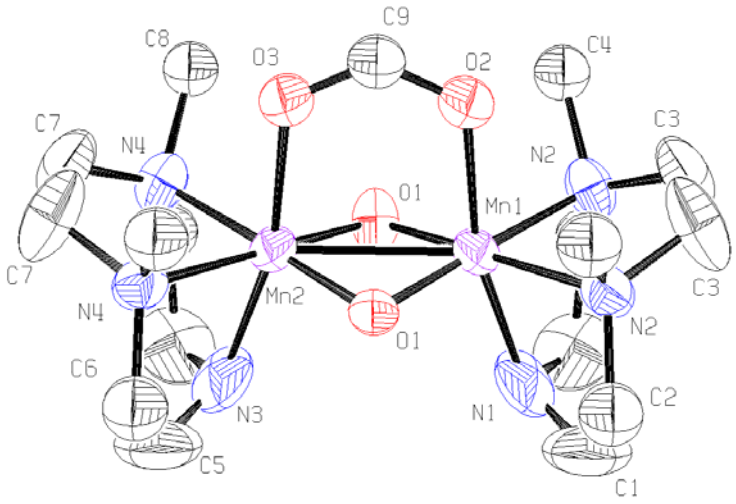

Figure 24. Ortep drawing of cation **Mn1** in [**Mn1**][PF_6]$_{1.5}$[Cl]$_{0.5}$ · 1.5 H_2O at the 50% probability level. Hydrogen atoms, solvent molecules, chloride and hexafluorophosphate anions are omitted for clarity.

The molecular structures of the green Mn(III)-Mn(IV) dioxo complexes [(L-Me_2)$_2$$Mn_2(O)_2$(OOCH)]$^{2+}$ (**Mn1**) and [(L-Me_2)$_2$$Mn_2(O)_2$(OOCMe)]$^{2+}$ (**Mn3**), show a metal-metal distance of 2.620(1) and 2.628(4) Å, respectively. These distances compare well to the isoelectronic Mn(III)-Mn(IV) cation [L_2Mn_2(O)$_2$(OOCMe)]$^{2+}$ (2.588(2) Å) [136]. In contrast, the red-violet Mn(III)-Mn(III) complex [(L-Me_2)$_2$$Mn_2$(O)(OOCMe)$_2$]$^{2+}$ (**Mn4**) possesses a longer metal-metal distance: the molecular structure of **Mn4** reveals a distance of 3.1416(8) Å, comparable to those observed in the analogous Mn(III)-Mn(III) complexes [L_2Mn_2(O)(OOCMe)$_2$]$^{2+}$ (3.096(2) Å) [137] and [L(L-Me_3)Mn_2(O)(OOCMe)$_2$]$^{2+}$ (3.121(2) Å) [138].

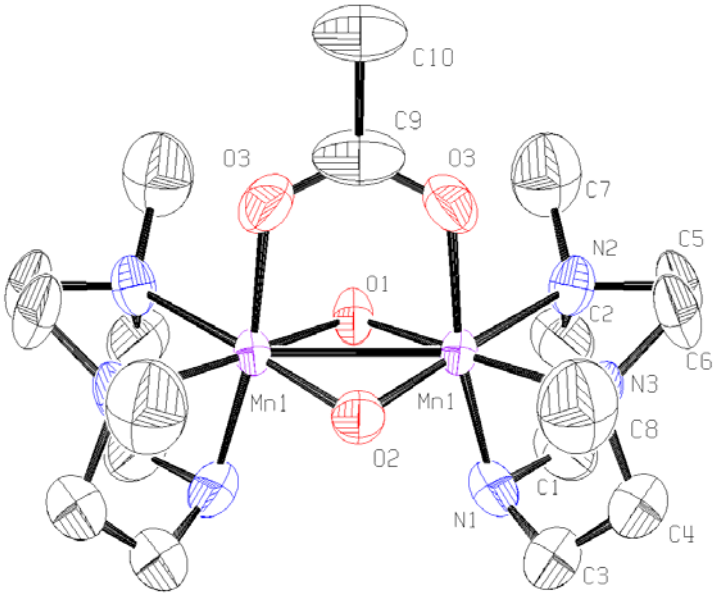

Figure 25. Ortep drawing of one crystallographically independent cation **Mn3** in [**Mn3**][PF_6]$_2$ · $(CH_3)_2CO$ at the 50% probability level. Hydrogen atoms, solvent molecules and hexafluorophosphate anions are omitted for clarity

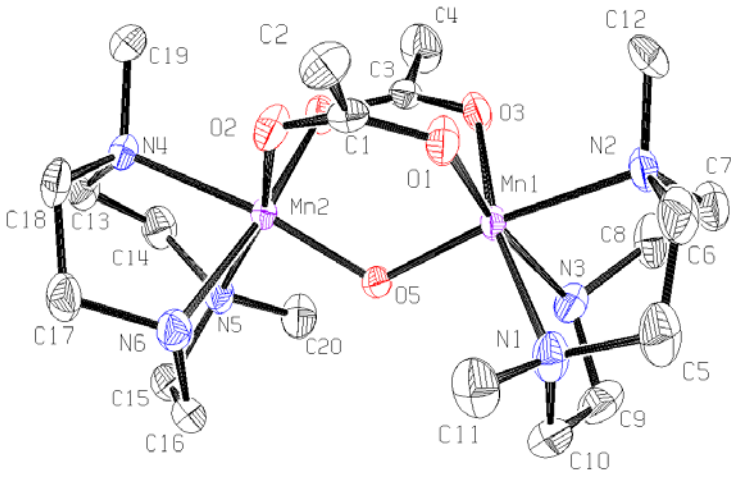

Figure 26. Ortep drawing of cation **Mn4** in [**Mn4**][PF_6]$_2$ at the 50% probability level. Hydrogen atoms and hexafluorophosphate anions are omitted for clarity

Selected bond lengths and angles of complexes [**Mn1**][PF_6]$_{1.5}$[Cl]$_{0.5}$ · 1.5 H_2O, [**Mn3**][PF_6]$_2$ · $(CH_3)_2CO$ and [**Mn4**][PF_6]$_2$ are listed in Table 6.

Table 6. Selected bond lengths (Å) and angles (°) for [**Mn1**][PF_6]$_{1.5}$[Cl]$_{0.5}$ · 1.5 H_2O, [**Mn3**][PF_6]$_2$ · $(CH_3)_2CO$ and [**Mn4**][PF_6]$_2$

	[**Mn1**][PF_6]$_{1.5}$[Cl]$_{0.5}$	[**Mn3**][PF_6]$_2$	[**Mn4**][PF_6]$_2$
Interatomic distances			
Mn-Mn	2.620(1)	2.628(4)	3.1416(8)
Mn-Mn		2.599(4)	
Mn-O (oxo)	1.811(2)	1.797(7)	1.796(3)
Mn-O (oxo)	1.811(2)	1.781(7)	1.799(2)
Mn-O (oxo)		1.814(7)	
Mn-O (oxo)		1.836(8)	
Mn-O (carboxylato)	2.110(3)	2.082(8)	2.008(3)
Mn-O (carboxylato)	2.109(3)	2.064(8)	2.074(3)
Mn-O (carboxylato)			2.022(3)
Mn-O (carboxylato)			2.123(3)
Mn-N (H)	2.091(6)	2.16(1)	2.141(3)
Mn-N (H)	2.093(6)	2.150(8)	2.144(4)
Mn-N (Me)	2.113(3)	2.11(1)	2.107(3)
Mn-N (Me)	2.115(3)	2.11(1)	2.236(3)
Mn-N (Me)		2.11(1)	2.246(4)
Mn-N (Me)		2.12(1)	2.118(3)
Angles			
Mn-O-Mn (oxo)	92.7(1)	92.6(5)	121.8(2)
Mn-O-Mn (oxo)		92.8(5)	
O-C-O (carboxylato)	128.6(5)	123(2)	124.1(4)
O-C-O (carboxylato)		125(2)	124.9(4)

Interestingly, all complexes show intermolecular interactions with solvent molecules or anions, due to the presence of an N-H moiety within the ligand L-Me_2. Therefore, in [**Mn1**][PF_6]$_{1.5}$[Cl]$_{0.5}$ · 1.5 H_2O, the hydrogen atoms of the two N-H amino groups interact strongly with a chloride anion, see Figure 27. The distances between the nitrogen atoms and the chloride anion are 3.220(5) Å (for N1) and 3.227(5) Å (for N3) with N-H···Cl angles of 153.2° and 153.4° respectively.

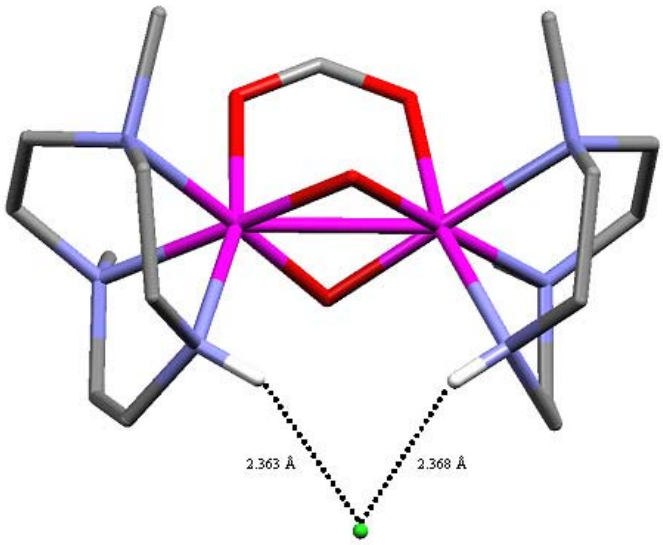

Figure 27. Capped sticks representation of cation **Mn1** in [**Mn1**][PF_6]$_{1.5}$[Cl]$_{0.5}$ · 1.5 H_2O, showing the intermolecular interactions with the chloride anion

In [**Mn3**][PF_6]$_2$ · $(CH_3)_2CO$ where two crystallographically independent molecules of **Mn3** are present per unit cell, two different intermolecular interactions are observed, see Figure 28. One cation of **Mn3** interacts with a hexafluorophosphate anion, whereas the second cation forms hydrogen bonds with an acetone molecule. In the intermolecular hydrogen bonded system involving the acetone molecule, the N···O distance is 2.78(1) Å with an N-H···O angle of 144.9°, whereas with the fluorine atoms of the hexafluorophosphate, the N···F distances are 3.05(1) and 3.20(1) Å with angles of 166.6 and 133.2° respectively.

Finally, in [**Mn4**][PF_6]$_2$, the amino protons of the N-H moieties interact independently with the two hexafluorophosphate anions, see Figure 29. The distances between the nitrogen and fluorine atoms are 3.022(6) and 3.242(6) Å (for N3) and 3.234(9) and 3.134(9) Å (for N6) with N-H···F angles ranging from 127.2 to 146.1°.

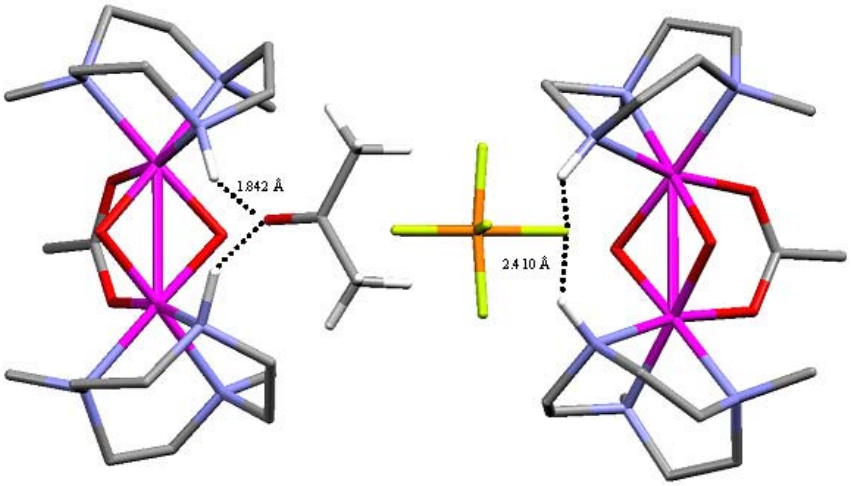

Figure 28. Capped sticks representation of cation **Mn3** in [**Mn3**][PF_6]$_2$ · $(CH_3)_2CO$, showing the intermolecular interactions with an acetone molecule and a hexafluorophosphate anion

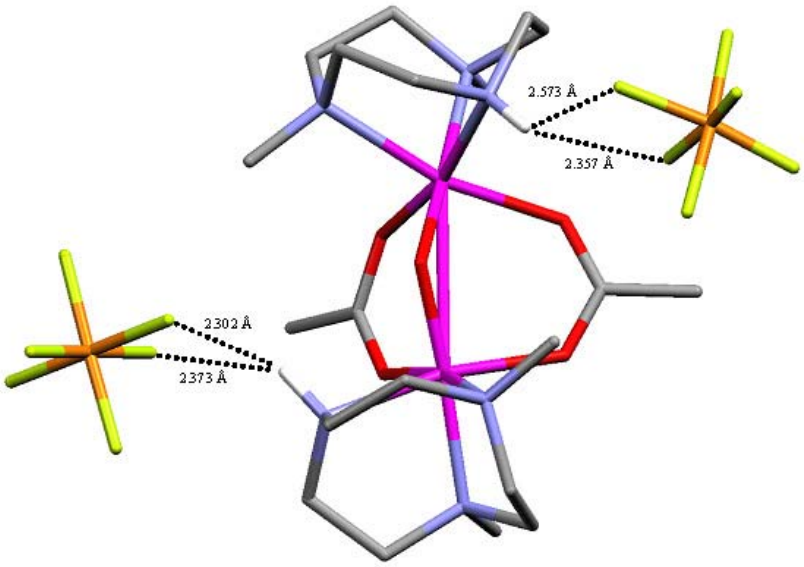

Figure 29. Capped sticks representation of cation **Mn4** in [**Mn4**][PF_6]$_2$, showing the intermolecular interactions with the hexafluorophosphate anions

We studied the catalytic potential of the complexes **Mn1** – **Mn4** for the oxidation of isopropanol with hydrogen peroxide to give acetone. The oxidation reaction was carried out in aqueous solution or in acetonitrile in the presence of ascorbic or oxalic acid as co-catalysts at 20 °C. The results are shown in Figure 30, Figure 31 and Table 7.

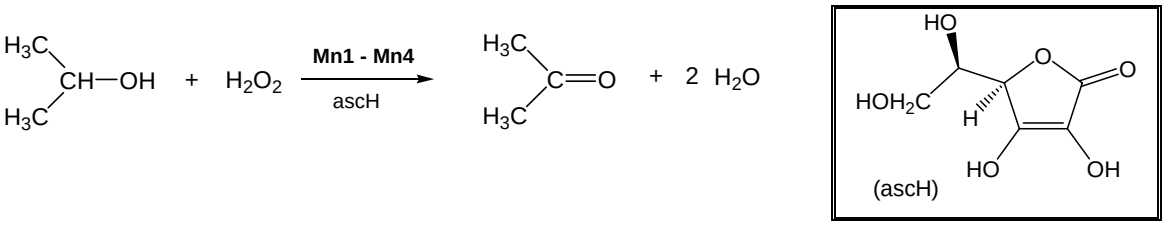

Scheme 25. Catalytic oxidation of isopropanol in water and ascorbic acid used as a co-catalyst

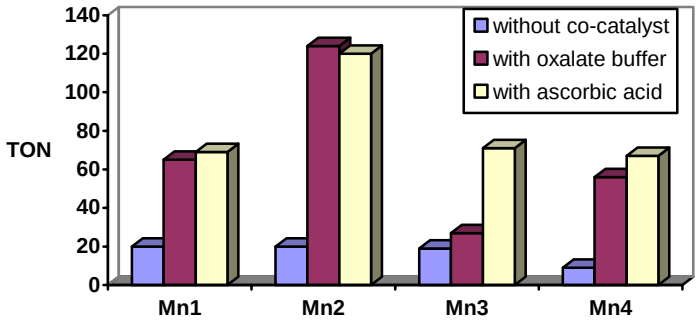

Figure 30. Oxidation of isopropanol in water, catalysed by the complexes **Mn1**–**Mn4** in the absence/presence of 0.01 M ascorbic acid or 0.02 M oxalate buffer as co-catalyst (20°C, 1h, 1.0 × 10^{-4} M complex **Mn1**−**Mn4**, 0.20 M isopropanol, 0.50 M H_2O_2

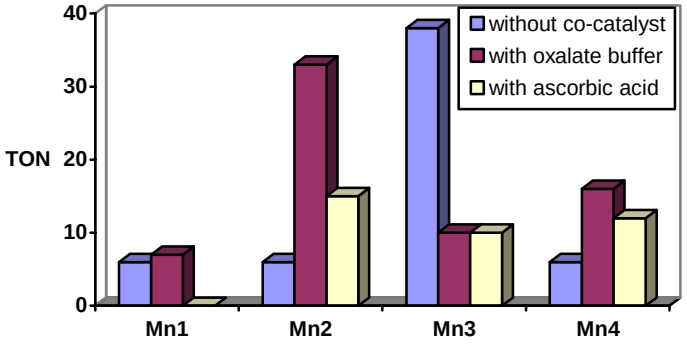

Figure 31. Oxidation of isopropanol in acetonitrile, catalysed by the complexes **Mn1**–**Mn4** in the absence/presence of 0.01 M ascorbic acid or 0.02 M oxalate buffer as co-catalyst (20°C, 1h, 1.0 × 10^{-4} M complex **Mn1**−**Mn4**, 0.20 M isopropanol, 0.50 M H_2O_2

The highest activity was observed for complex $[(L\text{-}Me_2)_2Mn_2(O)(OOCPh)_2)]^{2+}$ (**Mn2)** in water in the presence of oxalate buffer, the TON (catalyst turnover number, mol of products per mol of catalyst) being 124 after 1 hour at 20 °C, which is not as high as that of $[(L\text{-}Me_3)_2Mn_2(O)_3]^{2+}$, for which a TON of 3040 was observed under the same conditions (with 0.02 mM catalyst). However, while $[(L\text{-}Me_3)_2Mn_2(O)_3]^{2+}$ in combination with

carboxylic (typically acetic) acid as co-catalyst is more active in acetonitrile [108] than in water [64], the complexes **Mn1**–**Mn4** are more active in aqueous solution (Table 7).

Table 7. Oxidation of isopropanol in water and acetonitrile, catalysed by the complexes **Mn1**–**Mn4** in the absence/presence of 0.01 M ascorbic acid or 0.02 M oxalate buffer as co-catalyst (20 °C, 1h, 1.0×10^{-4} M $MnSO_4$, complex **Mn1**−**Mn6**, 0.20 M isopropanol, 0.50 M H_2O_2)

Catalyst	TON (after 1h) in water			TON (after 1h) in acetonitrile		
	Without co-catalyst	With oxalate	With ascorbic acid	Without co-catalyst	With oxalate	With ascorbic acid
Mn^{2+}/ L-Me_2	17	77	103			
Mn1	20	65	69	6	7	0
Mn2	20	124	120	6	33	15
Mn3	19	27	71	38	10	10
Mn4	9	56	67	6	16	12

The role of the co-catalyst (ascorbic or oxalic acid) is not clear, it may serve as a reducing agent and/or as a carboxylato ligand. The beneficial effect of ascorbic acid as co-catalyst has been observed in the oxidation of 2-pentanol to give 2-pentanone, catalysed by mixture of $Mn(OOCCH_3)_2 \cdot 4\ H_2O$ and L-Me_3 in moist acetonitrile [139].

3.3.2 Catalytic Potential of *In Situ* Prepared Manganese Complexes Containing New Macrocyclic Ligands

The manganese complexes containing the new ligands are made *in situ* by reaction of $MnSO_4 \cdot H_2O$ with L-Me_2, L^{SS}-Me_3, R^{1S}L-Me_2, R^{1R}L-Me_2, R^{2S}L-Me_2, Ac-L-Me_2 and Pr-L-Me_2 in water; the stock solution thus formed, is then added to the reaction mixture. The oxidation of isopropanol with hydrogen peroxide to give acetone is carried out in aqueous solution in the absence/presence of ascorbic or oxalic acid as co-catalysts at 20 °C. The results are shown in Figure 32 and Table 8.

Although, without co-catalyst the activity is low, the introduction of a pendant carboxylato arm into the L-Me_2 structure significantly increases both stability and

performance of the catalyst. This effect is more pronounced in the case of Pr-L-Me_2, in line with mechanistic investigations [111]. According to the MS-ESI spectra, the oxidation activity can be tentatively ascribed to the dinuclear manganese complexes with two carboxylato arms bridging two manganese centers. Indeed, the substitution of only one hydrogen atom in the 1,4,7-triazacyclononane ring (by *e.g.* methyl group) inhibits the tri- and tetranuclear complex formation [113, 140]. However, upon addition of 3 equivalents of hydrogen peroxide to the *in situ* prepared manganese complex containing Pr-L-Me_2, all the fragments in the MS-ESI spectrum represent di-, tri- and tetranuclear manganese complexes (*m/z* 1196, 1007, 976 (35%, tetranuclear); 945, 914, 685 (50%, trinuclear); 663, 584 (10%, dinuclear). Thus, in the case of Pr-L-Me_2 ligand the pendant propionato group has a strong tendency to bridge neighbouring manganese centers and even at high hydrogen peroxide concentration to keep them in the active dinuclear form (one of the principles of the carboxylate-promoted mechanism [111, 112]). In the case of Ac-L-Me_2, the MS-ESI spectrum consists of di- and mononuclear manganese fragments (*m/z* 594, 556, 548, 515 (60%, dinuclear); 331, 300, 269 (30%, mononuclear). Therefore, we can assume that in Ac-L-Me_2 three nitrogen atoms and the pendant acetato group are preferentially coordinated to the same manganese center and at high hydrogen peroxide concentration these dinuclear complexes are more subjected to the cleavage. However, we were not able to isolate these high-valent species which decomposed during crystallization even at low temperatures (−18 °C, 0 °C, decoloration).

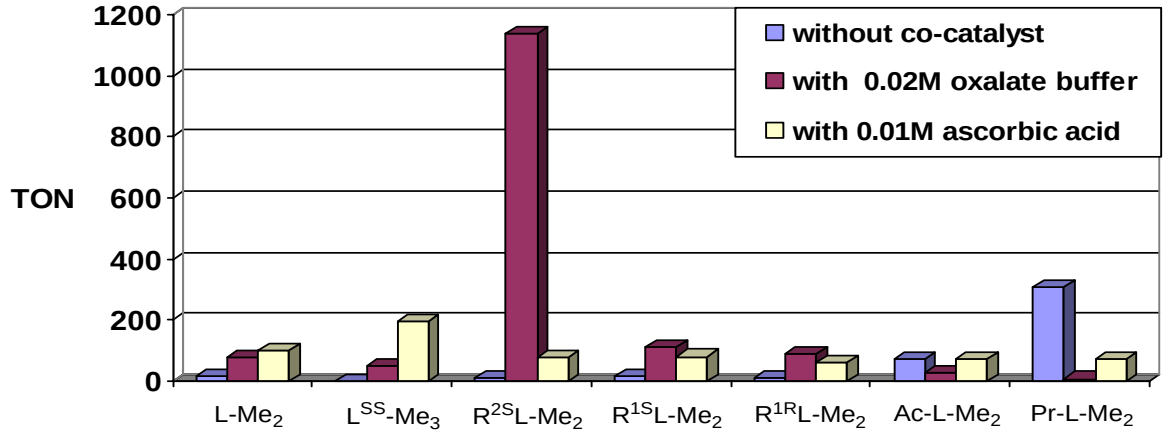

Figure 32. Oxidation of isopropanol in water, catalysed by the *in situ* prepared manganese complexes in the absence /presence of 0.01 M ascorbic acid or 0.02 M oxalate buffer as co-catalyst; $[MnSO_4]_o = 10^{-4}$ M, $[Ligand]_o = 1.5 \times 10^{-4}$ M, $[H_2O_2]_o = 0.50$ M, $[i\text{-PrOH}]_o = 0.20$ M, 20 °C; 1 hour (TON – catalyst turnover number)

Table 8. Oxidation of isopropanol in water, catalysed by *in situ* prepared manganese complexes in the absence/presence of 0.01 M ascorbic acid or 0.02 M oxalate buffer as co-catalyst; $[MnSO_4]_o = 10^{-4}$ M, $[Ligand]_o = 1.5 \times 10^{-4}$ M, $[H_2O_2]_o = 0.50$ M, $[i\text{-PrOH}]_o = 0.20$ M, 20 °C

Ligand	Name	TON (after 1h) in water		
		Without co-catalyst	With oxalate	With ascorbic acid
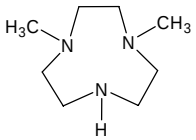	1,4-dimethyl-1,4,7-triazacyclononane **(L-Me$_2$)**	17	77	103
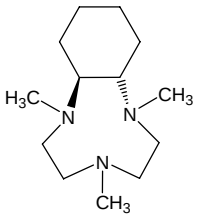	*SS-trans*-2,5,8-trimethyl-2,5,8-triazabicyclo-[7.4.0^{1,9}] tridecane **(L^{SS}-Me$_3$)**	0	51	198
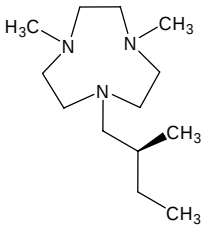	(*S*)-1-(2-methylbutyl)-4,7-dimethyl-1,4,7-triazacyclononane **(R^{2S}L-Me$_2$)**	10	1140	78
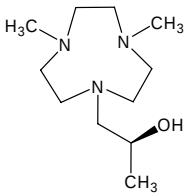	(*S*)-1-(2-hydroxypropyl)-4,7-dimethyl-1,4,7-triazacyclononane **(R^{1S}L-Me$_2$)**	15	112	81
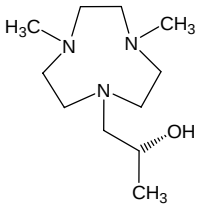	(*R*)-1-(2-hydroxypropyl)-4,7-dimethyl-1,4,7-triazacyclononane **(R^{1R}L-Me$_2$)**	13	91	61
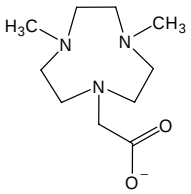	2-(4,7-dimethyl-1,4,7-triazacyclononan-1-yl)acetate **(Ac-L-Me$_2$)**	72	28	73
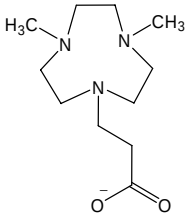	3-(4,7-dimethyl-1,4,7-triazacyclononan-1-yl)propionate **(Pr-L-Me$_2$)**	310	8	71

The addition of oxalate buffer (pH 3.5) causes an increase of the oxidation activity in the case of alkyl and hydroxyalkyl *N*-substituted ligands (L-Me_2, L^{SS}-Me_3, R^{1S}L-Me_2, R^{1R}L-Me_2 and R^{2S}L-Me_2), but a significant decrease in the case of the ligands containing pendant carboxylato arms (Ac-L-Me_2, Pr-L-Me_2). This can be explained by the competition of the bidentate oxalate ligand and hydrogen peroxide for the place in the coordination sphere of the manganese center, which is still occupied by three nitrogen atoms of the 1,4,7-triazacyclononane ring and an oxygen atom of the carboxylato pendant arm. The best catalytic performance was shown by the manganese complex containing trialkyl *N*-substituted R^{1S}L-Me_2 ligand, a TON of 1140 was observed after 1 hour of the reaction. However, the manganese complex with trimethyl *N*-substituted L^{SS}-Me_3 ligand is significantly less effective due to the coordination problems imposed by the rigid bicyclic structure of the macrocyclic ligand.

The addition of ascorbic acid accelerates the oxidation of isopropanol, the highest activity is observed in the case of L^{SS}-Me_3 (TON = 198, after 1h). The coordination of ascorbic acid to the manganese center is less effective comparing to the oxalate, therefore, the oxidation activity is higher also for the ligands with carboxylato pendant arms (Ac-L-Me_2, Pr-L-Me_2).

Given the fact the ligands L^{SS}-Me_3, R^{1S}L-Me_2, R^{1R}L-Me_2 and R^{2S}L-Me_2 are chiral, we studied the corresponding manganese complexes prepared *in situ* for enantioselective epoxidation reactions. Indene has been chosen as a model substrate (Scheme 26); it can be epoxidized to give the racemic mixture of (1*R*,2*S*) and (1*S*,2*R*) enantiomers of indene oxide using *m*-chloroperbenzoic acid [141] (2-indanone has been also detected), or to give (1*R*,2*S*)-indene oxide enriched mixture using the Jacobsen protocol with a *R*,*R*-(salen)-Mn-based complex [142, 143]. Both methods were used to prepare the calibration samples for the HPLC separation on the Daicel Chiracel OJ-H type column using nitrobenzene as internal standard. In the case of Mn^{2+}/L*, we observed by ^{1}H NMR and UV spectroscopy only the formation of both epoxides expected (Scheme 26). Only upon standing at room temperature for 3 days, formation of 2-indanone, 2-indanol and 1,2-indanediols was observed.

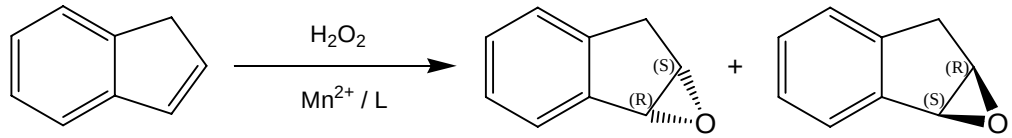

Scheme 26. Epoxidation of indene, catalyzed by *in situ* prepared manganese complexes

The catalytic epoxidation activity is best in aqueous acetonitrile (50% v/v), in water the solubility of indene is too low, while in acetonitrile $MnSO_4$ as well as oxalates or ascorbic acid precipitate from the solution. The results of epoxidation studies are shown in Figure 33 and Table 9.

Table 9. Epoxidation of indene in H_2O/MeCN 50% v/v, catalysed by *in situ* prepared manganese complexes in the absence/presence of 0.3 mM ascorbic or 0.3 mM oxalate buffer as co-catalyst; $[MnSO_4]_o = 10^{-4}$ M, $[Ligand]_o = 1.5 \times 10^{-4}$ M, $[H_2O_2]_o = 0.20$ M, $[indene]_o = 0.10$ M, 2 °C; the absolute configuration of indene oxide, which is preferentially formed, is shown in brackets

Ligand	Name	Without co-catalyst			With oxalate			With ascorbate		
		ee %	conv. %	TON 2h	ee %	conv. %	TON 2h	ee %	conv. %	TON 2h
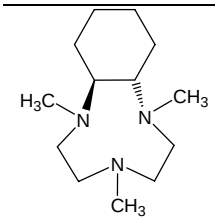	L^{SS}-Me_3	13.4 (1*S*,2*R*)	0.68	6.8	1.4 (1*S*,2*R*)	1.26	12.6	10.0 (1*S*,2*R*)	0.54	5.4
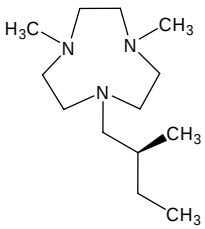	R^{2S}L-Me_2	5.9 (1*S*,2*R*)	1.46	14.6	4.1 (1*S*,2*R*)	6.0	60	17.2 (1*S*,2*R*)	0.55	5.5
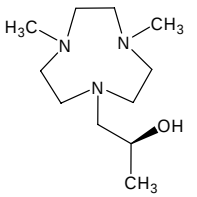	R^{1S}L-Me_2	17 (1*R*,2*S*)	4.2	42	3.5 (1*R*,2*S*)	15.9	159	3.3 (1*R*,2*S*)	0.51	5.1
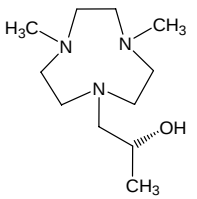	R^{1R}L-Me_2	17 (1*S*,2*R*)	4.2	42	3.5 (1*S*,2*R*)	16.3	163	3.3 (1*S*,2*R*)	0.49	4.9

Without co-catalyst the oxidation activity is low in the case of L^{SS}-Me_3 and $R^{2S}L$-Me_2, the corresponding catalytic turnover numbers are 6.8 (ee = 13.4%) and 14.6 (ee = 5.9%) after 2 hours of the reaction with a predominant formation of (1*S*,2*R*)-indene oxide. In the case of $R^{1R}L$-Me_2 and $R^{1S}L$-Me_2 ligands the TONs attain 42 (ee = 17%), the (1*S*,2*R*)-enantiomer being the major epoxidation product with $R^{1R}L$-Me_2, while with the $R^{1S}L$-Me_2 ligand (1*R*,2*S*)-indene oxide is preferentially formed.

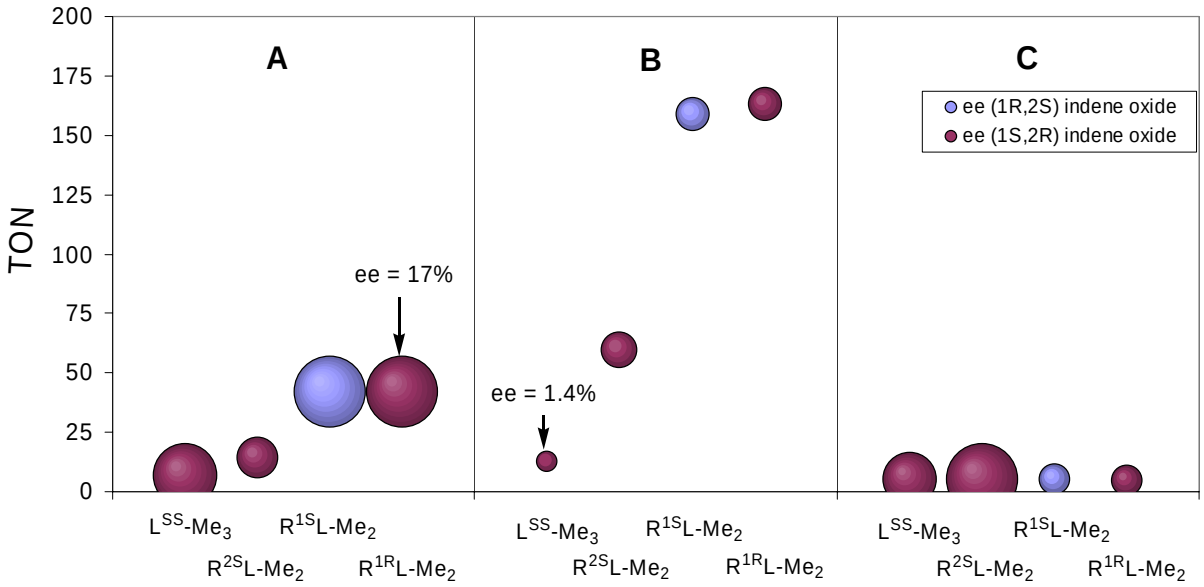

Figure 33. Activity and selectivity parameters in the indene epoxidation in H_2O/MeCN 50/50 v/v mixture, catalysed by *in situ* prepared manganese complexes in the absence (**A**) /presence of 0.3 mM oxalate buffer (**B**) or 0.3 mM ascorbate buffer (**C**) as co-catalyst; $[MnSO_4]_o = 10^{-4}$ M, $[Ligand]_o = 1.5 \times 10^{-4}$ M, $[H_2O_2]_o = 0.20$ M, $[indene]_o = 0.10$ M, 2 °C; 2 hours; the values of enantiomeric excess (%) are proportional to the surface of the corresponding bubbles

In the presence of oxalate (3 eq. respect to Mn^{2+}) the catalytic activity increases (TONs attain 160), but the enantioselectivity falls down to ee = 1−4% (Figure 33B). This fact demonstrates that in the presence of oxalates a different catalytically active species is formed. With ascorbic acid/sodium ascorbate used as a co-catalyst the catalytic activity is low and gives about 5 TON after 2 hours of the reaction (Figure 33C).

Manganese complexes with Ac-L-Me_2 and Pr-L-Me_2 ligands containing pendant carboxylato arms show a significant catalytic activity in the oxidation of isopropanol and do not require a co-catalyst. Using these *in situ* prepared complexes for the indene epoxidation under the conditions applied for the enantioselective catalysis (2 °C, 2 h, H_2O/MeCN 50% v/v, 0.1 M indene, 0.2 M H_2O_2, no co-catalyst added), the TONs values attain 326 and 450,

the conversions being 32.6% and 45% for Ac-L-Me_2 and Pr-L-Me_2 respectively (the product distribution shows 93% of indene oxide and 7% of indanone-2, Table 10).

Table 10. Epoxidation of indene in H_2O/MeCN 50% v/v, catalysed by *in situ* prepared manganese complexes; $[MnSO_4]_o = 10^{-4}$ M, $[Ligand]_o = 1.5 \times 10^{-4}$ M, $[H_2O_2]_o = 0.20$ M, $[indene]_o = 0.10$ M, 2 °C, 2 hours

Ligand	Name	catalyst µmol	(1*R*,2*S*)-Indene oxide, µmol	(1*S*,2*R*)-Indene oxide, µmol	Indanone-2 µmol	Conv. %	TON
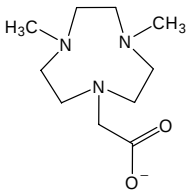	Ac-L-Me_2	0.2	30.26	30.22	4.67	32.6	326
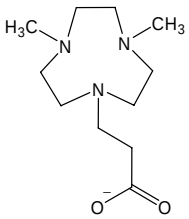	Pr-L-Me_2	0.2	41.91	41.92	6.27	45.0	450

Thus, a combination of $MnSO_4$ and either Ac-L-Me_2 or Pr-L-Me_2 ligands shows excellent catalytic activity, addition of a co-catalyst is not required. The best catalytic performance (450 turnover numbers after 2 hours) of the system $MnSO_4$/Pr-L-Me_2 is considerably higher than that of the system $MnSO_4$/L-Ac_3 ligand (Scheme 20), for which a TON of 66 was observed after 10 hours under optimized conditions [103]. To the best of our knowledge, the system $MnSO_4$/Pr-L-Me_2 ligand gives the highest catalytic turnover for epoxidation reaction without co-catalyst reported so far.

The isolation of manganese complexes containing L^{SS}-Me_3 in our hands was not successful, however, a low-yield synthesis for its (*R*,*R*) enantiomer has been reported [133]. For the R^{2S}L-Me_2 ligand no crystalline material could be obtained using manganese (II) chloride and manganese (III) acetate as a starting material. Fortunately, we succeeded in the isolation and the characterization of dinuclear manganese complexes containing R^{1R}L-Me_2 and R^{1S}L-Me_2 ligands, one of the most selective epoxidation catalyst precursors according to our results with *in situ* prepared complexes (Table 9).

3.3.3 Manganese Complexes Containing Chiral 1-(2-Hydroxypropyl)-4,7-Dimethyl Triazacyclononane Ligands

Two dinuclear Mn(III)-Mn(IV) complexes $[(R^{1R}L\text{-}Me_2)_2Mn_2(O)_2]^{3+}$ (**Mn5R**) and $[(R^{1S}L\text{-}Me_2)_2Mn_2(O)_2]^{3+}$ (**Mn5S**) can be synthesized by reacting $MnCl_2 \cdot H_2O$ with the chiral ligand in moist ethanol, followed by the addition of the alkaline solution of hydrogen peroxide (Scheme 27). Two manganese centers are bridged by two oxo ligands as well as by two chiral pendant arms introduced into the triazacyclononane ring. Both complexes **Mn5R** and **Mn5S** could be isolated as the hexafluorophosphate salts, which are well soluble in acetone and acetonitrile, but sparingly soluble in ethanol, isopropanol and water.

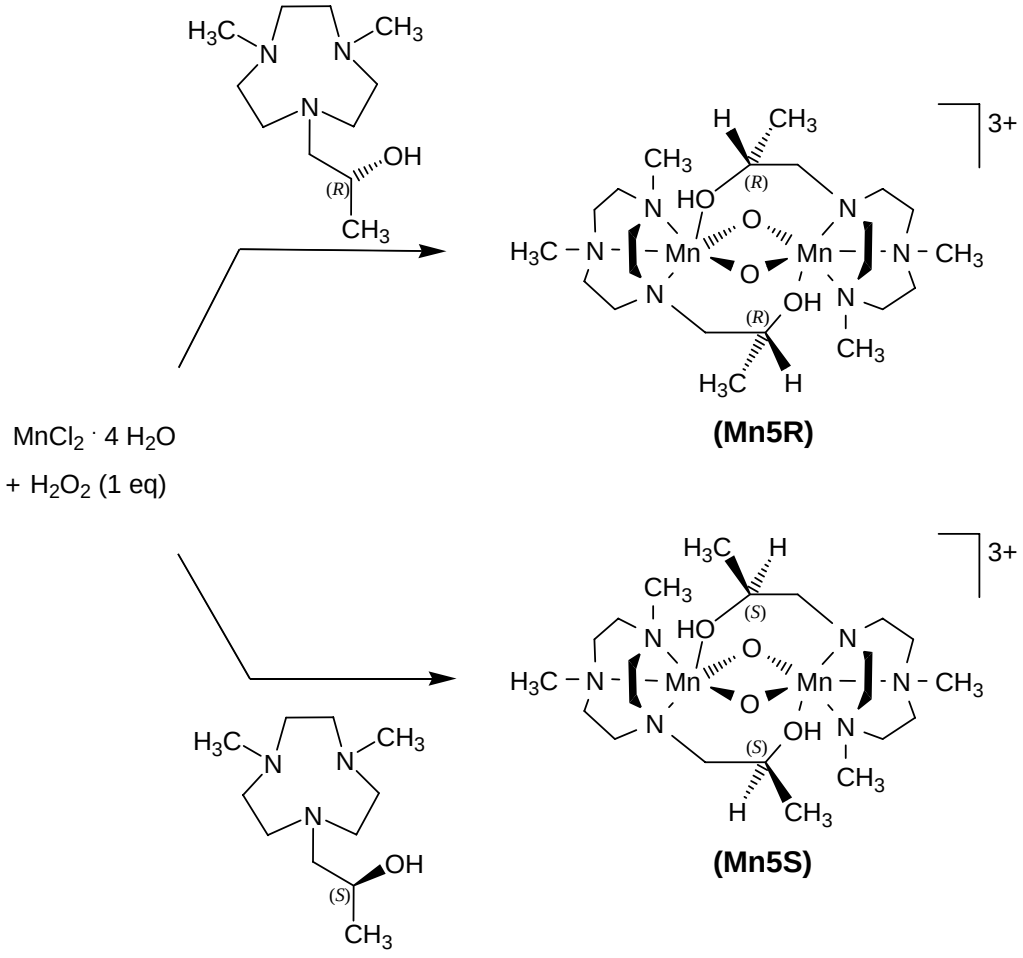

Scheme 27. Synthesis of the dinuclear Mn(III)-Mn(IV) complexes containing chiral 1-(2-hydroxypropyl)-4,7-dimethyl triazacyclononane as well as oxo ligands

The ESI-MS spectra of **Mn5R** and **Mn5S** show the parent peak at *m/z* 715.1 ([**Mn5** − 2H][PF_6]) in the positive mode. The absorptions at 648 cm^{-1}, observed in the infrared spectra,

can be ascribed to the breathing mode of the Mn_2O_2 core [144], which are shifted to the lower frequencies as compared to those observed for **Mn1** (690, 668 cm^{-1}) and **Mn3** (686, 661 cm^{-1}) containing a μ-carboxylato bridge. The presence of hydroxo groups in the bridging pendant arms of **Mn5R** and **Mn5S** is established by a O–H stretching frequency at 3674 cm^{-1}. In the UV/vis spectra, the acetonitrile solutions of **Mn5R** and **Mn5S** show three intense absorption maxima λ (ε, M^{-1} cm^{-1}) 575 (320), 281 (14700), 225 (12600) nm. The CD spectra of the **Mn5R** and **Mn5S** solutions in acetonitrile indicate the enantiomeric relationship between these two complexes and result in the mirror images of each other (Figure 34). The CD curves are bisignate and for **Mn5R** shows the maxima centered around λ (Δε, M^{-1} cm^{-1}) 474 (+ 1.5), 432 (– 0.4), 360 (+ 4.7), 310 (– 4.0), 256 (– 6.4) and 224 (+ 5.4) nm; for **Mn5S**: λ (Δε, M^{-1} cm^{-1}) 474 (– 1.5), 432 (+ 0.4), 360 (– 5.2), 310 (+ 5.0), 256 (+ 6.4) and 224 (– 6.2) nm.

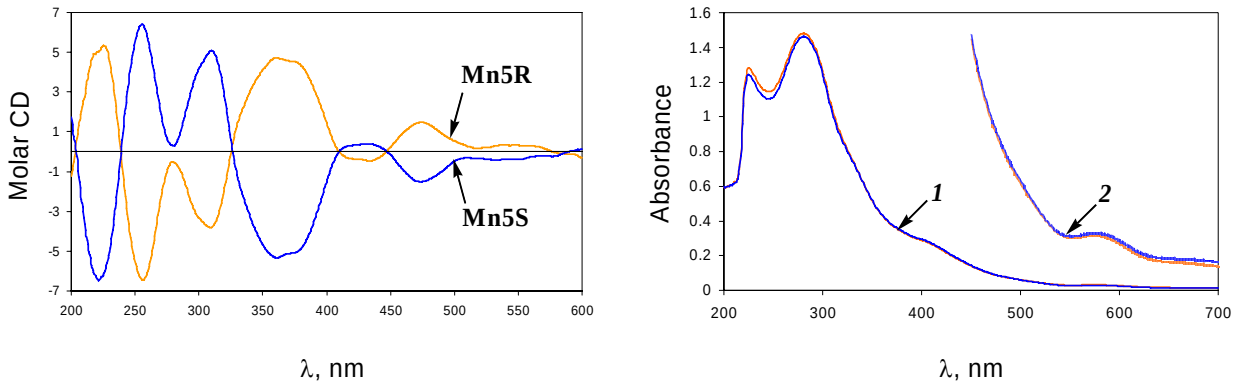

Figure 34. Molar circular dichroism (CD) and UV-Vis spectra of [**Mn5R**][PF_6]$_3$ and [**Mn5S**][PF_6]$_3$ in acetonitrile; in the UV-Vis spectra for ***1***: [**Mn5R**]$^{3+}$ = [**Mn5S**]$^{3+}$ = 1.0 × 10^{-4} M; for ***2***: [**Mn5R**]$^{3+}$ = [**Mn5S**]$^{3+}$ = 1.0 × 10^{-3} M

Brown-green X-ray quality crystals of [**Mn5R**][PF_6]$_3$ · 0.5 $(CH_3)_2CO$ and [**Mn5S**][PF_6]$_3$ · 0.5 $(CH_3)_2CO$ were obtained by slow diffusion of ether into an acetone solution containing **Mn5R** and **Mn5S** respectively. The molecular structures of **Mn5R** and **Mn5S** are shown in Figure 35 – 38. **Mn5R** and **Mn5S** are the first examples of a dinuclear manganese complex bridged by two chiral pendant arms.

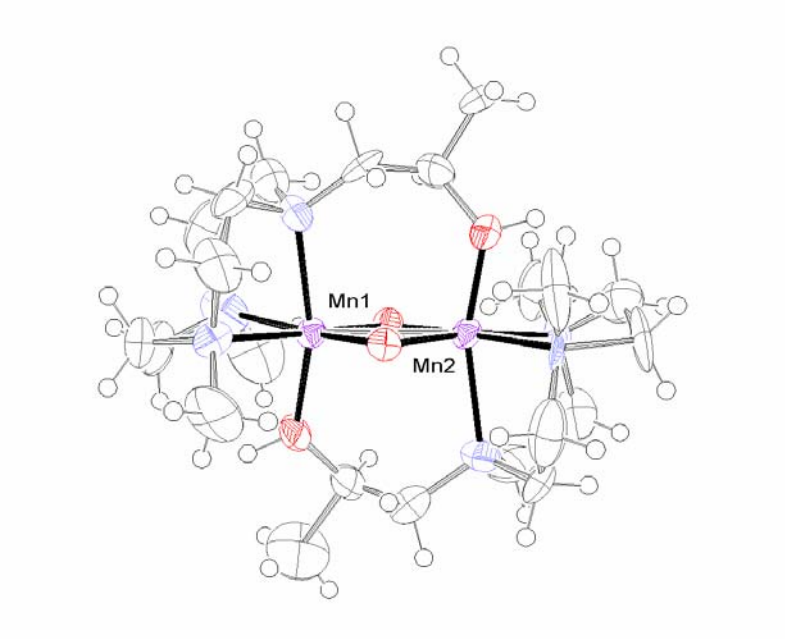

Figure 35. Ortep drawing of cation **Mn5R** in [**Mn5R**][PF_6]$_3$ at the 50% probability level. Hexafluorophosphate anions and acetone molecule are omitted for clarity

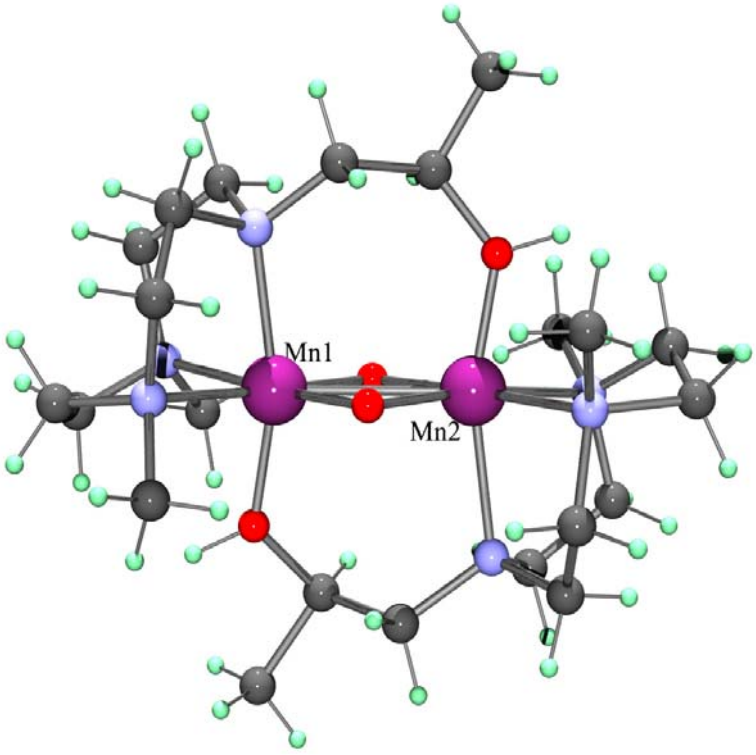

Figure 36. Structural representation of cation **Mn5R** showing coordination mode of the two manganese centers in [**Mn5R**][PF_6]$_3$. Hexafluorophosphate anions and acetone molecule are omitted for clarity

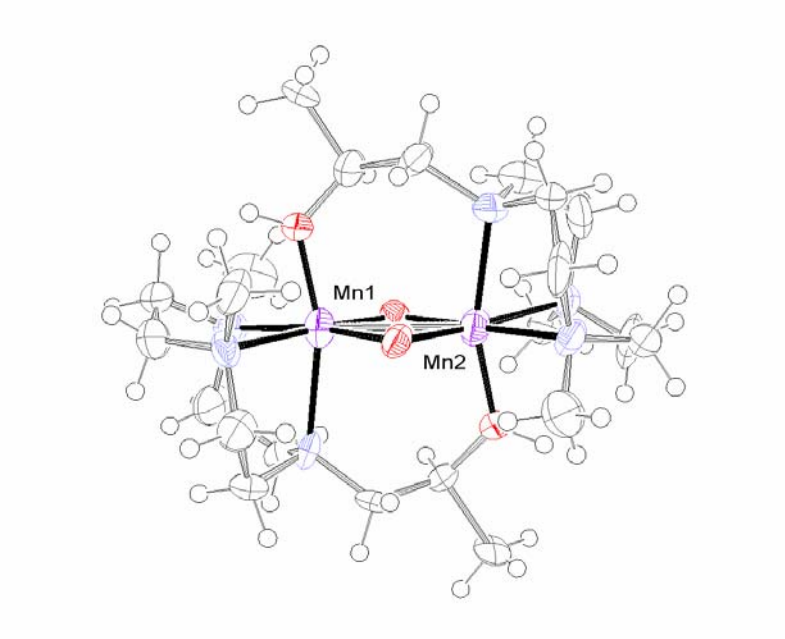

Figure 37. Ortep drawing of cation **Mn5S** in [**Mn5S**][PF_6]$_3$ at the 50% probability level. Hexafluorophosphate anions and acetone molecule are omitted for clarity

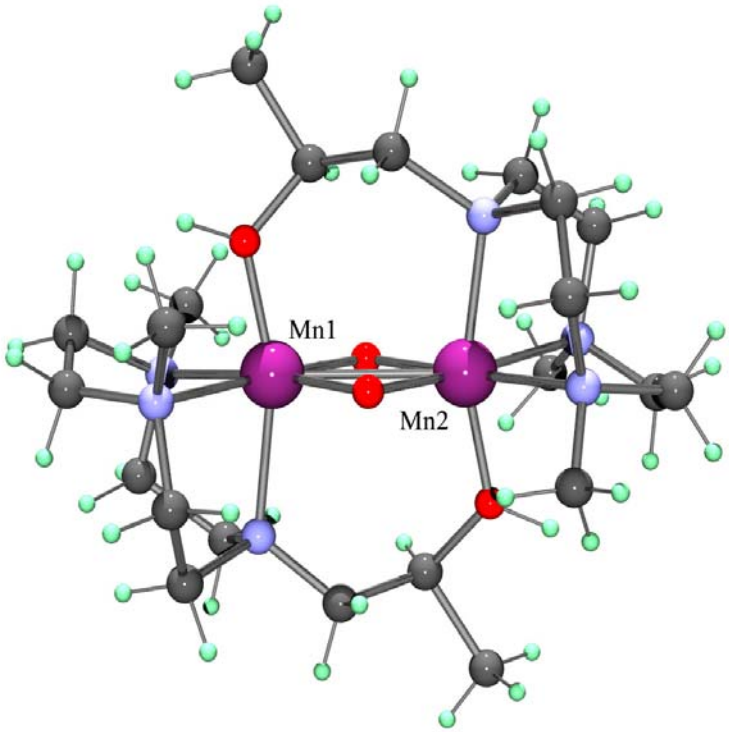

Figure 38. Structural representation of cation **Mn5S** showing coordination mode of the two manganese centers in [**Mn5S**][PF_6]$_3$. Hexafluorophosphate anions and acetone molecule are omitted for clarity

Table 11. Selected bond lengths (Å) and angles (°) for [**Mn5R**][PF_6]$_3$ · 0.5 · $(CH_3)_2CO$ and [**Mn5S**][PF_6]$_3$ · 0.5 · $(CH_3)_2CO$

	[**Mn5R**][PF_6]$_3$	[**Mn5S**][PF_6]$_3$
Interatomic distances		
Mn1-Mn2	2.699(2)	2.695(3)
Mn1-O1 (hydroxo)	1.813(7)	1.799(6)
Mn2-O2 (hydroxo)	1.794(7)	1.806(7)
Mn1-O3 (oxo)	1.784(8)	1.804(7)
Mn1-O4 (oxo)	1.763(9)	1.778(7)
Mn2-O3 (oxo)	1.846(11)	1.813(7)
Mn2-O4 (oxo)	1.836(9)	1.832(8)
Mn1-N (R^{1R} arm)	2.116(10)	2.176(10)
Mn1-N (Me)	2.142(16)	2.128(10)
Mn1-N (Me)	2.103(12)	2.100(9)
Mn2-N (R^{1R} arm)	2.145(9)	2.090(9)
Mn2-N (Me)	2.073(11)	2.155(10)
Mn2-N (Me)	2.138(12)	2.169(9)
Angles		
Mn1-O3-Mn2 (oxo)	96.0(3)	96.3(3)
Mn1-O4-Mn2 (oxo)	97.1(3)	96.5(3)
O1-Mn1-Mn2	99.7(4)	101.7(3)
O2-Mn2-Mn1	100.6(4)	101.5(3)

The molecular structures of the Mn(III)-Mn(IV) dioxo complexes $[(R^{1R}L\text{-}Me_2)_2Mn_2(O)_2]^{3+}$ (**Mn5R**) and $[(R^{1S}L\text{-}Me_2)_2Mn_2(O)_2]^{3+}$ (**Mn5S**), show a metal-metal distance of 2.699(2) and 2.695(3) Å, respectively. This distances are slightly longer then those in the isoelectronic Mn(III)-Mn(IV) cations $[(L\text{-}Me_2)_2Mn_2(O)_2(OOCH)]^{2+}$ (**Mn1**, 2.620(1) Å), $[(L\text{-}Me_2)_2Mn_2(O)_2(OOCMe)]^{2+}$ (**Mn3**, 2.628(4) Å) and $[L_2Mn_2(O)_2(OOCMe)]^{2+}$ (2.588(2) Å)

[136], but compares well to those in the dinuclear Mn(III)-Mn(IV) cation $[(L^t)_2Mn_2(O)_2]^{3+}$ (2.679(1) Å, L^t = 2,2',2"-triaminoethylamine) containing two bridging ethylenediamine and two oxo fragments between clearly distinguishable Mn(III) and Mn(IV) centers [145]. In our case the differentiation of Mn(III) and Mn(IV) centers is problematic, because the environment of the two manganese atoms (imposed by the triazacyclononane ring) is practically identical. The selected bond lengths and angles are listed in Table 11.

The **Mn5R** and **Mn5S** complexes were tested for the oxidation of isopropanol with hydrogen peroxide to give acetone in aqueous solution and in acetonitrile in the absence and in the presence of ascorbic or oxalic acid as co-catalysts at 20 °C. The results are shown in Table 12. In the absence of co-catalyst both complexes are more active in acetonitrile solution, however, in aqueous solution the accelerating effect of the added co-catalyst is more pronounced.

Table 12. Oxidation of isopropanol in water and acetonitrile, catalysed by the complexes **Mn5R**–**Mn5S** in the absence/presence of 0.01 M ascorbic acid or 0.02 M oxalic buffer in water, 0.02 M oxalic acid in acetonitrile as co-catalyst (20 °C, 1h, 1.0×10^{-4} M catalyst, 0.20 M isopropanol, 0.50 M H_2O_2)

Catalyst	TON (after 1h) in water			TON (after 1h) in acetonitrile		
	Without co-catalyst	With oxalate	With ascorbic acid	Without co-catalyst	With oxalate	With ascorbic acid
Mn5R	12	276	58	15	53	5
Mn5S	12	285	57	15	45	5

It is interesting to check the enantioselectivity of these two chiral dimanganese complexes in the oxidative kinetic resolution of racemic 1-phenylethanol to give acetophenone (Scheme 28). The results are shown in Table 13.

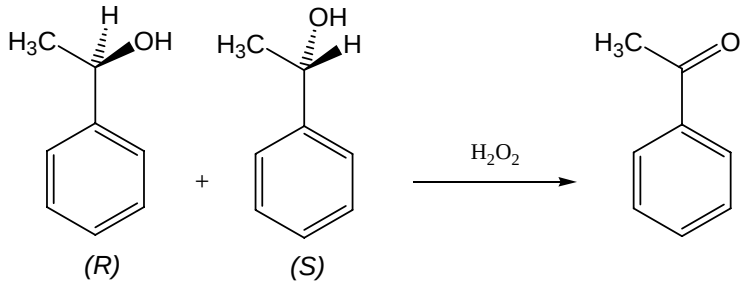

Scheme 28. Oxidative kinetic resolution of racemic 1-phenylethanol to give acetophenone

Even at low temperature (2 °C) there is no enantioselectivity observed for the oxidation of (*R*)- and (*S*)-1-phenylethanol. This means that both enantiomers are kinetically equivalent in the reactivity toward H-atom abstraction catalyzed by **Mn5R** and **Mn5S** both in the absence and in the presence of co-catalyst (including the chiral one – ascorbic acid). On the other hand, in the presence of oxalic and ascorbic acid the overall catalytic performance increases and attains 145 turnover numbers after 2 hours of the reaction in the case of **Mn5S** (Table 13).

Table 13. Oxidation of racemic 1-phenylethanol in H_2O/MeCN 50% v/v, catalysed by **Mn5R** and **Mn5S** complexes in the absence/presence of 0.3 mM ascorbic or 0.3 mM oxalate buffer as co-catalyst; $[catalyst]_o = 10^{-4}$ M, $[H_2O_2]_o = 0.20$ M, $[1\text{-phenylethanol}]_o = 0.05$ M, 2 °C; the absolute configuration of 1-phenylethanol, which is preferentially oxidized, is shown in brackets

Complex	Without co-catalyst			With oxalate			With ascorbate		
	ee %	conv. %	TON 2h	ee %	conv. %	TON 2h	ee %	conv. %	TON 2h
Mn5R	0.0	2.4	12	0.3 (*S*-)	29	145	0.1 (*R*-)	26	130
Mn5S	0.2 (*S*-)	2.4	12	0.1 (*S*-)	29	145	0.2 (*S*-)	26	130

The epoxidation of indene using **Mn5S** and **Mn5R** complexes reveals that in moist acetonitrile the catalytic activity and enantioselectivity is comparable to those observed for the parent *in situ* prepared manganese complexes with R^{1S}L-Me_2 and R^{1R}L-Me_2 ligands (Table 14, Figure 39). However, upon addition of ascorbic acid/sodium ascorbate **Mn5S** and **Mn5R** complexes are about 10 times more active and 3 times more selective with respect to the corresponding *in situ* prepared systems (Table 9, Table 14). In acetonitrile solution the catalytic activity and enantioselectivity of **Mn5S** and **Mn5R** complexes are low and upon addition of oxalic acid (500 equivalents with respect to the catalyst) only 2-indanone is observed with TONs 12 under the same conditions. This means that in acetonitrile solution the nature of the oxidizing species formed from **Mn5S** and **Mn5R** is substantially different from those derived from Wieghardt's type $[(L\text{-}Me_3)_2Mn_2(O)_3]^{2+}$ precursor, where oxalic acid dramatically increases the catalytic performance [112].

Table 14. Epoxidation of indene in MeCN and H_2O/MeCN 50% v/v mixtures, catalysed by **Mn5S** and **Mn5R** complexes in the absence/presence of 0.3 mM ascorbic or 0.3 mM oxalate buffer as co-catalyst; $[catalyst]_o = 10^{-4}$ M, $[H_2O_2]_o = 0.20$ M, $[indene]_o = 0.10$ M, 2 °C; 2 hours; the absolute configuration of indene oxide, which is preferentially formed, is shown in brackets

Complex	In acetonitrile			In water/acetonitrile (50/50 v/v)								
	Without co-catalyst			Without co-catalyst			With oxalate			With ascorbate		
	ee %	conv. %	TON	ee %	conv. %	TON	ee %	conv. %	TON	ee %	conv. %	TON
Mn5S	7 (1*R*,2*S*)	2.1	21	13 (1*R*,2*S*)	2.9	29	4.2 (1*R*,2*S*)	10.4	104	11 (1*R*,2*S*)	6.2	62
Mn5R	7 (1*S*,2*R*)	2.1	21	13 (1*S*,2*R*)	2.9	29	4.4 (1*S*,2*R*)	10.5	105	11 (1*S*,2*R*)	6.2	62

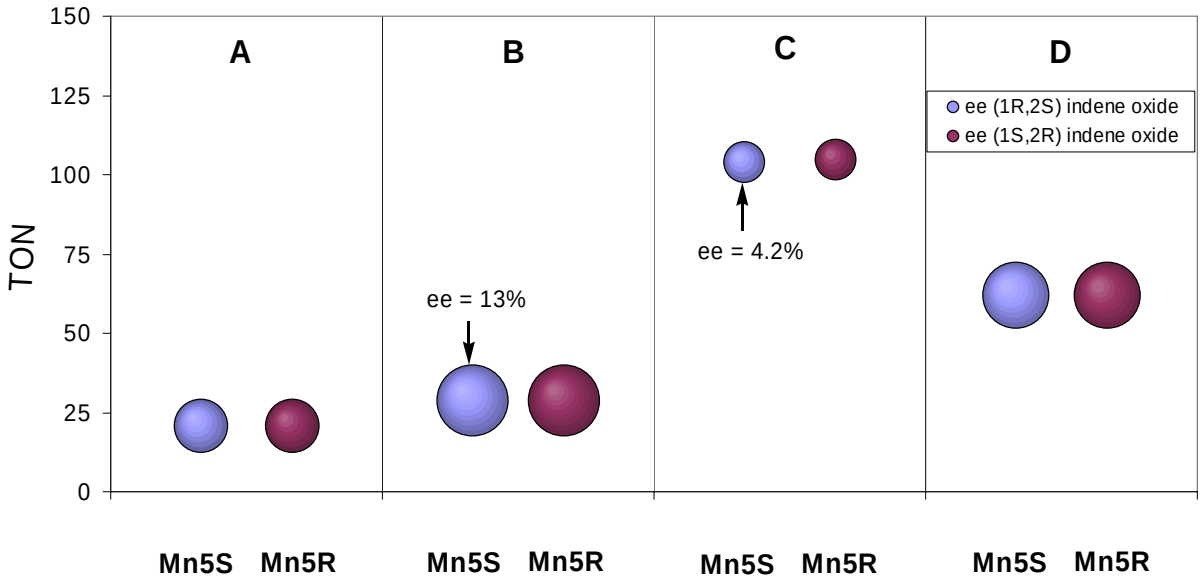

Figure 39. Activity and selectivity parameters in the indene epoxidation, catalysed by **Mn5S** and **Mn5R** complexes in MeCN (**A**) and H_2O/MeCN 50% v/v mixture in the absence (**B**) /presence of 0.3 mM oxalic (**C**) or 0.3 mM ascorbic buffer (**D**) as co-catalyst; $[catalyst]_o = 10^{-4}$ M, $[H_2O_2]_o$ = 0.20 M, $[indene]_o$ = 0.10 M, 2 °C; 2 hours; the values of enantiomeric excess (%) are proportional to the surface of the corresponding bubbles

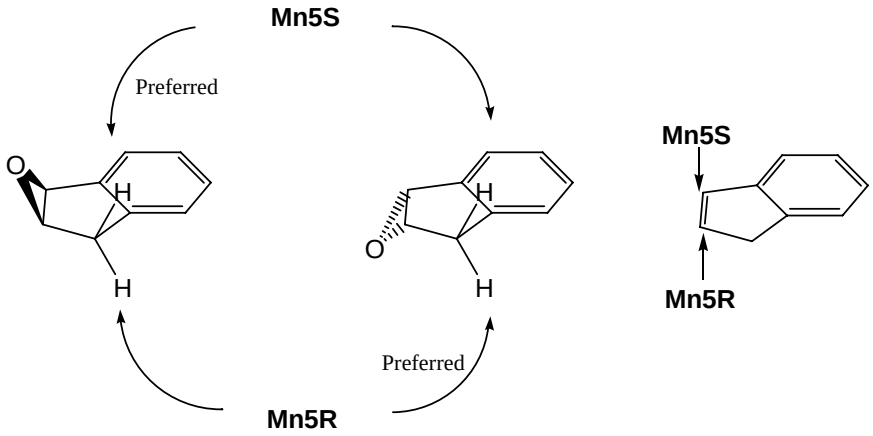

Figure 40. Stereoselectivity mnemonics for the epoxidation of indene with hydrogen peroxide using **Mn5S** and **Mn5R** complexes

Although the selectivity parameters for the epoxidation reaction with **Mn5S** and **Mn5R** are far from the practical applications, they represent one more example of the chiral high-valent manganese complexes with enantioselective properties in the catalytic oxidation with H_2O_2. Moreover, they provide additional insights into the oxidation mechanism and could serve as a basic model for the further catalyst design.

3.3.4 Oxidation of Alkanes Catalyzed by the Isolated Dinuclear Mn(III)-Mn(IV) Complex Containing Chiral (*R*)-1-(2-Hydroxypropyl)-4,7-Dimethyl Triazacyclononane Ligands

With the isolated compound $[(R^{1R}L\text{-}Me_2)_2Mn_2(O)_2][PF_6]_3$ (**[Mn5R][**$PF_6]_3$), we studied the oxidation of cyclohexane with hydrogen peroxide in acetonitrile solution at 25 °C.

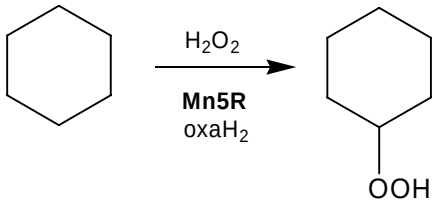

The oxidation of cyclohexane takes place only in the presence of a co-catalyst such as oxalic acid, and cyclohexyl hydroperoxide is formed as the major product (measured by using the triphenylphosphine method [146], Figure 41). The total catalyst turnover number attains 68 after 5 hours of the reaction.

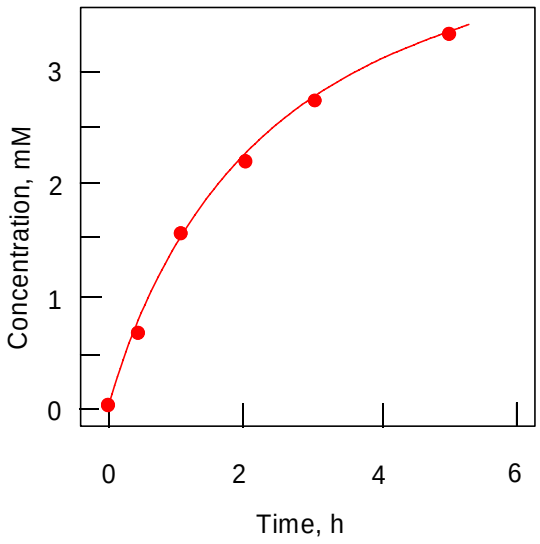

Figure 41. Accumulation of cyclohexyl hydroperoxide in the oxidation of cyclohexane (0.46 M) with H_2O_2 (0.6 M) in MeCN at 25 °C catalyzed by **Mn5R** (0.05 mM) and oxalic acid (0.05 M) measured with the triphenylphosphine method

In order to shed light on the nature of the oxidizing species generated from **Mn5R** upon addition of hydrogen peroxide, we studied also the oxidation of higher linear and branched alkanes (*n*-hexane, *n*-heptane, *n*-octane and isooctane). The selectivity parameters are given in Table 15. All parameters were measured after reduction of the reaction mixtures with

triphenylphosphine before the GC analysis and calculated based on the ratios of isomeric alcohols. The parameter C(1):C(2):C(3):C(4) indicates the relative normalized reactivities of hydrogen atoms at carbons 1, 2, 3 and 4 of the chain of unbranched alkanes (*i.e.*, calculated taking into account the number of hydrogen atoms at each carbon). The parameter 1°:2°:3° indicates the relative normalized reactivities of hydrogen atoms at primary, secondary and tertiary carbons of isooctane.

Table 15. Selectivity parameters in oxidation of alkanes in acetonitrile catalyzed by **Mn5R** in the presence of oxalic ($oxaH_2$) and acetic acid (AcOH)

System	C(1) : C(2) : C(3) : C(4)			1º : 2º : 3º
	n-Hexane	*n*-Heptane	*n*-Octane	Isooctane
Mn5R / $oxaH_2$	1 : 71 : 78	1 : 91 : 99 : 68	1 : 94 : 99 : 51	1 : 5 : 17
Mn5R / AcOH	1 : 42 : 43			1 : 3 : 20
$[(L\text{-}Me_3)_2Mn_2O_3]^{2+}/oxaH_2$		1 : 74 : 78 : 78		1 : 2 : 130
$[(L\text{-}Me_3)_2Mn_2O_3]^{2+}$/AcOH		1 : 46 : 35 : 35	1 : 29 : 25 : 24	1 : 8 : 40

Compared to the known catalytic systems $[(L\text{-}Me_3)_2Mn_2(O)_3]^{2+}/oxaH_2$ or $[(L\text{-}Me_3)_2Mn_2(O)_3]^{2+}$/AcOH [64, 109], which are believed to proceed via abstraction of hydrogen atoms from the alkane by a reactive Mn=O species, the selectivity parameters are similar, suggesting that also in the case of **Mn5R** the oxygenation occurs via reactive manganese-oxo species capable to discriminate between primary and secondary hydrocarbon bonds.

In the isooctane molecule, the secondary C–H bonds are surrounded by bulky *t*-butyl and *i*-propyl groups; therefore, the selectivity parameter 2°/1° reflects the sterical hindrance for the oxidizing species. Given the parameter (C(2):C(1))/(2°:1°) for **Mn5R** to be in the range from 12 to 18 (3−4 in the case of hydroxyl radicals [163]), we can assume that the oxidizing species generated from **Mn5R** have the pronounced sterical restrictions.

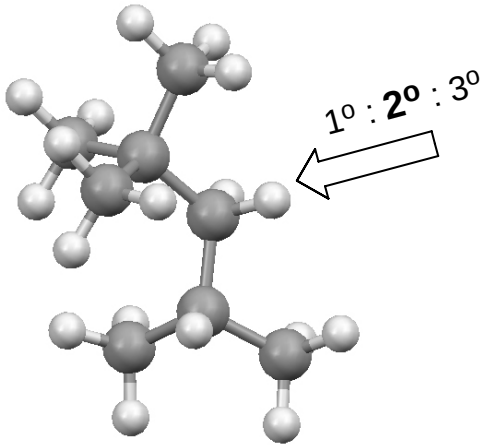

Figure 42. Selectivity parameter toward secondary C–H bonds in isooctane

The oxidation of *cis*- and *trans*-1,2-dimethylcyclohexane is a simple test for the reaction stereoselectivity (Figure 43). While retention of the stereochemical configuration is characteristic of a concerted reaction mechanism (in enzymes, however, the retention can be imposed by the active site geometry), loss of the stereochemical configuration is indicative of a nonconcerted mechanism, going through an intermediate.

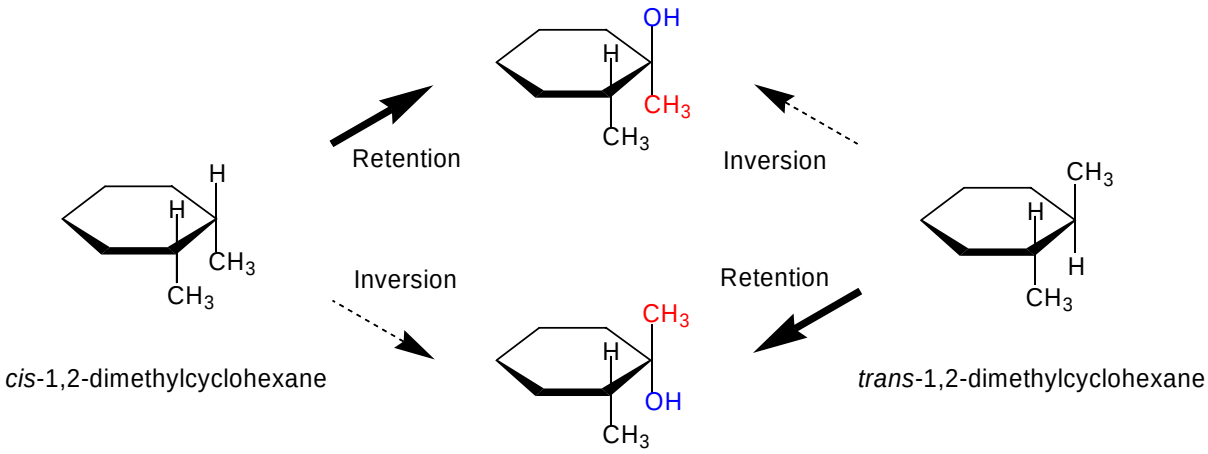

Figure 43. Stereoselectivity in the oxidation of *cis*- and *trans*-1,2-dimethylcyclohexane with H_2O_2 to give *cis*- and *trans*-1,2-dimethyl-cyclohexanol catalyzed by **Mn5R**

The selectivity parameters for the oxidation of *cis*- and *trans*-1,2-dimethylcyclohexane with H_2O_2, catalyzed by **Mn5R** in acetonitrile are given in Table 16. The parameter *trans*/*cis* indicates the ratio of *trans*- and *cis*-isomers of *tert*-alcohols formed in the reaction.

Table 16. Selectivity parameters in oxidation of cis- and trans-1,2-dimethylcyclohexane in acetonitrile catalyzed by **Mn5R** in the presence of oxalic ($oxaH_2$) and acetic acid (AcOH)

System	*Trans* / *cis* product ratio	
	From *cis*-1,2-dimethylcyclohexane	From *trans*-1,2-dimethylcyclohexane
Mn5R / $oxaH_2$	0.3	13
Mn5R / AcOH	0.7	45
$[(L\text{-}Me_3)_2Mn_2O_3]^{2+}/oxaH_2$	0.1	8
$[(L\text{-}Me_3)_2Mn_2O_3]^{2+}$/AcOH	0.35	4

In the oxidation of *trans*-1,2-dimethylcyclohexane the retention of configuration is unambiguous and is more pronounced in the case of acetic acid used as co-catalyst. In the oxidation of *cis*-1,2-dimethylcyclohexane, the retention of configuration is also observed, the *cis*-isomers of 1,2-dimethyl-1,2-cyclohexyldiol being preferentially formed; however, in the case of acetic acid as co-catalyst a significant amount of *trans*-isomers is also detected. In conclusion, we can assume that the oxidation occurs by a concerted reaction mechanism (hydrogen atom abstraction and hydroperoxydation taking place in a single step without formation of an intermediate), the high degree of the stereochemical retention being due to the implication of sterically hindered high-valent manganese-oxo species.

3.4 Conclusion

The manganese complexes containing 1,4,7-trimethyl-1,4,7-triazacyclononane ($L\text{-}Me_3$) are versatile catalysts for the oxidation of a wide range of organic functional groups by the clean oxidant H_2O_2.

Six new 1,4,7-triazacyclononane derived ligands have been synthesized and characterized. The corresponding manganese complexes prepared *in situ* show a significant catalytic activity in the oxidation of alcohols and the epoxidation of olefins with H_2O_2. The reactivity and the selectivity of the catalysts can be tuned: a) using oxalic and ascorbic acids, which act as coligands or/and reducing agents for the manganese centers, b) introducing a

functionality (carboxylato or hydroxo pendant arm) or/and chirality into the 1,4,7-triazacyclononane macrocycle. The manganese complex containing 3-(4,7-dimethyl-1,4,7-triazacyclononan-1-yl)propionate ligand **(**Pr-L-Me_2) shows the best performance in the oxidation of alcohols and in epoxidation of alkenes reported so far with H_2O_2; if no co-catalyst is added, the reaction proceeds smoothly in water under mild conditions. The MS-ESI spectra of the reaction mixture show that the propionato pendant arm in Pr-L-Me_2 has a strong tendency to bind two neighboring manganese centers and is capable of proton transfer during the oxidation. The catalytic activity could be tentatively attributed to the dinuclear manganese complexes with two carboxylato pendant arms bridging two manganese centers.

Five new dinuclear manganese complexes containing 1,4-dimethyl-1,4,7-triazacyclononane (**Mn1**–**Mn3**) and enantiomerically pure (*R*)- and (*S*)-1-(2-hydroxypropyl)-4,7-dimethyl-1,4,7-triazacyclononane **(Mn5R**, **Mn5S)** ligands have been isolated. The molecular structures of **Mn5R** and **Mn5S** provide the first examples of dinuclear manganese complexes bridged by two chiral pendant arms.

The epoxidation of indene with H_2O_2 using **Mn5S** or **Mn5R** as catalyst gives the mixture of (1*R*,2*S*)- and (1*S*,2*R*)-indene oxide with the enantiomeric excess up to 14.4%. Thus, the catalysts present one more example of the chiral high-valent manganese complexes with enantioselective properties in the catalytic oxidation with H_2O_2. The oxidation of linear and branched alkanes proceeds only in the presence of oxalic or acetic acid. The high degree of regio and stereoselectivity allow us to assume the oxidation to preferentially proceed via concerted mechanism with participation of high-valent manganese-oxo species as oxidizing species. Finally, **Mn5S** and **Mn5R** provide additional insights into the oxidation mechanism and can serve as a basic model for the further catalyst design.

4 Iron-Based Systems

Over the last decade a number of iron-based catalytic systems have been reported [38, 147, 148], some of them are capable of activating C–H bonds by a mechanism different from that involved in the classical Fenton chemistry (a radical autooxidation), giving rise to the formation of high-valent iron(IV) and iron(V) oxo species [37, 149, 150]. Since such species have been identified as the key oxidants in iron-containing enzymes [37, 15137], there is a growing interest in modelling enzyme active sites and in developing biomimetic alkane hydroxylation catalysts [152].

4.1 Modelling Metalloenzymes with Iron Complexes Containing Triazacyclononane-Derived Ligands: State of the Art

Iron complexes containing macrocyclic ligands with three nitrogen-donor atoms as well as carboxylato and oxo bridges have found much interest as model complexes relevant to biocatalysis [153, 154]. Thus, 1,4,7-triazacyclononane (L) was found to react with iron(III) chloride hexahydrate and ammonium acetate to give the dinuclear Fe(III)-Fe(III) complex $[L_2Fe_2(O)(OOCMe)_2]^{2+}$ [155] which has been described as model for the active centre of hemerythrin. Starting from 1,4,7-trimethyl-1,4,7-triazacyclononane (L-Me_3), iron(II) perchlorate hexahydrate and iron(III) chloride hexahydrate, the dinuclear Fe(II)-Fe(II) $[(L\text{-}Me_3)_2Fe_2(OH)(OOCMe)_2]^{+}$ and the corresponding Fe(III)-Fe(III) $[(L\text{-}Me_3)_2Fe_2(O)(OOCMe)_2]^{2+}$ are accessible [156]; they have been studied by S. Lippard as functional models for methane monooxygenase [157] (Scheme 29, see also Scheme 9). A mixed-valent Fe(III)-Fe(IV) complex $[L_2Fe_2(O)(OOCMe)_2]^{3+}$ can be generated electrochemically or chemically with aminyl radical cations at −30 °C in acetonitrile [158].

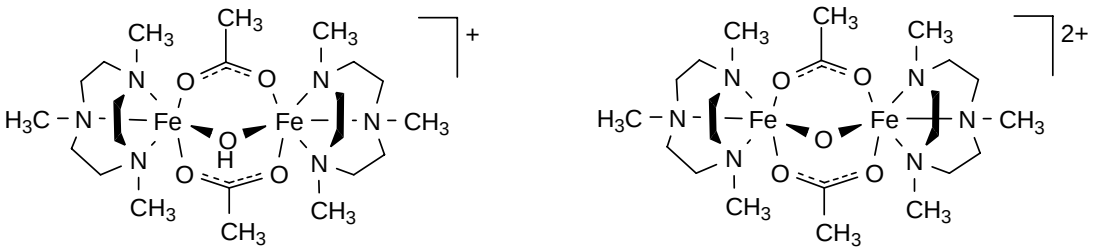

Scheme 29. Dinuclear Fe(II)-Fe(II) and Fe(III)-Fe(III) complexes containing 1,4,7-trimethyl-1,4,7-triazacyclononane (L-Me_3) ligand described as functional model for methane monooxygenase [157]

After the discovery of the catalytic activity of iron(III) complexes containing 1,4,7-trimethyl-1,4,7-triazacyclononane for low-temperature bleaching [159], the catalytic oxidation potential of this type of complexes has been demonstrated for the oxidation of phosphines [160] and sulfides [161] with dioxygen and benzylic groups with hydrogen peroxide [162]. In our laboratory it was showed that the presence of pyrazine-2-carboxylic acid strongly increases the catalytic oxidation potential of the dinuclear Fe(III)-Fe(III) complex $[L_2Fe_2(O)(OOCMe)_2]^{2+}$ [163], so that even alkanes, including ethane and methane can be oxidised with hydrogen peroxide in acetonitrile.

The synthesis of the Fe(III)-Fe(III) complexes $[L_2Fe_2(O)(OOCMe)_2]^{2+}$ and $[(L\text{-}Me_3)_2Fe_2(O)(OOCMe)_2]^{2+}$ from iron(III) chloride and L or L-Me_3 by a two-step procedure has been described by K. Wieghardt and co-workers. [155, 156]. With the analogous ligand 1,4-dimethyl-1,4,7-triazacyclononane (L-Me_2) we developed a simple one-pot synthesis of the Mn(III)-Mn(III) and Mn(III)-Mn(IV) complexes **Mn1**–**Mn4** (Chapter 3.3.1). We now extended this method to the synthesis of $(L\text{-}Me_2)_2Fe_2$ complexes containing various carboxylato bridges.

4.2 New Results with Dinuclear Iron Complexes Containing 1,4-Dimethyl-1,4,7-Triazacyclononane Ligands as well as Carboxylato and Oxo Bridges

Three dinuclear Fe(III)-Fe(III) complexes $[(L\text{-}Me_2)_2Fe_2(O)(OOCH)_2]^{2+}$ (**Fe1**), $[(L\text{-}Me_2)_2Fe_2(O)(OOCMe)_2]^{2+}$ (**Fe2**) and $[(L\text{-}Me_2)_2Fe_2(O)(OOCPh)_2]^{2+}$ (**Fe3**) have been obtained in moderate to good yields (Scheme 30).

All complexes **Fe1**–**Fe3** could be isolated as the hexafluorophosphate salts, which are well soluble in acetone and acetonitrile, but sparingly soluble in ethanol, isopropanol and water. The Fe–O–Fe deformation modes for **Fe2** (725 cm^{-1}) and for **Fe3** (724 cm^{-1}), observed in the infrared spectra, are comparable to those in $[L_2Fe_2(O)(OOCMe)_2]^{2+}$ (730 cm^{-1}) [155], whereas for **Fe1** it is shifted to 750 cm^{-1}. In the UV/vis spectra, the acetonitrile solutions of **Fe1**–**Fe3** show three intense absorption maxima (**Fe1**: 240, 339 and 474 nm, **Fe2**: 230, 341 and 473 nm, **Fe3**: 237, 338, and 476 nm).

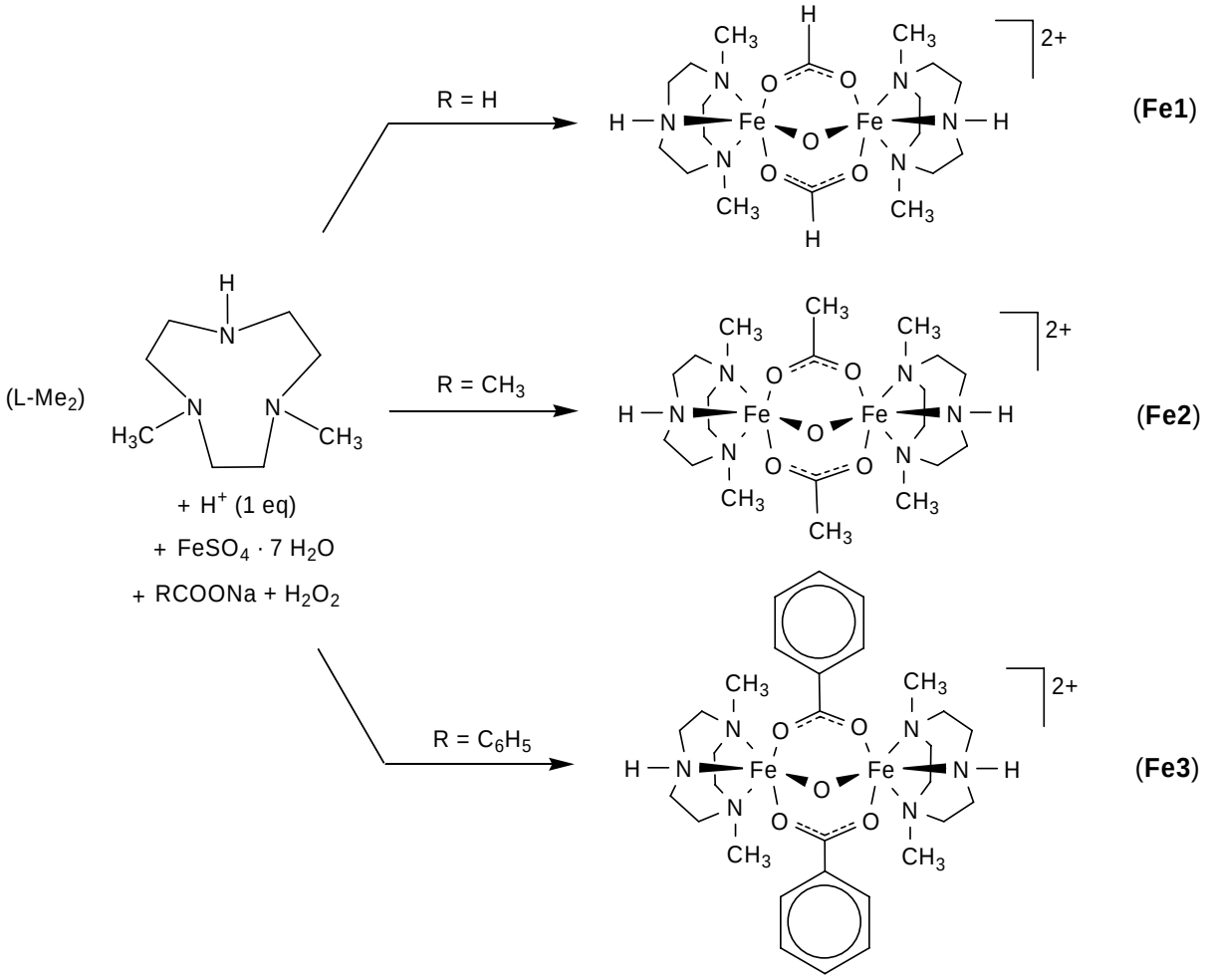

Scheme 30. Reaction of 1,4-dimethyl-1,4,7-triazacyclononane (L-Me_2) with iron(II) sulfate heptahydrate in the presence of hydrogen peroxide and the corresponding sodium carboxylate

The molecular structure of **Fe2**, solved by single-crystal X-ray structure analysis of the hexafluorophosphate salt presents two iron(III) centers linked by two acetato bridges and by an oxo bridge. Iron centers are facially coordinated to a L-Me_2 ligand through the three

nitrogen atoms. For the orange crystals of [**Fe2**][PF_6]$_2$ (Figure 44) a Fe–Fe distance equals to 3.104(1) Å, which compares well to the isoelectronic Fe(III)-Fe(III) cations [(L-Me_3)$_2$$Fe_2$(O)(OOMe)$_2$]$^{2+}$ [3.12(4) Å] [156] and [(L-Me_3)$_2$$Fe_2$(O)(OOC^{t}Bu)$_2$]$^{2+}$ [3.121(2) Å] [164].

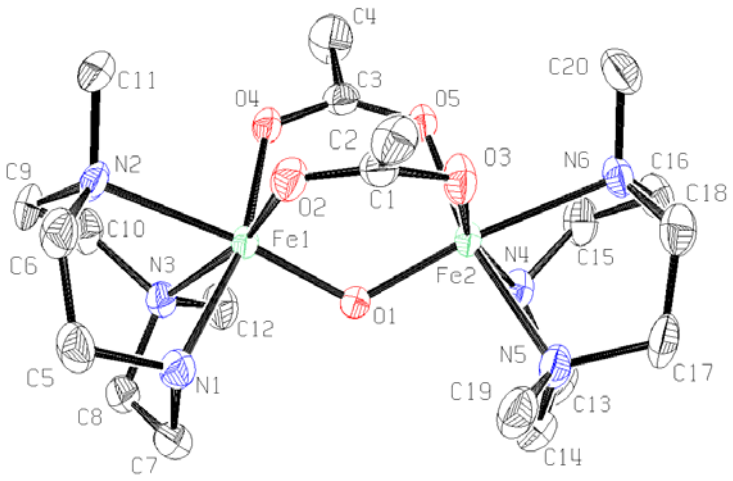

Figure 44. The molecular structure of [(L-Me_2)$_2$$Fe_2$(O)(OOCMe)$_2$]$^{2+}$ (**Fe2**), displacement ellipsoids are drawn at the 50% probability level, hydrogen atoms and hexafluorophosphate molecules are omitted for clarity. Selected bond lengths (Å) and angles (º): Fe(1)-Fe(2) 3.1038(11), Fe(1)-N(1) 2.151(5), Fe(1)-N(2) 2.243(5), Fe(1)-N(3) 2.193(5), Fe(2)-N(4) 2.159(5), Fe(2)-N(5) 2.197(5), Fe(2)-N(6) 2.252(5), Fe(1)-O(1) 1.788(4), Fe(2)-O(1) 1.796(4), Fe(1)-O(2) 2.027(4), Fe(1)-O(4) 2.023(4), Fe(2)-O(3) 2.018(4), Fe(2)-O(5) 2.040(4); Fe(1)-O(1)-Fe(2) 120.0(2), O(2)-C(1)-O(3) 124.6(6), O(4)-C(3)-O(5) 125.0(6).

Interestingly, **Fe2** complex shows intermolecular interactions with the hexafluorophosphate anions, owing to the presence of an N-H moiety within the ligand L-Me_2. In [**Fe2**][PF_6]$_2$ the distances between the nitrogen atoms and the fluorine atoms of the hexafluorophosphate anion vary from 2.998(7) to 3.285(7) Å with N-H···F angles of 165.3 and 132.3° respectively.

We studied the catalytic potential of the complexes **Fe1**–**Fe3** for the oxidation of isopropanol with hydrogen peroxide to give acetone. The oxidation reaction was carried out in aqueous solution or acetonitrile in the presence of ascorbic acid at 20 °C. Ascorbic acid was used as a co-catalyst, it may act as proton donor and as reducing agent. Reducing agents are obligatory components for oxygenation in most of the biologically active systems [1]. The results are shown in Table 17.

Table 17. Oxidation of isopropanol in water and acetonitrile, catalyzed by the complexes **Fe1**–**Fe3** in the absence/presence of ascorbic acid as co-catalyst (20 °C, 1h, 1.0×10^{-4} M $FeCl_2$, complex **Fe1**–**Fe3**, 0.20 M isopropanol, 0.50 M H_2O_2)

Catalyst	TON (after 1h) in water		TON (after 1h) in acetonitrile	
	no co-catalyst	with ascorbic acid	no co-catalyst	with ascorbic acid
$FeCl_2$	5	243	2	37
Fe1	17	274	5	29
Fe2	9	320	3	32
Fe3	6	306	3	34

The highest catalytic activity was observed for $[(L\text{-}Me_2)_2Fe_2(O)(OOCMe)_2]^{2+}$ (**Fe2**) in the presence of ascorbic acid in water, the TON being 320 after 1 hour at 20 °C, which is considerably higher than that of the analogous manganese complex $[(L\text{-}Me_2)_2Mn_2(O)(OOCMe)_2]^{2+}$ (**Mn4**), for which a TON of 67 was observed under the same conditions (Chapter 3.3.1).

The dinuclear Fe(III)-Fe(III) complexes **Fe1**–**Fe3** can be effectively reduced with ascorbic acid in aqueous solution at room temperature. In the case of $[(L\text{-}Me_2)_2Fe_2(O)(OOCMe)_2]^{2+}$ (**Fe2**), the intensity of the absorption at 475 nm is reduced by a factor of 10 upon addition of ascorbic acid (Figure 45), while a new band centered around 590 nm appears with an isosbestic point at 530 nm.

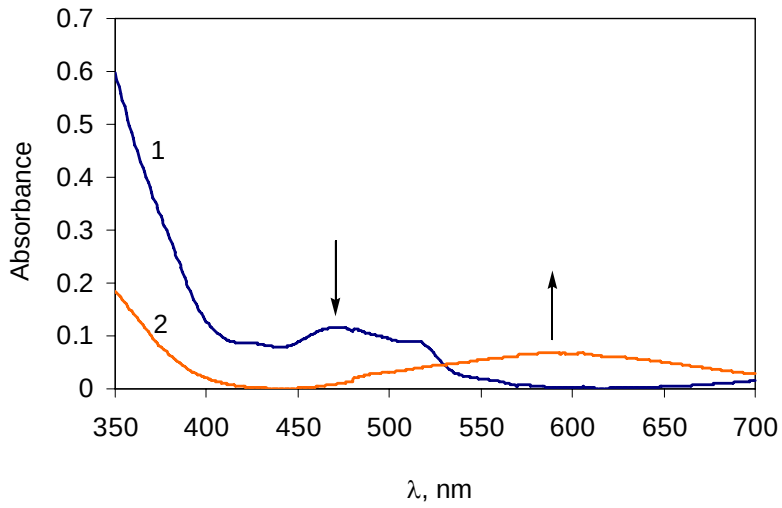

Figure 45. UV/vis spectrum of $[(L\text{-}Me_2)_2Fe_2(O)(OOCMe)_2]^{2+}$ (**Fe2**) (1.0×10^{-4} M) in the absence (**1**) and presence (**2**) of ascorbic acid (1.0×10^{-2} M, 20 °C, 5 min, H_2O)

All complexes **Fe1**–**Fe3** in combination with ascorbic acid as co-catalyst are much more active in water than in acetonitrile (Table 17), in line with the complexes $[(L\text{-}Me_2)_2Mn_2(O)(OOCMe)_2]^{2+}$ (**Mn4**) and $[(L\text{-}Me_2)_2Mn_2(O)(OOCPh)_2]^{2+}$ (**Mn2**) in combination with oxalic or ascorbic acid as co-catalyst (Chapter 3.3.1).

4.3 Toward Methane Monooxygenase: Complexation of Iron with 1,4-Dimethyl-1,4,7-Triazacyclononane Containing a Pendant Carboxylato Arm

Soluble methane monooxygenase (sMMO), isolated from methanotrophic organisms catalyzes the transformation of methane into methanol using molecular oxygen as the oxidant in the presence of biological reducing agent NADH. A great variety of alkanes and alkenes are also substrates for sMMO [165]. Hydrogen peroxide can be used as the oxidant, with no need for a reducing agent.

Polynuclear iron complexes containing oxo and carboxylato bridges reported as structural models for sMMO proved to have the potential in the catalytic alkane hydroxylation with hydrogen peroxide, alkylhydroperoxides or peracids [150, 151, 166]. However, the efficiency of these systems is still very low: The catalysts turnover numbers do not exceed 30 in the methane oxidation [1, 163]. Moreover, the reaction mixture usually contains a large excess of the reducing agent that effectively competes with the substrate. In order to avoid this problem, in sMMO the metal site and the substrate binding site are close [52, 151], resulting in a very high local substrate concentration with a finely tuned electrons flow.

In an effort to approach this situation, we decided to use the polydentate ligand Ac-L-Me_2, containing both carboxylate and nitrogen chelating moieties, which can mimic the aspartate-glutamate-histidine coordination environment in sMMO (the sMMO active site is shown in Scheme 9).

4.3.1 Syntheses and Characterization

Iron(II) sulfate heptahydrate reacts readily with Ac-L-Me_2 ligand in moist ethanol and, after the subsequent oxidation with hydrogen peroxide, the resulting brown-green product can be extracted into acetonitrile. Upon standing for a week at room temperature, two iron(III)

complexes can be isolated from this solution by column chromatography on silica in the form of the hexafluorophosphate salts. The green fraction represents the tetranuclear $[(Ac\text{-}L\text{-}Me_2)_4Fe_4(O)_2]^{4+}$ (**Fe4**) complex, while the major product crystallizes as a brown-orange dinuclear Fe(III)-Fe(III) complex considered to be $[(Ac\text{-}L\text{-}Me_2)_2Fe_2(O)(OOCMe)]^{+}$ (**Fe5**), see Scheme 31. A similar interconversion of the dinuclear iron(III) complex $[Fe_2L'_2(O)(OOCMe)]$ into the tetranuclear $[Fe_4L'_4(O)_2]$ complex containing ethylenediamine diacetate derived ligand (L' = *N,N'*-bis(3,4,5-trimethoxybenzyl)-ethylenediamine *N,N'*-diacetate) in moist acetonitrile has been reported by S. Ménage *et al*. [167]. Later, an analogous phenomenon was observed with tripodal tetradentate pyridyl-amino acid ligands [168, 169].

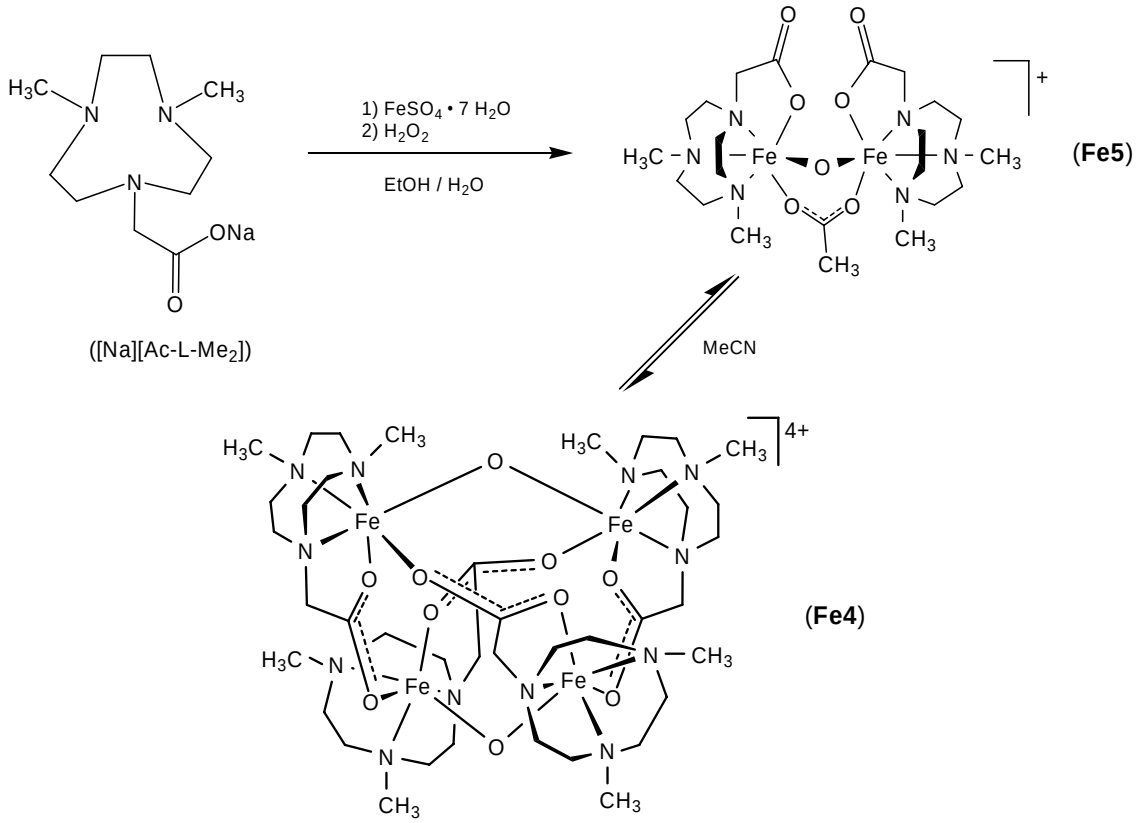

Scheme 31. Reaction of sodium 2-(4,7-dimethyl-1,4,7-triazacyclononan-1-yl) acetate ([Na][Ac-L-Me_2]) with iron(II) sulphate heptahydrate in the presence of hydrogen peroxide

Green X-ray quality crystals of [**Fe4**][PF_6]$_4$ · 5 MeCN were obtained by slow diffusion of ether into an acetonitrile solution containing **Fe4**. A microcrystalline brown-orange powder of [**Fe5**][PF_6] · 2 KPF_6 was obtained by slow diffusion of ether into an acetone solution containing **Fe5**. The molecular structure of **Fe4** is shown in Figure 46, selected bond lengths and angles are given in Table 18.

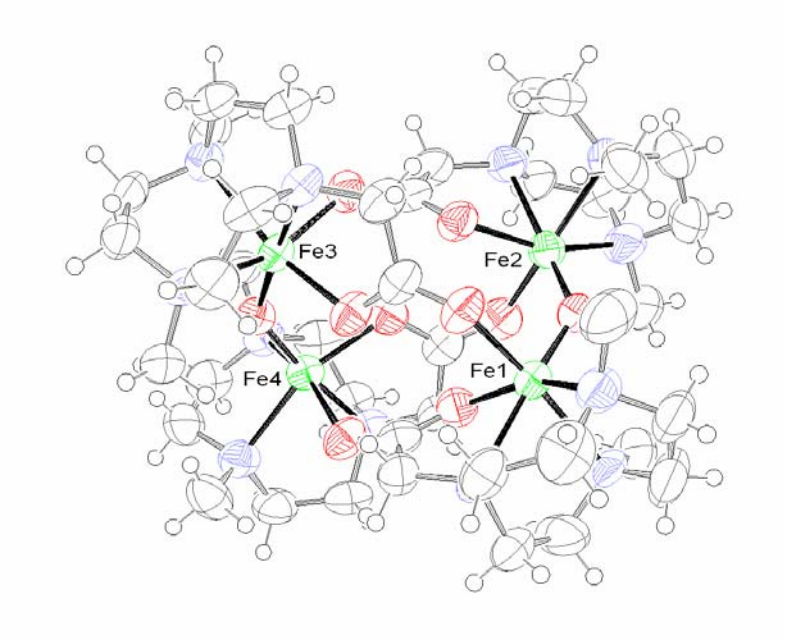

Figure 46. The molecular structure of $[(Ac\text{-}L\text{-}Me_2)_4Fe_4(O)_2]^{4+}$ (**Fe4**) in [**Fe4**][PF_6]$_4$ · 5 MeCN, displacement ellipsoids are drawn at the 50% probability level, MeCN and hexafluorophosphate molecules are omitted for clarity.

Table 18. Selected bond lengths (Å) and angles (°) for [**Fe4**][PF_6]$_4$ · 5 MeCN

	Fe(1)	Fe(2)	Fe(3)	Fe(4)
Interatomic distances				
Fe-Fe (through oxo)	3.347	3.347	3.328	3.328
Fe-Fe (through acetato)	5.324	5.330	5.334	5.337
Fe-O (oxo)	1.803(5)	1.803(6)	1.805(5)	1.791(5)
Fe-O (own acetato)	1.997(5)	1.997(6)	2.002(5)	1.991(5)
Fe-O (bridged acetato)	2.092(6)	2.071(6)	2.064(6)	2.086(6)
Fe-N (acetato substituted)	2.269(6)	2.271(7)	2.257(6)	2.250(6)
Fe-N (Me)	2.179(7)	2.175(7)	2.189(6)	2.197(7)
Fe-N (Me)	2.207(6)	2.208(7)	2.211(6)	2.204(6)
Angles				
Fe-O-Fe (oxo)	136.2(8)	136.2(8)	135.4(5)	135.4(5)
O-C-O (own acetato arm)	122.7(5)	123.8(7)	123.9(9)	122.7(1)

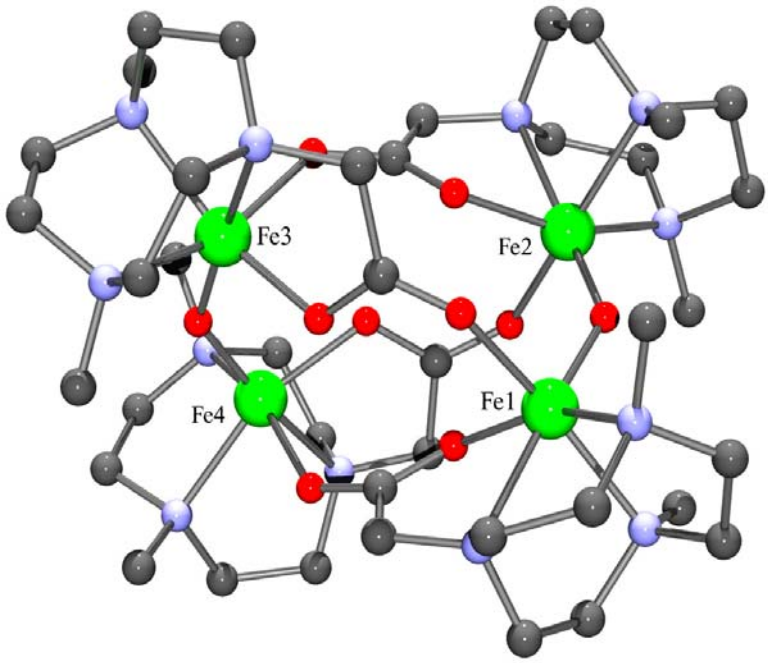

Figure 47. Simplified structural picture of **Fe4** showing coordination mode of the four iron(III) centers in [**Fe4**][PF_6]$_4$ · 5 MeCN; hydrogen atoms, MeCN and hexafluorophosphate molecules are omitted for clarity

A single-crystal X-ray structure analysis of [**Fe4**][PF_6]$_4$ · 5 MeCN reveals **Fe4** to contain four iron(III) centers (Figure 47), each of which being coordinated to three nitrogen atoms of a triazacyclononane ligand, and each of which being bridged by one oxo and by two carboxylato bridges, a structural feature known from the active center of methane monooxygenase [54]. The tetrairon core represents a tetrahedron with two short edges (μ-oxo-bridges) and four long ones (μ-carboxylato-bridges). Fe–Fe distances of the oxo-bridged iron(III) centers are in the range of 3.328–3.347 Å, which are longer than those in the dinuclear Fe(III)-Fe(III) cations [(L-Me_2)$_2$$Fe_2(O)(OOCMe)_2]^{2+}$ (**Fe2**) [3.104(1) Å] and [(L-Me_3)$_2$$Fe_2(O)(OOCMe)_2]^{2+}$ [3.12(4) Å] [156], but compare well to those in tetranuclear [Fe_4L'$_4$$(O)_2$] [3.389(4) Å] [167]. The Fe–N (acetato substituted) bonds are always in *trans* coordination to the oxo bridge and they are slightly lengthened relative to those *trans* to the acetato bridges due to the greater *trans* influence of the oxo bridge. Furthermore, in **Fe4** the Fe–O–Fe angles of the μ-oxo-bridges are in the range of 135.4(5)–136.2(8)^o, which are substantially larger than those in dinuclear **Fe2** [120.0(2)^o], but comparable to 142.7(7)^o in the tetranuclear [Fe_4L'$_4$$(O)_2$] complexes [167]. This means, that upon dimerization of the dinuclear Fe(III)-Fe(III) precursor the μ-oxo-bridges adopt a more "open" configuration, reflecting also the constraints imposed by two carboxylato bridge moieties. The tetranuclear

structure of **Fe4** is quite unique and represents a new example of the binding versatility of carboxylates.

The ESI-MS spectrum of **Fe4** in acetone shows the parent peak at *m/z* 575 ([(Ac-L-Me_2)$_2$$Fe_2$(O) + H + H_2O]$^{3+}$), in line with the tetrameric iron(III) core rupture observed in ESI-MS spectra for analogous complexes [167, 169]. Absorptions at 753 cm^{-1} and 773 cm^{-1}, observed in the infrared spectrum, can be ascribed to the asymmetric Fe–O–Fe stretch modes, which are shifted to the high values as compared with those for the dinuclear complexes **Fe2** (725 cm^{-1}) and **Fe3** (724 cm^{-1}). This can be rationalized by the fact that the energy of vibration increases as the Fe–O–Fe angle increases [170, 171]. Therefore, in the more "open" configuration of **Fe4** these resonances should have higher values. The ν_{as}(C–O) stretching frequency for **Fe4** is observed at 1622 cm^{-1}, while ν_s(C–O) frequency appears at 1407 cm^{-1}. The UV/vis spectrum shows for the acetonitrile solutions of **Fe4** the absorption maxima around λ (ε, M^{-1} cm^{-1}) 578 (300), 501 (670), 491 (710), 325 (24500) nm.

The brown microcrystalline product, [**Fe5**][PF_6] · 2 KPF_6, is considered to be [(*N_3O*-Ac-L-Me_2)$_2$$Fe_2$(μ-O)(μ-OOCMe)][$PF_6$] · 2 KPF_6 on the basis of the analytical and spectroscopic data, by analogy to the known compound [(*N_3O*-Ac-L)$_2$$Fe_2$(μ-O)(μ-OOCMe)][$ClO_4$] · $NaClO_4$ · 2 H_2O, containing the non-methylated ligand Ac-L instead of Ac-L-Me_2, for which the molecular structure is known by single-crystal X-ray analysis [172].

The presence of an acetato bridge in **Fe5** is surprising, since in the reaction of $FeSO_4$ · 7 H_2O with Ac-L-Me_2 in aqueous ethanol, which yields **Fe4** and **Fe5**, no acetate is added. However, we found that, upon addition of hydrogen peroxide to the aqueous ethanol solution of Fe^{2+}/Ac-L-Me_2 followed by stirring in air for 2 hours at room temperature, a significant quantity of acetic acid is formed (detected after acidification and GC analysis), which apparently originates from the iron-catalyzed oxidation of ethanol.

The NMR spectra of paramagnetic dinuclear Fe(III)-Fe(III) complexes containing L, L-Me_3 ligands as well as acetato and oxo bridges have been reported and interpreted using labelling experiments [173]. The strong coupling between the iron(III) centers causes the smaller range of chemical shifts (from 0 to +35 ppm) as compared to the analogous Mn(III)-Mn(III) complexes (from –160 to +120 ppm). The ^{1}H NMR (400 MHz) spectrum of **Fe5** in CD_3CN is shown in Figure 48.

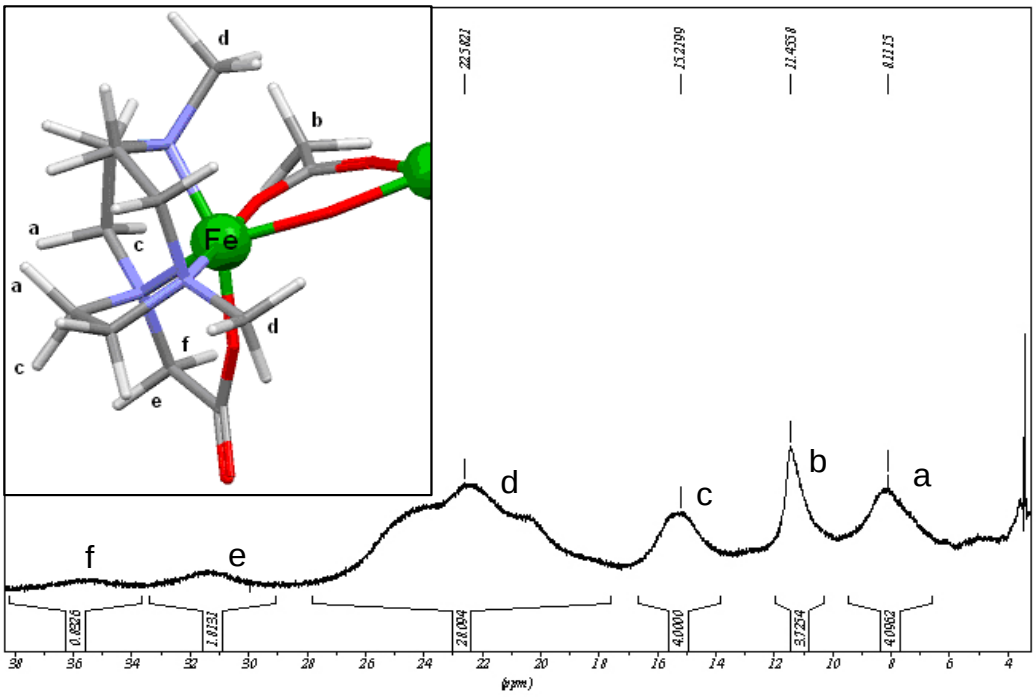

Figure 48. ^{1}H NMR spectrum of the paramagnetic complex [(Ac-L-Me_2)$_2$$Fe_2$(O)(OOCMe)][$PF_6$] ([**Fe5**][$PF_6$]) measured in CD_3CN at 27 °C

The sharp resonance at δ 11.5 ppm (b) corresponds to the methyl group of the bridging μ-acetato ligand and compares well to δ 11.4 ppm reported for those in [(L-Me_3)$_2$$Fe_2(O)(OOCMe)_2]^{2+}$ and [$L_2Fe_2(O)(OOCMe)_2]^{2+}$ [173]. Since three N-CH_3 moieties of the macrocycle ligand in [(L-Me_3)$_2$$Fe_2(O)(OOCMe)_2]^{2+}$ are not equivalent, one of the methyl groups that is *trans* coordinated with respect to the oxo bridge gives rise to the upfield signal around 14.8 ppm [173]. The resonance around δ 15.2 ppm in the spectrum of **Fe5** we assign to four "axial" methylene protons (c) near the nitrogen atoms *trans*-coordinated to the oxo bridge, which are more deshielded than the four "equatorial" methylene protons (a) with δ 8.1 ppm. This assumption is consistent with the relative intensities of these resonances as well with the literature data [173, 174] and the X-ray analyses of [**Fe4**][PF_6]$_4$ · 5 MeCN and [(N_3O-Ac-L)$_2$$Fe_2$(μ-O)(μ-OOCMe)][$ClO_4$] · $NaClO_4$ · 2 H_2O. Two broad resonances centered around δ 31.5 and 35.5 ppm can be attributed to the equatorial (e) and axial (f) methylene protons of the pendant acetato arms, the axial ones being more deshielded and expected to be shifted to downfield values. Due to the significant overlap between the signals from 18 to 28 ppm (d) the detailed assignment is problematical, but N-methyl protons (non-equivalent, near δ 22 ppm [173]) as well as the other methylene protons in the Ac-L-Me_2 ligand can be assigned to the signal d.

The ESI-MS spectrum of **Fe5** in acetonitrile shows the parent peak at *m/z* 634 (70%, [**Fe5** + H + H_2O]$^{2+}$) and minor peaks at *m/z* 651 (10%, [**Fe5** + 2 H_2O]$^{+}$), 615 (10%, [**Fe5**]$^{+}$), 416 (10%, [**(**Ac-L-Me_2)Fe + PF_6]$^{+}$). Absorptions at 781 cm^{-1} and 740 cm^{-1}, observed in the infrared spectrum, can be assigned to the asymmetric Fe−O−Fe stretch modes, shifted to higher values as those in dinuclear **Fe2** (725 cm^{-1}) and **Fe3** (724 cm^{-1}), but are comparable to those in **Fe4**. Since the vibration energies are indicative of the Fe−O−Fe angle parameters, we can assume that in **Fe5** the Fe−O−Fe angle falls in the range from 130 to 135° (129° in [(Ac-L)$_2$$Fe_2$(O)(OOCMe)]$^{+}$ and 136° in **Fe4**). The ν_{as}(C−O) stretching frequency of the bridging acetate in **Fe5** is observed at 1578 cm^{-1}, ν_s(C−O) frequency appears at 1466 cm^{-1}, while bands at 1646 and 1359 cm^{-1} are due to the monodentate pendant carboxyl groups of the ligand. These bands are shifted by 10−30 cm^{-1} to higher values as compared to those in [(Ac-L)$_2$$Fe_2$(O)(OOCMe)]$^{+}$, which could indicate incorporation of voluminous KPF_6 ion pairs between two acetato pendant arms. The UV/vis spectra of **Fe5** and [(Ac-L)$_2$$Fe_2$(O)-(OOCMe)]$^{+}$ are very similar [172], in acetonitrile both complexes show absorption maxima around λ (ε, for **Fe5**, M^{-1} cm^{-1}) 663 (160), 503 (1040), 449 (1600), 421 (1800), 326 (15500) nm. The elemental analysis of [**Fe5**][PF_6] · 2 KPF_6 gives 23.22% (C), 3.80% (H) and 7.25% (N), as compared to the calculated values of 23.40, 3.93 and 7.44% respectively.

4.3.2 Iron Complexes as Alcohol Oxidation Catalysts

We studied the catalytic activity of **Fe4** and **Fe5** for the oxidation of isopropanol with hydrogen peroxide to give acetone. The reaction was carried out in aqueous solution or acetonitrile in the absence and in the presence of ascorbic or pyrazin-2-carboxylic acid at 20 °C. The results are shown in Table 19.

The highest catalytic activity was observed for [(Ac-L-Me_2)$_4$$Fe_4$$(O)_2$]$^{4+}$ (**Fe4**) in the presence of pcaH in water, the TON being 463 after 1 hour at 20 °C. If added to the catalytic mixture, pcaH significantly suppresses the catalase activity of **Fe4** and **Fe5**, apparently it acts as a co-ligand to the iron centers. Surprisingly, the oxidation activity of **Fe4** and **Fe5** are close, regardless of the difference in the number of iron centers per molecule. Both complexes are much more active in water than in acetonitrile solution.

Table 19. Oxidation of isopropanol in water and acetonitrile, catalysed by the complexes **Fe4** and **Fe5** in the absence/presence of 0.001 M pyrazine-2-carboxylic acid (pcaH) or 0.01 M ascorbic acid (ascH) as co-catalyst (20 °C, 1h, 1.0×10^{-4} M $FeCl_2$, **Fe4**, **Fe5**, 0.20 M isopropanol, 0.50 M H_2O_2)

Catalyst	TON (after 1h) in water			TON (after 1h) in acetonitrile		
	without co-catalyst	with pcaH	with ascH	without co-catalyst	with pcaH	with ascH
$FeCl_2$	5	56	243	2	26	37
Fe4	226	463	301	26	19	40
Fe5	190	431	268	16	9	42

In aqueous solution **Fe4** and **Fe5** efficiently catalyze isopropanol oxidation without any co-catalyst added due to the presence of the pendant acetato arm within the macrocyclic ligand. Indeed, complexes **Fe1**–**Fe3** containing only bridging carboxylato groups are almost inactive in the absence of co-catalyst. With ascorbic acid as co-catalyst all five iron complexes as well as iron(II) chloride give comparable TONs, regardless of the nature and the quantity of iron centers. Therefore, we can assume that in the oxidation of isopropanol, ascH acts preferentially as a stoichiometric reducing agent.

4.3.3 Oxidation of Higher Alkanes

We studied at first the oxidation of cyclohexane with hydrogen peroxide catalyzed by **Fe4** and **Fe5** in acetonitrile solution at 25 °C.

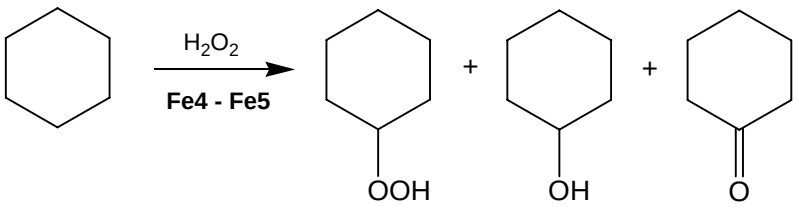

In the case of **Fe5**, the oxidation takes place during the initial period of 15 minutes, cyclohexyl hydroperoxide being the major product of the reaction (curve *1*, Figure 49). However, after this period the oxygenase activity of the complex is blocked and a slow decomposition of cyclohexyl hydroperoxide into the mixture of cyclohexanol (curve *2*) and cyclohexanone (curve *3*) is observed. Presumably, this decomposition is catalyzed by an iron

complex generated from **Fe5** in the course of the reaction, cyclohexanol is predominantly formed with the alcohol/ketone ratio about 10, the total catalyst turnover number attains 13.

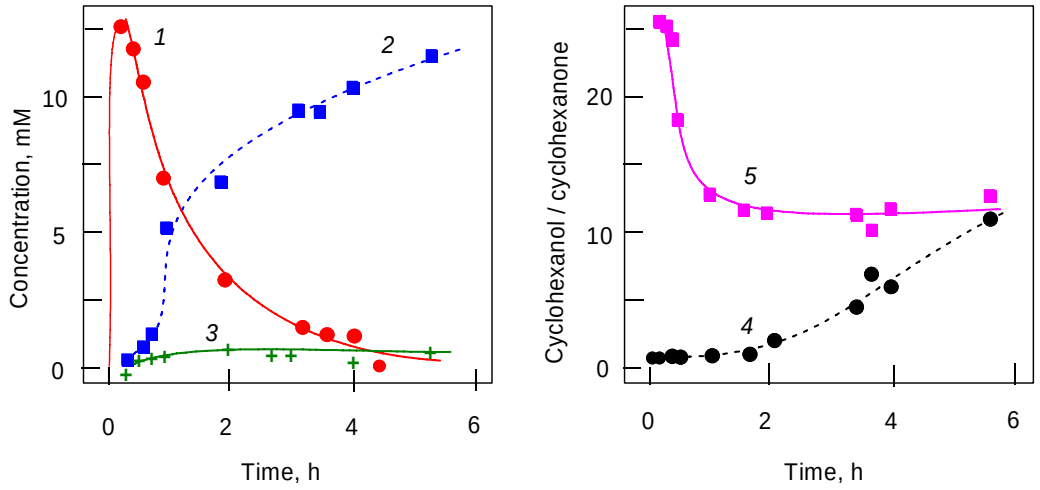

Figure 49. Oxidation of cyclohexane (0.46 M) with H_2O_2 (0.6 M) in MeCN at 25 °C catalyzed by complex **Fe5** (1 mM); the following curves are shown: accumulation of cyclohexyl hydroperoxide (curve *1*), cyclohexanol (*2*), cyclohexanone (*3*) as well as the alcohol/ketone ratio measured before (*4*) and after (*5*) the reduction of the samples with triphenylphosphine

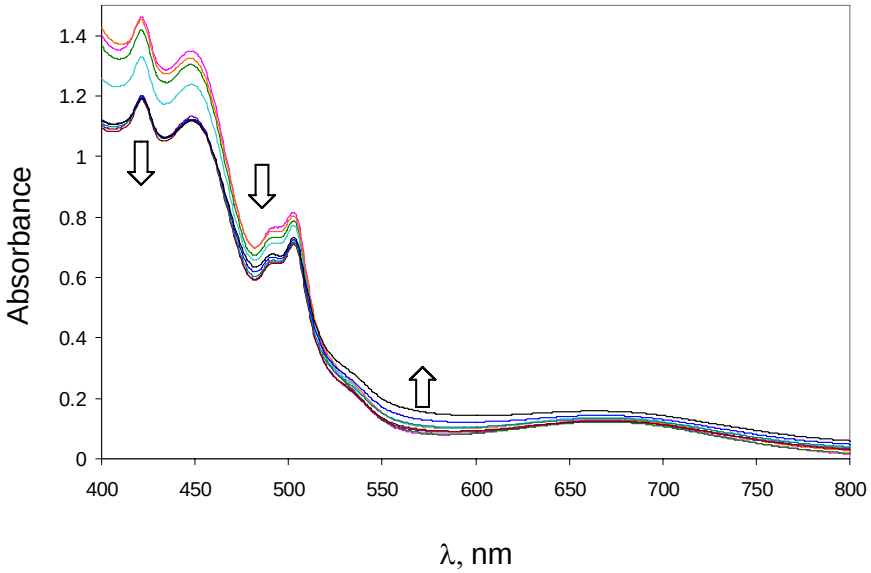

Figure 50. Oxidation of cyclohexane (0.46 M) with H_2O_2 (0.6 M) in MeCN at 25 °C catalyzed by **Fe5** (1 mM), electronic spectra of the catalytic reaction mixture (0–4 hours)

Since the electronic spectra of the catalytic mixture do not change much (Figure 50), we propose that the structure of **Fe5** is slightly transformed, presumably, the μ-acetato bridge being exchanged with water/solvent molecules. Diaqua Fe(III)-Fe(III) complexes with similar

tetradentate ligands have been isolated [169] and postulated as the intermediates for the dimerization process and for the catalytic oxidation with hydrogen peroxide [167, 169, 175].

With **Fe4** the oxidation of cyclohexane possesses the same features as in the case of **Fe5**, but the catalyst intermediate is more robust and maintains the oxygenase activity for at least 6 hours of the reaction at 25°C (Figure 51). Cyclohexyl hydroperoxide is the major oxygenation product in the initial period of the reaction (curve *1*), while it slowly decomposes in the course of the reaction to give the mixture of cyclohexanol (curve *2*) and cyclohexanone (curve *3*) in the presence of an iron complex generated from **Fe4**. Cyclohexanol is the predominant product after 6 hours of reaction. The alcohol/ketone ratio decreases to 6, what could indicate that the catalytically active species are also involved in the oxidation of cyclohexanol to give cyclohexanone. The total catalyst turnover number attains 43 and is significantly higher than that of **Fe5** (TON = 13) and a recently reported Fe(III) tetramer (TON = 6.5) [175].

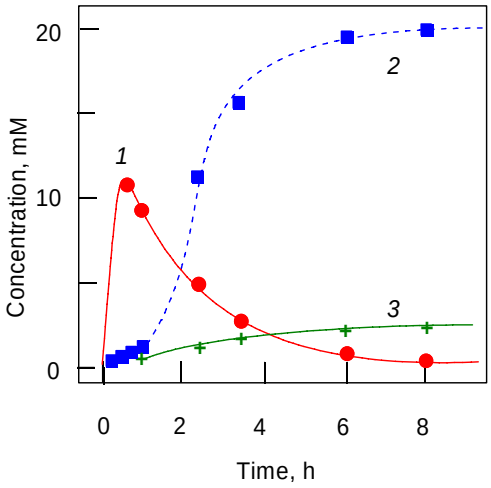

Figure 51. Oxidation of cyclohexane (0.46 M) with H_2O_2 (0.6 M) in MeCN at 25 °C catalyzed by **Fe4** (0.5 mM); the following curves are shown: accumulation of cyclohexyl hydroperoxide (curve *1*), cyclohexanol (*2*), and cyclohexanone (*3*)

The electronic spectra of **Fe4** in the presence of H_2O_2 and cyclohexane are shown in Figure 52. The transformation of **Fe4** into an intermediate iron (III) complex is almost completed after 2 hours of the reaction. This intermediate has no oxygenase activity – the addition of a new portions of H_2O_2 results in no subsequent product formation, but in H_2O_2 decomposition and further complex degradation.

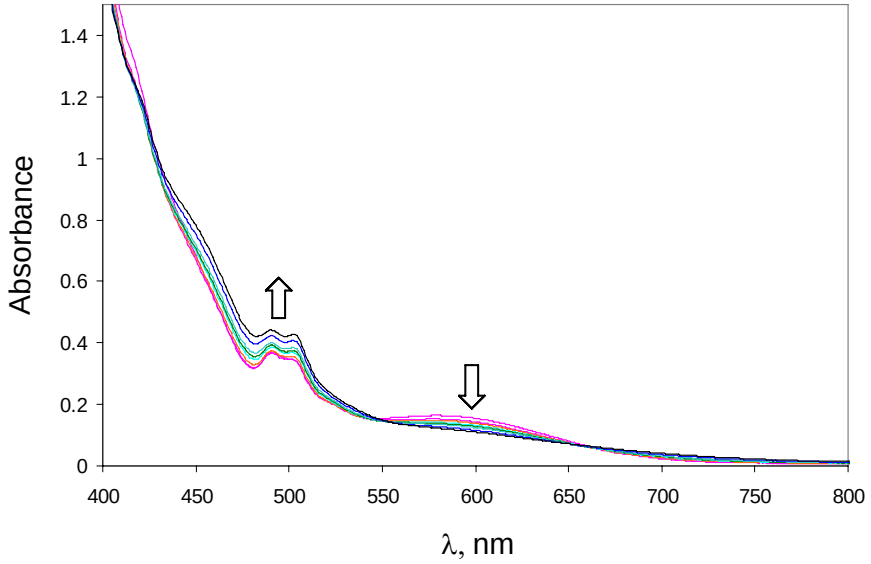

Figure 52. Oxidation of cyclohexane (0.46 M) with H_2O_2 (0.6 M) in MeCN at 25 °C catalyzed by **Fe4** (0.5 mM), electronic spectra of the catalytic reaction mixture (0–6 hours)

In order to elucidate the nature of the oxidizing species generated from **Fe4** and **Fe5** upon addition of hydrogen peroxide, we studied the oxidation of higher linear and branched alkanes (*n*-hexane, *n*-heptane, *n*-octane and isooctane). The selectivity parameters are given in Table 20. All parameters were measured after reduction of the reaction mixtures with triphenylphosphine before the GC analysis and calculated based on the ratios of isomeric alcohols. The parameter C(1):C(2):C(3):C(4) indicates the relative normalized reactivities of hydrogen atoms at carbons 1, 2, 3 and 4 of the chain of unbranched alkanes (i.e., calculated taking into account the number of hydrogen atoms at each carbon). The parameter 1°:2°:3° indicates the relative normalized reactivities of hydrogen atoms at primary, secondary and tertiary carbons of isooctane.

Table 20. Selectivity parameters in oxidation of alkanes in acetonitrile catalyzed by **Fe4** and **Fe5**

System	C(1) : C(2) : C(3) : C(4)			1º : 2º : 3º
	n-Hexane	*n*-Heptane	*n*-Octane	Isooctane
Fe4 – H_2O_2 (25 ºC)	1 : 13 : 13	1 : 15 : 14 : 11	1 : 10 : 12 : 9	1 : 5 : 11
Fe5 – H_2O_2 (25 ºC)	1 : 13 : 13	1 : 10 : 10 : 6	1 : 8 : 9 : 7	1 : 2 : 21
hν – H_2O_2 (20 ºC)	1 : 10 : 7	1 : 7 : 6 : 7		1 : 2 : 6
$FeSO_4$ – H_2O_2 (20 ºC)		1 : 5 : 5 : 5		1 : 3 : 6

If compared to known hydroxyl radical generation systems (photochemical activation and Fenton's reagent [163], Table 20), **Fe4** and **Fe5** complexes produce oxidizing species, which are more selective, – they have a higher tendency to discriminate between primary and secondary hydrocarbon bonds. However, in both cases we deal with radical species (C(2)/C(1) < 20), which are presumably ferryl-oxo radicals (Fe–O·).

In the isooctane molecule, the secondary C–H bonds are surrounded by bulky *t*-butyl and *i*-propyl groups, and the selectivity parameter C(2)/C(1) in linear alkanes compared to 2º/1º for isooctane reflects the sterical hindrance for the oxidizing species. Given the parameters (C(2):C(1))/(2°:1°) for **Fe4** and **Fe5** complexes being similar to those for hν – H_2O_2 system, we can assume that the oxidizing species generated from **Fe4** and **Fe5** have minimal sterical restrictions and are situated on the surface of the complexes or, once generated, escape the catalyst and attack the substrate from the solvent cage. This is also consistent with the fact, that in the oxidation of *cis*- and *trans*-1,2-dimethylcyclohexane with H_2O_2 catalyzed by **Fe4** and **Fe5** no stereoselectivity have been observed.

The data obtained show that the mechanism of alkanes oxidation catalysed by **Fe4** and **Fe5** complexes is relevant to those in sMMO, which is characterized by the nonconcerted reaction mechanism (hydrogen atom abstraction preceding hydroxylation) with no retention of stereochemistry and a preference to the activation of secondary C–H bonds [165]. Since MMO is one of two enzymes capable of methane hydroxylation (the second one is ammonia oxygenase AMO [176]), we also studied the catalytic oxygenation of methane by **Fe4** and **Fe5** complexes.

4.3.4 Methane Oxidation in Water

The oxidation of methane (50 bars) is carried out in the 100 mL stainless steel autoclave equipped with a glass reactor in the presence of air (10 bars). D_2O is used as solvent.

$$CH_4 + H_2O_2 + 1/2\ O_2 \xrightarrow[\textbf{Fe4 - Fe5}]{} CH_3OOH + H_2O$$

The product distribution was analysed by ^1H NMR (MeCN as internal standard) and confirmed by GC analysis performed after reduction of the reaction mixture with $NaBH_4$ (*i*-PrOH as internal standard). Since no formaldehyde has been detected (Nash reagent [177]),

we provide data on methanol/methyl hydroperoxide and formic acid accumulation after 4 hours of the reaction. The results are summarized in Table 21.

Table 21. Oxidation of methane in D_2O catalyzed by **Fe4** and **Fe5**. Conditions : 10^{-4} M catalyst, 0.50 M H_2O_2, 10 bars air, 50 bars of methane, product distribution contains MeOH / MeOOH / HCOOH ratios in the catalyst turnover numbers after 4 hours of the reaction, [pcaH] = 1.6×10^{-3} M.

	TON in water							
	50 °C		60 °C		70 °C		80 °C	
Catalyst	MeOH/MeOOH/ HCOOH	Σ	MeOH/MeOOH/ HCOOH	Σ	MeOH/MeOOH/ HCOOH	Σ	MeOH/MeOOH/ HCOOH	Σ
Fe5	1.7 / 1.3 / 0	3	2 / 2 / 0	4	6.5 / 8.5 / 0	15	5 / 13 / 0	18
Fe4	3.5 / 6.5 / 0	10	8 / 11 / 0	19	8 / 3 / 11	22	15 / 9 / 0	24
Fe4/pcaH	5 / 6 / 0	11	10 / 3 / 28	41	8 / 6 / 14	28	8 / 3 / 14	25

We found that after four hours the oxidation of higher alkanes catalyzed by **Fe4** and **Fe5** complexes is almost complete. In the case of methane the oxidation reaction has the same timescale. Since **Fe4** is more robust than **Fe5**, it catalyzes the methane oxygenation more efficiently (Figure 53); especially this effect is pronounced at moderate temperatures 50–60 °C. However, at higher temperatures **Fe4** and **Fe5** show comparable activities, the tetrameric structure of **Fe4** presumably undergoes decomposition, and the oxygenase activity of both catalysts is comparable.

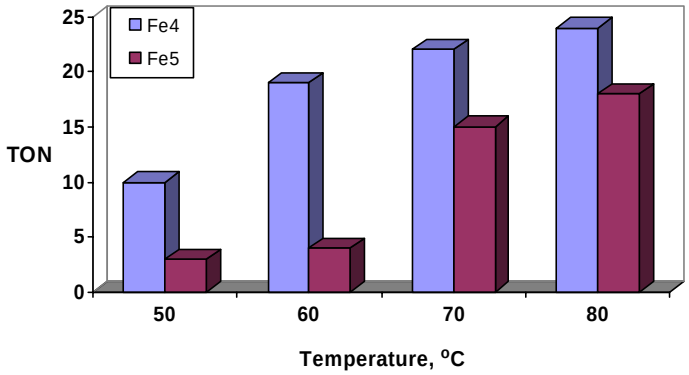

Figure 53. Oxidation of methane in D_2O catalyzed by **Fe4** and **Fe5** complexes. Conditions : 10^{-4} M catalyst, 0.50 M H_2O_2, 10 bars air, 50 bars of methane, TON – catalyst turnover number after 4 hours of the reaction.

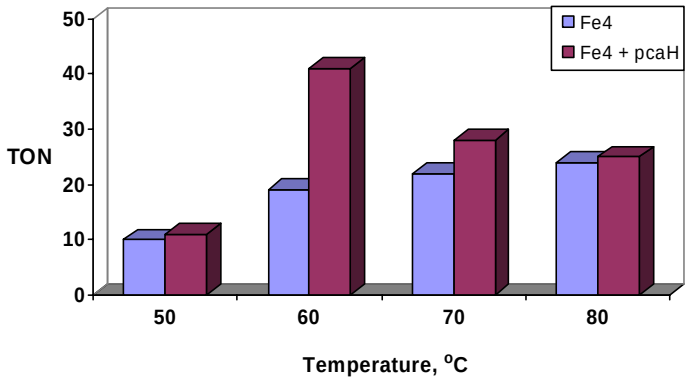

Figure 54. Oxidation of methane in D_2O catalyzed by **Fe4** complex in the absence/presence of pcaH (1.6×10^{-3} M). Conditions : 10^{-4} M **Fe4**, 0.50 M H_2O_2, 10 bars air, 50 bars of methane, TON – catalyst turnover number after 4 hours of the reaction.

In the presence of pcaH, the oxygenase activity of **Fe4** complex increases, what is in line with a reduced catalase activity of **Fe4** under these conditions observed in the isopropanol oxidation. This effect is more pronounced at 60 °C, however, at higher temperatures pcaH is not stable under the catalytic conditions, as we reported in Chapter 2.2.1, and the oxygenase activities of both systems are close. With pcaH added as co-catalyst, the main oxidation product is formic acid, the same was observed in blank experiments with iron(II) sulphate[*]. In the case of **Fe4** and **Fe5** complexes the main oxidation products are methanol and methyl hydroperoxide in line with the predominant alcohols formation observed in the oxidation of higher alkanes catalyzed by these complexes.

4.4 Conclusion

Iron complexes containing 1,4,7-triazacyclononane-derived ligands have been reported as functional models of important oxygen activating enzymes hemerythrin and methane monooxygenase (sMMO). The latter is the only well-studied enzyme that is able to hydroxylate methane affording methanol under mild conditions. Starting from 1,4-dimethyl-

[*] The methane oxidation with $FeSO_4/H_2O_2$ system (Fenton-type reagent; 10^{-4} M $FeSO_4$, 0.50 M H_2O_2, 10 bars air, 50 bars of methane) gives the following product distribution and catalytic turnover numbers after 1 hour: MeOH / MeOOH / HCOOH / $\mathbf{\Sigma_{TON}}$: (50 °C) 4 / 3 / 3 / **10**; (60 °C) 5 / 4 / 13 / **22**; (80 °C) 8 / 15 / 82 / **105**.

1,4,7-triazacyclononane (L-Me_2), we opted to model the sMMO active site and develop biomimetic alkane hydroxylation using air and H_2O_2 as oxidants.

In this chapter we reported a straightforward synthesis for dinuclear Fe(III)-Fe(III) complexes containing L-Me_2 ligands as well as carboxylato and oxo bridges. Three new **Fe1** –**Fe3** complexes have been synthesized and characterized. These complexes show a significant catalytic activity in the oxidation of alcohols only in the presence of ascorbic acid, which acts as stoichiometric reducing agent. With $[(L\text{-}Me_2)_2Fe_2(O)(OOCMe)_2]^{2+}$ (**Fe2**) used in the oxidation of methane with H_2O_2 in aqueous solution, no oxygenation product has been detected.

We therefore introduced a carboxylate function directly into the 1,4,7-triazacyclononane macrocycle. Two new iron(III) complexes containing the 2-(4,7-dimethyl-1,4,7-triazacyclononan-1-yl)acetate ligand **(**Ac-L-Me_2) have been synthesized. While **Fe5** represents a dinuclear Fe(III)-Fe(III) complex, $[(N_3O\text{-Ac-L-}Me_2)_2Fe_2(\mu\text{-O})(\mu\text{-OOCMe})]^{+}$, with pendant acetato arms being monodentately coordinated to iron(III) centers, **Fe4** is a tetranuclear complex, $[(N_3O_2\text{-Ac-L-}Me_2)_4Fe_4(O)_2]^{4+}$; the bidentate mode of pendant acetato arms coordination bridging two dimeric subunits into the "dimer of dimers" has been observed. The tetranuclear structure of **Fe4** represents a new example of the binding versatility of carboxylates.

The complexes **Fe4** and **Fe5** show significant catalytic oxygenase activity in the oxidation of alcohols and alkanes with H_2O_2; without addition of co-catalyst the reaction proceeds under mild conditions. The addition of an aminoacid (pcaH) decreases the catalase activity of these complexes in aqueous solution, improving the catalytic performance in the oxidation of isopropanol. The tetrameric **Fe4** complex is more robust than the dimeric **Fe5** complex and maintains the oxygenase activity for hours under catalytic conditions at room temperature. The selectivity pattern in the oxidation of linear and branched alkanes catalyzed by **Fe4** and **Fe5** complexes allows us to assume that the oxidizing species have a radical nature and can be tentatively assigned to ferryl-oxo radical species (Fe–O·). Since both complexes have structural and selectivity features close to those observed for sMMO, we used **Fe4** and **Fe5** for the oxygenation of methane with H_2O_2 in aqueous solution. We found that both complexes are active in this reaction under moderate temperatures (50–80 °C) and pressures (60 bars).

Finally, **Fe4** and **Fe5** can be used for the oxidation of alcohols and alkanes with H_2O_2 without addition of reducing agents or co-ligands. Both complexes can serve as structural and functional models for methane monooxygenase and provide new insights into the oxidation mechanism.

5 Ruthenium- and Cobalt-Based Systems

The oxidation of alcohols to give carbonyl compounds is an important transformation in synthetic organic chemistry. Although several stoichiometric reagents based on activated dimethyl sulfoxide (Swern oxidation) [178], hypervalent iodine compounds (Dess-Martin) [179], and reactive oxometal compounds (MnO_2 and pyridinium chlorochromate) [35] have been developed as selective oxidation reagents, the search for new catalytic procedures for selective alcohol oxidations using inexpensive and environmentally friendly oxidants such as H_2O_2 [180] remains an area of intensive interest.

5.1 Catalytic Oxygenation with Ruthenium and Cobalt Complexes Containing Triazacyclononane Ligands: State of the Art

Ruthenium and cobalt complexes with nitrogen containing ligands are known to catalyse alcohol oxidations under mild conditions [180, 181, 182]. In the case of ruthenium, using 1,4,7-trimethyl-1,4,7-triazacyclononane as a tripodal ligand, the Ru(IV) oxidation state of the metal centre is accessible: thus, reaction of the dimethylsulfoxide complex $RuCl_2(dmso)_4$ with 1,4,7-trimethyl-1,4,7-triazacyclononane in ethanol, followed by treatment with HCl in air, yields $(L\text{-}Me_3)RuCl_3 \cdot H_2O$, which can be converted in the presence of carboxylate anions into dinuclear Ru(III)-Ru(III) (μ-oxo)bis(μ-carboxylato) complexes [174]. In the case of sodium acetate, two Ru(III)-Ru(III) complexes $[(L\text{-}Me_3)_2Ru_2(OH)(OOCMe)_2]^{3+}$ and $[(L\text{-}Me_3)_2Ru_2(O)(OOCMe)_2]^{2+}$ can be isolated, the latter one can be oxidized into the Ru(III)-Ru(IV) complex $[(L\text{-}Me_3)_2Ru_2(O)(OOCMe)_2]^{3+}$ [174], or converted into the Ru(II)-Ru(III), Ru(III)-Ru(III) and Ru(IV)-Ru(IV) complexes $[(L\text{-}Me_3)_2Ru_2(OH)_3]^{2+}$, $[(L\text{-}Me_3)_2Ru_2(OH)_3]^{3+}$ and $[(L\text{-}Me_3)_2Ru_2(O)_3]^{2+}$ [183].

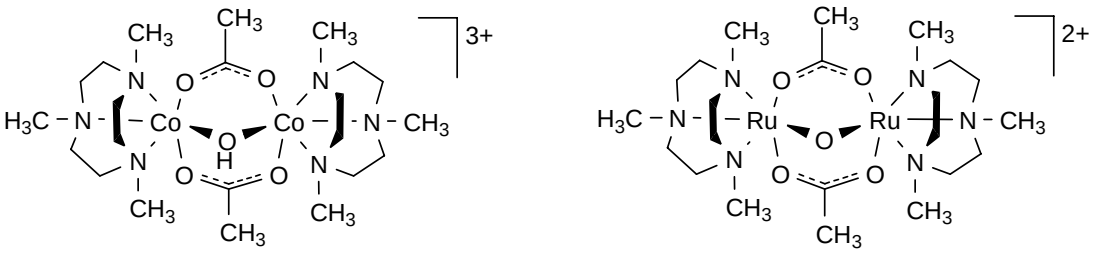

Scheme 32. Dinuclear Co(III)-Co(III) and Ru(III)-Ru(III) complexes containing 1,4,7-trimethyl-1,4,7-triazacyclononane (L-Me_3) ligand

The mononuclear ruthenium(III) complex [(L-Me_3)Ru($OOCCF_3$)$_3$] has been reported as an effective catalyst for the epoxidation of alkenes [184] and for the oxidation of alcohols with *t*-butyl hydroperoxide under mild conditions [185].

Dinuclear carboxylato-bridged complexes of cobalt are surprisingly rare, considering the enormous structural variety of such compounds. A full series of dinuclear Co(II)-Co(II), Co(II)-Co(III) and Co(III)-Co(III) di-μ-acetato complexes, containing 1,4,7-trimethyl-1,4,7-triazacyclononane, $[(L\text{-}Me_3)_2Co_2(OH)(OOCMe)_2]^+$, $[(L\text{-}Me_3)_2Co_2(OH)(OOCMe)_2]^{2+}$ and $[(L\text{-}Me_3)_2Co_2(OH)(OOCMe)_2]^{3+}$ (Scheme 32), has been reported by Wieghardt [186].

In this chapter we describe a straight-forward synthesis for dinuclear Co(III)-Co(III) complex containing 1,4-dimethyl-1,4,7-triazacyclononane (L-Me_2) ligands as well as acetato and hydroxo bridges, and a synthetic route to the Ru(III)-Ru(III) analogue $[(L\text{-}Me_2)_2Ru_2(O)(OOCMe)_2]^{2+}$; both cations can be isolated as the hexafluorophosphate salts. The catalytic oxidation properties of these compounds are discussed.

5.2 New Results with Dinuclear Ruthenium and Cobalt Complexes Containing 1,4-Dimethyl-1,4,7-Triazacyclononane Ligands as well as Carboxylato and Oxo or Hydroxo Bridges

5.2.1 Syntheses and Characterization

Unlike the complexation of iron salts with 1,4,7-triazacyclononane-derived ligands [156], the corresponding reaction with $RuCl_3 \cdot n\ H_2O$ does not work; however, the analogous Ru(III)-Ru(III) complex $[(L\text{-}Me_2)_2Ru_2(O)(OOCMe)_2]^{2+}$ (**Ru2**) can be synthesised by reacting Ru(dmso)$_4Cl_2$ with L-Me_2, HCl and air in refluxing ethanol, followed by addition of sodium

acetate (Scheme 33), by analogy to Wieghardt's method for the synthesis of the L-Me_3 derivative [183]. The mononuclear intermediate (L-Me_2)$RuCl_3 \cdot H_2O$ (**Ru1**) has also been isolated, it precipitates upon addition of water. The ν_{as}(C−O) stretching frequency for **Ru2** at 1559 cm^{-1} as well as ν_s(C−O) frequency at 1428 cm^{-1} are comparable to those in [(L-Me_3)$_2$$Ru_2(O)(OOCMe)_2]^{2+}$ (1548 cm^{-1} and 1425 cm^{-1}) [174]. The UV/vis spectrum shows for **Ru2** very intense absorption maxima at 233, 279 and 538 nm, which compare well to those in [(L-Me_3)$_2$$Ru_2(O)(OOCMe)_2]^{2+}$ [174].

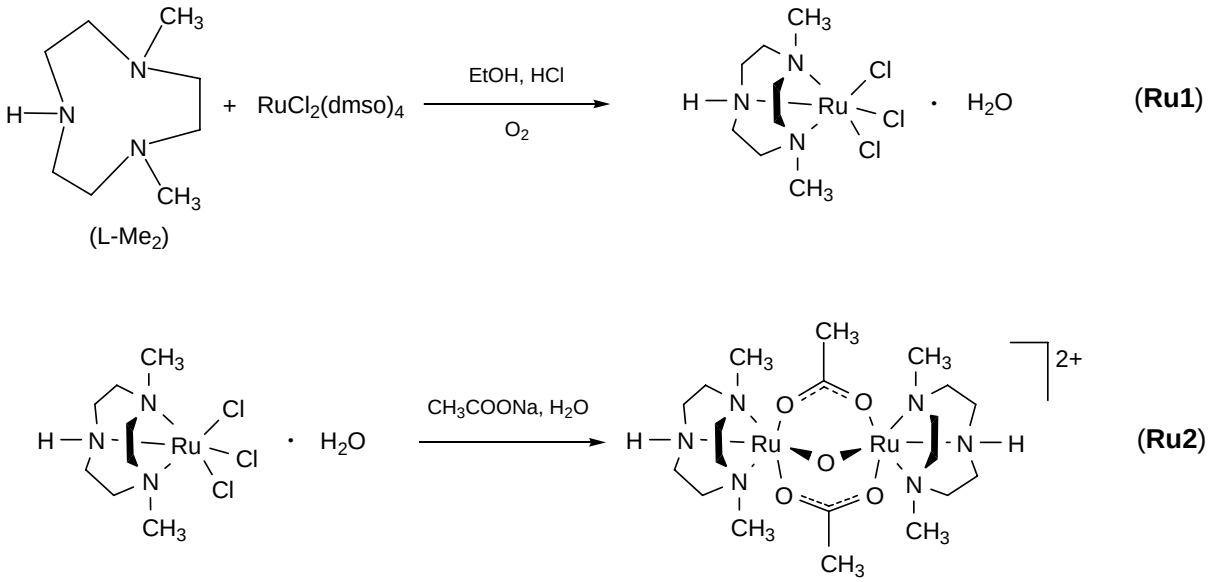

Scheme 33. Reaction of 1,4-dimethyl-1,4,7-triazacyclononane (L-Me_2) with $RuCl_2(dmso)_4$ in the presence of sodium acetate

The reaction of L-Me_2, sodium acetate, hydrogen peroxide and triethylamine with $CoCl_2 \cdot 6\ H_2O$ in acetonitrile yields a dinuclear hydroxo-bridged Co(III)-Co(III) complex [(L-Me_2)$_2$$Co_2(OH)(OOCMe)_2]^{3+}$ (**Co1**), see Scheme 34. The presence of the μ-OH bridge is clearly established by a sharp O−H stretching frequency at 3568 cm^{-1}. The ν_{as}(C−O) stretching frequency for **Co1** at 1590 cm^{-1} is comparable to those of [(L-Me_3)$_2$$Co_2(OH)(OOCMe)_2]^{3+}$ (1588 cm^{-1}), while the ν_s(C−O) frequency is shifted to higher values (1452 cm^{-1} in **Co1** versus 1418 cm^{-1} in the known L-Me_3 analogue) [186].

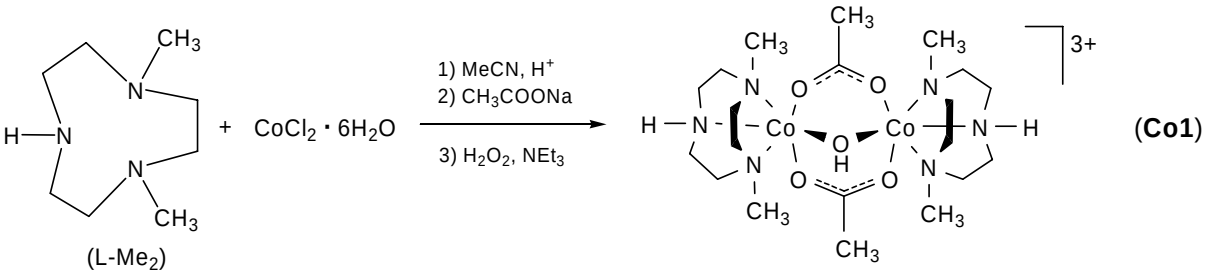

Scheme 34. Reaction of 1,4-dimethyl-1,4,7-triazacyclononane (L-Me_2) with cobalt(II) chloride hexahydrate in the presence of hydrogen peroxide and sodium acetate

The molecular structures of **Ru2** and **Co1**, solved by single-crystal X-ray structure analyses of the hexafluorophosphate salts, are very similar. The two metal centres are linked by two acetato bridges and by an oxo (**Ru2**) or a hydroxo bridge (**Co1**), and all metal centres are facially coordinated to a L-Me_2 ligand through the three nitrogen atoms. The single-crystal X-ray structure analyses reveal for the purple crystals of [**Ru2**][PF_6]$_2$ (Figure 55) a Ru-Ru distance of 3.230(1) Å, and for the violet crystals of [**Co1**][PF_6]$_3$ (Figure 56) a Co-Co distance of 3.358(1) Å. The Ru-Ru distance in **Ru2** compares well to those in the isoelectronic Ru(III)-Ru(III) cations [(1-methylimidazole)$_6$$Ru_2$(O)(OOCMe)$_2$]$^{2+}$ [3.266(1) Å] [187] and [(L-Me_3)$_2$$Ru_2$(O)(OOCMe)$_2$]$^{2+}$ [3.258(1) Å] [188], whereas the Co-Co distance in **Co1** is shorter than those in the Co(II)-Co(III) cation [(L-Me_3)$_2$$Co_2$(OH)(OOCMe)$_2$]$^{2+}$ [3.435(4) Å] [186]. Surprisingly, the **Co1** analysis presents the first example of X-ray resolved structure of dinuclear Co(III)-Co(III) carboxylato bridged complex.

Interestingly, both **Ru2** and **Co1** complexes show intermolecular interactions with solvent molecules or anions, owing to the presence of an N-H moiety within the ligand L-Me_2. Thus, in [**Ru2**][PF_6]$_2$ the hydrogen atoms of the N-H amino groups interact strongly with the hexafluorophosphate anions: the N-F distance is 3.234(13) Å with a N-H···F angle of 159.8°. In [**Co1**][PF_6]$_3$ · $(CH_3)_2CO$, strong hydrogen bonds are formed with an acetone molecule, see Figure 57.

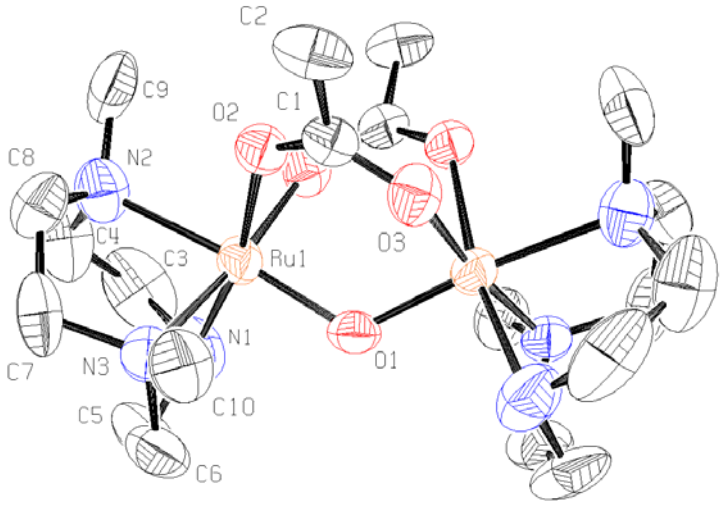

Figure 55. The molecular structure of $[(L\text{-}Me_2)_2Ru_2(O)(OOCMe)_2]^{2+}$ (**Ru2**), displacement ellipsoids are drawn at the 50% probability level, hydrogen atoms and hexafluorophosphate molecules are omitted for clarity. Selected bond lengths (Å) and angles (º): Ru(1)-Ru(1)^{i} 3.2299(12), Ru(1)-N(1) 2.068(6), Ru(1)-N(2) 2.172(7), Ru(1)-N(3) 2.092(8), Ru(1)-O(1) 1.850(4), Ru(1)-O(2) 2.084(5), Ru(1)^{i}-O(3) 2.079(6); Ru(1)-O(1)-Ru(1)^{i} 121.6(4), O(2)-C(1)-O(3) 124.8(7). ^{i} = x, -y, 1-z

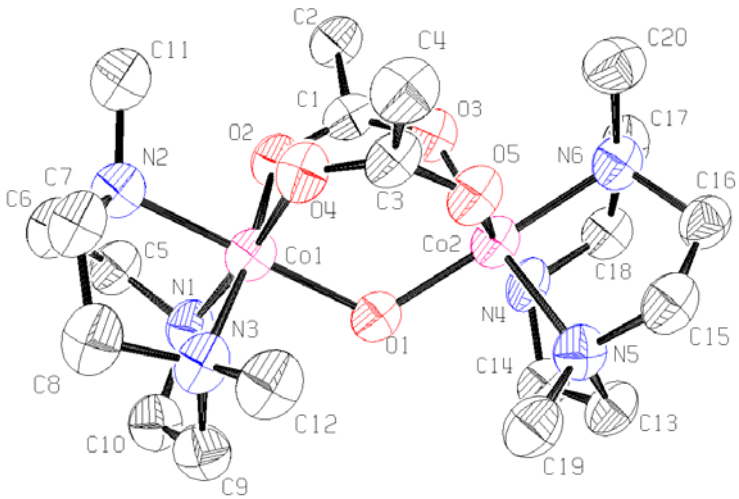

Figure 56. The molecular structure of $[(L\text{-}Me_2)_2Co_2(OH)(OOCMe)_2]^{3+}$ (**Co1**), displacement ellipsoids are drawn at the 50% probability level, hydrogen atoms, acetone and hexafluorophosphate molecules are omitted for clarity. Selected bond lengths (Å) and angles (º): Co(1)-Co(2) 3.3584(14), Co(1)-N(1) 1.930(5), Co(1)-N(2) 1.987(6), Co(1)-N(3) 1.969(6), Co(2)-N(4) 1.939(5), Co(2)-N(5) 1.968(5), Co(2)-N(6) 1.989(6), Co(1)-O(1) 1.936(4), Co(2)-O(1) 1.927(4), Co(1)-O(2) 1.863(4), Co(1)-O(4) 1.894(4), Co(2)-O(3) 1.912(4), Co(2)-O(5) 1.895(4); Co(1)-O(1)-Co(2) 120.8(2), O(2)-C(1)-O(3) 125.8(6), O(4)-C(3)-O(5) 125.9(6)

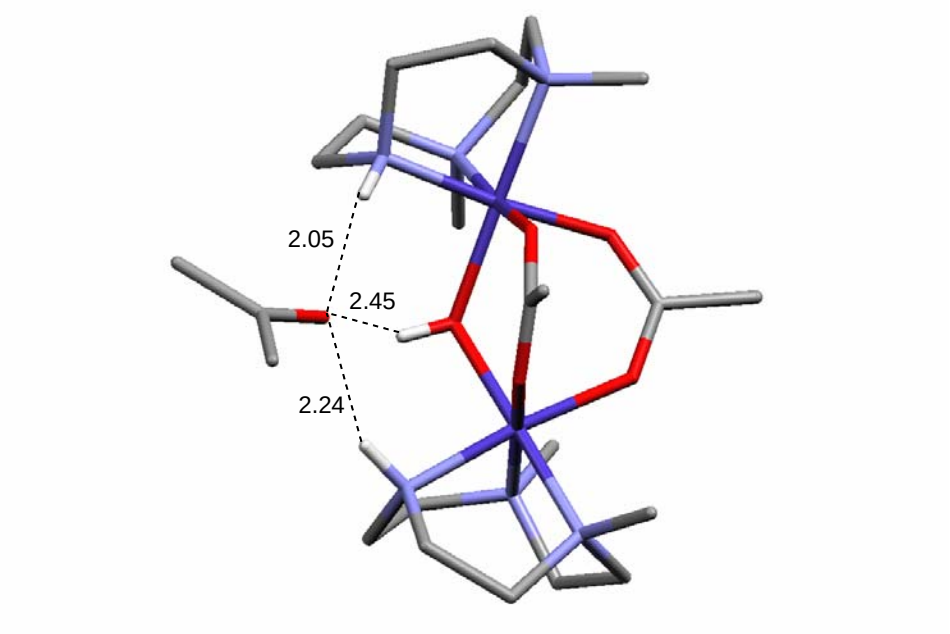

Figure 57. Capped sticks representation of cation **Co1** in [**Co1**][PF_6]$_3$ · $(CH_3)_2CO$, showing the intermolecular interactions with the acetone molecule

The intermolecular hydrogen-bonded system in [**Co1**][PF_6]$_3$ · $(CH_3)_2CO$ involves the two N-H moieties, as well as the hydroxo bridging ligand. The N···O distances are 2.895(7) and 3.087(8) Å with N-H···O angles of 153.9 and 153.0° respectively, whereas the O···O distance is 3.080(6) Å with an O-H···O angle of 134.2°.

5.2.2 Oxidation of 2-Propanol in Water

We studied the catalytic potential of the complexes **Ru1**, **Ru2** and **Co1** for the oxidation of isopropanol with hydrogen peroxide to give acetone. The oxidation reaction was carried out in aqueous solution or acetonitrile at 20 °C in the presence of ascorbic acid used as a co-catalyst. The results are shown in Table 22.

The highest catalytic activity was observed for $[(L\text{-}Me_2)_2Ru_2(O)(OOCMe)_2]^{2+}$ (**Ru2**) in the presence of ascorbic acid in water, the catalyst turnover number being 72 after 1 hour at 20 °C, which is comparable to that of the analogous manganese complex $[(L\text{-}Me_2)_2Mn_2(O)(OOCMe)_2]^{2+}$ (**Mn4**), for which a TON of 67 was observed under the same conditions (Chapter 3.3.1). However, this catalytic performance is considerably lower than those of the

corresponding iron(III) complexes: for $[(L\text{-}Me_2)_2Fe_2(O)(OOCMe)_2]^{2+}$ (**Fe2**) in the presence of ascorbic acid in water, the TON being 320 after 1 hour at 20 °C.

Table 22. Oxidation of isopropanol in water and acetonitrile, catalyzed by the complexes **Ru1**, **Ru2** and **Co1** in the absence/presence of ascorbic acid as co-catalyst (20 °C, 1h, 1.0×10^{-4} M catalyst, 0.20 M isopropanol, 0.50 M H_2O_2)

Catalyst	TON (after 1h) in water		TON (after 1h) in acetonitrile	
	no co-catalyst	with ascorbic acid	no co-catalyst	with ascorbic acid
Ru1	2	63	0	5
Ru2	0	72	0	3
Co1	1	28	0	3

While the dinuclear Fe(III)-Fe(III) complexes **Fe1**–**Fe3** can be effectively reduced with ascorbic acid in aqueous solution at room temperature, the complexes **Ru1**, **Ru2** and **Co1** are quite stable in the presence of ascorbic acid and thus less active in the oxidation of isopropanol. All complexes **Ru1**, **Ru2** and **Co1** in combination with ascorbic acid as co-catalyst are much more active in water than in acetonitrile (Table 22), in line with the analogous complexes $[(L\text{-}Me_2)_2Mn_2(O)(OOCMe)_2]^{2+}$ (**Mn4**) and $[(L\text{-}Me_2)_2Fe_2(O)(OOCMe)_2]^{2+}$ (**Fe2**) in combination with oxalic or ascorbic acid as co-catalyst.

5.3 Conclusion

The straightforward synthesis for a dinuclear Co(III)-Co(III) complex containing 1,4-dimethyl-1,4,7-triazacyclononane ($L\text{-}Me_2$) ligands as well as carboxylato and hydroxo bridges (**Co1**), as well as the synthetic route to the Ru(III)-Ru(III) complex $[(L\text{-}Me_2)_2Ru_2(O)(OOCMe)_2]^{2+}$ (**Ru2**) have been described, the mononuclear intermediate $(L\text{-}Me_2)RuCl_3 \cdot H_2O$ (**Ru1**) being also isolated and characterised. The molecular structures of **Ru2** and **Co1**, solved by single-crystal X-ray structure analyses of the hexafluorophosphate salts, reveal for the purple crystals of [**Ru2**][PF_6]$_2$ a Ru-Ru distance of 3.230(1) Å, and for the violet crystals of [**Co1**][PF_6]$_3$ · $(CH_3)_2CO$ a Co-Co distance of 3.358(1) Å. The molecular structure of **Co1** provide the first example of an X-ray resolved structure of a dinuclear Co(III)-Co(III) carboxylato-bridged complex.

All three complexes show catalytic activity for the oxidation of isopropanol with hydrogen peroxide in water to give acetone in the presence of ascorbic acid as co-catalyst.

6 Regioselective Alkane Oxidation Catalyzed by Redox-Active Molecular Sieves

Molecular sieves are highly structured microporous inorganic solids, containing channels and pores of a precise and uniform size. Among them zeolites and zeotypes represent the most industrially important class of crystalline solids made up of silicon, aluminium, phosphorus and oxygen as the essential elements. In these solids, the phosphorus, silicon and aluminium atoms occupy the centers of tetrahedral sites and the oxygen atoms link the corner positions [189] (Figure 58).

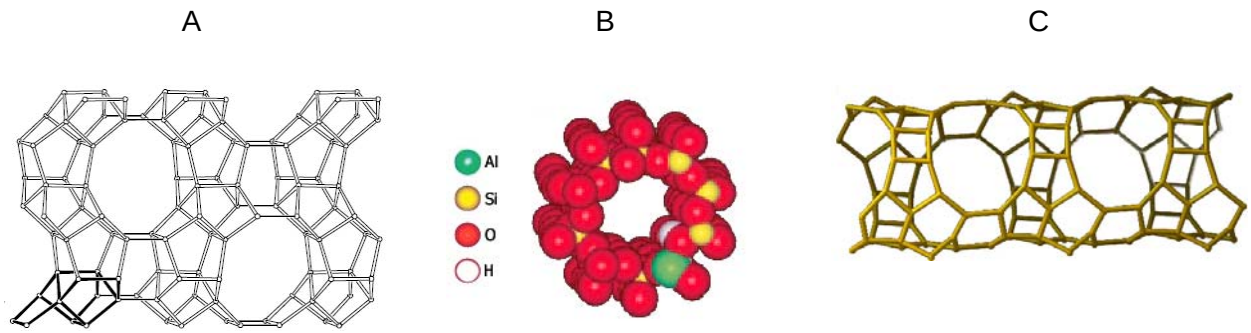

Figure 58. Channels and cavities in zeolites : (A) MFI-type framework, (B) loosely attached proton (white) is bound to a neighboring framework oxygen atom in the acid centers Al-O(H)-Si, (C) UTL-type framework

6.1 Micro- and Mesoporous Materials as “Inorganic Enzymes”

Framework-substituted, molecular-sieve microporous solids are the centerpieces of a new approach to the aerobic oxyfunctionalization of saturated hydrocarbons [190]. The solids, where some of the tetrahedral sites are replaced by catalytically active, transition-metal ions in high oxidation states (Co^{3+}, Mn^{3+}, Fe^{3+}) [191], are specially designed to allow free access of oxygen into the interior of these high-area solids. Certain metal-substituted molecular sieves allow only the end-on approach of linear alkanes to the active centers, thereby favoring an enhanced reactivity of the terminal methyl groups [192]. By optimizing the cage

dimension, choosing the molecular sieve with the appropriate pore aperture as well as adjusting the average separation of active centers within a cage, highly selective oxidation of hydrocarbons may be achieved under mild conditions (Scheme 35) [193, 194].

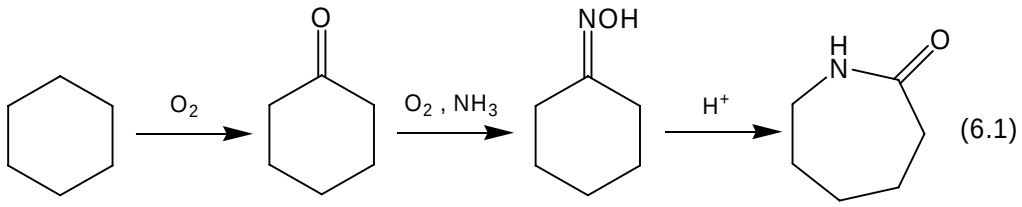

Scheme 35. Shape-selective catalytic transformation of cyclohexane to ε–caprolactam using redox active aluminophosphates, the first step being catalyzed by $Cr_{0.03}AlP_{0.97}O_4$, the second and third step by $Mn_{0.02}Mg_{0.02}Al_{0.96}PO_4$

The incorporation of redox-active metals (Ti^{4+} [195, 196], V^{3+}, Cr^{3+}, Fe^{3+} [197]) into the framework of microporous (pore diameters < 2 nm) and mesoporous (pore diameters 2−50 nm) molecular sieves has received much attention since the 1990s. The resulting redox-active molecular sieves catalyze a variety of selective oxidations under mild conditions [198]. Their structural diversity provides the possibility of designing tailor-made solid catalysts (mineral enzymes) for liquid-phase oxidations with clean oxidants such as O_2, H_2O_2, and alkylhydroperoxides.

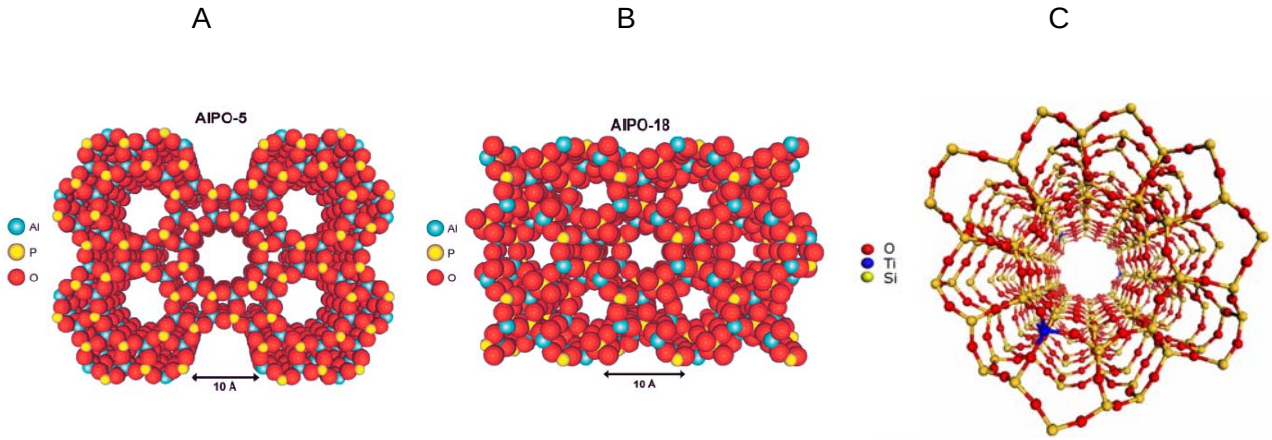

Figure 59. Three-dimensional representation of the pore structures of aluminophosphates (A) AlPO-5, (B) AlPO-18 and titanosilicalite (C) TS-1 (pore apertures are respectively 7.5 Å, 3.8 Å and 5.5 Å)

Micro- and mesoporous materials containing relatively small cavities or narrow channels are excellent examples of catalysts for regioselective functionalization of long-chain

alkanes [199]. Thus, aerobic oxidation of *n*-dodecane over Mn-ALPO*-18 (with pores 3.8 Å × 3.8 Å, Figure 59) gives, preferentially, products of oxidation at C_1 and C_2, whereas oxidation over Mn-ALPO-5 (pores 7.5 Å × 7.5 Å) produces only the C_3, C_4 and C_4 oxygenates [200]. The selectivity pattern for Fe-AlPO-31 (pores diameter 5.4 Å) is completely different from that of Fe-AlPO-5 (pores 7.5 Å × 7.5 Å) in aerobic oxidation of cyclohexane, even though the active sites are identical (Scheme 36, Figure 60) [201].

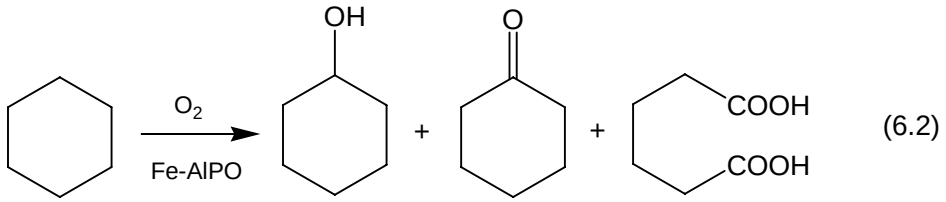

Scheme 36. Aerobic oxidation of cyclohexane catalysed by Fe-AlPOs

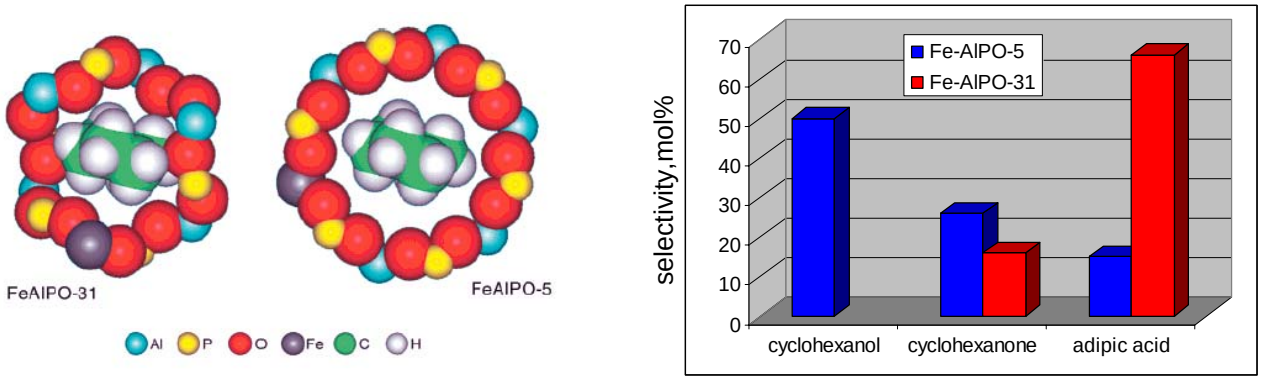

Figure 60. Product selectivities (in mol% at similar levels of conversion) in the aerial oxidation of cyclohexane, after 24h, at 373 K, with Fe-AlPO-31 and Fe-AlPO-5.

These differences in product selectivity are rationalized in terms of the differences in pore dimensions: the diffusion of cyclohexane and the cyclic intermediates in the oxidation reaction within the FeAlPO-31 channel system is severely limited, and therefore further oxidation of the cyclic intermediates to linear products such as adipic acid is facilitated.

In 1983, Taramasso, Perego, and Notari reported the synthesis of a titanium-substituted analogue of silicalite, given the name titanium silicalite or TS-1 [202]. The product contains

* ALPO - aluminophosphate

low levels (up to 2.5 atom %) of titanium substituting silicon in tetrahedral positions of the silicalite (MFI) framework, a system of straight and sinusoidal intersecting channels of approximately 0.55 nm in diameter [203]. Microporous titanosilicalite TS-1 is known as a catalyst for H_2O_2 oxidation of various organic compounds [198, 204] including alkanes [205, 206].

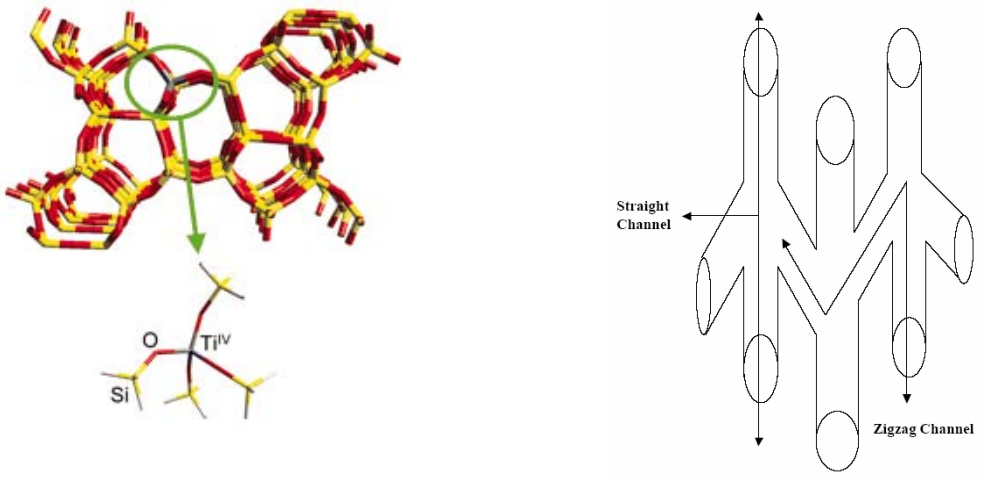

Figure 61. Straight and sinusoidal intersecting channels in TS-1

Due to the relatively narrow pores (Figure 61), TS-1 catalyses efficiently the H_2O_2 oxidation of small organic molecules [207], whereas the bulky oxidant, *tert*-butyl hydroperoxide, is inactive in TS-1-catalysed reactions. Nevertheless, cyclohexane can react with H_2O_2, and addition of acetic acid to the reaction mixture leads to activity enhancement [208].

The preparation of TS-1 by incorporation of Ti^{4+} cations into the framework of silicalite is not trivial and limited to 3 wt% [209]. One of the reasons is that these cations have a radius larger than that of Si^{4+}, and their incorporation in a zeotype framework distorts the structure of silicalite. Thus, the product can only crystallize with a small metal content. The pH values of the gels for the synthesis of the metallo-silicates are normally around 9−13. Under these alkaline conditions, Ti^{4+} has a strong tendency to form insoluble amorphous TiO_2 species, unlike silicates or aluminates which dissolve under alkaline conditions. Therefore, the titanium-containing silicalite TS-1 is prepared by hydrothermal crystallisation of a silicon-titanium gel, stabilized with H_2O_2, and tetrapropylammonium bromide was used as template (Figure 62) [208].

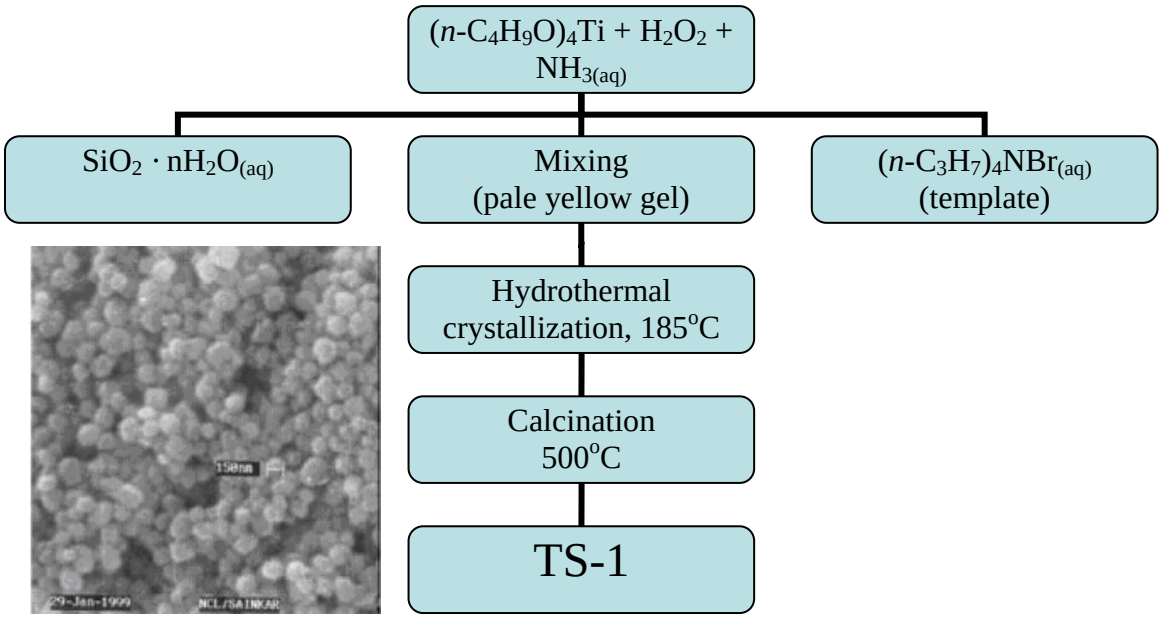

Figure 62. The synthesis procedure and a Scanning Electron Microscope (SEM) picture of a TS-1 sample

The Si/Ti ratio of 20 for this white crystalline powder was obtained by spectroscopic methods and the specific surface area, measured by gas adsorption (BET), was approximately 373 $m^2\ g^{-1}$.

6.2 New Results with Titanosilicalite TS-1

Hydrogen atoms at primary (1^o), secondary (2^o) and tertiary (3^o) carbon atoms of branched alkane chains (*e.g.*, in 2-methylhexane) usually react with oxidizing reagents with different reactivities which change in the following order: 1° < 2° < 3°. The value of the parameter 1°:2°:3°, which is normalized taking into account the number of hydrogen atoms at each position, gives the relative reactivities of hydrogen atoms at primary, secondary and tertiary carbons, respectively, and allows conclusions about the nature of an oxidizing species. The regioselectivity (*i.e.*, the selective functionalization of certain positions in a long alkane chain) can be enhanced by reagents, in which the reaction centers are surrounded by bulky substituents or are situated in hydrophobic pockets. Thus, enzymes [210], certain metal-complex catalysts [211, 212] and metal-based biomimetic systems [213] are known to induce regioselective transformations of alkanes.

6.2.1 Light Alkanes Oxygenation

The oxidation of gaseous saturated hydrocarbons is carried out in a glass-lined stainless-steel autoclave with intensive stirring using hydrogen peroxide as oxidant (Scheme 37). The autoclave is charged with air under atmospheric pressure prior to addition of the gaseous alkane. The reactions are stopped by cooling with ice, and acetonitrile containing a small amount of nitromethane (an internal standard for the GC) is then added to the reaction mixture in order to obtain (after filtering off the solid TS-1) a homogeneous solution.

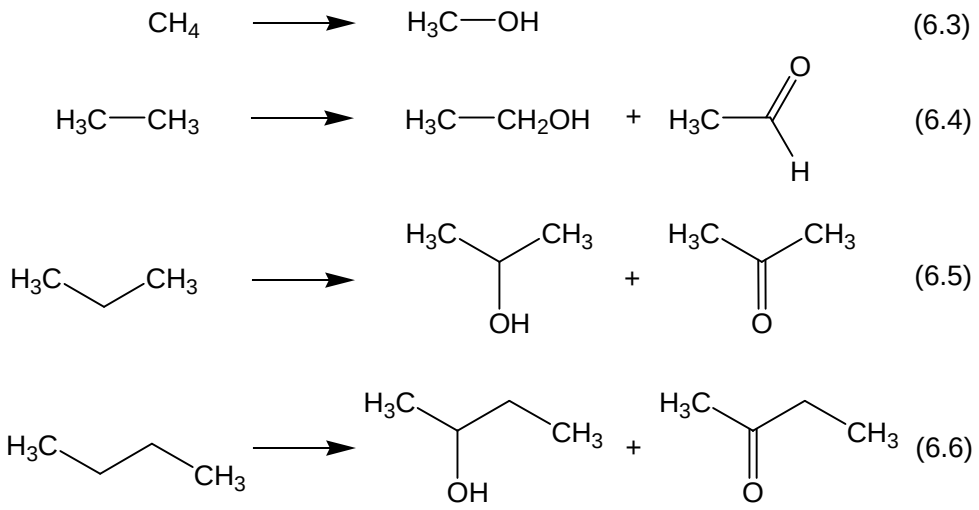

Scheme 37. Light alkanes oxygenation with H_2O_2 catalyzed by titanosilicalite TS-1

The samples are analyzed by GC upon addition of solid PPh_3, which converts the hydroperoxides quantitatively into the corresponding alcohol, so that only alcohols and ketones/aldehydes are detected in the sample. The results are shown in Table 23.

Table 23. Oxidation of various alkanes with hydrogen peroxide catalyzed by TS-1, 60 °C, H_2O_2 (35% wt) 1 mL

Entry	Alkane	TS-1 (mg)	Pressure (bar)	Time (h)	Products (μmol)
1	Methane	10	50	24	Methanol (1.1)
2	Ethane	10	30	12	Acetaldehyde (28), ethanol (1.7)
3	Propane	10	5	4	Acetone (10), isopropanol (4.7)
4	*n*-Butane	10	2	4	Butan-2-one (12), butan-2-ol (1.5)

If a light alkane does not contain methylene groups, such as ethane or methane, the methyl C–H bonds are functionalized by the H_2O_2–TS-1 system, but the reaction takes much longer time (entries 1, 2). In the two other gaseous alkanes, propane and *n*-butane, the methylene groups are predominantly oxidized (entries 3 and 4, respectively). The major oxidation products being the corresponding ketones. This can be explained by the fact, that the diffusion of corresponding alcohols, formed as initial products in the oxidation reaction, is restricted within the TS-1 channel system, so that further oxidation to the carbonyl products is facilitated. In the case of methanol, the steric limitations are negligible, therefore, methane gives only methanol as oxidation product.

6.2.2 Unusual Regioselectivity in the Oxidation of Higher Alkanes

The reactions of liquid alkanes are carried out in air in a solid-liquid-liquid triphasic system using a thermostated cylindrical pyrex vessel with vigorous stirring and worked up as described for the case of gaseous hydrocarbons. The results of the *n*-heptane oxidation are summarized in Scheme 38 and in Figure 63.

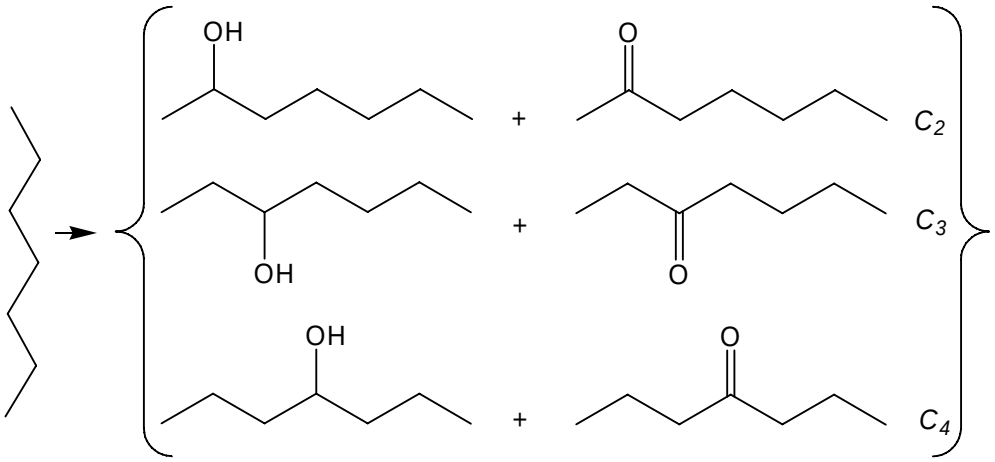

Scheme 38. Reaction products of the *n*-heptane oxidation with H_2O_2 and air catalyzed by TS-1 after treatment with PPh_3.

We found that *n*-heptane is oxidized at a relatively low temperature (50 °C) in the absence of any organic additives to give a mixture of isomeric alcohols and ketones. We analyzed the reaction solutions both before and after addition of triphenylphosphine and demonstrated that only small amounts of the corresponding alkyl hydroperoxides are formed. The second interesting feature of the reaction is that only oxidation of methylene groups is observed, whereas the reactivity of the more inert methyl groups is negligible (the CH_2 groups

are 80–100 times more reactive than the CH_3 groups). This observation, which is in accordance with other findings [206], clearly testifies that the alkane oxidation does not involve free hydroxyl radicals or, possibly, metal-oxo species. Indeed, the normalized selectivity parameter C_1:C_2:C_3:C_4 for the relative reactivities of the hydrogen atoms in positions *1*, *2*, *3* and *4* of the hydrocarbon chain equals approximately 0:60:145:76 (Figure 63A). For the reaction of *n*-heptane with hydroxyl radicals generators (the "vanadate ion–pyrazine-2-carboxylic acid–H_2O_2" reagent, hν–H_2O_2, $FeSO_4$–H_2O_2) this parameter was found equal to 6.7:60:47:47 [73, 78, 79], for the oxidation with the "H_2O_2–$[(L\text{-}Me_3)_2Mn_2(O)_3]^{2+}$–$CH_3COOH$" system (L-$Me_3$ = 1,4,7-trimethyl-1,4,7-triazacyclononane), believed to proceed via abstraction of hydrogen atoms from the alkane by the Mn=O fragment, this parameter was found to be 1.3:60:46:46 [64, 109]. Thus, it is reasonable to assume that the alkane oxygenation with the H_2O_2–TS-1 system occurs with participation of certain titanium peroxy species [214, 215, 216]. We also found that a branched isomer of heptane, 2-methylhexane gives only a very small amount of oxygenates. In the case of the more bulky 3-methylhexane we did not detect any traces of oxygenates. Therefore, it can be concluded that the oxidation of light and higher linear alkanes proceeds only in the narrow channels of TS-1.

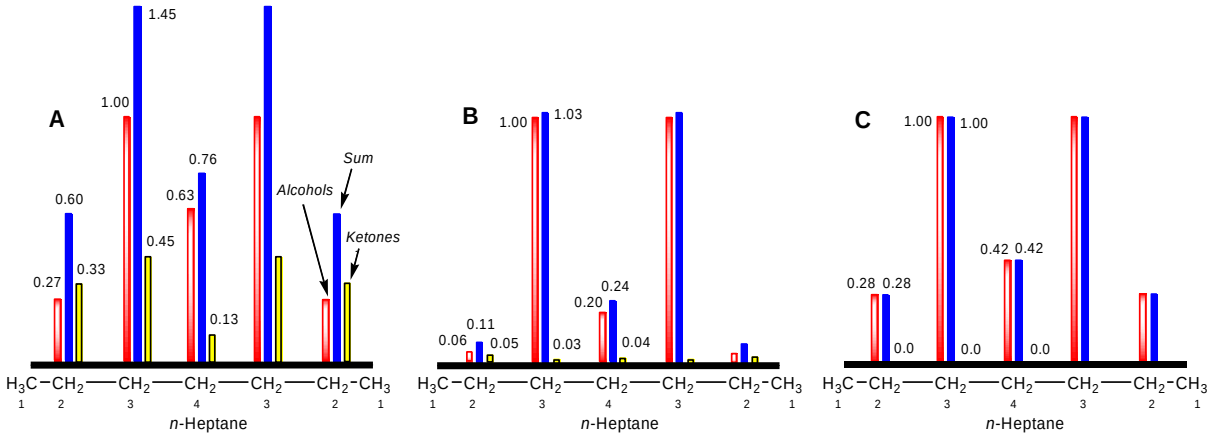

Figure 63. Distribution of isomers (normalized reactivities of methylenes in positions 2, 3 and 4) in the oxidation of *n*-heptane with H_2O_2 catalyzed by TS-1. The reactivity of the 3-methylene hydrogens in the corresponding isomeric alcohol formation is accepted to equal 1.00 (TS-1, 5 mg; H_2O_2, 0.25 mL; *n*-heptane, 0.05 mL; 0.5 h, 50 °C). (A) without additives; (B) in the presence of hexan-3-ol (0.05 mL); (C) in the presence of butan-2-ol (0.05 mL)

The most striking peculiarity of the reaction with *n*-heptane is an unusual distribution of regioisomers formed by the functionalization of methylene groups (Figure 63). Thus, the

normalized reactivities of the methylenes in positions *2* and *4* are approximately two times lower than that of the *3*-CH_2 group. If hexan-3-ol is added to the reaction mixture (Figure 63B) the regioselectivity increases dramatically: the reactivity of the *3*-CH_2 group is now ten and five times higher than the reactivities of hydrogens in positions *2* and *4*. It is noteworthy that in this case, the 3- and 4-oxygenates consist of the almost pure isomeric alcohols, whereas the mixture of 2-oxygenates (formed in a very small amount) consists of approximately equal portions of the alcohol and ketone. In the course of the reaction, hexan-3-ol is oxidized to hexan-3-one with conversion of only 2.5%. Butan-2-ol also enhances the regioselectivity (Figure 63C), although less efficiently in comparison with hexan-3-ol.

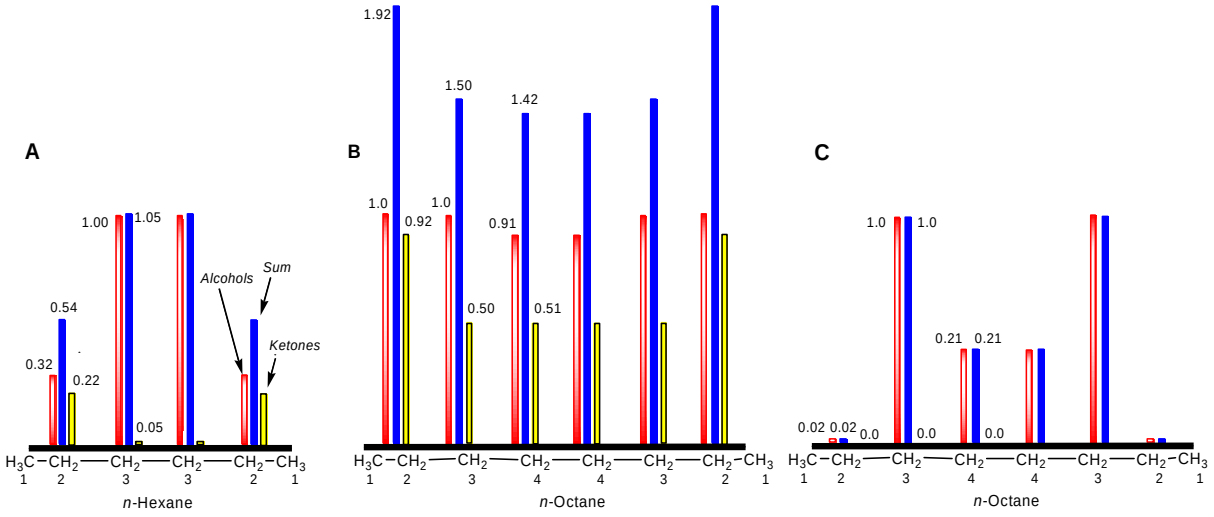

Figure 64. Reactivities of methylenes in various positions of the alkane chain in the oxidation of *n*-hexane (A) and n-octane (B) with H_2O_2 catalyzed by TS-1. The reactivity of the 3- or 2-methylene hydrogens in the corresponding isomeric alcohol formation is accepted to equal 1.00. (C) in the presence of hexan-3-ol.

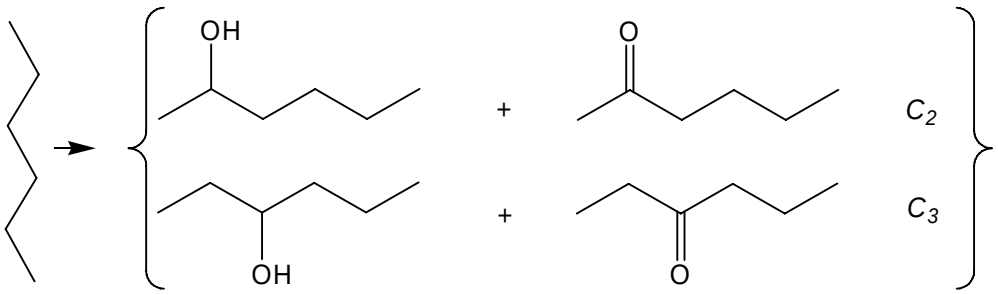

Scheme 39. Reaction products of the *n*-hexane oxidation with H_2O_2 and air catalyzed by TS-1 after treatment with PPh_3.

The oxidation of *n*-hexane (Scheme 39, Figure 64A) occurs under the same conditions with the predominant formation of the 3-oxygenate (consisting of the almost pure alcohol). In contrast, the oxidation of *n*-octane gives the "usual" distribution of regioisomers (Figure 64B): the amount of the 2-oxygenates is slightly larger than that of the other isomers. However, as in the case of *n*-heptane, adding hexan-3-ol improves dramatically the selectivity to give only the 3- and 4-alcohols (Figure 64C, Scheme 40).

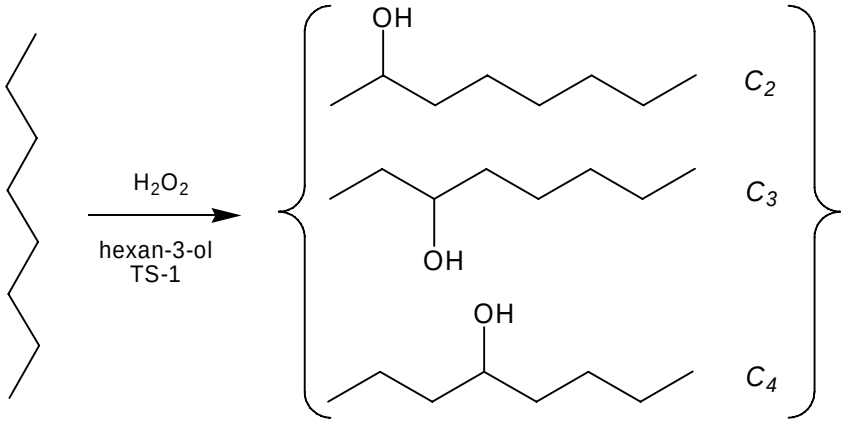

Scheme 40. Improved selectivity of the n-octane oxidation with H_2O_2 and air in the presence of hexan-3-ol, catalyzed by TS-1 (after treatment with PPh_3).

The reaction with *n*-nonane (Figure 3) gives an isomer distribution in which the amount of C_2 oxygenates is 2.5 times higher than the amount of the 3-isomers.

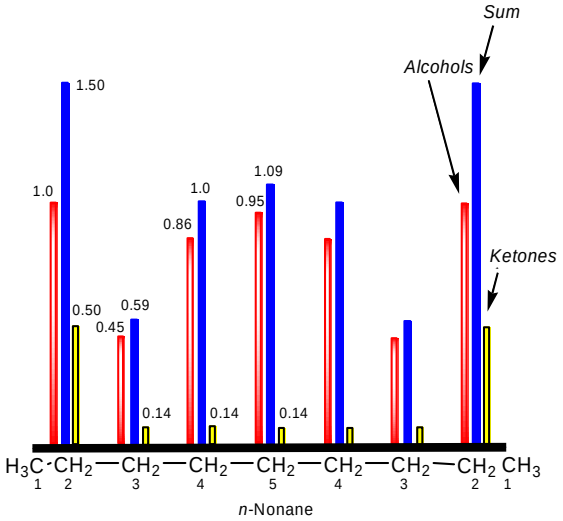

Figure 65. Normalized reactivities of methylenes in various positions of the *n*-nonane chain in its oxidation with H_2O_2 catalyzed by TS-1. The reactivity of the 2-methylene hydrogens in the corresponding isomeric alcohol formation is accepted to equal 1.00.

We can assume that this unusual regioselectivity is due to the narrow hydrophobic cavities of TS-1 in which the oxygenation of alkanes proceeds. If adsorbed [217, 218] in the silicalite *n*-heptane adopts a U-shape conformation [219, 220], the C–H bonds in position *3* will be in close contact with reaction centers (titanium-peroxy species), whereas the *4*-CH_2 groups are situated (in the form of a "hairpin bend") in the middle of the channel and cannot be efficiently attacked by the oxidizing species. Molecules of higher alcohols are apparently adsorbed in the cavity modifying it, and this leads to an increase in the regioselectivity.

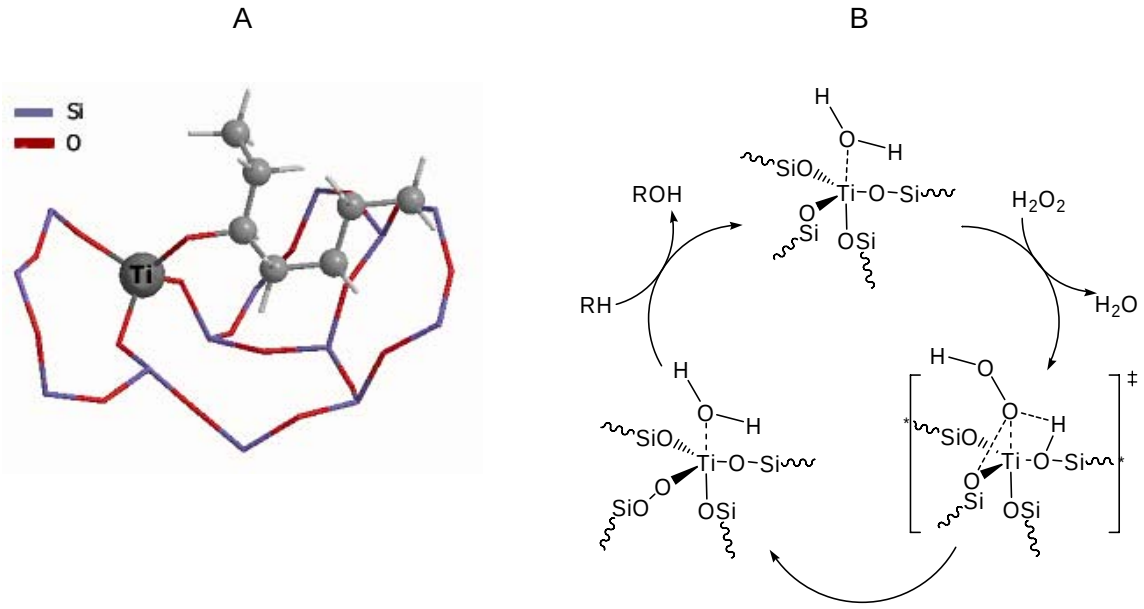

Figure 66. Oxygenation of alkanes with H_2O_2 catalyzed by TS-1; (A) - *n*-heptane in a hydrophobic channel of TS-1 approaches Ti^{4+} active site, (B) – possible mechanism of oxygenation supported by DFT calculations including Ti-peroxo (Ti)-OO-(Si) moieties as an active species [214]

Recently, it was found that in the reaction of *n*-heptane with the "H_2O_2–$[(L\text{-}Me_3)_2Mn_2(O)_3]^{2+}$– carboxylic acid" system in water the CH_2 groups in position 4 are oxidized more easily than the methylenes in positions *3* and *2* [64]. This phenomenon can also be explained if we assume that *n*-heptane in aqueous solution adopts U-shape conformations and the *4*-CH_2 group has some preference in approaching the Mn-containing reaction center situated between two voluminous macrocyclic ligands.

6.3 Conclusion

Titanosilicalite TS-1 catalyses the oxidation of light (methane, ethane, propane and *n*-butane) and higher normal alkanes (hexane, heptane, octane and nonane) to give the corresponding isomeric alcohols and ketones. The oxidation of higher alkanes proceeds with a unique regioselectivity. Thus, in the reaction with *n*-heptane the CH_2 groups in position *3* exhibit a reactivity 2.5 times higher than those of the other methylene groups. This selectivity can be enhanced if hexanol-3 is added to the reaction mixture, the 3-CH_2/2-CH_2 ratio attaining 10. It is assumed that the unusual selectivity in oxidation of *n*-heptane (and other higher alkanes) is due to steric hindrance in the catalyst cavity. As a result the catalytically active species situated on the catalyst walls can react easily only with certain methylene groups of the alkane which is adsorbed in the cavity taking U-shape (hairpin) conformations.

This work demonstrates that by using solid catalysts with nanopores we can control regioselectivity in the oxidative functionalization of higher normal alkanes, and this selectivity can be improved if we introduce into the reaction mixture certain other molecules such as alcohols.

7 General Conclusions and Perspectives

The project of this work deals with one of the most intriguing and important topics of contemporary chemical research, the catalytic activation and functionalization of hydrocarbons that are still regarded mainly as energy supplies. The aim of the present work was to get new mechanistic insights into the oxidation of alkanes, alkenes and alcohols starting from known catalytic systems and to develop new catalysts on the basis of transition metal complexes, using cheap and environmentally benign oxidants.

$$CH_4 + H_2O_2 + 1/2\ O_2 \longrightarrow CH_3OOH + H_2O$$

In the first part of this thesis, the known binary vanadate/pyrazine-2-carboxylic acid (VO_3^-/pcaH) system was found to oxidize alkanes and alcohols with hydrogen peroxide by different radical-based reaction mechanisms. In the catalytic cycle two different radicals are released: the hydroperoxyl and hydroxyl radicals, which both attack the substrates with activated C−H bonds (alcohols), whereas in the alkane oxidation only hydroxyl radicals are the oxidizing species.

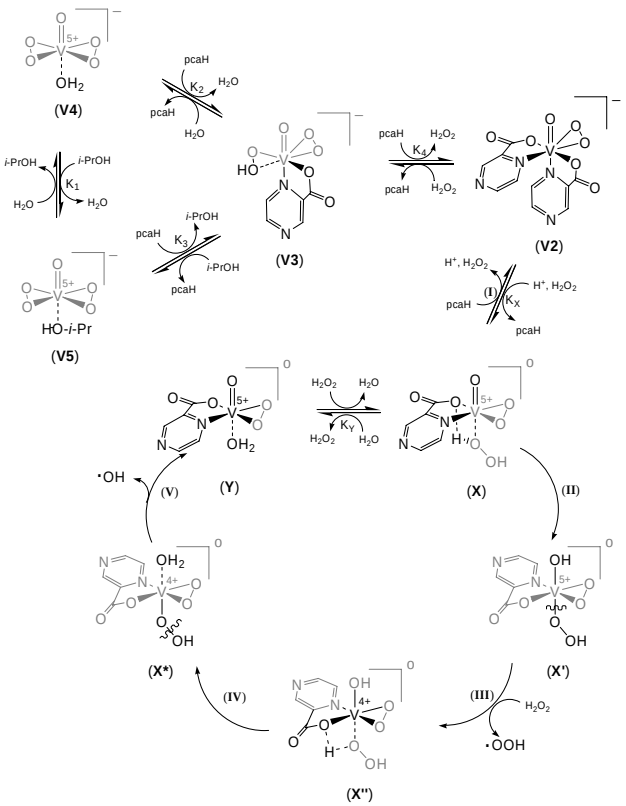

Detailed spectroscopic and kinetic studies revealed that the rate-limiting step is the monomolecular decomposition of a diperoxo vanadium complex containing one pca ligand, tentatively assigned [V(O)(OO)(H_2O_2)(pca)] (**X**). However, there are two consecutive steps with comparable activation barriers (steps II and III). The mechanistic scheme proposed satisfactorily interprets the experimental data and is supported by recent DFT studies of the system. Water substentially decreases the catalytic activity of the vanadate/pcaH system. However, in aqueous solution methane can be oxygenated using an excess of pcaH at elevated temperatures (70–90 °C).

The second part of this thesis is inspired by biomimetics and centered on manganese and iron complexes which can mimic methane monooxygenase and other oxygen-activating enzymes. In this context, the 1,4,7-triazacyclononane macrocycle was found to be a very useful framework for the synthesis of new ligands, which allows to tune the electronic and steric properties of the resulting transition metal complexes. Six new 1,4,7-triazacyclononane-derived ligands as well as thirteen new manganese, iron, cobalt and ruthenium complexes have been synthesized and characterized.

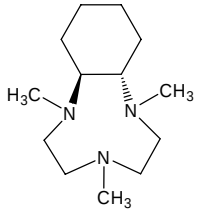

(L^{SS}-Me_3)

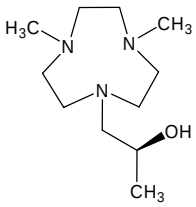

(R^{1S}L-Me_2)

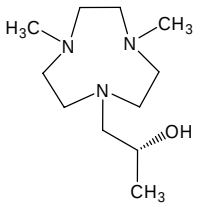

(R^{1R}L-Me_2)

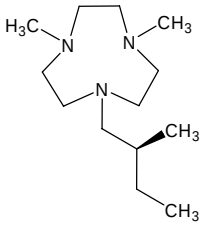

(R^{2S}L-Me_2)

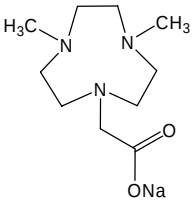

([Na][Ac-L-Me_2])

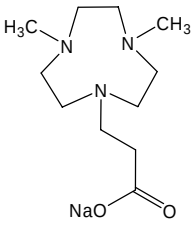

([Na][Pr-L-Me_2])

The catalytic activities and the selectivities of the manganese, iron, cobalt and ruthenium catalysts containing 1,4,7-triazacyclononane-derived ligands can be tuned by: a) using a co-catalyst (oxalic, ascorbic and pyrazin-2-carboxylic acids), which acts as ligand or/and reducing agent for the metal centers, b) introducing a functionality (carboxylato or hydroxo pendant arm) or/and chirality into the 1,4,7-triazacyclononane macrocycle. The $MnSO_4$/Pr-L-Me_2 system, where Pr-L-Me_2 is 3-(4,7-dimethyl-1,4,7-triazacyclononan-1-

yl)propionate ligand, shows the best performance in the oxidation of alcohols and in epoxidation of alkenes with H_2O_2 reported to date, the reaction proceeds smoothly in water under mild conditions.

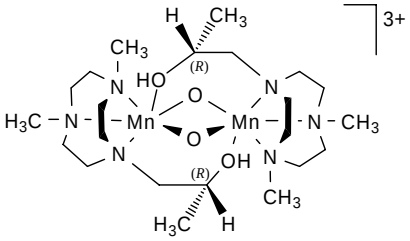

(**Mn5R**)

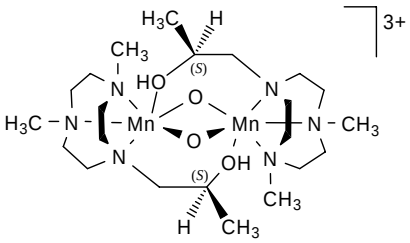

(**Mn5S**)

Five new dinuclear manganese complexes containing 1,4-dimethyl-1,4,7-triazacyclononane (**Mn1**–**Mn3**) and enantiomerically pure (*R*)- and (*S*)-1-(2-hydroxypropyl)-4,7-dimethyl-1,4,7-triazacyclononane **(Mn5R**, **Mn5S)** ligands have been isolated and characterized. The molecular structures of **Mn5R** and **Mn5S** provide the first examples of dinuclear manganese complexes bridged by two chiral pendant arms and present one more example of the chiral high-valent manganese complexes with enantioselective and stereoselective properties in the catalytic oxidation with H_2O_2.

A straight-forward synthesis for new dinuclear Fe(III)-Fe(III) complexes **Fe1**–**Fe3** containing 1,4-dimethyl-1,4,7-triazacyclononane ligands as well as carboxylato and oxo bridges has been developed. With 2-(4,7-dimethyl-1,4,7-triazacyclononan-1-yl)acetate ligand **(**Ac-L-Me_2) two iron(III) complexes have been isolated: **Fe5** represents the dinuclear Fe(III)-Fe(III) complex $[(N_3O\text{-Ac-L-}Me_2)_2Fe_2(\mu\text{-O})(\mu\text{-OOCCH}_3)]^+$ with pendant acetato arms being μ_1-coordinated to iron(III) centers; **Fe4** is a tetranuclear $[(N_3O_2\text{-Ac-L-}Me_2)_4Fe_4(O)_2]^{4+}$ complex with μ_2-coordinating mode of the pendant acetato arms. The tetranuclear structure of **Fe4** represents a new example of the binding versatility of carboxylates.

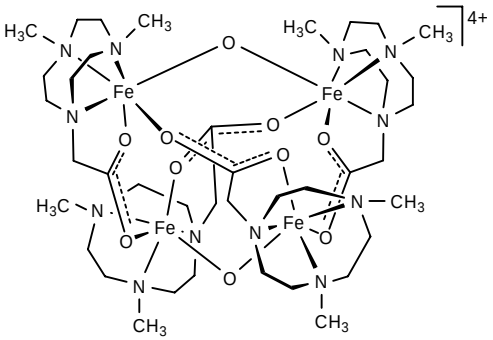

(**Fe4**)

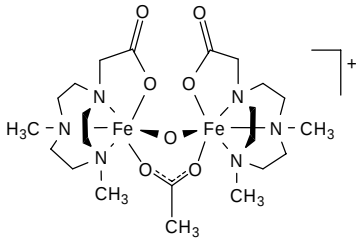

(**Fe5**)

Fe4 and **Fe5** can be used for alcohol and alkane oxidation with H_2O_2, the addition of reducing agents or co-ligands is not necessary. Given that the active oxidizing species in both cases present a radical selectivity pattern, they can be assumed to be ferryl-oxo radicals. **Fe4** and **Fe5** complexes can serve as structural and functional models for methane monooxygenase, since they have common structural and selectivity features; both complexes are active in the oxidation of methane with H_2O_2.

Two ruthenium(III) complexes **Ru1**, **Ru2** as well as the dinuclear Co(III)-Co(III) complex **Co1** containing 1,4-dimethyl-1,4,7-triazacyclononane ligands have been isolated and characterized. The molecular structure of **Co1** provides the first example of an X-ray resolved structure of a dinuclear Co(III)-Co(III) carboxylato-bridged complex. All three compounds show catalytic activity for the oxidation of isopropanol with hydrogen peroxide in water to give acetone in the presence of ascorbic acid as co-catalyst.

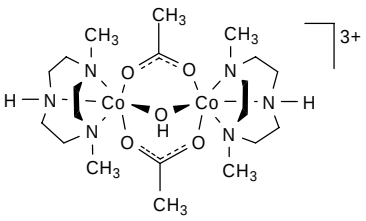

(**Co1**)

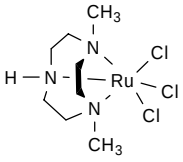

(**Ru1**)

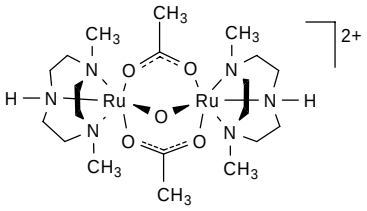

(**Ru2**)

The third part of this thesis tackles regio- and shape-selectivity problems. Using a solid titanosilicalite catalyst with nanopores (TS-1), we can control regioselectivity in the oxidative functionalization of higher normal alkanes, and this selectivity can be improved dramatically if we introduce into the reaction mixture certain alcohols, which compete with the substrate for the nanopores.

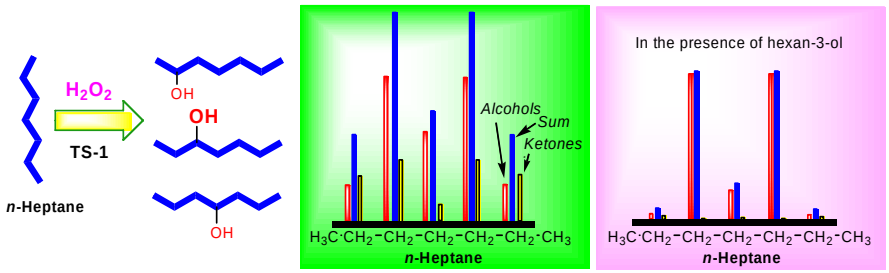

It is assumed that the unusual selectivity in the oxidation of *n*-heptane (and other higher alkanes) is due to steric hindrance in the catalyst cavity. The catalytically active species situated on the catalyst walls can react easily only with exposed methylene groups of the alkane chain, which is adsorbed in the cavity taking U-shape (hairpin) conformations.

This work demonstrates that the biomimetic approach combined with detailed mechanistic investigations provide new insights into the selective oxidation pathways. Nature can serve as a model for developing new concepts and strategies in the catalyst design.

8 Experimental Section

8.1 Solvents, Gases and Starting Materials

Solvents for the catalytic experiments were of analytical grade (Acros, Merck or Cambridge Isotope Laboratories) and used without distillation, only stored over molecular sieve and under a nitrogen atmosphere. Solvents for synthesis were of technical grade and were purified by distillation under nitrogen atmosphere and dried according to standard laboratory practices [221]. Water was bidistilled and stored under nitrogen. Laboratory gases were purchased from Carbagas and used directly from the cylinders without further purification.

Commercial salts of vanadium, manganese, iron and cobalt were used as received (Aldrich and Merck). The compounds NBu_4VO_3 [222], $RuCl_2(dmso)_4$ [223] were synthesized as described previously. The macrocyclic ligands precursors L_N [119], L_O [119], L-Ts_3 [118], L [119], L-Me_2 [129], L-Me_3 [118], L-CH [224], L_{NO} [133], $L^{SS}{}_N$ [116, 133] and L^{SS}-Ts_3 [116, 133] were synthesized and purified according to the published methods. All other commercial organic compounds were of analytical grade and used as received (Acros, Aldrich and Fluka). Hydrogen peroxide was used as a solution in water (30%, not stabilized, Fluka) and stored at 4 °C. The exact concentration was determined using potassium permanganate titration and by UV-spectroscopy (230 nm, $\varepsilon = 81\ M^{-1}\ cm^{-1}$). Formaldehyde was used as a solution in water (37 %, stabilized with 10% methanol, Acros) and stored at room temperature. Hydrobromic acid was used as a solution in glacial acetic acid (33%, Riedel de Haën).

The TS-1 samples, prepared according to references [208, 209], were given to us by Prof. Tawan Sooknoi, Department of Chemistry, King Mongkut's Institute of Technology, Bangkok, Thailand.

8.2 Instrumentation and Analyses

Synthetic Techniques. All syntheses were carried out by standard Schlenk techniques under nitrogen or argon atmosphere unless stated otherwise. Silica (63-200, 60 Å) and

aluminum oxide (pH 7.0) for the column chromatography was purchased from Chemie Brunschwig AG and Fluka respectively.

UV-Vis Spectrophotometry. UV-Vis spectra were recorded using an UVICON-930 spectrophotometer; the samples were placed in quartz 2 mm or 10 mm high-precision cells with an appropriate solvent used as reference. Microsoft Excel was used for data analysis.

IR Spectroscopy. Infrared spectra were recorded with a Perkin-Elmer Spectrum One spectrometer in transmission mode where the absorptions are given in reciprocal centimeters (cm^{-1}). A standard press was used to produce KBr pellets. Intensity data are described with the following abbreviations: vs = very strong, s = strong, m = medium, w = weak, sh = shoulder.

CD Spectroscopy. Circular dichroism spectra were recorded using a JASCO J-710 instrument with 2 nm band width, 0.5 nm step resolution, 4 s response time in quartz 10 mm high-precision cells with an appropriate solvent used as reference. Microsoft Excel was used for data analysis.

NMR Spectroscopy. Nuclear magnetic resonance spectra were recorded using a Varian Gemini 200 BB instrument or a Bruker AMX 400 spectrometer and referenced by using the resonances of the residual non-deuterated solvents. ^{1}H and ^{13}C {^{1}H - decoupled} NMR: internal standard solvent, external standard TMS. ^{51}V NMR spectra were recorded by Dr. Alex Kitaygorodskiy (Clemson University, Clemson, USA) using a Bruker Avance 500 at 500.13 MHz (^{1}H) and 131.46 MHz (^{51}V). A typical vanadium spectrum for a 1 mM solution was obtained from the accumulation of 20,000 transients with a 700 ppm spectral window, at about 12 scans per second. An exponential line broadening up to 200 Hz was applied before Fourier transformation. The vanadium chemical shifts are quoted relative to external $VOCl_3$ (0 ppm). The spectra in 2-propanol were collected with the magnetic field unlocked. Unless it is stated otherwise, spectra were recorded at room temperature (297 K). Chemical shifts are given in ppm and coupling constants *J* in Hz (s = singlet, d = doublet, t = triplet, dd = doublet of doublet, m = multiplet)

Potentiometric Titration. pH-potentiometric measurements were done by Dr. Péter Buglyó from University of Debrecen, Hungary. The measurements were carried out at an ionic strength of 0.2 mol dm^{-3} (KCl) and at 25.0 ± 0.1 ^{o}C in aqueous solution. Carbonate-free KOH solution of known concentration (*ca.* 0.2 M) was used as titrant. A Radiometer pHM 84

instrument equipped with Metrohm combined electrode (type 6.0234.110) and Metrohm 715 Dosimat burette was used for the pH-metric measurements. The electrode system was calibrated according to Irving *et al.* [225]; the pH-metric readings could therefore be converted directly into hydrogen ion concentration. The water ionization constant, pK_w, is 13.76 ± 0.01 under the conditions employed. The pH-metric titrations were performed in the pH range 2.0−11.0. The initial volume of the samples was 10.00 mL. The ligand concentrations were varied in the range 2–4 mM and the metal ion to ligand ratios in the range 1:1−1:4. The samples were in all cases completely deoxygenated by bubbling purified argon for *ca*. 20 min before the measurements. About 200 titration points were used to find the stoichiometry of the species and calculate their concentration stability constants in the vanadate/pcaH system. The calculations were performed by the PSEQUAD computer program [226] using the literature data (log β) of the vanadium(V) [227] hydrolytic. The accepted fitting of the titration curves was always less than 0.01 mL.

Mass Spectra. ESI mass spectra were measured by the Analytical Service of the University of Neuchâtel (Switzerland) using a LCQ Finnigan spectrometer.

Elemental Analyses. Microanalyses were carried out by the Laboratory of Pharmaceutical Chemistry, University of Geneva (Switzerland) or by the Laboratory of Organic Chemistry, ETH Zurich (Switzerland).

Crystallographic Analyses. The crystallographic analyses were done by Dr. Bruno Therrien and the crystallographic group of the University of Neuchâtel directed by Professor Helen Stoeckli-Evans. Generally, single X-ray quality crystals were mounted on a Stoe Image Plate Diffraction system equipped with a ϕ circle goniometer, using Mo-Kα graphite monochromated radiation (λ = 0.71073 Å) with ϕ range 0−200°, increment of 1.5, 1.4 and 1.5° respectively, D_{max}-D_{min} = 12.45−0.81 Å. The structures were solved by direct methods using the program SHELXS-97 [228]. The refinement and all further calculations were carried out using SHELXL-97 [229]. In all compounds the hydrogen atoms have been included in calculated positions and treated as riding atoms using the SHELXL default parameters. All non-H atoms were refined anisotropically, using weighted full-matrix least-square on F^2. A semi-empirical absorption correction was applied using MULABS (PLATON03 [230], T_{min}=0.776, T_{max}=0.961). Molecular structure representations were drawn with ORTEP [231], MERCURY [232] and POV-RAY [233]. The experimental data for these analyses are shown in Appendix.

Gas Chromatography. GC-analysis was performed on a Dani 86.10 gas chromatograph equipped with a split-mode capillary injection system and flame ionisation detector using a CP-WAX52CB capillary column (25 m × 0.32 mm × 0.25 μm), integrator SP-4400, carrier gas was helium. Acetonitrile or nitromethane was used as internal standards. The flame ionization detector response factors were obtained after calibration experiments, using a standard substrate mixtures.

Gaseous mixtures (O_2, N_2, CH_4, CO and CO_2) were quantified after injection of 500 μl with a gas-tight syringe on a packed column (Carboxen-1000 60/80, 4.5 m × 3.1 mm, Supelco) using a thermal conductivity detector (TCD).

High Performance Liquid Chromatography. The HPLC analyses were done on a Agilent/Hewlett-Packard 1100 modular HPLC system equipped with a UV-detector using nitrobenzene as internal standard. The chiral product separation was performed using Daicel Chiracel OB-H (25 cm × 4.6 mm, for 1-phenylethanol) and Daicel Chiracel OJ-H (25 cm × 4.6 mm, with pre-column, for indene oxide) columns and analysed with Agilent Chemport software. In isocratic conditions the retention times were: (hexane/isopropanol 50/1, 0.9 mL/min) 11 (nitrobenzene), 16 (*S*-1-phenylethanol), 17 (acetophenone) and 25 minutes (*R*-1-phenylethanol); (hexane/isopropanol 50/1, 0.8 mL/min) 7 (indene), 11 (nitrobenzene), 16 (indanone-2), 18 (1*R*,2*S*-indene oxide), 20 (1*S*,2*R*-indene oxide) and 29 minutes (indanol-2). The calibration experiments were performed using standard substrate mixtures and verified by ^{1}H NMR and UV-spectroscopy. The mixture of racemic indene oxide and indanone-2 was obtained according to the published procedure [141] and fractionalized on silica column (eluent CH_2Cl_2, ^{1}H NMR analysis). The 1*R*,2*S*-indene oxide enriched sample was prepared (Jacobsen protocol [142, 143]) using Mn(III)-*R*,*R*-salen complex (Aldrich), *N*-pyridine oxide as terminal ligand and chlorobenzene as solvent.

Kinetic Calculations. The kinetic parameters and equations in this work were calculated with Dr. Yuriy N. Kozlov from the Semenov Institute of Chemical Physics, Russian Academy of Sciences, Moscow, Russia.

8.3 Syntheses

(*S*)-1-(2-methylbutyl)-4,7-diaza-1-azoniatricyclo[5.2.1.0^{4,10}]decane iodide ([R^{2S}L-CH][I]). In a 50 mL Schlenk tube 1.11 g (8.0 mmol) of freshly distilled methine-bridged triamine L-CH (1,4,7-triazatricyclo[5.2.1.0^{4,10}]decane) was dissolved in 5 mL of absolute THF at 0 °C, and a solution of (*S*)-1-iodo-2-methylbutane in 5 mL of THF was added dropwise (10 minutes). After stirring at 0 °C for one hour, the mixture was warmed to the room temperature and stirred in the darkness for 96 hours. The resulting white-yellowish crystals precipitated from the solution were filtered under nitrogen atmosphere, washed 4 times with 5 mL of THF and dryed *in vacuo* (0.05 mbar, 20 °C, 24h).

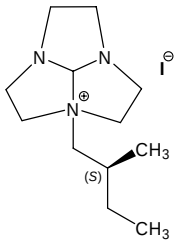

([R^{2S}L-CH][I])

[R^{2S}L-CH][I]: Yield 42–52%. ^{1}H NMR (400 MHz, CD_3OD) δ = 5.65 (s, 1H, N_3CH), 3.82–3.68 (m, 6H, NCH*H*CH*H*N), 3.4–3.2 (m, 7H, NC*H*HC*H*HN, NC*H*HCH(CH_3)C_2H_5), 3.00 (m, 1H, NCH*H*CH(CH_3)C_2H_5), 2.13 (m, 1H, NCH_2CH(CH_3)C_2H_5), 1.61 (m, 1H, $NCH_2CH(CH_3)CHHCH_3$), 1.42 (m, 1H, $NCH_2CH(CH_3)CHHCH_3$), 1.18 (d, 3H, NCH_2CH-(CH_3)CH_2CH_3, ^{3}J = 6.8 Hz) and 1.03 ppm (t, 3H, $NCH_2CH(CH_3)CH_2CH_3$, ^{3}J = 7.4 Hz). ^{13}C NMR {^{1}H decoupled} (100 MHz, CD_3OD) δ = 129.4, 64.3, 58.3, 57.6, 57.3, 53.2, 52.9, 33.1, 29.6, 19.0 and 11.4 ppm. MS (ESI positive mode, CH_3OH): *m/z* 210.2 (60%, [R^{2S}L-CH]$^{+}$), 200.4 (24%, [R^{2S}L + H]$^{+}$), 228 (8%, [R^{2S}L-COH + H]$^{+}$, methine-bridge opening) and 340.3 (6%, [R^{2S}L-CH + I + 3H]$^{3+}$); MS/MS {*m/z* 210.2 fragment} *m/z* 140.1 ([R^{2S}L-CH + H − $CH_2CH(CH_3)CH_2CH_3$]$^{+}$). IR (KBr pellets) ν (cm^{-1}): 2962 (s), 2881 (s), 1462 (s), 1385 (s), 1288 (s), 1214 (s), 1085 (vs), 713 (s) and 601 (m). UV-vis (CH_3CN) λ_{max} (nm): 214 (ε = 10200 M^{-1} cm^{-1}), 247 (12500). CD (CH_3CN) λ_{max} (nm): 243 (Δε = + 2.34 M^{-1} cm^{-1}), 239.5 (– 5.1).

8.3.1 Ligands

(*S*)-1-(2-methylbutyl)-4,7-dimethyl-1,4,7-triazacyclononane ($R^{2S}L\text{-}Me_2$). In a 100 mL flask (*S*)-1-(2-methylbutyl)-4,7-diaza-1-azoniatricyclo [5.2.1.$0^{4,10}$]decane iodide ([R^{2S}L-CH][I]) (1.40 g, 4.15 mmol) was dissolved in the mixture of 37% formaldehyde (20 mL) and formic acid (20 mL) and heated to reflux for 24 hours. After subsequent cooling an excess of 37% HCl (30 mL) was added and the solution was rotary evaporated. The yellow-brownish solids were dissolved in 20 mL 5M NaOH (pH > 12) and then extracted with chloroform (3 × 30 mL), dryed over anhydrous Na_2SO_4 and rotary evaporated. The crude product was distilled (bulb to bulb) under reduced pressure (0.1 mbar, 95 °C) in the nitrogen atmosphere to give a colorless oil.

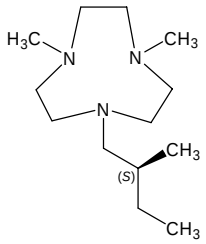

($R^{2S}L\text{-}Me_2$)

$R^{2S}L\text{-}Me_2$: Yield 75–81%. ^{1}H NMR (400 MHz, CD_3OD) δ = 2.93–2.62 (m, 12H, NC*H*$_2$C*H*$_2$N), 2.37 (s, 6H, NC*H*$_3$), 2.25 (m, 1H, NC*H*HCH(CH_3)C_2H_5), 2.19 (m, 1H, NCH*H*CH(CH_3)C_2H_5), 1.54 (m, 1H, NCH_2C*H*(CH_3)C_2H_5), 1.49 (m, 1H, $NCH_2CH(CH_3)C$*H*HCH_3), 1.12 (m, 1H, $NCH_2CH(CH_3)CH$*H*CH_3), 0.93 (d, 3H, NCH_2CH-(C*H*$_3$)CH_2CH_3, ^3J = 6.6 Hz) and 0.90 ppm (t, 3H, $NCH_2CH(CH_3)CH_2C$*H*$_3$, ^3J = 7.4 Hz). ^{13}C NMR {^{1}H decoupled} (100 MHz, $CDCl_3$) δ = 67.3 (1 × N*C*H$_2$CH(CH_3)CH_2CH_3), 57.6 , 57.3, 56.5 (6 × N*C*H$_2$*C*H$_2$N), 46.2 (2 × N*C*H$_3$), 33.7 (1 × NCH_2*C*H(CH_3)CH_2CH_3), 27.7 (1 × $NCH_2CH(CH_3)$*C*H$_2CH_3$), 18.1 (1 × NCH_2CH(*C*H$_3$)CH_2CH_3) and 11.4 ppm (1 × NCH_2CH-(CH_3)CH_2*C*H$_3$). MS (ESI positive mode, CH_3OH): *m/z* 228.2 ([$R^{2S}L\text{-}Me_2$ + H]$^+$). IR (film) ν (cm^{-1}): 2923 (s), 2782 (s), 1454 (s), 1368 (s), 1298 (m), 1109 (s), 1031 (s), 869 (m) and 752 (m). UV-vis (CH_3CN) λ_{max} (nm): 212 (ε = 7700 M^{-1} cm^{-1}). CD (CH_3CN) λ_{max} (nm): 232.5 ($\Delta\varepsilon$ = – 1.7 M^{-1} cm^{-1}), 229 (+ 0.87).

General procedure for **(*S*)-1-(2-hydroxypropyl)-4,7-dimethyl-1,4,7-triazacyclononane** (R^{1S}L-Me_2) and **(*R*)-1-(2-hydroxypropyl)-4,7-dimethyl-1,4,7-triazacyclononane** (R^{1R}L-Me_2). In a 20 mL Schlenk tube 1.57 g (10.0 mmol) of freshly distilled 1,4-dimethyl-1,4,7-triazacyclononane (L-Me_2) was dissolved in 3 mL of absolute ethanol at −10 °C, and a solution of corresponding enantiopure (*S*)-propylene oxide (0.82 g, 15 mmol, for R^{1S}L-Me_2) or (*R*)-propylene oxide (0.82 g, 15 mmol, for R^{1S}L-Me_2) in 3 mL of ethanol was added dropwise through a septum (5 minutes). After stirring at −10 °C for one hour, the mixture was warmed to the room temperature and stirred in the darkness for 48 hours. The low-boiling components were evaporated before the crude product was distilled (bulb to bulb) under reduced pressure (0.1 mbar, 95 °C) in the nitrogen atmosphere to give a colorless oil.

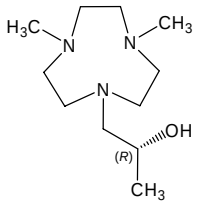

(R^{1R}L-Me_2)

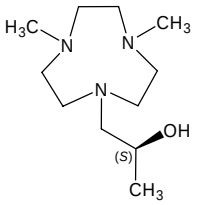

(R^{1S}L-Me_2)

R^{1R}L-Me_2: Yield 70%. ^{1}H NMR (400 MHz, $CDCl_3$) δ = 3.76 (m, 1H, $NCH_2CH(OH)CH_3$), 2.70–2.60 (m, 12H, NCH_2CH_2N), 2.60–2.37 (m, 2H, $NCH_2CH(OH)CH_3$), 2.20 (s, 6H, NCH_3) and 1.03 (d, 3H, $NCH_2CH(OH)CH_3$, ^3J = 6.3 Hz). ^{13}C NMR {^{1}H decoupled} (100 MHz, $CDCl_3$) δ = 66.1 ($NCH_2CH(OH)CH_3$), 65.9 ($NCH_2CH(OH)CH_3$), 58.7, 58.1, 57.0 (3 × NCH_2CH_2N), 46.3 (NCH_3) and 19.6 ($NCH_2CH(OH)CH_3$) ppm. MS (ESI positive mode, CH_3OH): *m/z* 216 ([R^{1R}L-Me_2 + H]$^+$). IR (film) ν (cm^{-1}): 3207 (s), 2928 (s), 2796 (s), 1455 (s), 1367 (s), 1319 (s), 1089 (s), 1035 (s), 986 (s) 878 (m) and 775 (m). UV-vis (hexane) λ_{max} (nm): 212 (ε = 1800 M^{-1} cm^{-1}). CD (hexane) λ_{max} (nm): 249 (Δε = – 0.15 M^{-1} cm^{-1}), 238 (+ 0.38), 233 (– 0.62) and 228 (+ 0.78).

R^{1S}L-Me_2: Yield 70%. ^{1}H NMR (400 MHz, C_6D_6) δ = 5.54 (br, 1H, $NCH_2CH(OH)CH_3$), 3.83 (m, 1H, $NCH_2CH(OH)CH_3$), 2.57 (m, 4H, R*NCH_2CH_2N), 2.49 (m, 8H, NCH_2CH_2N), 2.34–2.27 (m, 2H, $NCH_2CH(OH)CH_3$), 2.20 (s, 6H, NCH_3) and 1.17 (d, 3H, $NCH_2CH(OH)CH_3$, ^3J = 6.2 Hz). ^{13}C NMR {^{1}H decoupled} (100 MHz, C_6D_6) δ 66.5 ($NCH_2CH(OH)CH_3$), 65.7 ($NCH_2CH(OH)CH_3$), 59.2, 58.5, 56.9 (3 × NCH_2CH_2N), 46.4 (NCH_3) and 20.4 ($NCH_2CH(OH)CH_3$) ppm. MS (ESI positive mode, acetone): *m/z* 216

($[R^{1S}L\text{-}Me_2 + H]^+$). IR (film) ν ($cm^{-1}$): 3217 (s), 2933 (s), 2796 (s), 1455 (s), 1367 (s), 1318 (s), 1089 (s), 1035 (s), 986 (s) 878 (m) and 775 (m). UV-vis (hexane) λ_{max} (nm): 212 (ε = 1800 M^{-1} cm^{-1}). CD (hexane) λ_{max} (nm): 249 ($\Delta\varepsilon$ = + 0.15 M^{-1} cm^{-1}), 238 (– 0.24), 234 (+ 0.65) and 229 (– 0.73).

Sodium 2-(4,7-dimethyl-1,4,7-triazacyclononan-1-yl)acetate ([Na][Ac-L-Me_2]). In a 100 mL Schlenk tube 3.14 g (20.0 mmol) of freshly distilled 1,4-dimethyl-1,4,7-triazacyclononane (L-Me_2) was dissolved in 10 mL of water at room temperature and an aqueous solution of sodium bromoacetate (20 mmol, 10 mL), prepared by neutralization of 2.78 g (20 mmol) of bromoacetic acid with 0.80 g (20 mmol) NaOH, was added dropwise (5 minutes). The temperature was raised to 80 °C and 1.00 g (25 mmol) of NaOH dissolved in 5 mL of water was added dropwise. The temperature was maintained at 80 °C for 2 hours, until the reaction was complete. The light-yellow solution was evaporated (0.05 mbar, 50 °C) and the solid product was extracted with CH_2Cl_2 (3 × 50 mL), dryed over anhydrous Na_2SO_4 and filtered under the nitrogen atmosphere. A white-yellowish hygroscopic powder was obtained after solvent evaporation and drying *in vacuo* (0.01 mbar, 50 °C, 48 hours).

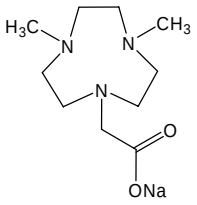

([Na][Ac-L-Me_2])

[Na][Ac-L-Me_2]: Yield 70−83%. ^{1}H NMR (400 MHz, $CDCl_3$) δ = 3.10 (s, 2H, NC*H*$_2$COONa), 2.55−2.48 (m, 12H, NC*H*$_2$C*H*$_2$N) and 2.33 (s, 6H, NC*H*$_3$). ^{13}C NMR {^{1}H decoupled} (100 MHz, $CDCl_3$) δ = 177.2 (NCH$_2$*C*OONa), 63.7 (N*C*H$_2$COONa), 55.0, 54.8, 53.2 (3 × N*C*H$_2$*C*H$_2$N) and 45.9 (N*C*H$_3$). MS (ESI negative mode, acetone): *m/z* 215 ([Ac-L-Me_2]$^-$). IR (KBr pellets) ν (cm^{-1}): 3418 (s), 2945 (s), 2853 (s), 2792 (s), 1594 (s), 1454 (s), 1405 (s), 1367 (s), 1078 (m), 1036 (s), 830 (m), 748 (m) and 612 (m). *Anal*. Calc. for $C_{10}H_{20}N_3O_2Na \cdot 1.5\ CH_2Cl_2$: C, 37.88; H, 6.36; N, 11.52. Found: C, 38.07; H, 6.50; N, 11.52 %.

Sodium 3-(4,7-dimethyl-1,4,7-triazacyclononan-1-yl)propionate ([Na][Pr-L-Me_2]). In a 100 mL Schlenk tube 3.14 g (20.0 mmol) of freshly distilled 1,4-dimethyl-1,4,7-triazacyclononane (L-Me_2) was dissolved in 10 mL of water at room temperature and an aqueous solution of sodium 3-bromopropionate (20 mmol, 10 mL), prepared by neutralization of 3.06 g (20 mmol) of 3-bromopropionic acid with 0.80 g (20 mmol) NaOH, was added dropwise (5 minutes). The temperature was raised to 50 °C and 1.00 g (25 mmol) of NaOH dissolved in 5 mL of water was added dropwise. The temperature was maintained at 50 °C for 2 hours, until the reaction was complete. The light-yellow solution was evaporated (0.05 mbar, 50 °C) and the solid product was extracted with $CHCl_3$ (3 × 50 mL), dryed over anhydrous Na_2SO_4 and filtered under the nitrogen atmosphere. The white-yellowish hygroscopic powder was obtained after solvent evaporation and drying *in vacuo* (0.01 mbar, 50 °C, 48 hours).

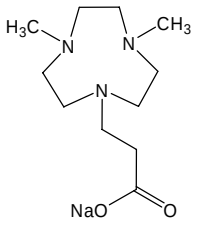

([Na][Pr-L-Me_2])

[Na][Pr-L-Me_2]: Yield 75%. ^{1}H NMR (400 MHz, CD_3OD) δ = 2.80 (t, 2H, NC$H_2$$CH_2$COONa, ^3J = 7.0 Hz), 2.65−2.63 (m, 12H, NCH_2CH_2N), 2.38 (s, 6H, NCH_3) and 2.36 (t, 2H, NCH_2CH_2COONa, ^3J = 9.9 Hz). ^{13}C NMR {^{1}H decoupled} (100 MHz, CD_3OD) δ = 181.1 (NCH_2CH_2*C*OONa), 56.5, 56.1, 55.5 (3 × N*C*H_2*C*H_2N), 53.7 (N*C*H_2*C*H_2COONa), 46.1 (N*C*H_3) and 36.6 (NCH_2*C*H_2COONa). MS (ESI negative mode, acetone): *m/z* 228.3 ([Pr-L-Me_2]$^-$), (ESI positive mode, acetone): *m/z* 230.3 ([Pr-L-Me_2 + 2H]$^+$) and 252.1 ([Pr-L-Me_2 + H + Na]$^+$). IR (KBr pellets) ν (cm^{-1}): 3459 (s), 2934 (s), 2852 (s), 2784 (s), 1611 (vs), 1581 (vs), 1464 (s), 1420 (s), 1367 (s), 1320 (m), 1077 (s), 1033 (s), 752 (m) and 623 (m). *Anal*. Calc. for $C_{11}H_{22}N_3O_2Na \cdot 0.5\ CHCl_3 \cdot H_2O$: C, 41.98; H, 7.51; N, 12.77. Found: C, 42.25; H, 7.71; N, 13.16 %.

***SS-trans*-2,5,8-trimethyl-2,5,8-triazabicyclo[7.4.0^{1,9}]tridecane** (L^{SS}-Me_3). In a 100 mL flask *SS-trans*-2,5,8-tritosyl-2,5,8-triazabicyclo[7.4.0^{1,9}]tridecane (L^{SS}-Ts_3) (2.09 g, 3.23 mmol) was dissolved in 25 mL of 96% sulfuric acid and heated at 130 °C for 72 hours. After

cooling to 0 °C 15 mL of ether was added and the dark viscous precipitate was separated by decantation and dryed in vacuo (0.05 mbar, 20 °C, 15 minutes). An ice-cold 10 M NaOH (50 mL) solution was slowly added to the slurry (pH > 12), and the resulting solution was extracted with $CHCl_3$ (3 × 50 mL), and organic fractions were rotary evaporated affording a yellow oil. This product was dissolved in a mixture of 37% formaldehyde (15 mL) and formic acid (15 mL) and heated to reflux for 24 hours. After subsequent cooling an excess of 37% HCl (25 mL) was added and the solution was rotary evaporated. The yellow-brownish solids were dissolved in 20 mL 5M NaOH (pH > 12) and then extracted with chloroform (3 × 30 mL), dryed over anhydrous Na_2SO_4 and rotary evaporated. The crude product was distilled (bulb to bulb) under reduced pressure (0.1 mbar, 105 °C) in the nitrogen atmosphere to give a colorless oil.

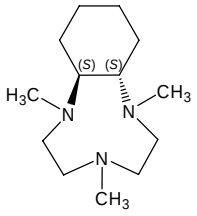

(L^{SS}-Me_3)

R^{SS}L-Me_3: Yield 20%. ^{1}H NMR (400 MHz, $CDCl_3$) δ = 2.7–2.4 (m, 8H, NC*H*$_2$C*H*$_2$N), 2.35 (br, 2H, NC**H*C**H*N), 2.26 (s, 3H, NC*H*$_3$), 2.22 (s, 6H, NC*H*$_3$), 1.80 (br, 2H), 1.71 (br, 2H) and 1.13 (br, 4H, cyclohexyl ring) ppm. ^{13}C NMR {^{1}H decoupled} (100 MHz, $CDCl_3$) δ = 64.2, 63.9, 55.0, 46.1, 40.6, 26.1 and 23.2 ppm. MS (ESI positive mode, acetone): *m/z* 226.2 ([R^{SS}L-Me_3 + H]$^+$). IR (film) ν (cm^{-1}): 2923 (s), 2775 (s), 1455 (s), 1366 (s), 1272 (s), 1172 (s), 1065 (s), 1026 (s), 951 (m), 877 (m), 853 (m) and 545 (m). UV-vis (CH_3CN) λ_{max} (nm): 229 (ε = 2200 M^{-1} cm^{-1}). CD (CH_3CN) λ_{max} (nm): 263 ($\Delta\varepsilon$ = + 0.49 M^{-1} cm^{-1}), 245 (– 0.33), 230 (+ 0.57), 222 (– 1.41) and 210 (+ 0.45).

8.3.2 Complexes

Manganese Complexes

General procedure for [(L-Me_2)$_2$$Mn_2(O)_2$(OOC-R)][$PF_6$]$_2$ ([**Mn1**][PF_6]$_2$, [**Mn3**][PF_6]$_2$) and [(L-Me_2)$_2$$Mn_2$(O)(OOC-R)$_2$][$PF_6$]$_2$ ([**Mn2**][PF_6]$_2$, [**Mn4**][PF_6]$_2$). In a 50 ml Schlenk tube, a mixture of L-Me_2 (157.3 mg, 1.00 mmol) and *p*-toluenesulfonic acid monohydrate (190.2

mg, 1.00 mmol) was dissolved in 15 mL of acetonitrile. To this clear light-yellow solution, solid $MnCl_2 \cdot 4\ H_2O$ (198 mg, 1.00 mmol) was added under vigorous stirring. The mixture was treated with ultrasound (10-15 minutes) and then stirred for half an hour. Then, KPF_6 (276 mg, 1.50 mmol) and the corresponding sodium carboxylate (**Mn1**: $HCOONa \cdot H_2O$, 129 mg, 1.50 mmol; **Mn2**: C_6H_5COONa, 216 mg, 1.50 mmol; **Mn3**: $CH_3COONa \cdot 3\ H_2O$, 68 mg, 0.50 mmol; **Mn4**: $CH_3COONa \cdot 3\ H_2O$, 204 mg, 1.50 mmol) were added to the slurry. After stirring at 45 °C for 20 minutes, the suspension was cooled to 0 °C, before 5 mL of an acetonitrile solution of H_2O_2 (102 µL, 1.0 mmol) and of triethylamine (278 µL, 2.0 mmol) was added. Then the green-brown suspension was stirred at 20 °C for 2h. After filtration through celite and washing with 2 ml of acetone, the volume of the filtrate was reduced to 3 mL *in vacuo*, and 3 mL of water was added. The dark solution was again concentrated *in vacuo* without heating, until a solid precipitated. The product was filtered off, washed with ethanol, ether and dried under vacuum. Single crystals suitable for X-ray analysis were grown from an acetone solution into which the ether was allowed to slowly diffuse within 48 hours.

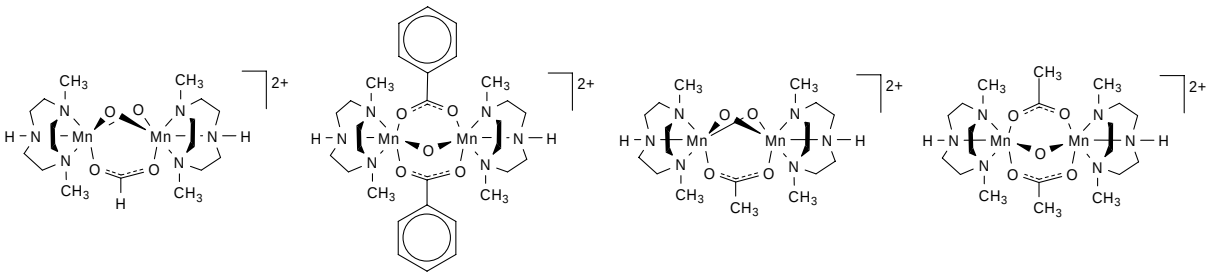

(**Mn1**) (**Mn2**) (**Mn3**) (**Mn4**)

$[(L\text{-}Me_2)_2Mn_2(O)_2(OOCH)][PF_6]_2$ ([**Mn1**][PF_6]$_2$): Yield 45%. IR (KBr pellets) ν (cm^{-1}): 3667 (m), 3593 (m), 3322 (m), 2947 (m), 2877 (m), 1617 (m), 1586 (s), 1458 (s), 1392 (m), 1326 (s), 1003 (m), 843 (vs), 690 (s), 558(s). *Anal*. Calc. for $C_{17}H_{39}F_{12}Mn_2N_6O_4P_2 \cdot H_2O$: C, 25.23; H, 5.11; N, 10.38. Found: C, 25.29; H, 5.14; N, 10.31%.

$[(L\text{-}Me_2)_2Mn_2(O)(OOCPh)_2)][PF_6]_2$ ([**Mn2**][PF_6]$_2$): Yield 75%. IR (KBr pellets) ν (cm^{-1}): 3435 (m), 3335 (m), 2991 (m), 2925 (m), 1610 (s), 1599 (s), 1558 (s), 1463(s), 1398(vs), 1181(s), 1034(m), 1011 (m), 840 (vs), 723(s), 697 (s), 558(s). *Anal*. Calc. for $C_{30}H_{48}F_{12}Mn_2N_6O_5P_2 \cdot H_2O \cdot (CH_3)_2CO$: C, 37.80; H, 5.38; N, 8.01. Found: C, 37.80; H, 5.40; N, 8.10%.

$[(L\text{-}Me_2)_2Mn_2(O)_2(OOCMe)][PF_6]_2$ ([**Mn3**][PF_6]$_2$): Yield 50%. IR (KBr pellets) ν (cm^{-1}): 3384 (m), 3334 (m), 2996 (m), 2949 (m), 1579 (s), 1463 (s), 1392 (s), 1342 (m), 1104 (m), 1033 (s), 1003 (s), 944 (m), 839 (vs), 740 (m), 686 (s), 613 (s), 558 (s). *Anal*. Calc. for $C_{18}H_{41}F_{12}Mn_2N_6O_4P_2 \cdot (CH_3)_2CO$: C, 29.21; H, 5.49; N, 9.73. Found: C, 29.25; H, 5.46; N, 9.69%.

$[(L\text{-}Me_2)_2Mn_2(O)(OOCMe)_2][PF_6]_2$ ([**Mn4**][PF_6]$_2$): Yield 55%. IR (KBr pellets) ν (cm^{-1}): 3436 (m), 3332 (s), 2984 (m), 2947 (m), 2917 (m), 1578 (s), 1459 (s), 1420 (s), 1091 (m), 1058 (m), 1024 (m), 1004 (m), 958 (m), 839 (vs), 713 (m), 694 (m), 558(s). *Anal*. Calc. for $C_{20}H_{44}F_{12}Mn_2N_6O_5P_2$: C, 28.31; H, 5.23; N, 9.91. Found: C, 28.29; H, 5.25; N, 9.82%.

General procedure for $[(R^{1S}L\text{-}Me_2)_2Mn_2(O)_2][PF_6]_3$ ([**Mn5S**][PF_6]$_3$ and $[(R^{1R}L\text{-}Me_2)_2Mn_2(O)_2][PF_6]_3$ ([**Mn5R**][PF_6]$_3$). In a 50 ml Schlenk tube, an aqueous ethanol (70%, 5 mL) solution containing a chiral $R^1L\text{-}Me_2$ ligand (140 mg, 0.65 mmol), $MnCl_2 \cdot 4\ H_2O$ (128 mg, 0.65 mmol) and KPF_6 (178 mg, 0.97 mmol) was stirred at room temperature (10 minutes) and then heated to 50 °C for 20 minutes. The resulting brown-red solution was cooled to 0 °C, before 1.5 mL of a freshly prepared aqueous solution containing H_2O_2 (65 µL, 0.65 mmol) and NaOH (31 mg, 0.78 mmol) was added. The pH of the brown-green solution was adjusted to 7.5 with 2M H_2SO_4 and stirred at 20 °C for 2h. After filtration through celite and washing with 2 mL of acetonitrile, the filtrate was evaporated *in vacuo.* The solid residue was washed 3 times with 10 mL of ethanol, dryed and extracted to acetone. Single crystals suitable for X-ray analysis were grown from an acetone solution into which the ether was allowed to slowly diffuse within 48 hours.

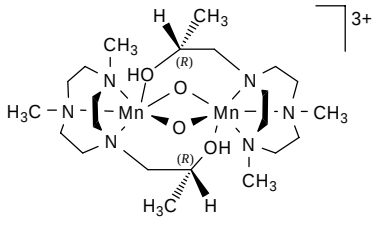

(**Mn5R**)

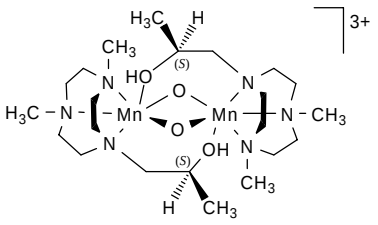

(**Mn5S**)

$[(R^{1R}L\text{-}Me_2)_2Mn_2(O)_2][PF_6]_3$ ([**Mn5R**][PF_6]$_3$: Yield 25−35%. MS (ESI positive mode, acetone): *m/z* 715.0 (40%, [**Mn5** − 2H][PF_6]), 548.2 (60%, [**Mn5** − $C(CH_3)OH$ + Na]). IR

(KBr pellets) ν (cm^{-1}): 3674 (m), 3435 (s), 2927 (m), 1631 (m), 1467 (s), 1145 (m), 1070 (s), 1015 (s) 838 (vs), 647 (s) and 558 (s). UV-vis (CH_3CN) λ_{max} (nm): 575 (ε = 320 M^{-1} cm^{-1}), 281 (14700) and 225 (12600). CD (CH_3CN) λ_{max} (nm): 474 ($\Delta\varepsilon$ = + 1.5 M^{-1} cm^{-1}), 432 (– 0.4), 360 (+ 4.7), 310 (– 4.0), 256 (– 6.4) and 224 (+ 5.4) nm. *Anal*. Calc. for $C_{22}H_{50}F_{18}Mn_2N_6O_4P_3$ · 0.5 acetone: C, 27.23; H, 5.15; N, 8.11. Found: C, 27.62; H, 5.19; N, 8.57%.

[(R^{1S}L-Me_2)$_2$$Mn_2(O)_2$][$PF_6$]$_3$ ([**Mn5S**][PF_6]$_3$: Yield 25−35%. MS (ESI positive mode, acetone): *m/z* 715.0 (55%, [**Mn5** − 2H][PF_6]), 548.2 (40%, [**Mn5** − C(CH_3)OH + Na]). IR (KBr pellets) ν (cm^{-1}): 3674 (m), 3436 (m), 2928 (m), 1583 (m), 1467 (s), 1014 (m), 839 (vs), 648 (s) and 558 (s). UV-vis (CH_3CN) λ_{max} (nm): 575 (ε = 320 M^{-1} cm^{-1}), 281 (14700) and 225 (12600). CD (CH_3CN) λ_{max} (nm): 474 ($\Delta\varepsilon$ = – 1.5 M^{-1} cm^{-1}), 432 (+ 0.4), 360 (– 5.2), 310 (+ 5.0), 256 (+ 6.4) and 224 (– 6.2) nm. *Anal*. Calc. for $C_{22}H_{50}F_{18}Mn_2N_6O_4P_3$ · 0.5 acetone: C, 27.23; H, 5.15; N, 8.11. Found: C, 27.33; H, 5.21; N, 8.53%.

Iron Complexes

General procedure for [(L-Me_2)$_2$$Fe_2$(O)(OOC-R)$_2$][$PF_6$]$_2$ ([**Fe1**][PF_6][SO_4]$_{0.5}$, [**Fe2**][PF_6]$_2$, [**Fe3**][PF_6]$_2$). In a 50 ml Schlenk tube, a mixture of L-Me_2 (157.3 mg, 1.00 mmol) and *p*-toluenesulfonic acid monohydrate (190.2 mg, 1.00 mmol) was dissolved in 10 mL of 80% aqueous ethanol. To this clear light-yellow solution, solid $FeSO_4$ · 7 H_2O (278 mg, 1.00 mmol) was added under vigorous stirring. The mixture was treated with ultrasound (10-15 minutes) and then stirred for half an hour. Then, KPF_6 (276 mg, 1.50 mmol) and the corresponding sodium carboxylate (**Fe1**: HCOONa · H_2O, 129 mg, 1.50 mmol; **Fe2**: CH_3COONa · 3 H_2O, 204 mg, 1.50 mmol; **Fe3**: C_6H_5COONa, 216 mg, 1.50 mmol) were added to the slurry. After stirring at 45 °C for 60 minutes, the suspension was cooled to 0 °C, before a freshly prepared aqueous solution (2 mL) of H_2O_2 (102 µL, 1.0 mmol) and NaOH (48 mg, 1.2 mmol) was added. Then the resulting orange suspension was stirred at 20 °C for 2h. After filtration through celite and washing 2 times with 2 mL of water, the orange solid on the celite bed was extracted with acetone, purified on neutral aluminum oxide (eluent

acetone/methanol 5:1) and isolated by evaporation of the solvent *in vacuo* (0.05 mbar, 20 °C, 24h). Single crystals suitable for X-ray analysis were grown from an acetone solution, into which ether was allowed to slowly diffuse within 48 hours.

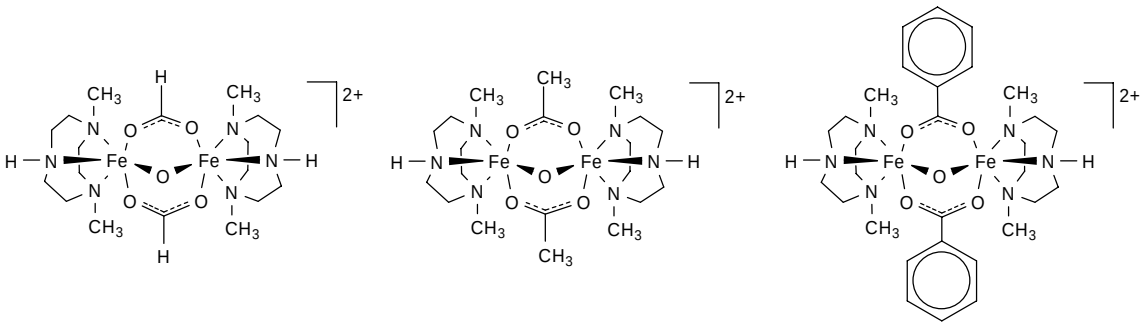

(**Fe1**) (**Fe2**) (**Fe3**)

$[(L\text{-}Me_2)_2Fe_2(O)(OOCH)_2][PF_6][SO_4]_{0.5}$ ([**Fe1**][PF_6][SO_4]$_{0.5}$): Yield 42–54%. UV-vis (CH_3CN) λ_{max} (nm): 240 (ε = 13800 M^{-1} cm^{-1}), 339 (7800), 474 (1100), 500 (sh) and 698 (150). IR (KBr pellets) ν (cm^{-1}): 3331 (m), 3263 (m), 2908 (s), 2871 (s), 1624 (s), 1566 (vs), 1496 (m), 1463 (s), 1362 (s), 1303 (m), 1100 (m), 1007 (s), 840 (vs), 750 (s), 558 (s) and 491 (m). *Anal*. Calc. for $C_{18}H_{40}F_6Fe_2N_6O_7P_1S_{0.5}$: C, 29.81; H, 5.56; N, 11.59. Found: C, 29.74; H, 5.68; N, 11.50%.

$[(L\text{-}Me_2)_2Fe_2(O)(OOCCH_3)_2][PF_6]_2$ ([**Fe2**][PF_6]$_2$): Yield 52–61%. UV-vis (CH_3CN) λ_{max} (nm): 230 (ε = 14600 M^{-1} cm^{-1}), 341 (6700), 473 (1460), 516 (1100), 550 (sh) and 748 (145). IR (KBr pellets) ν (cm^{-1}): 3332 (s), 2991 (m), 2951 (m), 1554 (s), 1495 (m), 1463 (s), 1425 (s), 1097 (m), 1028 (s), 1007 (s), 960 (m), 839 (vs), 725 (s), 664 (m) and 558 (s). *Anal*. Calc. for $C_{20}H_{44}F_{12}Fe_2N_6O_5P_2 \cdot 0.5\ (CH_3)_2CO$: C, 29.37; H, 5.39; N, 9.56. Found: C, 29.30; H, 5.34; N, 9.67%.

$[(L\text{-}Me_2)_2Fe_2(O)(OOCPh)_2)][PF_6]_2$ ([**Fe3**][PF_6]$_2$): Yield 75%. UV-vis (CH_3CN) λ_{max} (nm): 237 (ε = 27800 M^{-1} cm^{-1}), 338 (8200), 476 (1500), 517 (1140), 550 (sh) and 745 (140). IR (KBr pellets) ν (cm^{-1}): 3329 (m), 2981 (m), 2929 (m), 1593 (m), 1538 (s), 1494 (m), 1463 (s), 1400 (vs), 1178 (m), 1096 (m), 1027 (m), 1007 (s), 961 (m), 839 (vs), 724 (s), 677 (m), 558 (s) and 471 (m). *Anal*. Calc. for $C_{30}H_{48}F_{12}Fe_2N_6O_5P_2 \cdot 0.5\ (CH_3)_2CO$: C, 37.71; H, 5.12; N, 8.38. Found: C, 37.74; H, 5.32; N, 8.73%.

General procedure for $[(Ac\text{-}L\text{-}Me_2)_4Fe_4(O)_2][PF_6]_4$ ([**Fe4**][PF_6]$_4$) and $[(Ac\text{-}L\text{-}Me_2)_2Fe_2(O)(OOCMe)][PF_6]$ ([**Fe5**][PF_6]). In a 50 ml Schlenk tube, a mixture of $[Na][Ac\text{-}L\text{-}Me_2] \cdot 1.5\ CH_2Cl_2$ (364 mg, 1.00 mmol), $FeSO_4 \cdot 7\ H_2O$ (278 mg, 1.00 mmol) and KPF_6 (276 mg, 1.50 mmol) in aqueous ethanol (60%, 8 mL) was stirred under argon atmosphere at room temperature for two hours. The resulting dark green solution (pH 3.8 − 4.2) was cooled to 0 °C, before 2 mL of a freshly prepared aqueous solution containing H_2O_2 (100 µL, 1.00 mmol) and NaOH (48 mg, 1.20 mmol) was added. The brown-green mixture was stirred in air at 20 °C for 2h (pH 4.5), before celite (basic, pH 9) was added. After filtration the product was extracted from the celite bed by washing 2 times with 5 mL of acetonitrile and the combined washings were evaporated *in vacuo* (0.05 mbar, 20 °C, 2h). The green-brown solid residue was dissolved in acetonitrile and after standing for a week (TLC testing) two products were separated by column chromatography on silica (eluent MeCN:MeOH 5:1–2:1). The yield of the green product varied from 5 to 15% depending on dilution as well as on time. The green fraction containing [**Fe4**][PF_6]$_4$ was evaporated, washed 4 times with 10 mL of ethanol and dryed *in vacuo*. Single crystals of [**Fe4**][PF_6]$_4 \cdot 5$ MeCN suitable for X-ray analysis were grown from an acetonitrile solution into which the ether was allowed to slowly diffuse within 72 hours. The brown-orange fraction containing [**Fe5**][PF_6] was evaporated, extracted in acetone and crystallized with ether. A microcrystalline powder was obtained within 48 hours.

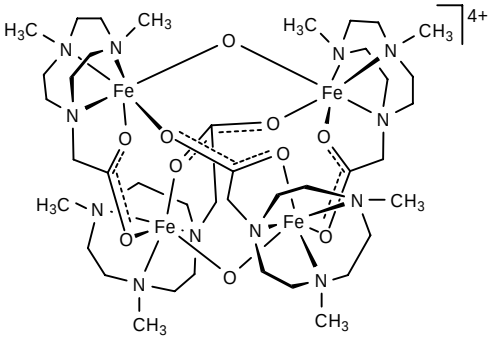

(**Fe4**)

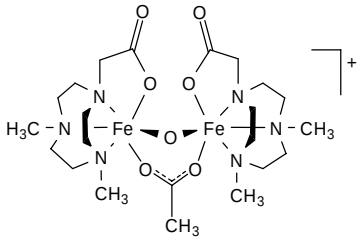

(**Fe5**)

$[(Ac\text{-}L\text{-}Me_2)_4Fe_4(O)_2][PF_6]_4$ ([**Fe4**][PF_6]$_4$): Yield 5−15%. MS (ESI, positive mode, acetone) *m/z* 575 ($[(Ac\text{-}L\text{-}Me_2)_2Fe_2(O) + H + H_2O]^{3+}$). UV-vis ($CH_3CN$) λ_{max} (nm): 578 (ε = 300 $M^{-1}\ cm^{-1}$), 501 (670), 491 (710) and 325 (24500). IR (KBr pellets) ν (cm^{-1}): 2925 (m), 1622 (vs), 1568 (m), 1407 (s), 1384 (m), 1304 (m), 1079 (m), 1023 (m), 841 (vs), 773 (s), 753 (s) and 559 (s). *Anal*. Calc. for $C_{40}H_{84}Fe_4N_{12}O_{10}P_4F_{24}$: C, 28.32; H, 4.99; N, 9.91. Found: C, 28.73; H, 4.67; N, 10.32%.

[(Ac-L-Me_2)$_2$$Fe_2$(O)(OOCMe)][$PF_6$] ([**Fe5**][$PF_6$]): Yield 28−40%. ^{1}H NMR (400 MHz, CD_3CN) δ = 35.5, 31.5 (br, 4H, NCH_2COO), 28−18 (br, 28H, NCH_2CH_2N, NCH_3), 15.2 (br, 4H, NCHHCH_2N), 11.5 (br, 3H, OOCCH_3) and 8.1 (br, 4H, NCHHCH_2N) ppm. MS (ESI, positive mode, MeCN) *m/z* 634 (70%, [**Fe5** + H + H_2O]$^{2+}$), 651 (10%, [**Fe5** + 2 H_2O]$^+$), 615 (10%, [**Fe5**]$^+$) and 416 (10%, [**(**Ac-L-Me_2)Fe + PF_6]$^+$). UV-vis (CH_3CN) λ_{max} (nm): 663 (ε = 160 M^{-1} cm^{-1}), 503 (1040), 449 (1600), 421 (1800) and 326 (15500). IR (KBr pellets) ν (cm^{-1}): 3435 (s), 2930 (m), 1643 (s), 1578 (s), 1466 (s), 1384 (s), 1357 (s), 1103 (m), 1024 (m), 842 (vs), 781 (s), 740 (m) and 559 (s). *Anal*. Calc. for $C_{22}H_{44}Fe_2N_6O_7PF_6 \cdot 2\ KPF_6$: C, 23.40; H, 3.93; N, 7.44. Found: C, 23.22; H, 3.80; N, 7.25%.

Ruthenium Complexes

(L-Me_2)$RuCl_3 \cdot H_2O$ (**Ru1**). In a 50 ml Schlenk tube, a mixture of L-Me_2 (315 mg, 2.00 mmol) and $RuCl_2$(dmso)$_4$ (436 mg, 0.90 mmol) was suspended in 10 mL of absolute ethanol. The mixture was stirred at 60 °C for 30 minutes, until a clear brown-red solution was obtained, and then refluxed for 2 hours. The solvent was removed by rotary evaporation and the solid was refluxed in 37% HCl (10 mL) for 30 minutes in the presence of air. The brown-orange solution was evaporated and the solid was suspended in 5 mL of water. The orange microcrystalline product was filtered, washed with water, ethanol, ether and dried *in vacuo*.

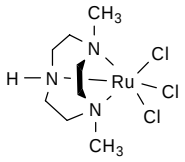

(**Ru1**)

(L-Me_2)$RuCl_3 \cdot H_2O$ (**Ru1**): Yield 41%. UV-vis (CH_3CN-H_2O) λ_{max} (nm): 229 (ε = 6800 M^{-1} cm^{-1}), 295 (1250) and 386 (2100). IR (KBr pellets) ν (cm^{-1}): 3391(vs), 3183 (vs), 2992 (m), 2925 (s), 1915 (m), 1632 (s), 1489 (m), 1449 (vs), 1384 (s), 1274 (m), 1095 (s), 1045 (s), 998 (s), 960 (s), 826 (s), 765 (m), 744 (m), 612 (m), 519 (m), 482 (m) and 436 (m). *Anal*. Calc. for $C_8H_{19}Cl_3N_3Ru \cdot H_2O$: C, 25.11; H, 5.53; N, 10.98. Found: C, 25.27; H, 5.35; N, 10.94%.

$[(L\text{-}Me_2)_2Ru_2(O)(OOCCH_3)_2][PF_6]_2$ ([**Ru2**][PF_6]$_2$): In a 50 ml Schlenk tube, (L-Me_2)$RuCl_3 \cdot H_2O$ (120 mg, 0.31 mmol) was suspended in 7 mL of water and $CH_3COONa \cdot 3\ H_2O$ (422 mg, 3.10 mmol) was added. The mixture was refluxed for 30 minutes, until a clear deep-violet solution was obtained. To this hot solution KPF_6 (350 mg, 1.90 mmol), dissolved in 5 mL of water, was added and the final product precipitated after 12 hours at 0 °C. The dark-violet microcrystalline solid was filtered, washed with water, ethanol, ether and dried *in vacuo*. Single X-ray quality crystals were grown from an acetone solution, into which ether was allowed to slowly diffuse within 48 hours.

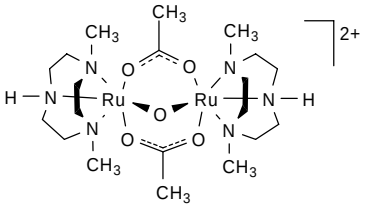

(**Ru2**)

$[(L\text{-}Me_2)_2Ru_2(O)(OOCCH_3)_2][PF_6]_2$ ([**Ru2**][PF_6]$_2$): Yield 73%. UV-vis (CH_3CN) λ_{max} (nm): 233 (ε = 10200 M^{-1} cm^{-1}), 279 (8900), 325 (sh) and 538 (6700). IR (KBr pellets) ν (cm^{-1}): 3435 (m), 3310 (s), 2933 (m), 1631 (m), 1559 (s), 1464 (s), 1428 (s), 1100 (m), 1037 (m), 1006 (m), 842 (vs), 766 (m), 684 (m), 558 (s), 520 (m), 471 (m) and 440 (m). *Anal*. Calc. for $C_{20}H_{44}F_{12}N_6O_5P_2Ru_2 \cdot 2\ H_2O$: C, 24.59; H, 4.95; N, 8.60. Found: C, 24.55; H, 4.42; N, 8.34%.

Cobalt Complexes

$[(L\text{-}Me_2)_2Co_2(OH)(OOCCH_3)_2][PF_6]_3$ ([**Co1**][PF_6]$_3$): In a 50 ml Schlenk tube, a mixture of L-Me_2 (157.3 mg, 1.00 mmol) and *p*-toluenesulfonic acid monohydrate (190.2 mg, 1.00 mmol) was dissolved in 15 mL of acetonitrile. To this clear light-yellow solution, solid $CoCl_2 \cdot 6\ H_2O$ (238 mg, 1.00 mmol) was added under vigorous stirring. The mixture was treated with ultrasound (10-15 minutes), before KPF_6 (276 mg, 1.50 mmol) and $CH_3COONa \cdot 3\ H_2O$ (204 mg, 1.50 mmol) were added to the deep blue suspension. After stirring at 60 °C for 20 minutes followed by cooling to 0 °C, an acetonitrile (5 mL) solution of H_2O_2 (102 µL, 1.0 mmol) and triethylamine (278 µL, 2.0 mmol) was added. Then the pink-brown suspension was stirred at 20 °C for 2h. After filtration through celite and washing with 2 mL of acetone,

the filtrate was evaporated *in vacuo*. The product was resuspended in water (2 mL), filtered, washed with water, ethanol, ether and dried under vacuum. Single crystals suitable for X-ray analysis were grown from an acetone solution into which the ether was allowed to slowly diffuse within 48 hours.

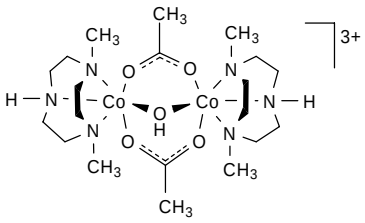

(**Co1**)

[(L-Me_2)$_2$$Co_2$(OH)($OOCCH_3$)$_2$][$PF_6$]$_3$ ([**Co1**][PF_6]$_3$): Yield 40%. UV-vis (CH_3CN) λ_{max} (nm): 535 (ε = 260 M^{-1} cm^{-1}), 330 (sh). IR (KBr pellets) ν (cm^{-1}): 3568 (m), 3436 (m), 3249 (m), 2958 (m), 1688 (s), 1590 (vs), 1502 (m), 1452 (s), 1080 (m), 1046 (m), 1011 (m), 981 (m), 841 (vs), 697 (m) and 558 (s). *Anal*. Calc. for $C_{20}H_{45}F_{18}Co_2N_6O_5P_3 \cdot (CH_3)_2CO \cdot H_2O$: C, 25.62; H, 4.95; N, 7.79. Found: C, 25.55; H, 4.90; N, 7.95%.

8.4 Catalytic Experiments

Oxidation of Light Alkanes

The experiments using gases as methane, ethane, propane or n-butane as substrates and synthetic air as oxidant were carried out in 100 ml autoclaves equipped with glass lined steel vessels containing a magnetic bar. In a typical experiment, the glass tube containing the solvent, catalyst, co-catalyst and the hydrogen peroxide was introduced in the steel vessel of the autoclave, which was closed hermetically and purged with air. After that, the autoclave was pressurized with air and with the hydrocarbon, in this order, to the corresponding pressures and heated to the corresponding temperature under vigorous stirring. (CAUTION: the combination of air or molecular oxygen and H_2O_2 with organic compounds at elevated pressures and temperatures may be explosive!) After the indicated reaction time, the autoclave was cooled in ice and the pressure was released; the samples of gaseous mixture were taken in

a 200 mL reservoir and analyzed by GC. Two aliquots of the reaction mixture were taken for ^{1}H NMR and for GC analysis using MeCN as internal standard.

With TS-1 used as a catalyst, the oxidations of gaseous saturated hydrocarbons were carried out in aqueous H_2O_2 (30 % solution, 1 mL) using the same techniques. The reactions were stopped by cooling with ice, and acetonitrile containing a small amount of nitromethane (an internal standard for the GC) was then added to the reaction mixture in order to obtain (after filtering off the solid TS-1) a homogeneous solution.

Oxidation of Higher Alkanes

The oxidation of higher alkanes was conducted with Prof. Dr. Georgiy B. Shul'pin from Semenov Institute of Chemical Physics, Russian Academy of Sciences, Moscow, Russia. The experiments were carried out in thermostated cylindrical vessels connected to a reflux tube, when the reaction temperature is higher than 40 °C and open to air. In a typical experiment, a portion of hydrogen peroxide was added to the solution of the catalyst and substrate in acetonitrile. After certain time intervals samples (0.6 mL) were taken. To one of the samples was added solid triphenylphosphine to reduce the alkyl hydroperoxide to the corresponding alcohol, reaction which is complete after 15 minutes. Each sample was injected in GC twice, 0.2 μl each time.

Oxidation of Alcohols

The oxidation of *i*-propanol and *n*-propanol was carried out in air in thermostated cylindrical pyrex vessels with vigorous stirring. The total volume of the reaction solution was 10 mL. In a typical experiment, hydrogen peroxide (30% aqueous solution, 0.50 M) was added to a mixture containing a catalyst, co-catalyst and a substrate in water, acetonitrile or in moist isopropanol. Blank experiments were carried out without catalyst. The samples of the reaction solution were analyzed by GC.

The oxidation of racemic 1-phenylethanol was carried out in air in ice-cooled bath with vigorous stirring. The total volume of the reaction solution was 2 mL. In a typical experiment, hydrogen peroxide (30% aqueous solution, 0.20 M) was added to a mixture containing a catalyst and a substrate in aqueous acetonitrile (50%). After 2 hours the reaction products were extracted with ether (3 × 2 mL), dryed over anhydrous Na_2SO_4 and filtered through silica using ether (10 mL) as eluent. To the resulting solution (total volume 15−16 mL) 10 μL

of nitrobenzene was added and the samples were analyzed by HPLC using Daicel Chiracel OB-H column.

Oxidation of Alkenes

The epoxidation of indene was carried out in air in ice-cooled bath with vigorous stirring. The total volume of the reaction solution was 2 mL. In a typical experiment, hydrogen peroxide (30% aqueous solution, 0.20 M) was added to a mixture containing a catalyst, co-catalyst and a substrate in aqueous acetonitrile (50%). After 2 hours the reaction products were extracted with ether (3 × 2 mL), dryed over anhydrous Na_2SO_4 and filtered through silica using ether (10 mL) as eluent. To the resulting solution (total volume 15−16 mL) 10 μL of nitrobenzene was added and the samples were analyzed by HPLC using Daicel Chiracel OJ-H column.

Determination of Oxygen Evolved

In experiments involving molecular oxygen evolution, the volume of molecular oxygen evolved was measured using a thermostated burette. The reaction system was connected to a manometric burette filled with water which was saturated with oxygen prior to use. After certain time intervals, the pressure was equilibrated using a separation funnel by adjusting the water level to the same heights.

9 References

[1] A. E. Shilov, G. B. Shul'pin, "Activation and Catalytic Reactions of Saturated Hydrocarbons in the Presence of Metal Complexes", Kluwer, Dordrecht, **2000**.

[2] H. Arakawa, M. Aresta, J. N. Armor, M. A. Barteau, E. J. Beckman, A. T. Bell, J. E. Bercaw, C. Creutz, E. Dinjus, D. A. Dixon, K. Domen, D. L. DuBois, J. Eckert, E. Fujita, D. H. Gibson, W. A. Goddard, D. W. Goodman, J. Keller, G. J. Kubas, H. H. Kung, J. E. Lyons, L. E. Manzer, T. J. Marks, K. Morokuma, K. M. Nicholas, R. A. Periana, L. Que, Jr., J. Rostrup-Nielson, W. M. H. Sachtler, L. D. Schmidt, A. Sen, G. A. Somorjai, P. C. Stair, B. R. Stults, W. Tumas, *Chem. Rev.* **2001**, *101*, 953.

[3] J.-P. Lange, *Ind. Eng. Chem. Res.* **1997**, *36*, 4282.

[4] B. L. Conley, W. J. Tenn III, K. J. H. Young, S. K. Ganesh, S. K. Meier, V. R. Ziatdinov, O. Mironov, J. Oxgaard, J. Gonzales, W. A. Goddard III, R. A. Periana, *J. Mol. Catal. A* **2006**, *251*, 8.

[5] C. L. Hill (editor), "Activation and Functionalization of Alkanes", Wiley-Interscience, New York, **1989**.

[6] A. E. Shilov, G. B. Shul'pin, *Chem. Rev*. **1997**, *97*, 2879.

[7] G. B. Shul'pin, "Oxidations of C-H Compounds Catalyzed by Metal Complexes", in: *Transition Metals for Organic Synthesis*, Eds. M. Beller and C. Bolm, Second Edition, WILEY-VCH Verlag, Weinheim, **2004**, *2*, 215.

[8] B. A. Arndtsen, R. G. Bergman, T. A. Mobley, T. H. Peterson, *Acc. Chem. Res*. **1995**, *28*, 154.

[9] T. R. Cundari, *Organometallics* **1994**, *13*, 2987.

[10] A. L. Suing, C. R. Dewan, P. S. White, H. H. Thorp, *Inorg. Chem.* **2000**, *39*, 6080.

[11] W. Cui, B. B. Wayland, *J. Am. Chem. Soc*. **2004**, *126*, 8266.

[12] R. Ramnauth, S. Al-Juaid, M. Motevalli, B. C. Parkin, A. C. Sullivan, *Inorg. Chem.* **2004**, *43*, 4072.

[13] R. A. Periana, D. J. Taube, S. Gamble, H. Taube, T. Satoh, H. Fujii, *Science* **1998**, *280*, 560.

[14] Y. Fujiwara, K. Takaki, Y. Taniguchi, *Synlett* **1996**, *7*, 591.

[15] R. A. Periana, O. Mironov, D. Taube, G. Bhalla, C. J. Jones, *Science* **2003**, *301*, 814.

[16] M. Lin, T. E. Hogan, A. Sen, *J. Am. Chem. Soc*. **1996**, *118*, 4574.

[17] C. J. Jones, D. Taube, V. R. Ziatdinov, R. A. Periana, R. J. Nielsen, J. Oxgaard, W. A. Goddard, III, *Angew. Chem. Int. Ed.* **2004**, *43*, 4626.

[18] D. E. De Vos, B. F. Sels, *Angew. Chem. Int. Ed.* **2005**, *44*, 30.

[19] R. A. Periana, D. J. Taube, E. R. Evitt, D. G. Löffler, P. R. Wentrcek, G. Voss, T. Masuda, *Science* **1993**, *259*, 340.

[20] R. A. Periana, G. Bhalla, W. J. Tenn, III, K. J. H. Young, X. Y. Liu, O. Mironov, C. J. Jones, V. R. Ziatdinov, *J. Mol. Catal. A* **2004**, *220*, 7.

[21] J. C. Snyder, A. V. Grosse, U.S. Patent 2493038, **1950.**

[22] N. F. Gol'dshleger, M. B. Tyabin, A. E. Shilov, A. A. Shteinman, *Russ. J. Phys. Chem. (Engl. Trans.)* **1969**, *43*, 1222.

[23] M. Lin, T. Hogan, A. Sen, *J. Am. Chem. Soc*. **1997**, *119*, 6048.

[24] E. D. Park, Y.-S. Hwang, C. W. Lee, J. S. Lee, *Appl. Catal. A* **2003**, *247*, 269.

[25] J. E. Remias, A. Sen, *J. Mol. Catal. A: Chemical* **2002**, *189*, 33.

[26] E. I. Solomon, *Inorg. Chem.* **2001**, *40*, 3656.

[27] D. Lee, S. J. Lippard, *Inorg. Chem.* **2002**, *41*, 827.

[28] P. D. Metelski, V. A. Adamian, J. H. Espenson, *Inorg. Chem.* **2000**, *39*, 2434.

[29] C. A. Tolman, J. D. Druliner, M. J. Nappa, H. Herron, in: [5], 303.

[30] Y. Ishii, S. Sakaguchi, T. Iwahama, *Adv. Synth. Catal.* **2001**, *343*, 393.

[31] A. A. Fokin, P. R. Schreiner, *Adv. Synth. Catal.* **2003**, *345*, 1035.

[32] V. Nardello, J.-M. Aubry, D. E. De Vos, R. Neumann, W. Adam, R. Zhang, J. E. ten Elshof, P. T. Witte, P. L. Alsters, *J. Mol. Catal. A* **2006**, *251*, 185.

[33] R. Hage, A. Lienke, *Angew. Chem. Int. Ed.* **2006**, *45*, 206.

[34] B. Meunier, *Chem. Rev*. **1992**, *92*, 1411.

[35] C. Limberg, *Angew. Chem. Int. Ed.* **2003**, *42*, 5932.

[36] D. H. R. Barton, *Tetrahedron* **1998**, *54*, 5805.

[37] M. Costas, M. P. Mehn, M. P. Jensen, L. Que, Jr., *Chem. Rev.* **2004**, *104*, 939.

[38] G. J. P. Britovsek, J. England, S. K. Spitzmesser, A. J. P. White, D. J. Williams, *Dalton Trans.* **2005**, 945.

[39] P. Battioni, J. P. Renaud, J. F. Bartoli, M. Reina-Artiles, M. Fort, D. Mansuy, *J. Am. Chem. Soc*. **1988**, *110*, 8462.

[40] E. N. Jacobsen, W. Zhang, A. R. Muci, J. R. Ecker, L. Deng, *J. Am. Chem. Soc*. **1991**, *113*, 7063.

[41] S.-I. Murahashi, S. Noji, N. Komiya, *Adv. Synth. Catal.* **2004**, *346*, 195.

[42] R. W. Murray, K. Iyanara, J. Chenb, J. T. Wearing, *Tetrahedron Lett*. **1995**, *36*, 6415.

[43] C. C. Romão, F. E. Kühn, W. A. Herrmann, *Chem. Rev*. **1997**, *97*, 3197.

[44] G. B. Shul'pin, *J. Mol. Catal. A: Chemical* **2002**, *189*, 39.

[45] P. E. M. Siegbahn, M. R. A. Blomberg, *Chem. Rev*. **2000**, *100*, 421.

[46] B. P. Hay, R. D. Hancock, *Coord. Chem. Rev*. **2001**, *212*, 61.

[47] G. H. Loew, D. L. Harris, *Chem. Rev.* **2000**, *100*, 407.

[48] M. T. Green, *J. Am. Chem. Soc*. **1999**, *121*, 7939.

[49] M. R. Bukowski, S. Zhu, K. D. Koehntop, W. W. Brennessel, L. Que, Jr., *J. Biol. Inorg. Chem*. **2004**, *9*, 39.

[50] F. Neese, J. M. Zaleski, K. Loeb Zaleski, E. I. Solomon, *J. Am. Chem. Soc*. **2000**, *122*, 11703.

[51] A. Kitmitto, N. Myronova, P. Basu, H. Dalton, *Biochemistry* **2005**, *44*, 10954.

[52] M. H. Sazinsky, S. J. Lippard, *J. Am. Chem. Soc*. **2005**, *127*, 5814.

[53] R. L. Lieberman, A. C. Rosenzweig, *Nature* **2005**, *434*, 177.

[54] D. A. Whittington, S. J. Lippard, *J. Am. Chem. Soc*. **2001**, *123*, 827.

[55] M. Costas, J.-U. Rohde, A. Stubna, R. Y. N. Ho, L. Quaroni, E. Münck, L. Que, Jr., *J. Am. Chem. Soc*. **2001**, *123*, 12931.

[56] B. Ensing, F. Buda, M. C. M. Gribnau, E. J. Baerends, *J. Am. Chem. Soc*. **2004**, *126*, 4355.

[57] M.-H. Baik, B. F. Gherman, R. A. Friesner, S. J. Lippard, *J. Am. Chem. Soc*. **2002**, *124*, 14608.

[58] D. A. Kopp, S. J. Lippard, *Current Opinion in Chemical Biology* **2002**, *6*, 568.

[59] E. I. Solomon, T. C. Brunold, M. I. Davis, J. N. Kemsley, S.-K. Lee, N. Lehnert, F. Neese, A. J. Skulan, Y.-S. Yang, J. Zhou, *Chem. Rev*. **2001**, *100*, 235.

[60] J. A. Labinger, J. E. Bercaw, *Nature* **2002**, *417*, 507.

[61] M. A. Johnson, E. V. Stefanovich, T. N. Truong, *J. Phys. Chem. A* **1997**, *101*, 3196.

[62] H. T. Thümmel, *J. Phys. Chem. A* **1998**, *102*, 2002.

[63] G. Süss-Fink, G. V. Nizova, S. Stanislas, G. B. Shul'pin, *J. Mol. Catal. A* **1998**, *130*, 163.

[64] G. B. Shul'pin, G. V. Nizova, Y. N. Kozlov, V. S. Arutyunov, A. C. M. Dos Santos, A. C. T. Ferreira, D. Mandelli, *J. Organomet. Chem*. **2005**, *690*, 4498.

[65] I. Bar-Nahum, A. M. Khenkin, R. Neumann, *J. Am. Chem. Soc*. **2004**, *126*, 10236.

[66] T. Hirao, *Chem. Rev*. **1997**, *97*, 2707.

[67] L. Gonzalez Cuervo, Y. N. Kozlov, G. Süss-Fink, G. B. Shul'pin, *J. Mol. Catal. A* **2004**, *218*, 171.

[68] N. Mizuno, Y. Nakagawa, K. Yamaguchi, *J. Mol. Catal. A* **2006**, *251*, 286.

[69] A. Butler, M. J. Clague, G. E. Meister, *Chem. Rev*. **1994**, *94*, 625.

[70] H. Mimoun, L. Saussine, E. Daire, M. Postel, J. Fischer, R. Weiss, *J. Am. Chem. Soc*. **1983**, *105*, 3101.

[71] G. B. Shul'pin, G. Süss-Fink, *J. Chem. Soc., Perkin Trans. 2* **1995**, *7*, 1459.

[72] G. B. Shul'pin, M. C. Guerreiro, U. Schuchardt, *Tetrahedron* **1996**, *52*, 13051.

[73] G. B. Shul'pin, D. Attanasio, L. Suber, *J. Catal.* **1993**, *142*, 147.

[74] G. V. Nizova, G. Süss-Fink, G. B. Shul'pin, *Chem. Comm*. **1997**, *4*, 397.

[75] G. V. Nizova, G. Süss-Fink, G. B. Shul'pin, *Tetrahedron* **1997**, *53*, 3603.

[76] G. Süss-Fink, S. Stanislas, G. B. Shul'pin, G. V. Nizova, *Appl. Organomet. Chem*. **2000**, *14*, 623.

[77] G. Süss-Fink, S. Stanislas, G. B. Shul'pin, G. V. Nizova, H. Stoeckli-Evans, A. Neels, C. Bobillier, C. Saturnin, *J. Chem. Soc., Dalton Trans.* **1999**, *18*, 3169.

[78] G. B. Shul'pin, Y. N. Kozlov, G. V. Nizova, G. Süss-Fink, S. Stanislas, A. Kitaygorodskiy, V. S. Kulikova, *J. Chem. Soc., Perkin Trans. 2* **2001**, 1351.

[79] R. Z. Khaliullin, A. T. Bell, M. Head-Gordon, *J. Phys. Chem. B* **2005**, *109*, 17984.

[80] Y. N. Kozlov, G. V. Nizova, G. B. Shul'pin, *J. Mol. Catal. A* **2005**, *227*, 247.

[81] M. Bonchio, O. Bortolini, V. Conte, S. Primon, *J. Chem. Soc., Perkin Trans. 2* **2001**, 763.

[82] P. Buglyo, D. C. Crans, E. M. Nagy, R. L. Lindo, L. Yang, J. J. Smee, W. Jin, L.-H. Chi, M. E. Godzala Iii, G. R. Willsky, *Inorg. Chem*. **2005**, *44*, 5416.

[83] K. Paulsen, D. Rehder, *Z. Naturforsch*. **1982**, *37a*, 139.

[84] W. Priebsch, D. Rehder, *Inorg. Chem*. **1985**, *24*, 3058.

[85] M. Bonchio, O. Bortolini, M. Carraro, V. Conte, S. Primon, *J. Inorg. Biochem*. **2000**, *80*, 191.

[86] V. Conte, F. Di Furia, S. Moro, *J. Mol. Catal. A* **1997**, *117*, 139.

[87] J. S. Jaswal, A. S. Tracey, *Inorg. Chem*. **1991**, *30*, 3718.

[88] G. Du, J. H. Espenson, *Inorg. Chem*. **2005**, *44*, 2465.

[89] A. F. Ghiron, R. C. Thompson, *Inorg. Chem*. **1990**, *29*, 4457.

[90] V. Conte, F. Di Furia, S. Moro, *J. Mol. Catal. A* **1994**, *94*, 323.

[91] L. M. Dorfman, G. E. Adams, "Reactivity of the Hydroxyl Radical in Aqueous Solutions", NSRDS-NBS 46, Washington DC, **1973**, 24.

[92] K. Wieghardt, *Angew. Chem., Int. Ed. Engl.* **1989**, *28*, 1153.

[93] K. Wieghardt, U. Bossek, D. Ventur, J. Weiss, *J. Chem. Soc., Chem. Comm.* **1985**, 347.

[94] K. Wieghardt, U. Bossek, B. Nuber, J. Weiss, J. Bonvoisin, M. Corbella, S. E. Vitols, J. J. Girerd, *J. Am. Chem. Soc.* **1988**, *110*, 7398.

[95] K. Wieghardt, U. Bossek, W. Gebert, *Angew. Chem.* **1983**, *95*, 320; *Angew. Chem., Int. Ed. Engl.* **1983**, *22*, 328.

[96] K. Wieghardt, U. Bossek, J. Bonvoisin, P. Beauvillain, J.-J. Girerd, B. Nuber, J. Weiss, J. Heinze, *Angew. Chem. Int. Ed. Engl.* **1986**, *25*, 1030.

[97] H. Diril, H.-R. Chang, M. J. Nilges, X. Zhang, J. A. Potenza, H. J. Schugar, S. S. Isied, D. N. Hendrickson, *J. Am. Chem. Soc.* **1989**, *111*, 5102.

[98] R. Hage, J. E. Iburg, J. Kerschner, J. H. Koek, E. L. M. Lempers, R. J. Martens, U. S. Racherla, S. W. Russell, T. Swarthoff, M. R. P. van Vliet, J. B. Warnaar, L. van der Wolf, B. Krijnen, *Nature.* **1994**, *369*, 637.

[99] B. C. Gilbert, N. W. J. Kamp, J. R. Lindsay Smith, J. Oakes, *J. Chem. Soc., Perkin Trans. 2*, **1998**, 1841.

[100] J. R. Lindsay Smith, B. C. Gilbert, A. Mairata i Payeras, J. Murray, T. R. Lowdon, J. Oakes, R. Pons i Prats, P. H. Walton, *J. Mol. Catal. A* **2006**, *251*, 114.

[101] D. H. R. Barton, W. Li, J. A. Smith, *Tetrahedron Lett.* **1998**, *39*, 7055.

[102] J. W. De Boer, J. Brinksma, W. R. Browne, A. Meetsma, P. L. Alsters, R. Hage, B. L. Feringa, *J. Am. Chem. Soc.* **2005**, *127*, 7990.

[103] D. E. De Vos, T. Bein, *J. Organomet. Chem.* **1996**, *520*, 195.

[104] C. Bolm, N. Meyer, G. Raabe, T. Weyhermüller, E. Bothe, *Chem. Commun.* **2000**, 2435.

[105] K. F. Sibbons, K. Shastri, M. Watkinson, *Dalton Trans.* **2006**, 645.

[106] J. R. Lindsay-Smith, G. B. Shul'pin, *Tetrahedron Lett.* **1998**, 4909.

[107] G. B. Shul'pin, J. R. Lindsay-Smith, *Russ. Chem. Bull.* **1998**, *47*, 2379.

[108] G. B. Shul'pin, G. Süss-Fink, L. S. Shul'pina, *J. Mol. Catal. A* **2001**, *170*, 17.

[109] G. B. Shul'pin, G. Süss-Fink, J. R. Lindsay-Smith, *Tetrahedron.* **1999**, *55*, 5345.

[110] T. H. Bennur, S. Sabne, S. S. Deshpande, D. Srinivas, S. Sivasanker, *J. Mol. Catal. A.* **2002**, *185*, 71.

[111] G. B. Shul'pin, G. V. Nizova, Y. N. Kozlov, I. G. Pechenkina, *New J. Chem.* **2002**, *26*, 1238.

[112] C. B. Woitiski, Y. N. Kozlov, D. Mandelli, G. V. Nizova, U. Schuchardt, G. B. Shul'pin, *J. Mol. Catal. A* **2004**, *222*, 103.

[113] J. H. Koek, E. W. M. J. Kohlen, S. W. Russell, L. van der Wolf, P. F. ter Steeg, J. C. Hellemons, *Inorg. Chim. Acta.* **1999**, *295*, 189.

[114] J. H. Koek, S. W. Russell, L. van der Wolf, R. Hage, J. B. Warnaar, A. L. Spek, J. Kerschner, L. DelPizzo, *J. Chem. Soc., Dalton Trans.* **1996**, 353.

[115] J. E. Richman, T. J. Atkins, *J. Am. Chem. Soc.* **1974**, *96*, 2268.

[116] S. W. Golding, T. W. Hambley, G. A. Lawrance, S. M. Luther, M. Maeder, P. Turner, *J. Chem. Soc., Dalton Trans.* **1999**, 1975.

[117] J. E. W. Scheuermann, K. F. Sibbons, D. M. Benoit, M. Motevalli, M. Watkinson, *Org. Biomol. Chem.* **2004**, *2*, 2664.

[118] A. J. Dickie, D. C. R. Hockless, A. C. Willis, J. A. McKeon, W. G. Jackson, *Inorg. Chem*. **2003**, *42*, 3822.

[119] A. McAuley, P. R. Norman, O. Olubuyide, *Inorg. Chem.* **1984**, *23*, 1938.

[120] R. Zhang, D. H. Busch, *Inorg. Chem.* **1993**, *32*, 4920.

[121] R. Hage, A. Lienke, *J. Mol. Catal. A* **2006**, *251*, 150.

[122] D. Schulz, T. Weyhermüller, K. Wieghardt, B. Nuber, *Inorg. Chim. Acta* **1995**, *240*, 217.

[123] B. Graham, B. Moubaraki, K. S. Murray, L. Spiccia, J. D. Cashion, D. C. R. Hockless, *J. Chem. Soc., Dalton Trans.* **1997**, 887.

[124] K. Wieghardt, U. Bossek, P. Chaudhuri, W. Herrmann, B. C. Menke, J. Weiss, *Inorg. Chem.* **1982**, *21*, 4308.

[125] G. V. Nizova, C. Bolm, S. Ceccarelli, C. Pavan, G. B. Shul'pin, *Adv. Synth. Catal*. **2002**, *344*, 899.

[126] D. A. Robson, S. Y. Bylikin, M. Cantuel, N. A. H. Male, L. H. Rees, P. Mountford, M. Schröder, *J. Chem. Soc., Dalton Trans.* **2001**, 157.

[127] A. A. Belal, L. J. Farrugia, R. D. Peacock, J. Robb, *J. Chem. Soc., Dalton Trans.* **1989**, 931.

[128] C. Bolm, D. Kadereit, M. Valacchi, *Synlett* **1997**, 687.

[129] C. Flassbeck, K. Wieghardt, *Z. Anorg. Allg. Chem.* **1992**, *608*, 60.

[130] J. L. Sessler, J. W. Sibert, V. Lynch, *Inorg. Chem.* **1990**, *29*, 4143.

[131] L. Wang, C. Wang, R. Bau, T. C. Flood, *Organometallics* **1996**, *15*, 491.

[132] E. M. McGarrigle, D. C. Gilheany, *Chem. Rev.* **2005**, *105*, 1563.

[133] M. Beller, A. Tafesh, R. W. Fischer, B. Scharbert, *Ger. Pat.*, Ger. DE 195 23 891, **1995**.

[134] D. E. De Vos, B. F. Sels, M. Reynaers, Y. V. S. Rao, P. A. Jacobs, *Tetrahedron Lett.* **1998**, *39*, 3221.

[135] T. H. Bennur, D. Srinivas, S. Sivasanker, V. G. Puranik, *J. Mol. Catal. A* **2004**, *219*, 209.

[136] K. Wieghardt, U. Bossek, L. Zsolnai, G. Huttner, G. Blondin, J.-J. Girerd, F. Babonneau, *J. Chem. Soc., Chem. Comm.* **1987**, 651.

[137] U. Bossek, K. Wieghardt, B. Nuber, J. Weiss, *Inorg. Chim. Acta* **1989**, *165*, 123.

[138] R. Hage, E. A. Gunnewegh, J. Niël, F. S. B. Tjan, T. Weyhermüller, K. Wieghardt, *Inorg. Chim. Acta* **1998**, *268*, 43.

[139] A. Berkessel, C. A. Sklorz, *Tetrahedron Lett.* **1999**, *40*, 7965.

[140] C. E. Dubé, S. Mukhopadhyay, P. J. Bonitatebus Jr., R. J. Staples, W. H. Armstrong, *Inorg. Chem.* **2005**, *44*, 5161.

[141] M. Imuta, H. Ziffer, *J. Org. Chem.* **1979**, *44*, 1351.

[142] J. F. Larrow, E. N. Jacobsen, *J. Am. Chem. Soc*. **1994**, *116*, 12129.

[143] C. H. Senanayake, G. B. Smith, K. M. Ryan, L. E. Fredenburgh, J. Liu, F. E. Roberts, D. L. Hughes, R. D. Larsen, T. R. Verhoeven, P. J. Reider, *Tetrahedron Lett.* **1996**, *37*, 3271.

[144] S. Pal, M. M. Olmstead, W. H. Armstrong, *Inorg. Chem*. **1995**, *34*, 4708.

[145] K. S. Hagen, W. H. Armstrong, H. Hope, *Inorg. Chem*. **1988**, *27*, 969.

[146] G. B. Shul'pin, *C. R. Chimie* **2003**, *6*, 163.

[147] F. Li, M. Wang, C. Ma, A. Gao, H. Chen, L. Sun, *Dalton Trans.* **2006**, *20*, 2427.

[148] J.-U. Rohde, J.-H. In, M. H. Lim, W. W. Brennessel, M. R. Bukowski, A. Stubna, E. Muenck, W. Nam, L. Que, Jr., *Science* **2003**, *299*, 1037.

[149] T. A. van den Berg, J. W. de Boer, W. R. Browne, G. Roelfes, B. L. Feringa, *Chem. Comm*. **2004**, *22*, 2550.

[150] S. Tanase, C. Foltz, R. de Gelder, R. Hage, E. Bouwman, J. Reedijk, *J. Mol. Catal. A* **2005**, *225*, 161.

[151] E. Y. Tshuva, S. J. Lippard, *Chem. Rev*. **2004**, *104*, 987.

[152] M. Costas, K. Chen, L. Que, Jr., *Coord. Chem. Rev*. **2000**, *200-202*, 517.

[153] A. L. Feig, S. J. Lippard, *Chem. Rev*. **1994**, *94*, 759.

[154] L. Que, Jr., W. B. Tolman, *Angew. Chem. Int. Ed.* **2002**, *41*, 1114.

[155] K. Wieghardt, K. Pohl, W. Gebert, *Angew. Chem.* **1983**, *95*, 739.

[156] J. R. Hartman, R. L. Rardin, P. Chaudhuri, K. Pohl, K. Wieghardt, B. Nuber, J. Weiss, G. C. Papaefthymiou, R. B. Frankel, S. J. Lippard, *J. Am. Chem. Soc*. **1987**, *109*, 7387.

[157] A. L. Feig, A. Masschelein, A. Bakac, S. J. Lippard, *J. Am. Chem. Soc.* **1997**, *119*, 334.

[158] L. D. Slep, A. Mijovilovich, W. Meyer-Klaucke, T. Weyhermüller, E. Bill, E. Bothe, F. Neese, K. Wieghardt, *J. Am. Chem. Soc.* **2003**, *125*, 15554.

[159] R. Hage, J. E. Iburg, *Eur. Pat. Appl*. **1993**, EP 549271.

[160] R. F. Moreira, E. Y. Tshuva, S. J. Lippard, *Inorg. Chem.* **2004**, *43*, 4427.

[161] E. Y. Tshuva, D. Lee, W. Bu, S. J. Lippard, *J. Am. Chem. Soc.* **2002**, *124*, 2416.

[162] M. Klopstra, R. Hage, R. M. Kellogg, B. L. Feringa, *Tetrahedron Lett.* **2003**, *44*, 4581.

[163] G. B. Shul'pin, G. V. Nizova, Y. N. Kozlov, L. Gonzalez Cuervo, G. Süss-Fink, *Adv. Synth. Catal.* **2004**, *346*, 317.

[164] U. Bossek, H. Hummel, T. Weyhermüller, E. Bili, K. Wieghardt, *Angew. Chem. Int. Ed. Engl.* **1995**, *34*, 2642.

[165] J. Green, H. Dalton, *J. Biol. Chem*. **1989**, *264*, 17698.

[166] G. V. Nizova, B. Krebs, G. Süss-Fink, S. Schindler, L. Westerheide, L. Gonzalez Cuervo, G. B. Shul'pin, *Tetrahedron* **2002**, *58*, 9231.

[167] S. Ménage, J.-B. Galey, J. Dumats, G. Hussler, M. Seite, I. G. Luneau, G. Chottard, M. Fontecave, *J. Am. Chem. Soc*. **1998**, *120*, 13370.

[168] S. Nishino, Y. Takahashi, Y. Nishida, *Inorg. Chem. Commun*. **2002**, *5*, 609.

[169] M. N. Mortensen, B. Jensen, A. Hazell, A. D. Bond, C. J. McKenzie, *Dalton Trans.* **2004**, 3396.

[170] J. Sanders-Loehr, W. D. Wheeler, A. K. Shiemke, B. A. Averill, T. M. Loehr, *J. Am. Chem. Soc.* **1989**, *111*, 8084.

[171] H. Zheng, Y. Zang, Y. Dong, V. G. Young, Jr., L. Que, Jr., *J. Am. Chem. Soc.* **1999**, *121*, 2226.

[172] B. Graham, B. Moubaraki, K. S. Murray, L. Spiccia, J. D. Cashion, D. C. R. Hockless, *J. Chem. Soc., Dalton Trans.* **1997**, *5*, 887.

[173] R. Hage, E. A. Gunnewegh, J. Niël, F. S. B. Tjan, T. Weyhermüller, K. Wieghardt, *Inorg. Chim. Acta* **1998**, *268*, 43.

[174] P. Neubold, K. Wieghardt, B. Nuber, J. Weiss, *Inorg. Chem.* **1989**, *28*, 459.

[175] E. A. Gutkina, V. M. Trukhan, C. G. Pierpont, S. Mkoyan, V. V. Strelets, E. Nordlander, A. A. Shteinman, *Dalton Trans.* **2006**, 492.

[176] R. L. Lieberman, A. C. Rosenzweig, *Critical Reviews in Biochemistry and Molecular Biology* **2004**, *39*, 147.

[177] T. Nash, *Biochem. J.*, **1953**, *55*, 416.

[178] A. Bisai, M. Chandrasekhar, V. K. Singh, *Tetrahedron Lett.* **2002**, *43*, 8355.

[179] S. D. Meyer, S. L. Schreiber, *J. Org. Chem.* **1994**, *59*, 7549.

[180] G. Strukul (editor), "Catalytic Oxidations with Hydrogen Peroxide as Oxidant", Kluwer, Dordrecht, **1992**.

[181] T. J. Meyer, M. H. V. Huynh, *Inorg. Chem.* **2003**, *42*, 8140.

[182] S. Das, T. Punniyamurthy, *Tetrahedron Lett.* **2003**, *44*, 6033.

[183] P. Neubold, B. S. P. C. Della Vedova, K. Wieghardt, B. Nuber, J. Weiss, *Inorg. Chem.* **1990**, *29*, 3355.

[184] W.-C. Cheng, W.-H. Fung, C.-M. Che, *J. Mol. Catal. A.* **1996**, *113*, 311.

[185] W.-H. Fung, W.-Y. Yu, C.-M. Che, *J. Org. Chem.* **1998**, *63*, 2873.

[186] P. Chaudhuri, J. Querbach, K. Wieghardt, B. Nuber, J. Weiss, *J. Chem. Soc., Dalton Trans.* **1990**, 271.

[187] C. Sudha, S. K. Mandal, A. R. Chakravarty, *Inorg. Chem.* **1993**, *32*, 3801.

[188] P. Neubold, K. Wieghardt, B. Nuber, J. Weiss, *Angew. Chem. Int. Ed. Engl.* **1988**, *27*, 933.

[189] D. J. Macquarrie, *Phil. Trans. R. Soc. Lond. A* **2000**, *358*, 419.

[190] J. M. Thomas, R. Raja, G. Sankar, R. G. Bell, *Acc. Chem. Res.* **2001**, *34*, 191.

[191] R. Raja, G. Sankar, J. M. Thomas, *J. Am. Chem. Soc.* **1999**, *121*, 11926.

[192] R. Raja, J. M. Thomas, *J. Mol. Catal. A* **2002**, *181*, 3.

[193] A. F. Masters, J. K. Beattie, A. L. Roa, *Catalysis Letters* **2001**, *75*, 159.

[194] J. M. Thomas, R. Raja, *P. N. A. S.* **2005**, *102*, 13732.

[195] Y.-W. Chen, H.-Y. Lin, *Journal of Porous Materials* **2002**, *9*, 175.

[196] G. Moretti, A. M. Salvi, M. R. Guascito, F. Langerame, *Surf. Interface Anal.* **2004**, *36*, 1402.

[197] A. Bhaumik, R. Kumar, *J. Chem. Soc., Chem. Commun.* **1995**, 869.

[198] I. W. C. E. Arends, R. A. Sheldon, M. Wallau, U. Schuchardt, *Angew. Chem. Int. Ed.* **1997**, *36*, 1144.

[199] J. M. Thomas, *Angew. Chem. Int. Ed.* **1999**, *38*, 3588.

[200] R. Raja, J. M. Thomas, *Chem. Commun.* **1998**, 1841.

[201] M. Dugal, G. Sankar, R. Raja, J. M. Thomas, *Angew. Chem., Int. Ed.* **2000**, *39*, 2313.

[202] M. Taramasso, G. Perego, B. Notari, *U.S. Patent 4.410.501*, **1983**.

[203] C. A. Hijar, R. M. Jacubinas, J. Eckert, N. J. Henson, P. J. Hay, K. C. Ott, *J. Phys. Chem. B* **2000**, *104*, 12157.

[204] P. Wu, T. Tatsumi, *J. Phys. Chem. B* **2002**, *106*, 748.

[205] P. J. Kooyman, G. C. A. Luijkx, A. Arafat, H. van Bekkum, *J. Mol. Catal. A* **1996**, *111*, 167.

[206] I. Halasz, M. Agarwal, E. Senderov, B. Markus, *Appl. Catal. A* **2003**, *241*, 167.

[207] P. Mukherjee, *PhD thesis*, University of Pune, **2000**.

[208] T. Sooknoi, J. Limtrakul, *Appl. Catal. A* **2002**, *233*, 227.

[209] A. Corma, M. T. Navarro, J. Perez-Pariente, *J. Chem. Soc., Chem. Comm.* **1994**, 147.

[210] M. W. Peters, P. Meinhold, A. Glieder, F. H. Arnold, *J. Am. Chem. Soc.* **2003**, *125*, 13442.

[211] J. F. Hartwig, K. S. Cook, M. Hapke, C. D. Incarvito, Y. Fan, C. E. Webster, M. B. Hall, *J. Am. Chem. Soc.* **2005**, *127*, 2538.

[212] J. Urbano, T. R. Belderrain, M. C. Nicasio, S. Trofimenko, M. M. Diaz-Requejo, P. J. Pérez, *Organometallics* **2005**, *24*, 1528.

[213] M. C. Feiters, A. E. Rowan, R. J. M. Nolte, *Chem. Soc. Rev*. **2000**, *29*, 375.

[214] H. Munakata, Y. Oumi, A. Miyamoto, *J. Phys. Chem. B* **2001**, *105*, 3493.

[215] D. H. Wells, Jr., W. N. Delgass, K. T. Thomson, *J. Am. Chem. Soc*. **2004**, *126*, 2956.

[216] J. Limtrakul, C. Inntam, T. N. Truong, *J. Mol. Catal. A* **2004**, *207*, 137.

[217] J. P. Fox, V. Rooy, S. P. Bates, *Micropor. Mesopor. Mater.* **2004**, *69*, 9.

[218] L. Lu, Q. Wang, Y. Liu, *J. Phys. Chem. B* **2005**, *109*, 8845.

[219] A. Wallqvist, D. G. Covell, *J. Phys. Chem*. **1995**, *99*, 13118.

[220] K. Nikki, H. Inakura, Wu-Le, N. Suzuki, T. Endo, *J. Chem. Soc., Perkin Trans. 2* **2001**, 2370.

[221] D. D. Perrin, W. L. F. Armarego, *Purification of Laboratory Chemicals*. Pergamon Press, Oxford, **1998**.

[222] V. W. Day, W. G. Klemperer, A. Yagasaki, *Chem. Lett*. **1990**, 1267.

[223] I. P. Evans, A. Spencer, G. Wilkinson, *J. Chem. Soc., Dalton Trans.* **1973**, 204.

[224] J. Kang, J. H. Jo, *Bull. Korean Chem. Soc*. **2003**, *24*, 1403.

[225] H. M. Irving, M. G. Miles, L. D. Pettit, *Anal. Chim. Acta*, **1967**, *38*, 475.

[226] L. Zékány, I. Nagypál, *Computational Methods for the Determination of Stability Constants*. Plenum Press, New York, **1985**, 291.

[227] L. Petterson, B. Hedman, I. Andersson, N. Ingri, *Chem. Scripta*, **1983**, *22*, 254.

[228] G. M. Sheldrick, *SHELXS-97-Program for crystal structure solution*, University of Göttingen, Göttingen, Germany (1997).

[229] G. M. Sheldrick, *SHELXL-97-Program for crystal structure refinement*, University of Göttingen, Göttingen, Germany (1997).

[230] A. L. Spek, *J. Appl. Cryst.* **2003**, *36*, 7.

[231] L. J. Farrugia, *J. Appl. Cryst*. **1997**, *30*, 565.

[232] I. J. Bruno, J. C. Cole, P.R. Edgington, M. Kessler, C. F. Macrae, P. McCabe, J. Pearson, R. Taylor, *Acta Cryst*. **2002**, *B58*, 389

[233] T. D. Fenn, D. Ringe, G. A. Petsko, *J. Appl. Cryst.* **2003**, *36*, 944.

Appendix

Table A. List of the new compounds synthesized in this work

1. Ligands

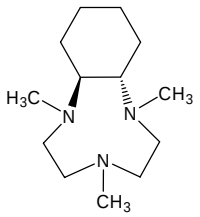

(L^{SS}-Me_3)

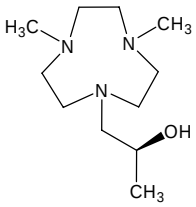

(R^{1S}L-Me_2)

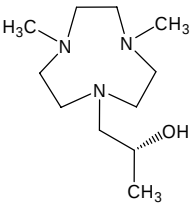

(R^{1R}L-Me_2)

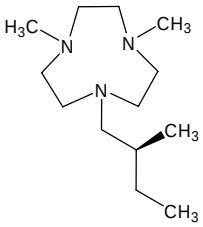

(R^{2S}L-Me_2)

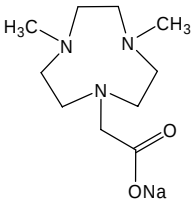

([Na][Ac-L-Me_2])

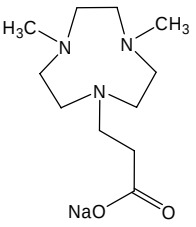

([Na][Pr-L-Me_2])

2. Manganese Complexes

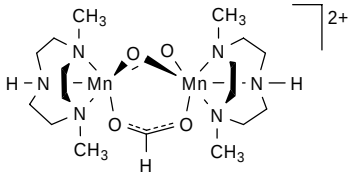

(**Mn1**)

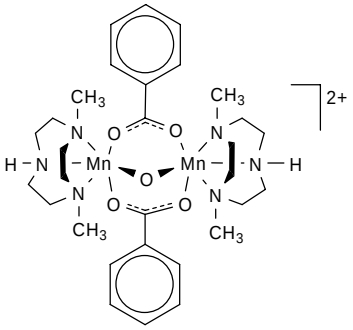

(**Mn2**)

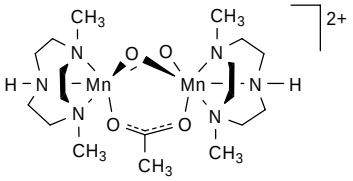

(**Mn3**)

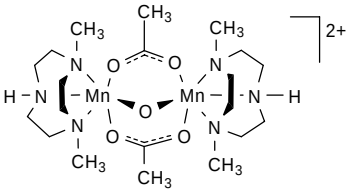

(**Mn4**)**

** − **Mn4** was already known, but not structurally characterized

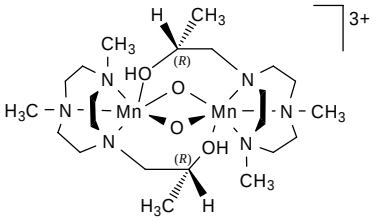

(**Mn5R**)

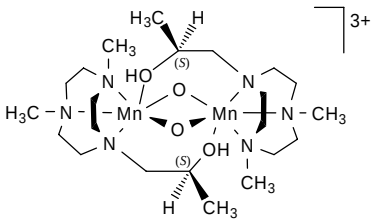

(**Mn5S**)

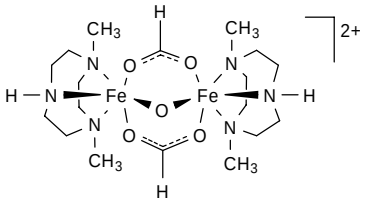

(**Fe1**)

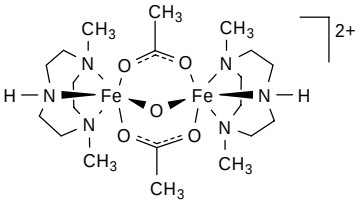

(**Fe2**)

3. Iron Complexes

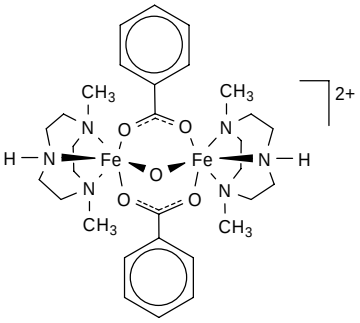

(**Fe3**)

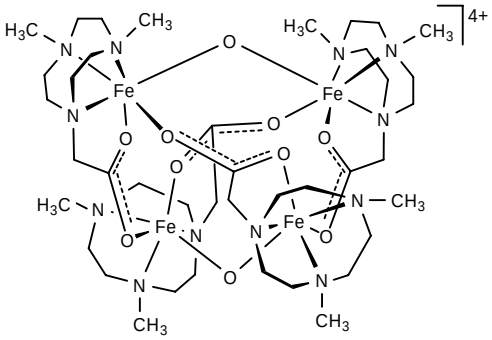

(**Fe4**)

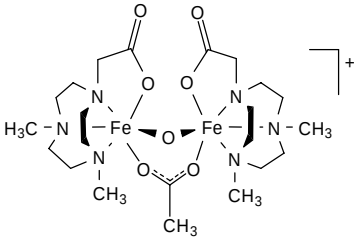

(**Fe5**)

4. Ruthenium Complexes

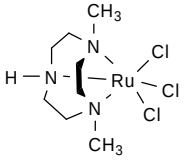

(**Ru1**)

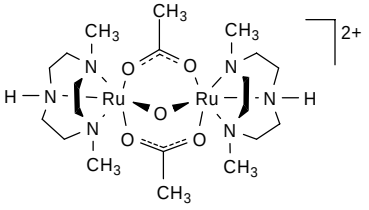

(**Ru2**)

5. Cobalt Complex

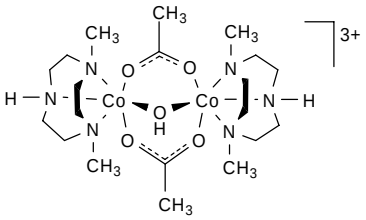

(**Co1**)

Table B. Crystallographic and selected experimental data for [**Mn1**][PF_6]$_{1.5}$[Cl]$_{0.5}$ · 1.5 H_2O, [**Mn3**][PF_6]$_2$ · $(CH_3)_2CO$ and [**Mn4**][PF_6]$_2$

	[**Mn1**][PF_6]$_{1.5}$[Cl]$_{0.5}$ · 1.5 H_2O	[**Mn3**][PF_6]$_2$ · $(CH_3)_2CO$	[**Mn4**][PF_6]$_2$
Chemical formula	$C_{17}H_{42}Cl_{0.5}F_9Mn_2N_6O_{5.5}P_{1.5}$	$C_{21}H_{47}F_{12}Mn_2N_6O_5P_2$	$C_{20}H_{44}F_{12}Mn_2N_6O_5P_2$
Formula weight	763.63	863.47	848.43
Crystal system	Monoclinic	Monoclinic	Monoclinic
Space group	P 2/m	C 2/m	P 2_1/n
Crystal colour and shape	Green plate	Green plate	Red rod
Crystal size	0.5 x 0.5 x 0.2	0.4 x 0.3 x 0.1	0.5 x 0.2 x 0.2
a (Å)	13.2587(11)	33.968(5)	14.3384(10)
b (Å)	8.5930(4)	11.9980(12)	16.6439(16)
c (Å)	16.2605(13)	19.298(2)	15.2611(11)
B (°)	114.227(9)	118.225(10)	115.683(7)
V (Å^3)	1689.4(2)	6929.7(14)	3282.2(5)
Z	2	8	4
T (K)	173(2)	173(2)	173(2)
D_c (g·cm^{-3})	1.501	1.655	1.717
μ (mm^{-1})	0.944	0.927	0.977
Scan range (°)	2.28 < θ < 25.90	2.15 < 2θ < 25.75	1.92 < 2θ < 26.02
Unique reflections	3504	7127	6202
Reflections used [I>2σ(I)]	2177	1829	4214
R_{int}	0.0680	0.2389	0.0653
Final *R* indices [I>2σ(I)]	0.0485, wR_2 0.1321	0.0825, wR_2 0.1829	0.0538, wR_2 0.1333
R indices (all data)	0.0748, wR_2 0.1405	0.2714, wR_2 0.2400	0.0819, wR_2 0.1441
Goodness-of-fit	0.885	0.737	1.014
Max, Min Δρ/e (Å^{-3})	0.531, -0.505	0.893, -0.956	1.463, -0.750

Table C. Crystallographic and selected experimental data for [**Fe2**][PF_6]$_2$, [**Ru2**][PF_6]$_2$ and [**Co1**][PF_6]$_3$ · $(CH_3)_2CO$

	[**Fe2**][PF_6]$_2$	[**Ru2**][PF_6]$_2$	[**Co1**][PF_6]$_3$ · $(CH_3)_2CO$
Chemical formula	$C_{20}H_{44}F_{12}Fe_2N_6O_5P_2$	$C_{20}H_{44}F_{12}N_6O_5P_2Ru_2$	$C_{23}H_{51}Co_2F_{18}N_6O_6P_3$
Formula weight	850.25	940.69	1060.47
Crystal system	Monoclinic	Orthorhombic	Triclinic
Space group	P 2_1/n	C mca	P -1
Crystal colour and shape	Orange block	Purple plate	Violet block
Crystal size	0.4 x 0.3 x 0.2	0.34 x 0.22 x 0.08	0.37 x 0.20 x 0.12
a (Å)	14.410(2)	33.806(7)	10.976(2)
b (Å)	16.547(2)	13.853(3)	11.246(2)
c (Å)	15.341(3)	15.199(3)	16.389(3)
α (°)			104.67(1)
β (°)	116.026(11)		92.67(1)
γ (°)			95.49(1)
V (Å^3)	3287.1(8)	7118(3)	1942.9(6)
Z	4	8	2
T (K)	173(2)	203(2)	203(2)
D_c (g·cm^{-3})	1.718	1.756	1.813
μ (mm^{-1})	1.090	1.040	1.110
Scan range (°)	1.62 < θ < 25.70	2.08 < θ < 26.00	1.29 < 2θ < 25.25
Unique reflections	6238	3281	6932
Reflections used [I>2σ(I)]	4185	1344	3923
R_{int}	0.1139	0.0904	0.1520
Final *R* indices [I>2σ(I)]	0.0692, wR_2 0.1610	0.0474, wR_2 0.1095	0.0683, wR_2 0.1532
R indices (all data)	0.1091, wR_2 0.1774	0.0890, wR_2 0.1491	0.1228, wR_2 0.1765
Goodness-of-fit	1.042	0.793	0.929
Max, Min Δρ/e (Å^{-3})	0.964, -1.352	0.448, -0.423	0.552, -1.264

Table D. Crystallographic and selected experimental data for [**Mn5R**][PF_6]$_3$, [**Mn5S**][PF_6]$_3$ and [**Fe4**][PF_6]$_4$ · 5 MeCN

	[**Mn5R**][PF_6]$_3$	[**Mn5S**][PF_6]$_3$	[**Fe4**][PF_6]$_4$ · 5 MeCN
Chemical formula	$C_{22}H_{50}F_{18}Mn_2N_6O_4P_3$	$C_{22}H_{50}F_{18}Mn_2N_6O_4P_3$	$C_{50}H_{95}F_{24}Fe_4N_{17}O_{10}P_4$
Formula weight	1007.47	1007.47	1897.71
Crystal system	Tetragonal	Tetragonal	Monoclinic
Space group	I 4	P 4	P 2_1/c
Crystal colour and shape	Brown block	Brown cube	Green plate
Crystal size	0.36 x 0.28 x 0.22	0.22 x 0.18 x 0.15	0.32 x 0.26 x 0.10
a (Å)	18.680(3)	18.884(1)	22.673(2)
b (Å)	18.680(3)	18.884(1)	14.8307(8)
c (Å)	24.730(5)	12.5586(6)	23.388(2)
B (°)	90	90	99.387(10)
V (Å^3)	8629(3)	4478.4(4)	7758.9(10)
Z	8	4	4
T (K)	173(2)	173(2)	173(2)
D_c (g·cm^{-3})	1.551	1.494	1.625
μ (mm^{-1})	0.809	0.780	0.935
Scan range (°)	2.18 < θ < 26.01	2.16 < 2θ < 25.98	2.11 < 2θ < 26.07
Unique reflections	5720	8742	15205
Reflections used [I>2σ(I)]	2349	3947	4675
R_{int}	0.1078	0.1228	0.1477
Final *R* indices [I>2σ(I)]	0.0611, wR_2 0.1287	0.1185, wR_2 0.2865	0.0701, wR_2 0.1667
R indices (all data)	0.1304, wR_2 0.1472	0.1644, wR_2 0.3169	0.2013, wR_2 0.2036
Goodness-of-fit	0.775	0.920	0.745
Max, Min Δρ/e (Å^{-3})	0.797, -0.431	0.821, -0.985	0.972, -0.755

Curriculum Vitae

Vladimir Bogdanovich Romakh,
PhD student, Assistant

Born December 1st, 1974 in Feodosiya (Ukraine)
Russian citizen

Carrier :

1991 Mathematician high school in Feodosiya, Ukraine

1991-1996 Moscow State University (Lomonosov), Moscow, Russia, MS degree with honours in Chemistry under the direction of Dr. Alevtina T. Mevkh. Project: *A Study of the Arachidonic Acid Conversion by Prostaglandin H Synthase in the Presence of Proteinaceous Drugs from a Blood Plasma*

1996-1999 Chemistry Department of Moscow State University in collaboration with A. N. Belozersky Institute of Physico-Chemical Biology, Russian Academy of Sciences, Moscow, Russia, postgraduate studies under the direction of Dr. Alevtina T. Mevkh. Project: *Oxygenation of Polyunsaturated Fatty Acids by Heme-Consistent Enzymes*

2000 Expert in an engineering company in Moscow, Russia

2001-2002 Semenov Institute of Chemical Physics, Russian Academy of Sciences, Moscow, Russia, research chemist under the direction of Prof. Georgiy B. Shul'pin. Project: *Metal Complex Catalysis, Biomimetic Oxidation of Organic Compounds*

2002-2006 Institut de Chimie, Université de Neuchâtel, Neuchâtel, Switzerland, PhD student and assistant under the direction of Prof. Georg Süss-Fink. Project: *Oxidation of Alkanes, Alkenes and Alcohols Catalyzed by Transition Metal Complexes*

2006- Heidelberg University, Germany, postdoctoral fellow under the direction of Prof. Peter Hofmann. Project: *Catalytic Research Laboratory of B.A.S.F.*

Professional Interests :

Activation of C-H Bonds, Catalytic Oxygenation, Biomimetic Models, Enzymatic Oxidation, Triazacyclononane Ligands, Chirality, Arene-Ruthenium, Arene-Osmium Clusters, Hydrogenation, Homogeneous Catalysis